

Alternative Wall-to-slab Connection Systems in Reinforced Concrete Structures

by

Johannes Daniël Gerber



*Thesis presented in partial fulfilment of the requirements for
the degree of Master of Engineering (Structural) in the
Faculty of Engineering at Stellenbosch University*

Supervisor: Prof. G.P.A.G van Zijl

December 2016

Declaration

By submitting this thesis electronically, I declare that the entirety of the work contained therein is my own, original work, that I am the sole author thereof (save to the extent explicitly otherwise stated), that reproduction and publication thereof by Stellenbosch University will not infringe any third party rights and that I have not previously in its entirety or in part submitted it for obtaining any qualification.

Date: 2016/08/20

Copyright © 2016 Stellenbosch University
All rights reserved.

Abstract

Alternative Wall-to-slab Connection Systems in Reinforced Concrete Structures

J.D. Gerber

*Department of Structural Engineering,
University of Stellenbosch,
Private Bag X1, Matieland 7602, South Africa.*

Thesis: MEng (Civil)

December 2016

In the construction of multi-storey buildings, the reinforced concrete (RC) core or shear walls normally precede the construction of the RC floors. A system is therefore required to connect the floors to the already cast walls. There are many different floor-to-wall connection systems available in South Africa, but their behaviour and capacity are not always fully understood, especially when the moment capacity of the joint is to be utilised in order to design more economical structures.

This research investigation focusses on four systems. The first is the conventional way of casting walls and floors by using continuous starter-bars that protrude through the formwork. The second system makes use of pre-bent site-installed starter-bars that are fixed within the wall, straightened after the wall is cast and then lapped with the slab reinforcement. The third system is also based on the principle of pre-bent starter bars, but they are pre-assembled inside a steel box to speed up the installation process and ease access to the bars once the wall is cast. Another system, that is not as popular in South Africa yet, is the use of cast-in anchors with mechanical couplers. The anchors are cast into the concrete wall and, once the form work is removed, threaded continuation bars are screwed into the couplers to make the connection between the floor and wall.

The design procedure for the continuous starter-bar system is well understood and documented in design codes, but not enough information is available on the design procedure for the other systems. Certain practical aspects of the installation process are also not fully understood.

Cold bending and straightening of the starter-bars are inevitable in both bend-out systems. Previous research shows that this cold working of the reinforcement can reduce the yield stress, ductility and E-modulus of the steel. In order to investigate these findings, a series of tensile tests are conducted on Y10 and Y12 reinforcement (high yield, deformed reinforcing bars). The results indicate that a significant reduction can be expected in both

the yield stress and modulus of elasticity of the steel. A low cycle fatigue test further confirmed that a reduction in the ductility of the steel is also present.

The next phase in the research investigation is to construct full scale models of the four connection systems. The systems are installed in four separate joints between a cantilever floor and a free-standing wall. The systems are designed to all have the same moment and shear capacity and are based on a typical wall-to-slab connection found in an office block. The construction of the models are done in such a way as to mimic the construction methods in practice as closely as possible. The entire process is done in a controlled environment, with a best practice approach adopted. Once the models are constructed, a load is applied at the tip of the cantilever floor in order to generate a bending moment and shear force at the wall-to-slab joint. The displacement of the specimen is monitored throughout the test. The structural performance is subsequently compared in terms of tip displacement, crack widths and ultimate resistance.

The effect of the cold bending on the starter-bars is clearly visible, as both the responses of the bend-out systems are less desirable than the results from the continuous starter-bar system. The experimental phase is followed by numerical analysis of the connection systems. Once the FE model is calibrated and verified with the data from the experimental phase, a sensitivity study is conducted. The effect of either varying the steel or the concrete properties on the structural performance of a slab-to-wall connection is investigated. The FE results shows that the structural performance is significantly more sensitive to a reduction in the yield stress of the starter-bars, than to the use of a lower concrete grade.

Finally, the systems are compared in terms of their constructibility, availability, material cost and their structural performance. Some recommendations on quality control matters and best-practice principles are also discussed. It is concluded that all the alternative connection systems can be successfully implemented in a moment-fixed wall-to-slab connection. The site-installed bend-out system performed the best structurally, but other practical considerations and project specific aspects might play an even bigger role in deciding which system to use in practice. Further, in order to ensure that the bend-out systems perform on the same level as the conventional system, it is recommended that the design should be conducted with a set of modified steel properties to allow for the negative effect of the cold working on the starter-bars.

Uittreksel

Alternatiewe Muur-tot-vloer Konneksiesisteme in Gewapende Beton Strukture

(“Alternative Wall-to-slab Connection Systems in Reinforced Concrete Structures”)

J.D. Gerber

*Departement Struktuur Ingenieurswese,
Universiteit van Stellenbosch,
Privaatsak X1, Matieland 7602, Suid Afrika.*

Tesis: MIng (Siviel)

Desember 2016

In die konstruksie van multi-verdieping geboue, word die gewapende beton kern of skuifmure gewoonlik vooruit gegiet, met die aanhegting van die bewapende vloere wat volg. 'n Stelsel is dus nodig om hierdie verbinding met die mure, wat alreeds gegiet is, te bewerkstellig. Alhoewel daar 'n wye reeks muur-tot-vloer konneksie sisteme beskikbaar is in Suid-Afrika, word hulle gedrag en kapasiteit nie altyd ten volle verstaan nie. Dit is veral so waar die moment kapasiteit van die konneksie in ag geneem word om sodoende meer ekonomies te kan ontwerp.

Hierdie navorsing fokus op vier verskillende muur-tot-vloer konneksie sisteme. Die eerste sisteem is die konvensionele manier om kontinuteit tussen die vloer en die muur te verseker: Die proses behels dat deurlopende bewapening deur die bekisting van die muur steek, om sodoende genoeg verankering met die bewapening van die vloer te verseker. Die tweede sisteem maak gebruik van voorafgebuigde stawe wat op die bousterrein geïnstalleer word. Die uit-buig stawe word aan die muur se bewapening vasgemaak en word eers uitgebuig nadat die muur gegiet is. Die derde stelsel maak ook gebruik van uitbuig-stawe, maar word vooraf geïnstalleer in 'n metaal kis om die installasieproses te vergemaklik en bespoedig. Die laaste sisteem wat ondersoek word is nog nie so bekend aan die Suid-Afrikaanse konstruksie bedryf nie. Dit maak gebruik van beton-ankers wat vasgeheg is aan meganiese koppelaars. Hierdie ankers word in die betonmuur ingegiet en sodra die bekisting verwyder is, word die bewapening eenvoudig ingeskroef om sodoende die verbinding tussen die muur en die vloer te maak.

Die ontwerpprocedure vir die deurlopende bewapening sisteem word goed verstaan en die proses is duidelik gedokumenteer in die ontwerp kodes, maar daar is nie genoeg inligting beskikbaar vir die ontwerp van die ander sisteme nie. Daar is ook heelwat onsekerheid oor van die praktiese aspekte rondom die installasie van die sisteme.

Koudbewerking van bewapening is onvermydelik in beide uit-buig sisteme aangesien die stawe eers teen 90° gebuig en in die muur geïnstalleer word, waarna dit weer reguit gebuig word sodra die muur gegiet is. Vorige navorsing toon dat hierdie koudbewerking 'n negatiewe effek op die einskappe van die staal het deurdat die E-modulus, duktiliteit asook die vloeispanning verlaag word. Hierdie bevindings word ondersoek deur 'n reeks trek toetse uit te voer op Y10 en Y12 bewapening (hoë vloeispanning, vervormde bewapeningstawe). Die resultate toon 'n beduidende afname in beide die vloeispanning en elastisiteitsmodulus van die staal.

Die volgende fase in die navorsingsondersoek is om volskaalse modelle van die vier verbinding stelsels te bou. Die stelsels word geïnstalleer in vier afsonderlike verbindings tussen 'n kantelbalk en 'n losstaande muur. Die onderskeie stelsels word op so 'n manier ontwerp dat hulle moment- en skuifkapasiteit verteenwoordigend is van 'n tipiese muur-tot-blad verbinding in 'n kantoorblok. Die praktyk word, sover as moontlik, nageboots in die konstruksie van die volskaalse modelle. Die hele proses vind plaas in 'n gekontroleerde omgewing en 'n beste-praktyk benadering word deurgaans gevolg. Sodra die volskaalse modelle gebou is, word hulle kapasiteit getoets deur 'n punt las op die kantelbalk te plaas om sodoende 'n buigmoment en skuifkrag by die muur-tot-blad konneksie te genereer. Die verplasing van die model word deurlopend gemonitor. Die sisteme word vergelyk op grond van die tempo in die verplasing van die kantelbalk, vorming van krake en maksimum weerstand.

Die negatiewe uitwerking wat die koudbewerking op die gedrag van die muur-tot-blad verbinding het, is duidelik sigbaar in die data wat tydens die volskaalse toetse ingesamel is. Albei uit-buig sisteme vertoon minder bevredigende gedrag in vergelyking met die deurlopende bewapening sisteem. Die eksperimentele fase word gevolg deur numeriese analise van die onderskeie stelsels. Sodra die eindige element model gekalibreer en geverifieer is met die fisiese eksperimentele data, word 'n sensitiwiteitsstudie uitgevoer. Die sensitiwiteit van die strukturele respons word gemeet teen 'n reeks wisselende staalen beton eienskappe. Die resultate van hierdie studie bewys dat die strukturele gedrag aansienlik meer sensitief is vir 'n verlaging in die vloeispanning van die bewapening as vir die gebruik van 'n swakker beton.

Uiteindelik word al die sisteme vergelyk met betrekking tot hulle praktiese uitvoerbaarheid, algemene beskikbaarheid, koste van materiaal en hulle strukturele gedrag. Daar word ook aanbevelings gemaak oor kwaliteitsbeheer op die bousterrein en beste-praktyk beginsels wat toegepas moet word. Ten slotte word daar bevind dat al drie alternatiewe sisteme suksesvol geïmplementeer kan word in 'n momentvaste muur-tot-vloer verbinding. Alhoewel die terrein geïnstalleerde uit-buig sisteem se strukturele gedrag die beste was, is dit moontlik dat ander faktore en projek spesifieke aspekte 'n groter rol kan speel wanneer daar op die gekose sisteem besluit moet word. Verder, om te verseker dat die strukturele gedrag van albei uitbuig-staaf konneksies in lyn is met die van die konvensionele metode, word daar aanbeveel dat die ontwerp van die konneksies aangepaste staal eienskappe in ag neem om voorsiening te maak vir die negatiewe uitwerking van die koudbewerking op die uitbuig-stawe.

Acknowledgements

I would like to express my sincere gratitude to the following people and organisations for their valuable contributions to this research investigation:

- Professor G.P.A.G van Zijl, as my promoter, for all his support, guidance, motivation and willingness to always help.
- Mr J. van der Merwe and S. Zarenka, for all their assistance in the structural workshop and laboratory.
- Mr T. Muzofa, for helping me with the physical experiments and conducting some of the supplementary tests, as part of his final year project.
- Mr E. Jeneke, C. van der Merve and F. Swanepoel, from PERI formwork, for sponsoring and supplying most of the material and equipment for the formwork used in the physical experiments.
- H. Proveda, from Ancon Building Products, for sponsoring some of the import cost for the cast-in anchor system.
- Dr. J Cairns, from Heriot Watt University, for providing me with his research on the Ancon KS Threaded Anchors.
- A. Layman, N Scheepers and the rest of the admin staff in the Structural Engineering Department, for all their assistance and help.
- Tertia Viljoen and Madelène Gerber, for the proof reading of this document.

I would also like to express my appreciation for all my family and friends for their continuous support, love and motivation. Lastly I would like to thank my Creator, for giving me the ability and strength to complete this project.

Dedications

Hierdie tesis word opgedra aan my beste vriend en lewensmaat, Madelène

Contents

Declaration	i
Abstract	ii
Uittreksel	iv
Acknowledgements	vi
Dedications	vii
Contents	viii
List of Figures	xii
List of Tables	xv
Nomenclature	xvii
1 Introduction	1
1.1 Background	1
1.2 Problem Statement	2
1.3 Scope	3
1.4 Objectives	3
1.5 Limitations	3
1.6 Thesis Layout	4
2 Connection Systems	6
2.1 Introduction	6
2.2 Continuous Starter-bar System	6
2.2.1 Description	6
2.2.2 Design Procedure	6
2.2.3 Additional Aspects	8
2.3 Site-installed Bend-out Bar System	8
2.3.1 Description	8
2.3.2 Effect of Cold Bending and Straightening	10
2.3.3 Design Procedure	13
2.3.4 Additional Aspects	13
2.4 Pre-assembled Bend-out Bar System	15
2.4.1 Description	15
2.4.2 Design Procedure	18

2.4.3	Additional Aspects	18
2.5	Cast-in Anchors System	18
2.5.1	Description	18
2.5.2	Modified Cone Behaviour	20
2.5.3	Design Procedure	23
2.5.3.1	Step 4 - Design for Flexure	24
2.5.3.2	Step 5 - Design for Shear	25
2.5.3.3	Step 6 - Rebar configuration	27
2.5.3.4	Step 7 - Anchorage and lap lengths	27
2.5.3.5	Step 8 - Detailing of reinforcement	27
2.5.4	Additional Aspects	28
3	Experimental Design	31
3.1	Introduction	31
3.2	Full-scale Tests	31
3.2.1	Test Configuration	33
3.2.2	Test Specimens	34
3.2.2.1	Design - Model A	35
3.2.2.2	Design - Model B	43
3.2.2.3	Design - Model C	45
3.2.2.4	Design - Model D	45
3.2.2.5	Construction	49
3.2.3	Test Frame Design	57
3.2.4	Measurement Instrumentation	60
3.2.5	Test Execution Methodology	62
3.3	Tensile Tests	62
3.3.1	Test Configuration	62
3.3.2	Test Specimens	63
3.3.3	Measurement Instrumentation	68
3.3.4	Test Execution Methodology	68
3.4	Low-cycle Fatigue Tests	70
3.4.1	Test Configuration	70
3.4.2	Test Specimens	70
3.4.3	Test Execution Methodology	71
3.5	Supplementary Tests	72
3.5.1	Compressive strength	73
3.5.2	E-modulus	73
4	Experimental Results	77
4.1	Introduction	77
4.2	Full-scale Tests	77
4.2.1	Test Observations	77
4.2.2	Test Results	83
4.3	Tensile Tests	86
4.3.1	Preliminary Tests	87
4.3.2	Reinforcement used in the Full-scale Models	93
4.4	Low-cycle Fatigue Tests	100
4.4.1	Test Observations	100
4.4.2	Test Results	101

4.5	Supplementary Tests	102
4.5.1	Compressive Strength	102
4.5.2	E-Modulus	103
5	Numerical Analysis	105
5.1	Introduction	105
5.2	Model Development	106
5.2.1	Elements	109
5.2.2	Mesh Configuration	111
5.2.3	Material Models	112
5.2.3.1	Concrete Models	112
5.2.3.2	Reinforcing Steel Models	116
5.2.4	Boundary Conditions	118
5.2.5	Load Conditions	119
5.3	Results	120
5.3.1	Comparison to Experimental Results	121
5.3.2	Sensitivity Study	123
6	Conclusions and Recommendations	133
6.1	Introduction	133
6.2	Conclusions	133
6.2.1	Constructibility of Systems	133
6.2.2	Effect of Cold Bending and Straightening	135
6.2.3	Structural Performance of Systems	136
6.2.4	FEM and Sensitivity Study	136
6.3	Recommendations	137
6.4	Future Work	138
	Appendices	140
A	Detailed Design Procedure - Continuous Starter-bar System	141
A.1	Step 1 - Determine loads	141
A.2	Step 2 - Calculate load combinations	142
A.3	Step 3 - Analyse structure	144
A.4	Step 4 - Design for Flexure	144
A.5	Step 5 - Design for Shear	146
A.6	Step 6 - Rebar configuration	147
A.7	Step 7 - Anchorage and lap lengths	147
A.8	Step 8 - Detailing Reinforcement	149
B	Tensile Test Results	151
C	Low Cycle Fatigue Test Results	158
D	Supplementary Test Results	161
E	Bending Schedules for Full Scale Models	163
E.1	Continuous Starter-bar System	164
E.2	Site-installed Bend-out Bar System	166
E.3	Pre-assembled Bend-out Bar System	167

<i>CONTENTS</i>	xi
E.4 Cast-in Anchors System	168
F Steel A-Frame Design Calculations	170
G Finite Element Material Models	182
H The Grubb's Test	187
List of References	189

List of Figures

2.1	Continuous Starter-bar System (reworked from Ancon Building Products (2011))	7
2.2	Bent-out Bar Shape: Site-installed (reworked from Ancon Building Products (2011))	9
2.3	Site-installed Bend-out Bar System (reworked from Ancon Building Products (2011))	10
2.4	Strain Reversal	11
2.5	Hysteresis Stress-strain Curves of Straightened Bars (reworked from Chun and Ha (2014))	12
2.6	Bend-out Starter-bar Bending Schedule	14
2.7	Sensitivity of Sectional Moment Resistance to Effective Depth of Flexural Reinforcement	15
2.8	Bend-out Starter-bar Unit (reworked from Ancon Building Products (2011))	16
2.9	Pre-assembled Bend-out Bar System (reworked from Ancon Building Products (2011))	17
2.10	Timber Anchor Carriers (reworked from Ancon Building Products (2014))	19
2.11	Cast-in Anchor with Mechanical Couplers (reworked from Ancon Building Products (2014))	20
2.12	Cone Failure for Cast-in Anchor in Direct Tension (reworked from Ancon Building Products (2014))	21
2.13	Modified Cone Failure for Cast-in Anchor in Moment Connections (reworked from Ancon Building Products (2014))	22
2.14	Notation for Joint Shear Resistance (reworked from Cairns (2010))	26
2.15	Anchor Edge Reinforcement Details (reworked from Ancon Building Products (2014))	28
2.16	Cast-in Anchor Continuation Bar Anchorage Detail (reworked from Ancon Building Products (2014))	29
3.1	Section Through Typical Office Block	32
3.2	Full-scale Specimen with Boundary Conditions and Applied Load	33
3.3	Full-scale Test Configuration	34
3.4	Sub Frame Analysis	37
3.5	a) Moment Diagram Envelope b) Shear Force Diagram Envelope	38
3.6	Continuous Starter-bar Dimensions	42
3.7	Shape Code 38	44
3.8	Wall Shuttering	50
3.9	Different Connection Systems	52
3.10	Discharging of Concrete	53
3.11	Wall-to-slab Joint Preparation	54
3.12	Floor Shuttering	56

3.13	Steel A-frame FE Model	58
3.14	Steel A-frame FEA Results	59
3.15	Steel A-frame	60
3.16	Full-scale Specimen LVDT Set-up	61
3.17	Tensile Testing Configuration	63
3.18	Typical Reinforcement Bending Table	64
3.19	Reinforcement Straightening Procedure	65
3.20	Machined Specimen	66
3.21	Tensile Testing LVDT Set-up	69
3.22	Determination of Yield Stress - Direct Method	71
3.23	Determination of Yield Stress - Offset Method	72
3.24	Degrees of Low-cycle Bending and Straightening	74
3.25	E-modulus Test Load Cycle	75
3.26	E-modulus Test Set-up	76
4.1	Cracks at Stage 1 - Wall Joint	78
4.2	Cracks at Stage 1 - Top of Floor	79
4.3	Cracks at Stage 2 - Wall Joint	80
4.4	Cracks at Stage 2 - Top of Floor	81
4.5	Cracks at Stage 3 - Wall Joint	82
4.6	Cracks at Stage 3 - Top of floor	83
4.7	Cantilever Tip Displacement vs Applied Load	84
4.8	Cantilever Centre Displacement vs Applied Load	85
4.9	Cantilever Rotation vs Applied Load	86
4.10	Stress-Strain Curve of Y10-S and Y10-B Reinforcement	88
4.11	Stress-Strain Curve of Y12-S and Y12-B Reinforcement	89
4.12	E-modulus Results of Y10-S and Y10-B Reinforcement	90
4.13	E-modulus Results of Y12-S and Y12-B Reinforcement	91
4.14	Yield Stress Calculation Methods for the Different Reinforcement Sets	92
4.15	Yield Stresses of Y10-S and Y10-B Reinforcement	93
4.16	Yield Stresses of Y12-S and Y12-B Reinforcement	94
4.17	Ultimate Stresses of Y10-S and Y10-B Reinforcement	95
4.18	Ultimate Stresses of Y12-S and Y12-B Reinforcement	96
4.19	Typical Stress-strain Relationships: Full-scale Model Reinforcement	97
4.20	E-modulus Results: Full Scale Model Reinforcement	98
4.21	Yield Stress Results: Full Scale Model Reinforcement	99
4.22	Ultimate Stress Results: Full Scale Model Reinforcement	100
4.23	Crack Formation and Discolouring of Rebar in Bent Region	101
4.24	Fatigue Test Results Summary	102
4.25	Summary of Uniaxial Compression Test Results	103
5.1	Finite Elements	109
5.2	CHX60, 20-node Solid Brick Element (Diana, 2014)	110
5.3	Embedded Reinforcement Element in Solid (Diana, 2014)	111
5.4	Reinforcement Segment Integration Points (Diana, 2014)	112
5.5	Effect of Mesh Size on FEM Results	113
5.6	a)Reinforcement Elements b)Concrete Mesh	114
5.7	a) Tensile Behaviour by Hordijk b) Compressive Behaviour by Thorenfeldt (Diana, 2014)	115

5.8	Equivalent Stress-strain Curve for the Reinforcement Material Model in Y12-A(40)	117
5.9	Rebar Stress-Strain Relationships used in Sensitivity Study	118
5.10	FE Model Boundary Conditions	119
5.11	FE Model Applied Displacement/Load	120
5.12	Comparison of Experimental data with FEA data of Model A	122
5.13	Comparison Of Experimental and Numerical Analysis of Model A	123
5.14	Results for Finite Element Analyses - 30 MPa Models	125
5.15	Results for Finite Element Analyses - 40 MPa Models	126
5.16	Results for Finite Element Analyses - 50 MPa Models	127
5.17	Results for Finite Element Analyses - S-Series Models	128
5.18	Results for Finite Element Analyses - B1-series Models	129
5.19	Results for Finite Element Analyses - B2-series Models	130
5.20	Tip Displacement Sensitivity to Change in Steel and Concrete Properties	131
5.21	Crack Width Sensitivity to Change in Steel and Concrete Properties	132
A.1	Pattern Loading on a Typical Subframe	145
A.2	Cast-in Starter-bar Anchorage Detail (reworked from Ancon Building Products (2014))	149
A.3	Shape Code 38	150
E.1	Model A Wall Reinforcing Bending Schedule	164
E.2	Model A Floor Reinforcing Bending Schedule	165
E.3	Model B Wall Reinforcing Bending Schedule	166
E.4	Model B Floor Reinforcing Bending Schedule	167
E.5	Model C Floor Reinforcing Bending Schedule	168
E.6	Model D Floor Reinforcing Bending Schedule	169
F.1	Steel A-frame Nodes	171
G.1	Equivalent Stress-strain Curve for the Reinforcement Material Model in Y12-S(30-50)	183
G.2	Equivalent Stress-strain Curve for the Reinforcement Material Model in Y12-B1(30-50)	184
G.3	Equivalent Stress-strain Curve for the Reinforcement Material Model in Y12-B2(30-50)	185

List of Tables

2.1	Material Cost Comparison in the United Kingdom	30
3.1	Ancon KSN12S Anchor Specifications (mm)	45
3.2	Parameters for Machined Specimens (mm)	67
3.3	Tensile Testing Specimen Sets	67
3.4	Low-cycle Fatigue Testing Specimen Sets	73
4.1	Cantilever Displacement Result Summary	87
4.2	Ultimate Capacity Summary	87
4.3	Modulus of Elasticity Results Summary (GPa)	90
4.4	Yield Stress Results Summary (MPa)	92
4.5	Ultimate Stress Results Summary (MPa)	94
4.6	Rebar used in Full-scale Models - E-modulus Summary (GPa)	97
4.7	Rebar used in Full-scale Models - Yield Stress Summary (MPa)	98
4.8	Rebar used in Full-scale Models - Ultimate Stress Summary (MPa)	99
4.9	Summary of Concrete E-Modulus Results	104
5.1	Summary of FE Analyses	106
5.2	Finite Element Model Summary	108
5.3	Summary of Sensitivity Study Results	124
6.1	Combined Material Cost Comparison	135
B.1	Preliminary Tensile Testing Results - Y10 Straight Rebar	152
B.2	Preliminary Tensile Testing Results - Y10 Straightened Rebar	153
B.3	Preliminary Tensile Testing Results - Y12 Straight Rebar	154
B.4	Preliminary Tensile Testing Results - Y12 Straightened Rebar	155
B.5	Full Scale Model A Floor Reinforcement - Y12 Straight Rebar	156
B.6	Full Scale Model B Floor Reinforcement - Y12 Straightened Rebar	156
B.7	Full Scale Model C Floor Reinforcement - Y12 Straightened Rebar	156
B.8	Full Scale Model D Floor Reinforcement - Y12 Straight Continuation Rebar	157
B.9	Full Scale Models Wall Reinforcement - Y12 Straight Rebar	157
C.1	Fatigue Test results - Y10-2 Set (straightened twice)	159
C.2	Fatigue Test results - Y10-3 Set (straightened thrice)	159
C.3	Fatigue Test results - Y12-2 Set (straightened twice)	160
C.4	Fatigue Test results - Y12-3 Set (straightened thrice)	160
D.1	Uniaxial Compression Test Results - Slab Specimens	161
D.2	Uniaxial Compression Test Results - Wall Specimens	162

*LIST OF TABLES***xvi**

G.1 FE Analysis - Material Model Inputs	186
H.1 Critical values of Grubbs Test	188

Nomenclature

Abbreviations

ACI	American Concrete Institute
ASTM	American Society for Testing and Materials
<i>c/c</i>	Centre-to-centre
CEB	Comity Euro-International de Beton
EN	European Design Codes
FE	Finite Element
FEA	Finite Element Analysis
FEM	Finite Element Modelling
LVDT	Linear Variable Differential Transformer
NZS	New Zealand Standards
RC	Reinforced Concrete
SLS	Serviceability Limit State
SABS	South African Bureau of Standards
SANS	South African National Standard
ULS	Ultimate Limit States

Variables

A	Area of Specimen
A_A	Accidental Action
A_E	Seismic Action
A_s	Area of Tension Reinforcement
$A_{s,w}$	Area of Outer Vertical Wall Reinforcement
a_v	Joint Shear Span

b	Effective Width
B_b	Percentage Redistribution
C_R	Empirical Coefficient
C_x	Anchor Edge Distance
d	Effective Depth
d_0	Original Diameter
d_a	Anchor Head Width
d_w	Wall Effective Depth
E	Young's Modulus of Elasticity
f_{bu}	Ultimate Anchorage Bond Stress
f_{ck}	Concrete Compressive Cylinder Stress
f_{cm}	Average Value of Concrete Compressive Strength Results
f_{cu}	Concrete Compressive Cube Stress
F_s	Applied Force
f_s	Stress in Reinforcement Bar
f_t	Concrete Tensile Stress
f_u	Ultimate Stress of Reinforcement Bar
f_y	Yield Stress of Reinforcement Bar
G	Permanent Action
G_f^I	Mode-I Fracture Energy
h	Crack Bandwidth
h_{eff}	Effective Anchor Embedment Depth
K	Weight of Bar
k	Empirical Coefficient
L	Length of Bar
l	Anchorage Length
L_0	Original Gauge Length
L_c	Parallel Length
L_t	Total Length of Test Piece

l_v	Joint Length
M	Design Moment
n_a	Number of Anchors in a Group
N_{Rd}^0	Nominal Pull-out Resistance for a Single Anchor
$N_{Rd,c}$	Modified Cone Pull-out Resistance for a Group of Anchors
$N_{Rd,s}$	Total Pull-out Resistance for a Group of Anchors
$N_{Rd,y}$	Capacity Yield Limit for Group of Continuation Rebar
Q	Variable Action
S_0	Original Cross-sectional Area of Parallel Length
$std(f_c)$	Standard deviation of Concrete Compressive Strength Results
S_x	Anchor Spacing
V	Design Shear Force
V_e	Volume of Element
v	Design Shear Stress
v_c	Shear Resistance
$V_{Rd,s}$	Nominal Shear Resistance for a Group of Anchors
V_w	Shear Force in Wall
x	Section Natural Axis Depth
z	Section Lever Arm
$z_{0.05}$	5 Percentage Point of the Random Variable
γ	Partial Factor
γ_c	Material Factor for Concrete
γ_m	Material Factor for Reinforcement
ε	Strain
ε_1	Total Principle Strain
$\varepsilon_{1,e}$	Elastic Principle Strain
$\varepsilon_{a,3}$	Average Strain at Upper Stress on Loading Cycle 3
ε_{cr}	Principle Crack Strain
$\varepsilon_{p,2}$	Average Lower Stress on Loading Cycle 2

σ	Stress
σ_1	Principle Stress
σ_a	Upper Stress
σ_a^m	Measured Stress Corresponding to Nominal Upper Stress, σ_a^m
σ_b	Lower Stress
σ_p	Applied Nominal Stress
σ_p^m	Measured Stress Corresponding to Nominal Preload Stress, σ_p^m
Φ	Reinforcement Bar Diameter
ψ	Combination Factor
Ψ	Reduction Factors
ω_{cr}	Principle Crack Width

Subscripts

<i>ave</i>	Available
<i>c</i>	Concrete
<i>hor</i>	Horizontal
<i>max</i>	Maximum
<i>min</i>	Minimum
<i>prov</i>	Provided
<i>req</i>	Required
<i>s</i>	Steel
<i>ver</i>	Vertical
<i>xx</i>	<i>xx</i> -Direction

Chapter 1

Introduction

1.1 Background

In the construction of multi-storey buildings the reinforced concrete (RC) core or shear walls, cast using slip or jump formwork, normally precede the construction of the RC floors. These systems are designed to increase the construction speed and efficiency, while minimising the cost of labour and material. Self-climbing jump formwork operates by using hydraulic jacks, connected to the already hardened concrete, to lift the formwork upwards. Slip formwork is similar in nature and application to jump formwork, but the formwork is raised vertically in a continuous process while wet concrete is being poured (Rupasinghe and Nolan, 2007). The sliding nature of these systems necessitate that there are no elements protruding from the wall, while under construction. This requirement prohibits the use of in-situ type connections where starter-bars are cast directly into the wall and fixed through the formwork, as presented in Figure 2.1 in section 2.2. The result of this limitation is that alternative methods are used to ensure rebar continuity between the floor and wall, without compromising the operation of the sliding formwork. Alternative systems are also used in cantilever balconies or walkways, or any structure where the wall is cast ahead of the connecting floor.

Currently, the most commonly used method in South Africa to ensure this continuity, is a rebar bend-out system. Rebar is pre-bent and fixed to the wall reinforcement and only straightened after the formwork is removed. This system is relatively simple to install and can be assembled on site, using regular rebar ordered from a bending yard. Although this system does not require highly skilled workers, the installation process can still be tedious and time consuming. Each starter-bar has to be securely placed at the correct position in the wall, in order to line up with the connecting floor. Refer to Figure 2.3 in section 2.3 for a visual representation of the system.

In order to make the installation process of the bend-out bars easier and faster, a modified approach is adopted, in which the pre-bent rebar is placed inside a steel casing, as shown in Figure 2.9, section 2.4. This modification improves the ease and speed of installation, but in turn makes the system more expensive. Another drawback is that only a few companies locally manufacture this system and it is therefore not readily available throughout South Africa.

More advanced alternatives usually involve pre-assembled elements cast inside the wall with continuation rebar screwed in afterwards, by means of mechanical couplers. These systems are rarely used in South Africa and can only be imported at a significant cost.

For specific applications these systems are an option, and as the demand for such products grow, locally manufactured alternatives might be available in the near future. Figure 2.11 in section 2.5 includes an illustration of the system.

Epoxy based adhesive dowels are also widely used in South Africa to anchor rebar in already cast concrete elements. However, due to the relatively high price of this system, its use is usually limited to projects where structural alterations or extensions necessitate the anchoring of rebar in existing concrete.

1.2 Problem Statement

In the case of epoxy based adhesive dowels, the performance and installation procedures are well researched and documented in the reference material provided by the manufacturers. The structural engineer has enough information to properly design a connection and prescribe the necessary installation procedures to ultimately have enough confidence that the connection will perform adequately. With most of the other advanced methods, this information is not available.

In the case of the bend-out systems, plastic deformation of the steel is unavoidable during the cold-bending and straightening of the rebar. Further, because rebar has a higher strength than ordinary steel, the mechanical properties of rebar are more prone to changes during cold bending. This change in mechanical properties has been observed to cause a reduction in the tensile yield strength, modulus of elasticity, ductility and even the ultimate strength of the steel (Chun and Ha, 2014). There is currently insufficient information available for engineers to accurately take this effect into account when designing a connection.

When looking at the modified bend-out system with the rebar encased in a steel box, further uncertainty arises as to what effect the steel casing has on the bond strength of the concrete connection, as it is permanently cast inside the structure.

The only reference in South African codes to bend-out bars is found in SANS 10144, where it is recommended that the size of the bend-out bars is limited to Y10 or R16 and that mechanical splices should be used if greater strength is required (SANS, 2012). Note that R16 denotes mild steel bars with a smooth surface and characteristic yield stress of 240 MPa, in this case with 16 mm diameter. Y10 denotes high strength, ribbed steel bars of characteristic yield strength of 450 MPa, in this case of diameter 10 mm. Rebar couplers connected to a cast-in steel anchor is an example of a mechanical splice, as mentioned in SANS 10144. Although the European codes give sufficient information to determine the direct pull-out resistance of anchors, recent research has shown that when the pull-out force is accompanied with a confining force in close proximity, the tensile capacity will increase. This is applicable when dealing with the design of wall-to-slab moment joints and can be used to design more economical connections(Cairns, 2010).

From the above it is evident that there are a number of different systems available for reinforced concrete wall-to-slab connections. The challenge for the design engineer remains to choose the most suitable system for the specific application at hand. In order to make an informed decision, more information is needed to understand how these systems perform structurally and what the aspects are to consider when designing them.

1.3 Scope

The focus of this research is to investigate how different types of connection systems compare to the conventional, in-situ type system, as described in section 2.2.

The research investigation includes the comparison between four different wall-to-slab connection systems, namely:

- Continuous Starter-bar (reference model)
- Site-installed Bend-out bar
- Pre-assembled Bend-out bar
- Cast-in Anchor

The investigation includes a study of each individual system, in order to gain an understanding of the critical aspects and parameters that will affect their structural performance. Preliminary tests are conducted to quantify these aspects, followed by full-scale testing and Finite Element Modelling (FEM) to confirm any local phenomena observed with the preliminary tests.

The principles and methodology for the design of the systems will also be discussed. The South African Standards are used as a basis for the design, with reference to other international standards and research where information is lacking. A comparison is drawn between the practical aspects of the systems, including ease and time of installation, cost, quality control and availability of products.

Floors are not normally designed to resist lateral loads, but their connectivity to the core walls is still important to ensure diaphragm / membrane action of the slabs subject to seismic or wind action, and to meet certain serviceability requirements. If a moment connection can be established between a wall-to-slab joint it can greatly assist the engineer to attain the required level of strength needed for the design and will also greatly reduce the deflection of the floor span directly adjacent to the connection. Consequently, this research will mainly focus on comparing connection systems based on their moment resistance capacity.

1.4 Objectives

The main objective of this study is to provide the engineer with recommendations on how to choose the most appropriate system for a wall-to-slab moment connection and conduct the design to be as economical as possible, without compromising the margin of safety as defined in typical design codes.

Secondly, construction guidelines are to be provided for safe application of these systems on site in order to comply with the designed connection.

1.5 Limitations

Only a single type of locally available rebar has been selected for the full study. Other locally available steel bars with rib configurations, some of which did not comply with

SANS 920:2011, have not been included in this study to limit the number of variables within the scope of investigation.

The equipment used to conduct the tensile testing was unable to accurately measure the total elongation of the steel rebar specimens. The reduced ductility of cold bent reinforcement could therefore not be quantified. The low cycle fatigue tests did, however, provide evidence that some reduction is present and previous research also confirmed this phenomenon (Chun *et al.*, 2003).

Only the material costs for the respective systems are being compared in this study. It is, however, important to note that other factors, not included in this study, can significantly influence the overall cost of a system. These factors include, but are not limited to, the cost of labour, the size of the building or project, material availability and the contractor's knowledge and previous experience in the use of a particular system.

1.6 Thesis Layout

The first chapter gave a brief background of the rationale behind using alternative wall-to-slab connection systems in high rise construction. Insight were provided on the most commonly used systems and their respective advantages and disadvantages. The scope of this research investigation was established and the specific problem statement was also defined. Finally the objectives were set and the limitations of this study discussed, with the layout of the research thesis included at the end of the chapter.

Chapter 2 provides more detail on the four different connection systems that fall within the scope of this research. All the systems are described in terms of their functionality, installation and design procedure, with a more in-depth discussion on the design procedure for the cast-in anchor system as this is not commonly used in South Africa. The effect of cold bending and straightening of reinforcement in the bend-out systems are also discussed, with some reference to previous research done on this subject.

The design and implementation of all the experimental testing performed in this study are included in Chapter 3. The results are presented in Chapter 4, with a short discussion on the observations made during the experimental phase.

In Chapter 5 the development of the Finite Element (FE) models are described. The chapter starts with a brief discussion of previous research conducted, followed by the development of the models. The second half of the chapter focusses on the results of the numerical analyses and how they compare to the experimental data. A sensitivity study is also included, in order to determine the effect of varying isolated properties in both the steel and the concrete.

Chapter 6 includes the final discussion on all the results obtained from both the physical and numerical analyses and the final conclusions derived from this research investigation. The chapter is concluded by providing a list of recommendations for the design and construction of moment fixed wall-to-floor connection systems.

Chapter 6 is followed by the list of references and appendices. Appendix A includes the detailed design procedure for the continuous starter-bar system. All the data captured in the tensile, fatigue and supplementary tests are presented in Appendices B, C and D. Examples of typical bending schedules are included in Appendix E, with the design calculations for the steel testing frame in Appendix F. Appendix G includes all the relevant

information used to establish the material models in the numerical analyses and, finally, Appendix H includes the procedure to detect a single outlier in a data set, using the Grubb's Test.

Chapter 2

Connection Systems

2.1 Introduction

This chapter provides the framework for the research investigation by introducing the four different connection systems that are studied. The format for each section is similar, with a brief description of how the system works, followed by a short overview of the design procedure. A more in-depth discussion is, however, included on the design procedure for the cast-in anchor system, as this is not commonly used in South Africa. Individual aspects that will influence the structural performance of the systems and any additional information regarding the use or installation of the systems, are also discussed.

2.2 Continuous Starter-bar System

2.2.1 Description

The conventional way of ensuring that the rebar is continuous in a wall-to-slab connection, is to cast the wall with floor starter-bars protruding orthogonally from the face of the wall. These starter-bars are fixed to the vertical reinforcement inside the wall at the correct position, in order to line up with the horizontal reinforcement intended for the floor. The starter-bars fit through pre-drilled holes in the formwork. It is important to ensure that there is a perfect alignment between the starter bars and the holes in the shuttering, in order to properly close the formwork. The exposed portion of the starter-bars should be long enough to ensure that a full lap length can be established with the connecting floor rebar.

Once the formwork is removed, the continuation reinforcement for the floor is put in place. This will ensure that the tensile force, in the top reinforcement of the floor, can be transferred into the adjacent wall. In order to ensure a proper shear connection, a shear key or pocket is also cast inside the wall as shown in Figure 2.1.

2.2.2 Design Procedure

When designing RC structures, the ultimate limit state (ULS) design usually governs (Robberts and Marshall, 2010). Therefore, the design procedure for the conditions at ULS and the principles, as set out in SANS 10100-1:2000, are used for the design of this type of connection. The procedure can be summarised in the following steps:

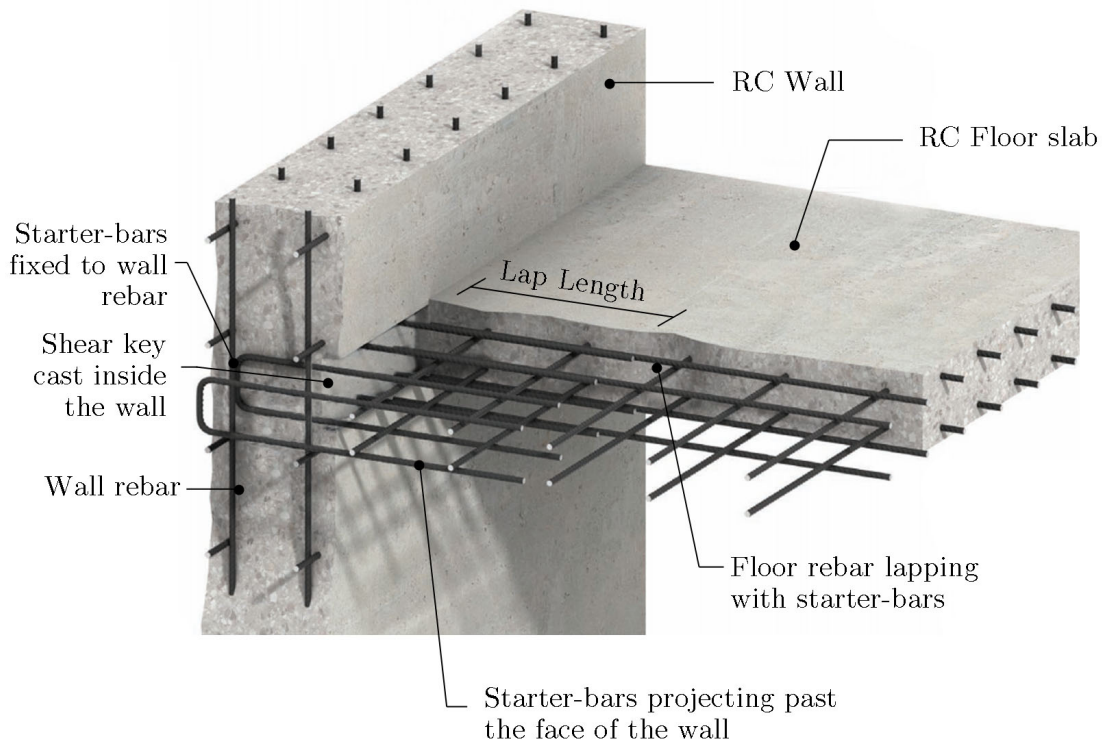


Figure 2.1: Continuous Starter-bar System (reworked from Ancon Building Products (2011))

Step 1: Determine forces acting on the structure

Step 2: Calculate possible load combinations

Step 3: Analyse structure to determine design forces and moments at ULS

Step 4: Design section for flexure

Step 5: Design section for shear

Step 6: Choose rebar configuration (size and spacing)

Step 7: Check anchorage and lap lengths

Step 8: Detail connection reinforcement

A detailed description of the design steps are presented in Appendix A.

2.2.3 Additional Aspects

The design procedure for the continuous starter-bar system is well understood and the codes provide clear guidelines for their design. Unfortunately, this system is very impractical and time consuming to install. To securely fix each individual starter-bar takes time, as it is physically difficult to manoeuvre through the wall reinforcement while retaining the correct level for the starter-bars (Ancon Building Products, 2014). The congestion of reinforcement is especially high in walls designed for seismic action and therefore more

problematic, as the design procedure requires the use of closely spaced horizontal reinforcement in the boundary zone i.e bottom levels of a building (SANS, 2011*b*).

It is also challenging to cut the holes in the shuttering at the correct position and to make them big enough to fit comfortably around the bars, without making them so big that the wet concrete spills from the gaps. The shuttering used to house the starter-bars can also not be re-used, as it is very unlikely that the holes will line-up exactly with the starter-bars in another connection. Further, the shuttering is almost always damaged during the removal process.

Finally, when the formwork is removed, the bars protrude from the face of the wall and this can limit the movement of material or equipment. More importantly, it also presents a safety hazard for workers in the vicinity (Ancon Building Products, 2014).

This system is available through-out South Africa and the starter-bars can be ordered from any bending yard. The material cost associated with this system is low and it can be installed by a regular rebar fixer. For a connection between a 300 mm thick wall and a 250 mm thick slab, with 25 mm cover and a rebar spacing of 150 mm c/c, the cost of the material is around R130 per meter of connection. This rate is based on information received in August 2016 from Staalmark, a local supplier in Cape Town. The time involved in proper installation of starter-bars will, however, negatively impact the overall cost of the system.

2.3 Site-installed Bend-out Bar System

2.3.1 Description

An alternative to the continuous system described in the previous section is the use of pre-bent rebar. This system is commonly used throughout South Africa and is referred to as either bend-out bars or pull-out bars. These pre-bent starter-bars are fixed with the reinforcement intended for the wall and placed at the same level as the proposed floor. They are covered with hard board or a similar material to ease access to the bent rebar after the wall has been cast. The rebar starters are pre-bent to a specific shape as shown in Figure 2.2.



Figure 2.2: Bent-out Bar Shape: Site-installed (reworked from Ancon Building Products (2011))

The next lift for the wall is subsequently cast with the pre-bent rebar and timber cover securely in place. The rebar will only be straightened once the wall has been cast, stripped

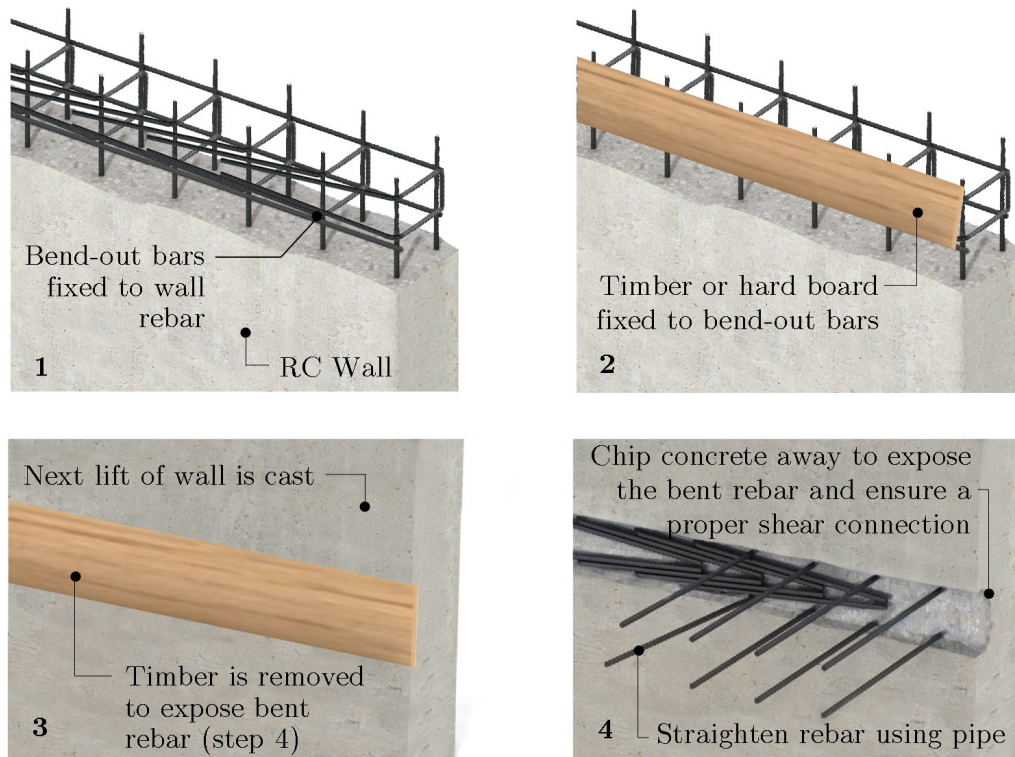


Figure 2.3: Site-installed Bend-out Bar System (reworked from Ancon Building Products (2011))

and the rebar for a specific floor needs to be put in place. At this time, the concrete surrounding the bend-out bars is carefully chipped away, in order to fully expose the bars and to form a shear key to enable a proper shear connection. The straightening of the rebar on site can be challenging as the position of the pre-bent bars might have shifted during the concreting of the wall. Usually, the bars are straightened manually by means of a pipe used as a lever arm. Caution should, however, be taken when straightening the rebar, as it has been reported to reduce rebar resistance and over-working of the steel might result in brittle fracture of the bars (Chun *et al.*, 2003).

Once all the rebar is bent out, the remainder of the installation process is similar to that of the starter-bar system in section 2.2. The bend-out bars are lapped with the floor rebar and cast conventionally to complete the wall-to-slab connection. Refer to Figure 2.3 for an illustration of the installation process.

2.3.2 Effect of Cold Bending and Straightening

Due to the nature of this system it is inevitable that the rebar will undergo cold bending and straightening. This cold working of the steel has an effect on the crystal structure of the alloy. When rebar is bent, the outer portion of the bar undergoes tensile deformation, while the inner portion of the bar is in compression. When the rebar is straightened afterwards, the opposite happens i.e. the inner portion is in tension and the outer portion in compression, as shown in Figure 2.4.

During the bending process the amount of strain on the outer portion of the bar surpasses

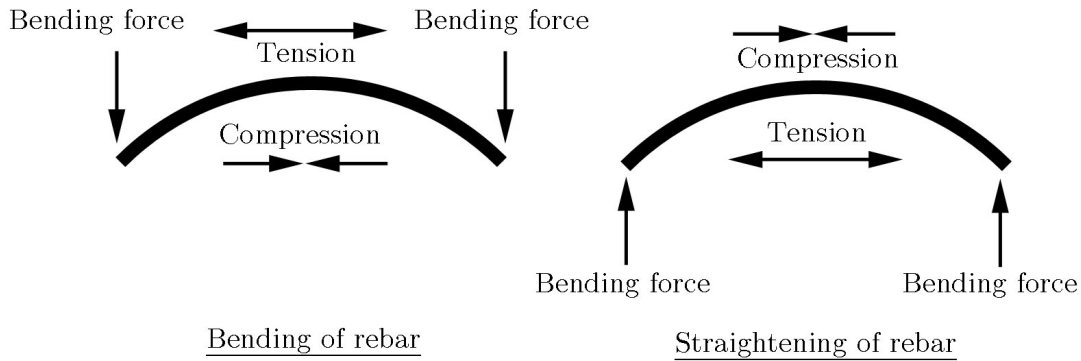


Figure 2.4: Strain Reversal

the level of tensile plastic hardening and will follow a curve similar to that in Figure 2.5(a) indicated as path 1. If this is followed by straightening of the rebar, the outer portion will continue with compressive plastic hardening along path 2 ending at the starting position in Figure 2.5(a) once the bar is fully straightened. When a tensile force is subsequently applied to the bar, an increase in the yield strength on the outer portion of the bar is observed along path 3.

The inner portion of the bar will undergo similar strain paths, but with compressive plastic hardening first, along path 4, followed by tensile hardening as shown in Figure 2.5(b) along path 5 and back to the starting position. When a tensile force is again applied to the bar, the inner portion will in this case experience a reduction in the yield strength as observed through the curve along path 6.

The combined behaviour of the inner and outer portion of the bar under a tensile force is shown in Figure 2.5(c). As the direction of the strain during straightening is opposite to that of the bending process, the dislocations form "pile-ups" which result in a decrease in the resistance to plastic deformation and ultimately a decrease in the yield strength of the steel. This is referred to as the Baushinger effect (Totten and Howes, 1997). This is evident when comparing the combined behaviour of both the inner and outer portions of the bar to the original curve with a bar that has not undergone any plastic deformation. There is also no clear yield plateau during plastic hardening and a reduction in the elongation of the steel is also observed. This further indicates reduced ductility of cold bent steel and previous research conducted by Chun and Ha (2014) recorded a reduction of up to 50% for high yield reinforcement.

On the other hand, rebar has a relatively high carbon content and over an extended period of time, after cold working, carbon will start to concentrate around the dislocations caused by cold bending. This will, in turn, prevent these deformed clusters from nucleating back to a homogeneous matrix when the rebar is straightened and will increase the resistance to plastic deformation, thus increasing the yield strength. This phenomena is called Age-Hardening. This hardening of the steel will, however, make it more brittle. (Totten and Howes, 1997)

Research has shown that if the time between the cold bending and straightening of the rebar is more than 3 months, the combined result of age-hardening and the Baushinger effect can, in fact, make the rebar stronger. (Chun and Ha, 2014) However, the time

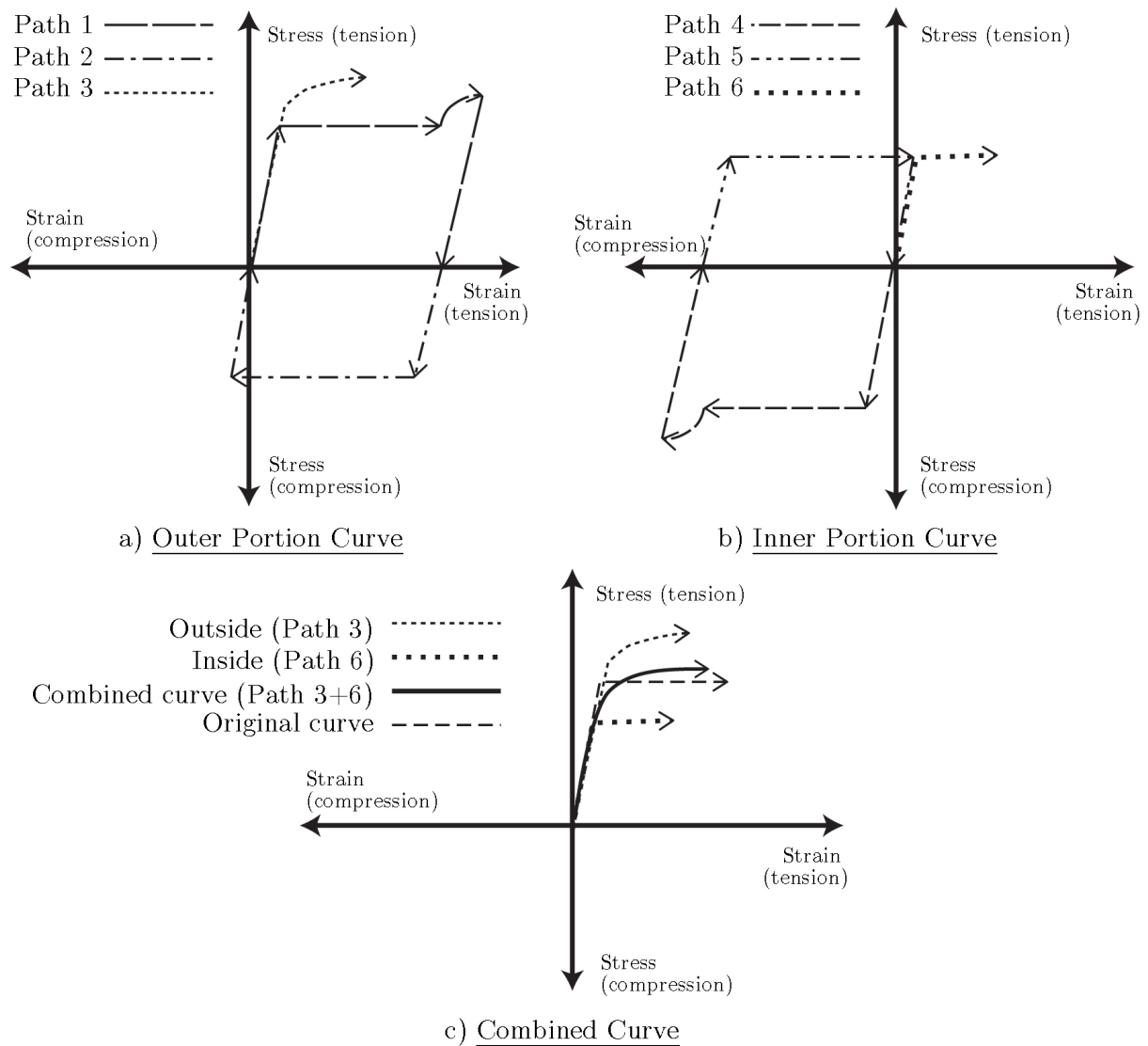


Figure 2.5: Hysteresis Stress-strain Curves of Straightened Bars (reworked from Chun and Ha (2014))

between bending and straightening of bend-out starter-bars is rarely available in practice and designers can therefore not rely on the possibility of an increase in the strength of the steel, but should rather assume that work hardening had no effect and that the yield strength and ductility is lower than anticipated.

2.3.3 Design Procedure

As the effect of the cold-bending and straightening is not fully understood and the reduction in yield strength not yet quantified, the steps in the design procedure for the bend-out system is currently almost identical to that of the continuous system in section 2.2. All the calculations for the bend-out system are based on the assumption that the rebar is already straightened and therefore reflecting the first system. The only difference is the detailing of the starter-bars.

The shape of the starter-bar used in the bend-out system is not one of the prescribed shapes found in SANS 10144:2012. The code, however, does permit the use of custom shapes, provided that the shapes are clearly dimensioned in the same format as standard shapes. The code number for a custom shape is usually the value 99. An example of a bending schedule containing a typical bend-out starter-bar is shown in Figure 2.6.

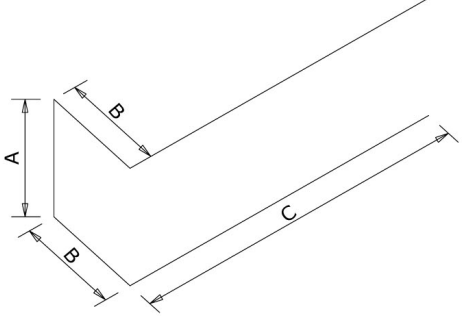

MEMBER	No OF	BARS PER MEMB	DIA	LENGTH	TOTAL NUM-BER	MARK	S C	BENDING					
								A	B	C	D	E/r	
Bend-out Bars	1	6	12	2000	6	a	99	200	325	500			
 <p>SHAPE CODE 99</p>													
	8	10	12	16	20	25	32	40	TOT	Date	2015/05/21		
R			11						11	Det by	JD GERBER		
Y										Ref Dwg			
TOT			11						11	Job No			
 UNIVERSITEIT STELLENBOSCH UNIVERSITY							BEND-OUT REBAR EXAMPLE			Revision		1	
										Schedule No		15422828	

Figure 2.6: Bend-out Starter-bar Bending Schedule

2.3.4 Additional Aspects

Although this system can theoretically be implemented in a wall that is cast by means of slip formwork, some practical aspects prevent it from being regularly used. Slip formwork is a continuous system that requires all work to be conducted at a high pace, including the fixing of rebar. This is not always possible with the site-installed bend-out system, as individual starter-bars have to be securely fixed one-by-one. It is very important to ensure that the starter-bars are fixed and kept at the correct position during the concreting of the floor, as an upward shift in the starter-bars can compromise the cover required on the reinforcement, while a downward shift will result in a reduction in the moment resistance of the connection. The downward movement of the rebar will reduce the effective depth of the section and subsequently reduce the flexural resistance. Figure 2.7, shows the percentage reduction in the moment resistance as a result of reducing the effective depth

due to downward shifting of the starter-bars. These results are based on the calculations as set out in SANS 10100-1:200, for a 250 mm thick slab, with 25 mm cover and Y12 rebar.

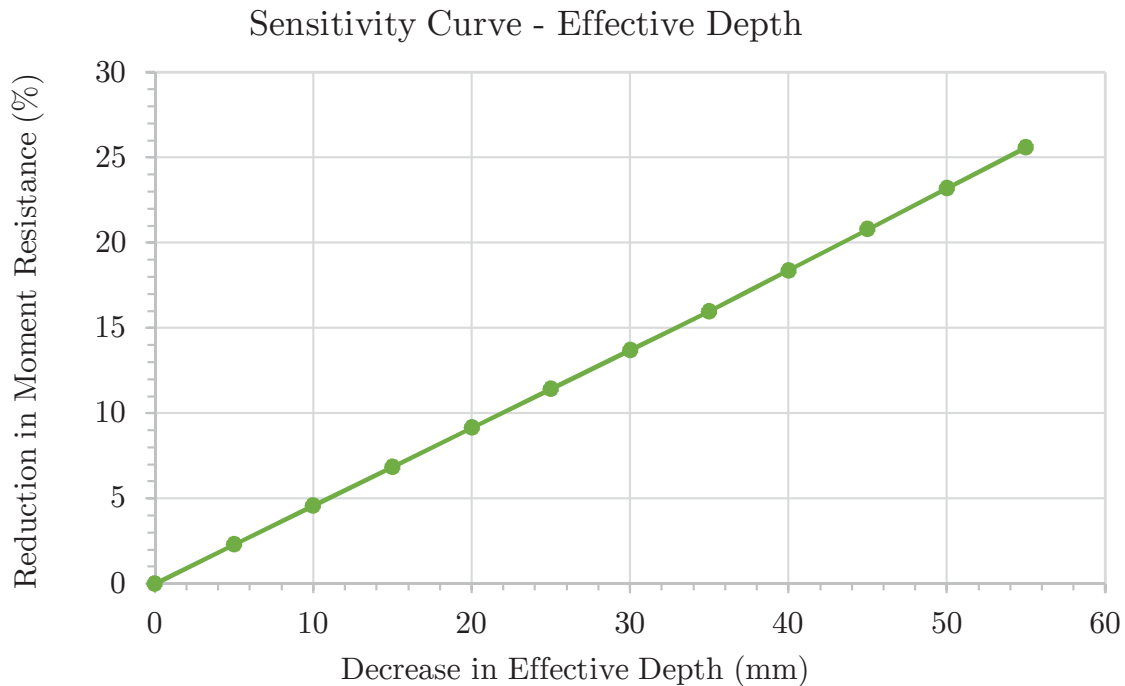


Figure 2.7: Sensitivity of Sectional Moment Resistance to Effective Depth of Flexural Reinforcement

The removal of the plywood cover (Figure 2.3(3)) can also be challenging if not enough releasing agent is applied to the inner surface of the plywood.

In order to straighten the bars, they first need to be fully exposed. This is done by using a jack hammer to chip away all the concrete surrounding the bent bars. Unfortunately this process takes a significant amount of time and is very labour intensive. It is also important not to damage the rebar when using the jack hammer.

One advantage is that the plywood can be kept in place until such time it is needed to connect a floor. This will avoid the safety hazard of projecting bars on site and will not restrict the movement of materials and equipment next to the wall.

This system is also available through-out South Africa and can be ordered through a normal bending yard. Similar to the continuous starter-bar system, the material cost associated with this type of connection is relatively low, at R130 per meter of connection. The rate was obtained from Staalmark, a local supplier. The amount of labour and time required for installation will, however, increase the price significantly.

2.4 Pre-assembled Bend-out Bar System

2.4.1 Description

In order to improve the time for installation of the bend-out bar system, a modification is made by which a number of starter-bars are pre-bent and placed inside a steel casing. This will allow a contractor to fix the starter-bars simultaneously as they are all confined in one steel box. The process of revealing the starter-bars is also less labour intensive and the probability of damaging the bars is reduced significantly.

The entire system with the pre-bent bars is ordered from a local supplier. Most suppliers have standard sizes that can be ordered, but with larger projects any size and rebar configuration can be custom-made to suit the design requirements. The pre-bent bars are fixed through a steel casing at the specified spacing and anchorage length. The shape of the bars is similar to the one depicted in Figure 2.6. A lid is placed on top of the steel box to ensure easy access once the system is cast inside the wall. Each end of the unit is sealed with a polystyrene block to prevent any ingress of concrete. The void that is created by the steel casing will also act as a shear key to ensure a proper shear connection. The steel casing also has a dimpled surface to ensure a better bond with the concrete (Ancon Building Products, 2011). Refer to Figure 2.8 for an illustration of a typical unit.

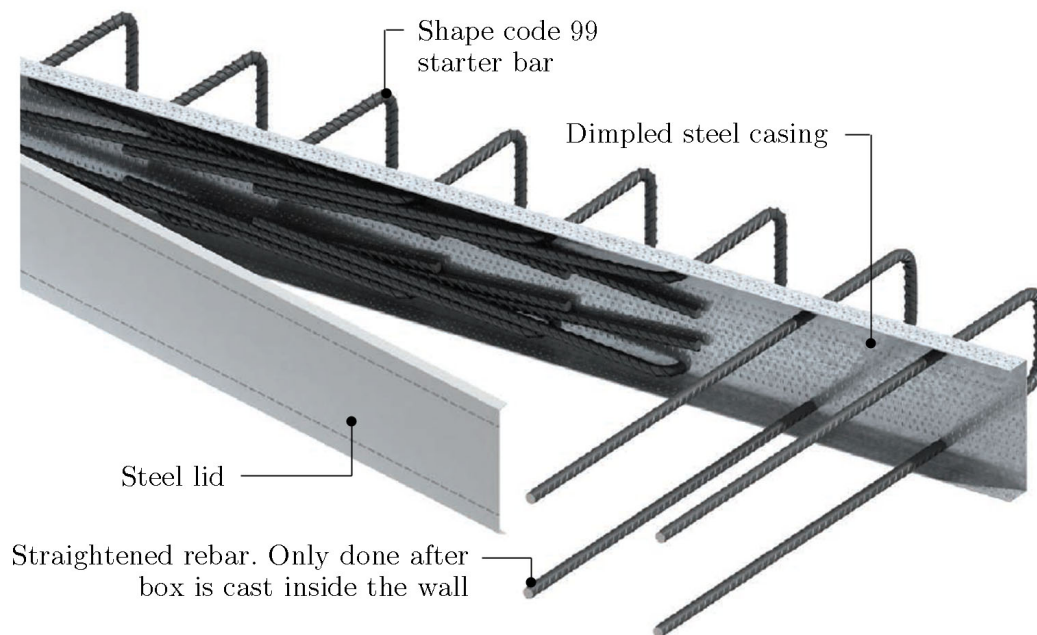


Figure 2.8: Bend-out Starter-bar Unit (reworked from Ancon Building Products (2011))

The complete unit is either nailed directly to the formwork or fixed securely to the main reinforcement in the wall. It is important that the box fits tightly against the formwork to prevent any concrete seepage between the two elements. Once the concrete is set and the formwork removed, the steel lid can be dismantled to reveal the bent bars. A modified pipe is used to straighten the rebar. The end of the pipe is cut at 45° to ensure a snug fit around the bars in their bent position. Finally, the continuation rebar for the floor is fixed. The steel box is filled when the concreting for the floor takes place and will act

as a shear key. This process is graphically illustrated in Figure 2.9. (Ancon Building Products, 2011)

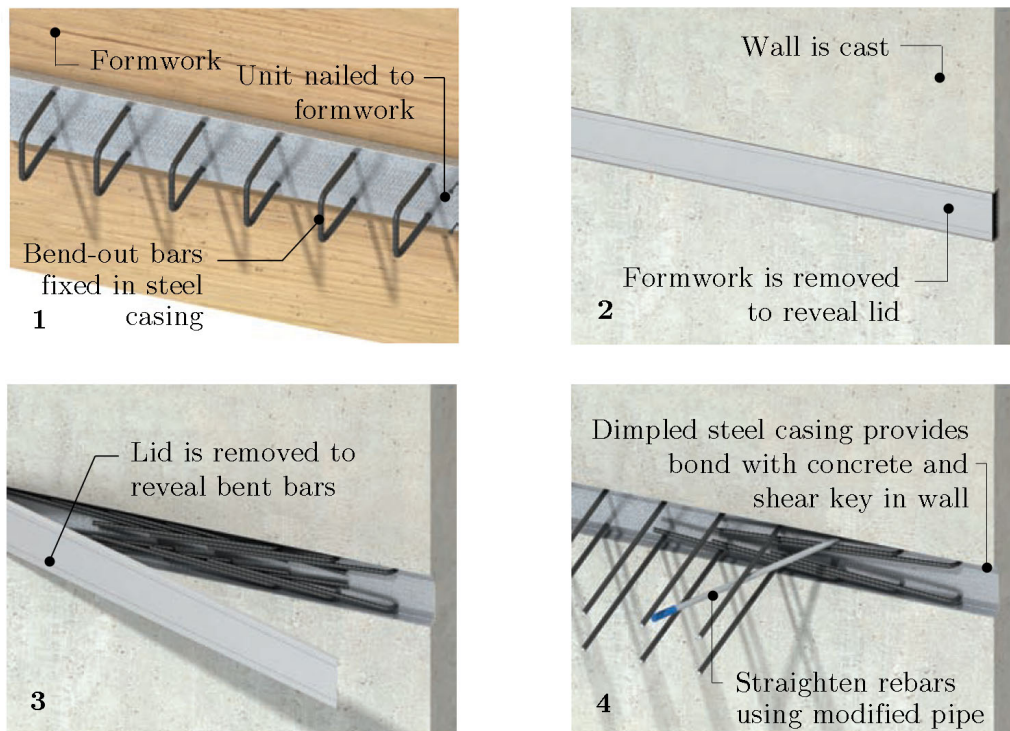


Figure 2.9: Pre-assembled Bend-out Bar System (reworked from Ancon Building Products (2011))

The cold bending and straightening of the rebar cannot be avoided and the effect on the strength of the steel is the same as in section 2.3.2, where a reduction in the yield strength and elongation is observed, with strain-hardening occurring without a clear yield plateau.

2.4.2 Design Procedure

The design procedure for the modified bend-out system is very similar to that of the site installed version. The assumption is still valid that the bars are already straightened and that the effect of the cold bending and straightening is currently not considered. The design steps are the same, with the only difference in the installation process as described in section 2.4.1.

2.4.3 Additional Aspects

This system is the most suitable for use in conjunction with jump formwork. The installation process is not labour intensive or overly complicated. The steel boxes can be securely fixed to the main rebar fast enough, not to compromise the continuous nature of the jump formwork system. The required accuracy, to ensure that the starter-bars are all in line and at the correct level, is easier to comply with when using this system, as the

starter-bars are all pre-assembled inside a steel casing and not individually fixed to the main rebar.

Similar to the previous system, the rebars remain bent inside the steel boxes until they are needed. They will therefore not pose any safety risk or be in the way of moving equipment or materials. Another major improvement on the previous system, is the ease of accessing the pre-bent bars. There is also no need for using a jack hammer and this eliminates the risk of damaging bars or surrounding concrete.

Currently only a handful of companies locally produce this system and it is therefore not readily available throughout South Africa. The material cost for using this system in a connection between a 300 mm thick wall and a 250 mm thick slab, with 25 mm cover and 150 mm rebar spacing, is R245 per meter connection, compared to the R130 for the site-installed alternative. However, on larger projects where time and efficiency play a greater role, the overall cost could be reduced significantly. The cost is based on the system supplied by Joluko in South Africa, quoted in August 2016.

2.5 Cast-in Anchors System

2.5.1 Description

A third alternative to the continuous starter-bar system, discussed in section 2.2, is the use of steel anchors with mechanical couplers. This system is not currently being used in the South African construction industry, but has many advantages that could make it an attractive alternative in specific applications.

The anchors are ordered in pre-assembled timber carriers, with the anchors securely fixed at the specified spacing - refer to Figure 2.10. The carriers are nailed directly to the formwork in the correct position to line up with the reinforcement intended for the connecting floor. The anchors can be ordered up to a Y20 rebar, with the carriers custom made to any rebar configuration. (Ancon Building Products, 2014)

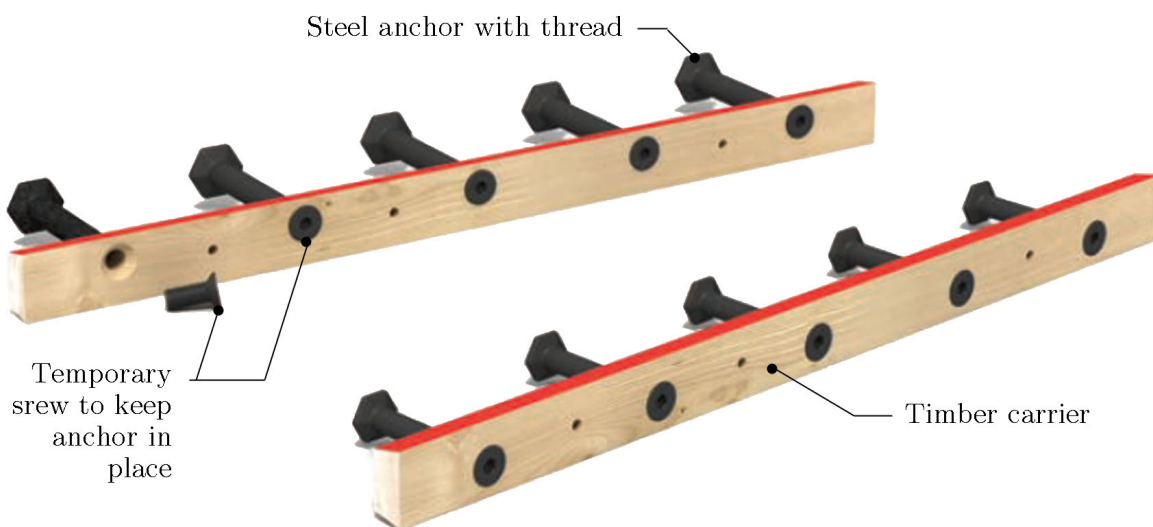


Figure 2.10: Timber Anchor Carriers (reworked from Ancon Building Products (2014))

The threaded continuation rebar is also supplied with the anchors in the correct diameter and cut to the specified length. In order to ensure continuity in the effective area of the rebar, the ends of the continuation bars are cut square and enlarged by cold forging, before being threaded. The thread is then cut to a size larger than the bar diameter to ensure that the effective area is not compromised. Standard metric sizes are usually used i.e a Y12 bar will receive a M16 thread.

Once the timber carriers are securely fixed to the formwork, releasing agent is applied to both the formwork and the timber carriers, before the wall is cast. When the concrete reaches the required strength the nails securing the carriers are removed and the formwork is dismantled. The temporary head-cap screws are unscrewed from the anchors to release the carriers and reveal the cast-in anchors. The carriers have a dual purpose by not only keeping the anchors in position, but also creating a shear key.

Finally the supplied continuation rebar is rotated to fit into the anchor thread and tightened using a hand wrench. No torquing is required. The rebar for the floor is fixed into position and the floor is cast conventionally to complete the floor-to-wall connection. Refer to Figure 2.11 for a graphical representation of the process as described.

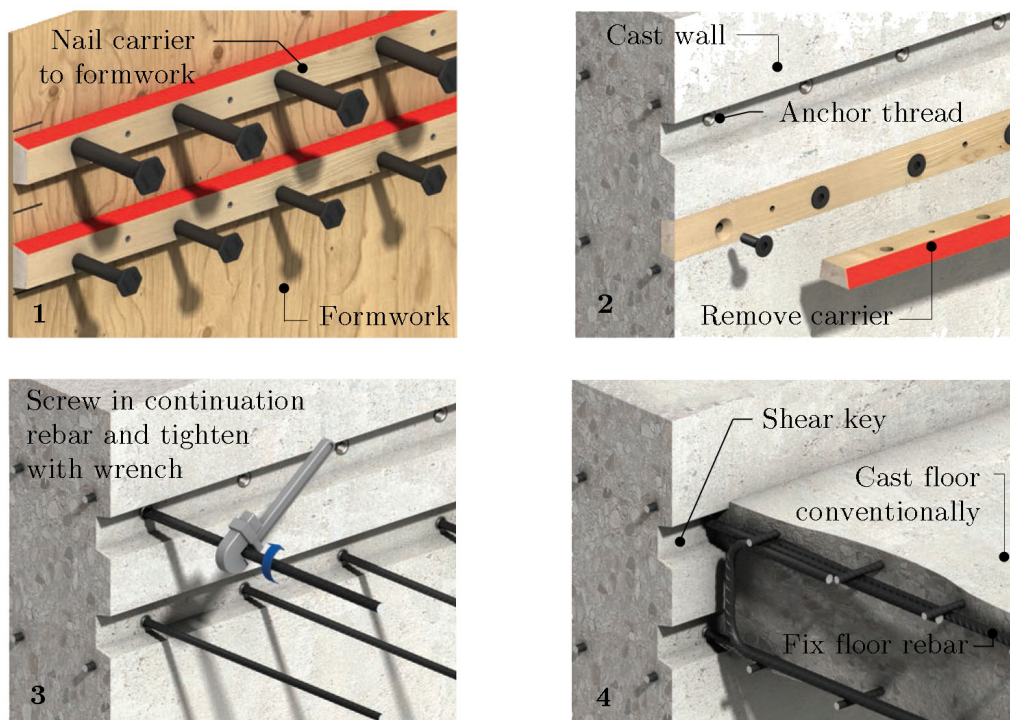


Figure 2.11: Cast-in Anchor with Mechanical Couplers (reworked from Ancon Building Products (2014))

2.5.2 Modified Cone Behaviour

The design procedures of cast-in anchors have been well established through extensive research over the past 50 years. The failure mode for direct tensile anchors is based on a model with a break-out prism with an angle of approximately 35° as shown in Figure

2.12. This can roughly be translated to a cone shape with a base equal to three times the effective anchor embedment depth i.e $3 \times h_{eff}$. This pull-out model is referred to as a cone failure mechanism. The design procedures for anchors in direct tension are well-established and documented in several design codes, such as the New Zealand Design Codes (NZS, 2006) and American Concrete Institute Codes (ACI, 2008). (Cairns, 2010)

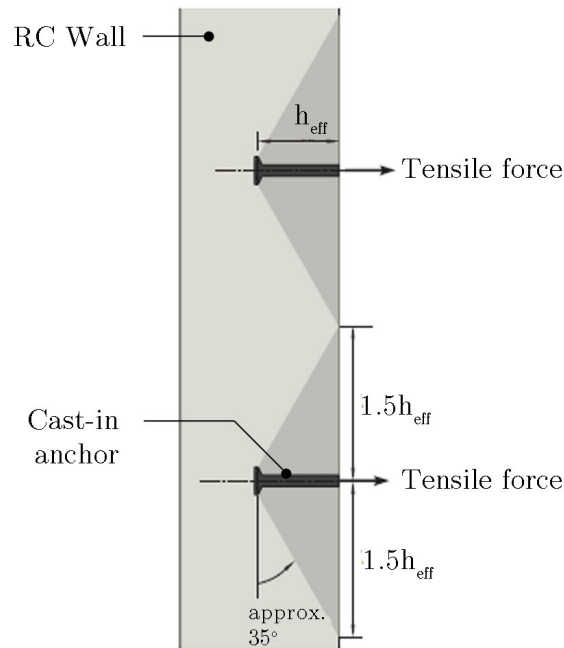


Figure 2.12: Cone Failure for Cast-in Anchor in Direct Tension (reworked from Ancon Building Products (2014))

These existing procedures, however, do not cover anchors within moment resisting connections, such as wall-to-slab applications. A recent research investigation, at Heriot Watt University, tested moment connections using cast-in anchors to determine the degree of enhancement in concrete pull-out capacity and to establish a design method based on the results.(Cairns, 2010)

In moment connections, such as wall-to-slab joints, the bottom portion of the slab will create a compression block in close proximity to the bearing surface of the anchor. The transmission of the force between the bearing face and the compression force, forming part of the moment couple in the slab, will tend to be taken by a direct compression strut rather than by shear or tension. This will decrease the break-out plane resisted by tension and will therefore create a modified cone shape, as illustrated in Figure 2.13. As concrete is stronger in compression than tension, the cone pull-out resistance will be increased. The tests also indicated that the enhancement is greatly impacted by the ratio of the depth of anchor head embedment (h_{eff}) to the effective depth of the anchor in the slab (d). The specific ratio being h_{eff}/d .(Cairns, 2010)

The nominal pull-out strength for a single cast-in anchor (N_{Rd}^0), without any modification, is given by Equation 2.1, with f_{ck} the characteristic cylinder compression strength of the

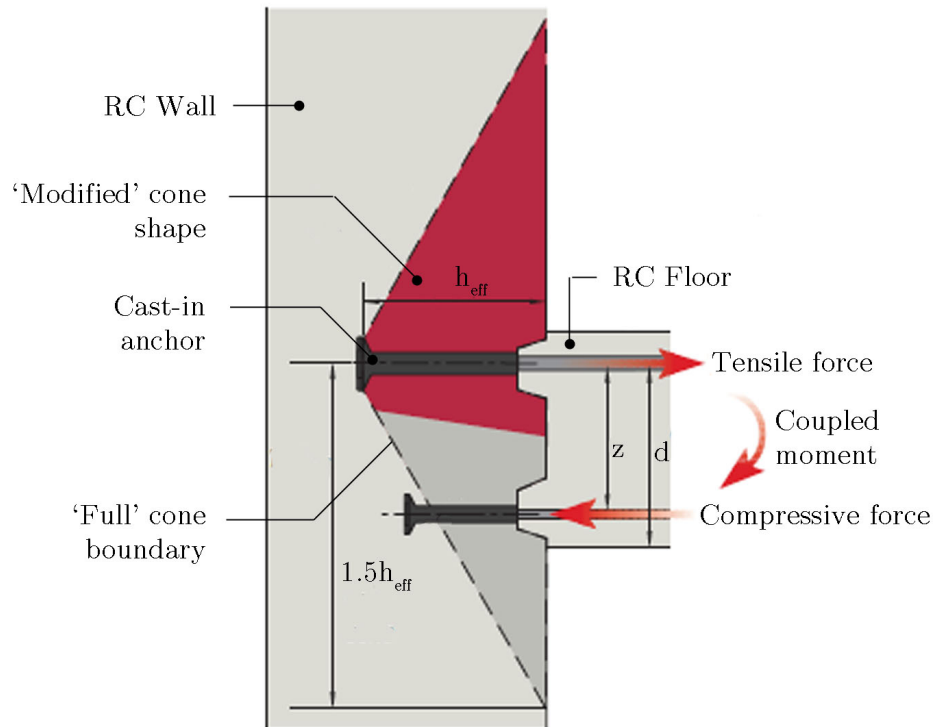


Figure 2.13: Modified Cone Failure for Cast-in Anchor in Moment Connections (reworked from Ancon Building Products (2014))

concrete, γ_c the material factor for concrete, h_{eff} the anchor head embedment and k an empirical coefficient taken as 12.5 (Telford, 1997).

$$N_{Rd}^0 = k \times f_{ck}^{\frac{1}{2}} \times h_{eff}^{\frac{3}{2}} / \gamma_c \quad (2.1)$$

Equation 2.3 was empirically developed as the best fit to the data gathered from the series of tests conducted at Heriot Watt University. The effect of the modified cone behaviour is established through Equation 2.2. $\Psi_{P,N}$ is limited to 1.25, which represents the upper bound to the available test data.

$$\Psi_{P,N} = -0.3 + 1.5 \frac{h_{eff}}{d} \leq 1.25 \quad (2.2)$$

The total modified cone resistance of a group of cast-in anchors (n_a) is given by Equation 2.3.

$$N_{Rd,s} = n_a \times N_{Rd}^0 \times \Psi_{P,N} \quad (2.3)$$

This equation will only govern while the h_{eff}/d ratio falls above a threshold value, after which the "unmodified" cone behaviour will predominate. The anchorage resistance will also be limited by the yield strength of the reinforcement.

2.5.3 Design Procedure

As with all concrete structures, the first steps in the design procedure is to calculate the design forces and moments. The design procedure for a wall-to-slab connection system using cast-in anchors will therefore start with the first three steps as described in section 2.2.

After the design forces and moments are determined, the design will follow the approach as set out in the CEB Design Guide, with additional research conducted at Heriot Watt University, for Ancon Building Products, presented in an unpublished report (Cairns, 2010). This approach is similar to what is presented in the New Zealand and ACI codes for cast-in anchors (NZS, 2006; ACI, 2008). A summary of the steps are set out below. The focus of this section will be from step 4 onwards, as the rest is presented in Appendix A.

Step 1: Determine forces acting on the structure

Step 2: Calculate possible load combinations

Step 3: Analyse structure to determine design forces and moments at ULS

Step 4: Design section for flexure

Step 5: Design section for shear

Step 6: Choose rebar configuration (size and spacing)

Step 7: Check anchorage and lap lengths

Step 8: Detail connection reinforcement

2.5.3.1 Step 4 - Design for Flexure

Cast-in anchors are predominately used to resist tensile forces. In a wall-to-slab application the anchors at the top of the connection will resist the tensile forces of the moment couple, while the bottom anchors will resist the compression forces. In order to uncouple the design moment in an equivalent tensile and compression force pair, the basic flexural design procedure, given in SANS 10100-1:200, is followed as described in section A.4. The following parameters are calculated from their respective equations:

- (z) lever arm in coupled moment - Equation A.7
- ($A_{s_{req}}$) required area of tension reinforcement - Equation A.9

The applied tensile force (F_s) associated with the applied moment (M) is subsequently determined by the following:

$$F_s = M/z \quad (2.4)$$

Once the applied tensile force is determined, the available resistance has to be calculated. The CEB Design Guide specifies that the total resistance for a group of cast-in anchors

to a direct tensile force, is determined by Equation 2.8. The combined resistance from a set of anchors is influenced by their spacing (s_x) and also by the distance from the last anchor to the edge of the slab on both sides (c_x) - refer to Figure 2.16 for a graphical definition of c_x . These effects are accounted for by multiplying the nominal resistance (N_{Rd}^0) of each anchor by a specific factor. Factors $\Psi_{A,N,1}$ and $\Psi_{A,N,2}$ are to account for the spacing of the internal anchors, while $\Psi_{S,N}$ is used to reduce the resistance of edge anchors. The values of all three factors (Equations 2.5 to 2.7) are limited to 1:

$$\Psi_{A,N,1} = \frac{S_x}{3 \times h_{eff}} \leq 1.0 \quad (2.5)$$

$$\Psi_{A,N,2} = \frac{C_x + S_x/2}{3 \times h_{eff}} \leq 1.0 \quad (2.6)$$

$$\Psi_{S,N} = 0.7 + \frac{0.3 \times C_x}{1.5 \times h_{eff}} \leq 1.0 \quad (2.7)$$

$$N_{Rd,c} = (n_a - 2) \times N_{Rd}^0 \times \Psi_{A,N,1} + 2 \times N_{Rd}^0 \times \Psi_{A,N,2} \times \Psi_{S,N} \quad (2.8)$$

As discussed in section 2.5.2 the modified cone behaviour enhances the total resistance $N_{Rd,s}$ and is determined by Equation 2.3.

The total capacity is therefore the greater of $N_{Rd,c}$ and $N_{Rd,s}$, but not greater than $N_{Rd,y}$. This limit is specified to ensure that the applied force does not result in stresses inside the top bars that exceed the yield limit for steel reinforcement.

$$N_{Rd,y} = n_a \times f_{yk} \times A_s / \gamma_m \quad (2.9)$$

f_{yk} is the characteristic strength of the reinforcement

γ_m is the material factor for reinforcement = 1.15

If the total capacity is more than the applied tensile force, the connection will be able to resist the applied moment. If this is not the case, either the effective depth of the slab should be increased, longer anchors should be used in order to increase h_{eff} or more anchors should be used.

2.5.3.2 Step 5 - Design for Shear

This section describes the procedure adopted to design the shear resistance for a cast-in anchor wall-to-slab joint. Experimental testing showed no evidence of distress that might be related to vertical shear in the slab directly adjacent to the joint. It is therefore assumed that the cast in shear keys provide sufficient resistance to shear. The shear capacity of such a connection can subsequently be determined with the procedure as set out in section A.5. (Cairns, 2010)

The main concern lies with the resistance of shear in the joint itself and the following procedure is adopted. It is based on the provisions of section 6.2.2 of the Eurocode 2

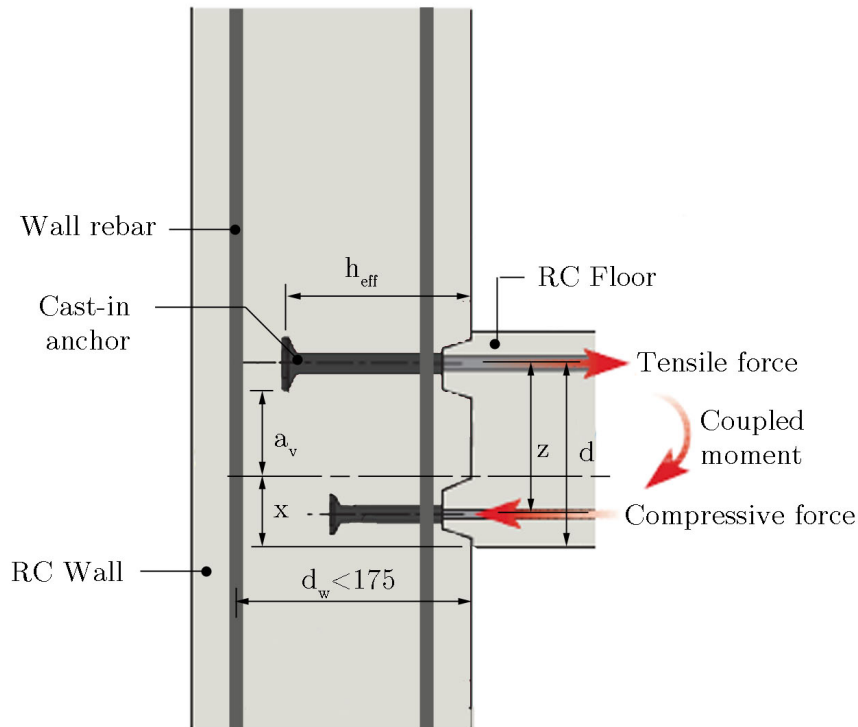


Figure 2.14: Notation for Joint Shear Resistance (reworked from Cairns (2010))

(BSI, 1992), with some modifications based on recent research conducted at Heriot Watt University (Cairns, 2010). Figure 2.14 graphically represents the joint parameters.

The anchorage of slab reinforcement here is significantly different to that of conventional bent rebar that is anchored to the back of the wall. Instead, the anchor terminates at a distance equal to the embedment depth (h_{eff}) inside the wall. The effective depth of the wall (d_w) is limited to 175 mm when calculating the shear resistance, as there is no experimental data available for thicker walls.

Following the provisions in section 6.2.2 of Eurocode 2, for members that do not require any additional shear reinforcement, Equation 2.10 for the characteristic joint shear resistance is derived from Equation 6.2 in Eurocode 2. Figure 2.14 illustrates the parameters used in the equations below.

$$V_{Rd,s} = C_R \times k_1 \times (100\rho_1 f_{ck})^{\frac{1}{3}} \times l_v \times d_w / \beta \quad (2.10)$$

C_R is taken as 0.18

f_{ck} is the characteristic cylinder compressive strength

l_v is the width of the joint

with

$$k_1 = 1 + \sqrt{\frac{200}{d_w}} \leq 2.0 \quad (2.11)$$

$$\rho_1 = \frac{A_{s,w}}{l_v \times d_w} \leq 0.02 \quad (2.12)$$

$$\beta = \frac{a_v}{2 \times d_w} \quad (2.13)$$

but with a minimum value of

$$V_{Rd,smin} = \left[0.05 \times k^{\frac{3}{2}} \times f_{ck}^{\frac{1}{2}} \right] \times l_v \times h_{eff} / \beta \quad (2.14)$$

and a maximum value of

$$V_{Rd,smax} = 0.05 \times b \times h_{eff} \times \Psi_v \times f_{ck} \quad (2.15)$$

$$\Psi_v = 0.6 \times \left[1 - \frac{f_{ck}}{250} \right] \quad (2.16)$$

The magnitude of the shear force applied to the joint is calculated by Equation 2.17:

$$V = T - V_w \quad (2.17)$$

$A_{s,w}$ is the area of vertical reinforcement in the wall on the outer face

a_v is the shear span of the joint

Ψ_v is a strength reduction factor for concrete cracked in shear

F_s is the applied tension force in the top anchor at ULS

V_w is the shear force in the wall just above the connection, determined through the structural analysis

If the capacity ($V_{Rd,s}$) is more than the applied shear force (V), the design requirement for joint shear resistance is satisfied.

2.5.3.3 Step 6 - Rebar configuration

All the standard precautions, as set out in section A.6, also apply to any rebar configuration when using cast-in anchors. There is, however, one additional requirement in a situation when the edge distance (c_x), from the last anchor to the edge of the wall, is more than $1.5 \times h_{eff}$. If this is the case, edge reinforcement, parallel to the anchor, is required as shown in Figure 2.15.

Once the reinforcement configuration is established, the anchorage and lap lengths are checked.

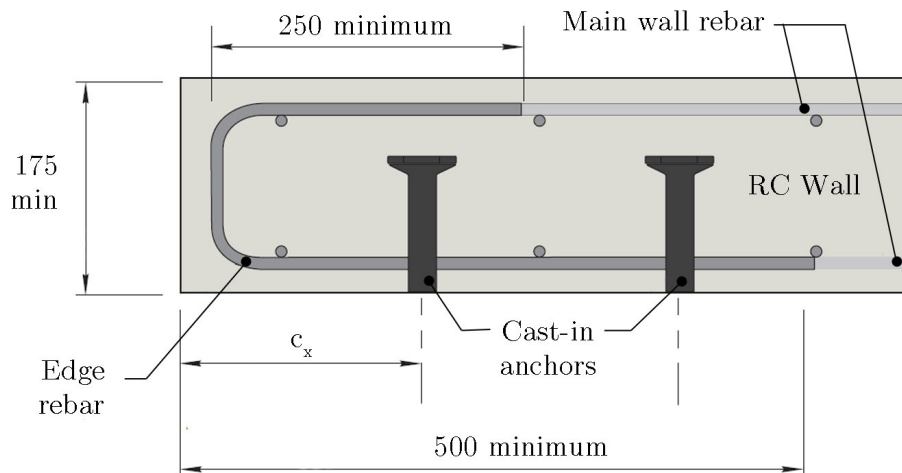


Figure 2.15: Anchor Edge Reinforcement Details (reworked from Ancon Building Products (2014))

2.5.3.4 Step 7 - Anchorage and lap lengths

Similar to conventional design principles, the tensile force is transferred through the top reinforcement of the floor to the continuation rebar screwed into the anchor. The force is then finally transmitted to the wall by the anchor pull-out resistance. In some moment connections, compression reinforcement is also required to be anchored to the wall, similar to the top rebar. To ensure the transfer of the force from the rebar in the slab to the continuation rebar, a proper lap length is required. The value can be calculated using Equation A.12 in section A.7 and is graphically represented in Figure 2.16 below. As the diameter of the required bottom/compression reinforcement is likely to be smaller than the top/tensile rebar, the lap length required will also be smaller.

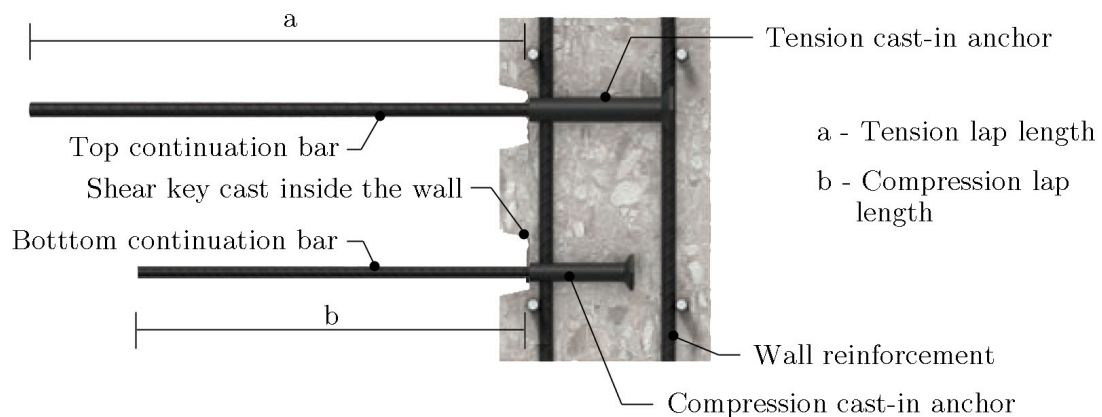


Figure 2.16: Cast-in Anchor Continuation Bar Anchorage Detail (reworked from Ancon Building Products (2014))

2.5.3.5 Step 8 - Detailing of reinforcement

The detailing procedure for the reinforcement in the wall and floor is identical to conventional systems. The only exception is that both the anchors and their continuation reinforcement bars are ordered from an approved supplier after the correct size, anchor imbedment depth and length of continuation bars are calculated. Refer to Appendix E, for an example of such a bending schedule.

2.5.4 Additional Aspects

This system can easily be adapted and used in conjunction with jump formwork. The installation process is easy to follow and great accuracy can be accomplished within the time limit associated with a continuous system.

Similar to the previous systems, there are no projecting rebars that could become a safety hazard, or impede moving equipment and material. The process of removing the timber carriers and exposing the threaded anchor ends is easy and well documented. Power equipment is not required. This system is also ideal in projects where high rebar quantities are required inside the wall, as the anchors fit easily through closely spaced reinforcement. The maximum capacity of a connection using these anchors is also larger than the bend-out alternatives, as the continuation rebars can be specified up to a Y20 bar.

This system is, unfortunately, not common in South Africa and there is currently no local company that manufactures it. A direct cost comparison to other systems is therefore not possible, as import costs will give unrealistic high values. When comparing prices in a market where all four systems are readily available, the material cost for the cast-in anchor system is still 3 times more expensive than the pre-assembled bend-out bar system. This comparison is presented in Table 2.1, comparing local prices in the United Kingdom.

Table 2.1: Material Cost Comparison in the United Kingdom

System	Cost (£/m)
Continuous Starter-bar	11
Site-installed Bend-out Bar	11
Pre-assembled Bend-out Bar	27
Cast-in Anchor	83

Prices obtained from Ancon Building Products

Chapter 3

Experimental Design

3.1 Introduction

This chapter describes the experimental testing conducted in this study. Each section starts by discussing the reason behind a specific experimental test and how it fits into the broader research investigation. Technical information relating to the configuration and set-up of each test is discussed, followed by details of the measurement instrumentation used. Finally the test execution methodology is also included.

In order to investigate the behaviour of the four different reinforced concrete wall-to-slab connection systems, full-scale models were constructed and tested under identical conditions. Section 3.2 presents all the details surrounding these full-scale tests.

An investigation on the effect of cold-bending and straightening of reinforcement was conducted in two stages. The first stage included a series of tensile tests in order to establish the effect on the steel properties, while stage two investigated the effect of low-cycle bending and straightening on the reinforcement.

Finally, information on the supplementary tests, to determine the concrete properties of the test specimens, are included.

3.2 Full-scale Tests

In order to compare the different connection systems, within the time constraint of this research, a best practice approach was adopted in the physical experimental phase. Four full-scale models of the different connection systems were built in the Stellenbosch University Structural Laboratory. The models represent a wall-to-slab moment connection found in a typical high rise office block. The structural system for the office block is assumed to be a concrete frame with masonry infill. The building has 250 mm thick reinforced concrete slabs, running continuously over columns spaced at 7.2 m in the one direction and 4 m in the other. All lateral forces are assumed to be resisted through boundary shear walls and will therefore not be considered in this investigation. The specific connection to be simulated in this experimental investigation is between the end of a continuous floor and a 300 mm thick core wall, as illustrated in Figure 3.1.

The full-scale models were constructed to represent this connection as closely as possible, by isolating a 1 m strip of the wall below and above the connection and keeping a portion of the slab, as shown in Figure 3.2. A load was subsequently applied to the tip of the

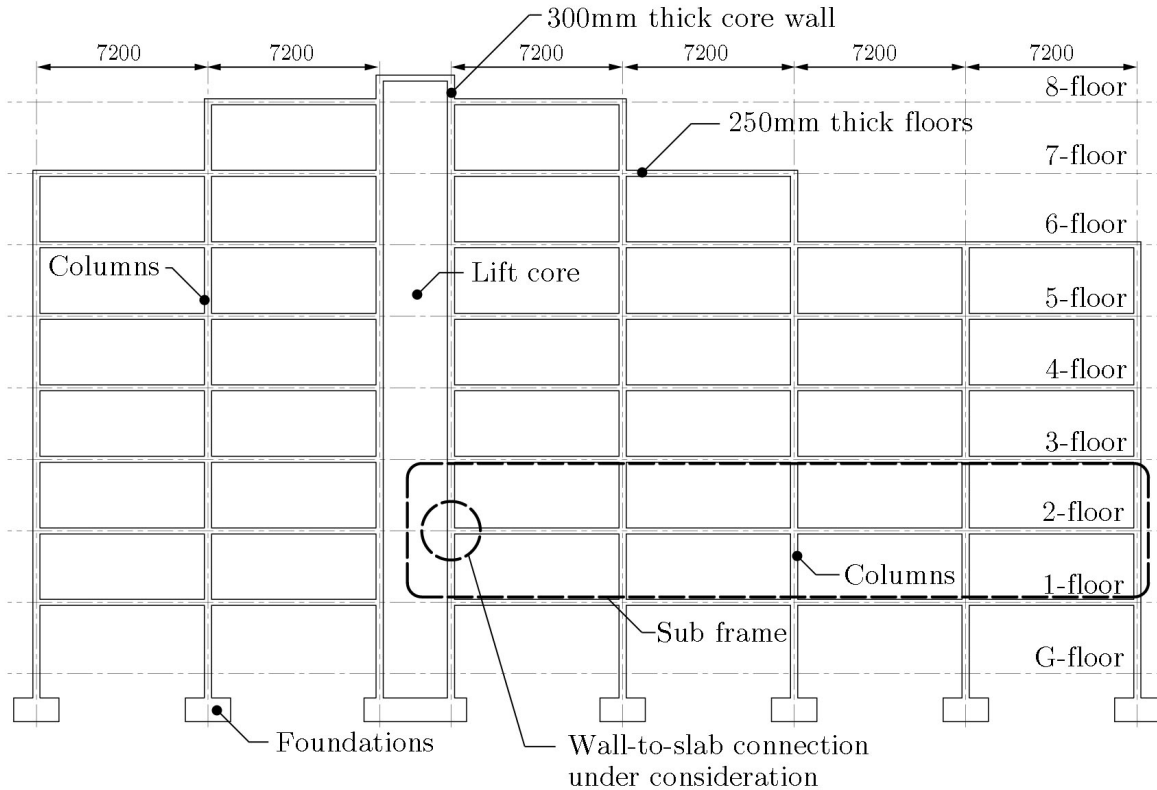


Figure 3.1: Section Through Typical Office Block

cantilever floor, in order to generate a moment and a shear force at the connection. Although the moment and shear force diagram for a cantilever structure is not the same as for a continuous floor, the focus of this research investigation is on the capacity at the connection and it is therefore only important to accurately simulate the conditions at the wall-to-slab joint. The distance between the applied load and the connection was further adjusted, in order to establish an appropriate moment to shear force ratio that corresponded to values obtained in the frame analysis of the building.

The models were all identical, with a 250 mm thick cantilever floor connected to a 300 mm thick wall. The systems were all designed to have the same moment and shear capacity, corresponding to an ULS design of a typical office block. The models were individually tested in a special steel frame designed to ensure that the desired boundary conditions are met. An illustration of the applied loads, boundary conditions and a full-scale specimen, is presented in Figure 3.2.

The results are presented through load-displacement curves and crack patterns, observed at applied loads, associated with the SLS, ULS and the load at failure. The practical aspects regarding the installation process are also discussed and presented in this section.

3.2.1 Test Configuration

The full-scale tests were conducted in the Stellenbosch University Structural Laboratory. The models were constructed simultaneously and stored in their original positions for 28 days. This ensured the concrete reached its full characteristic strength before being

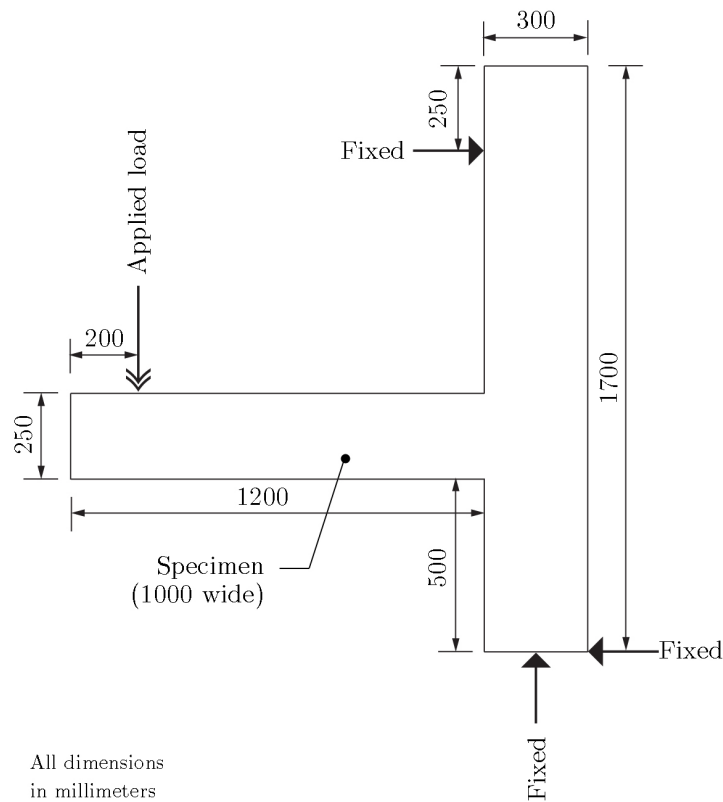


Figure 3.2: Full-scale Specimen with Boundary Conditions and Applied Load

tested. The models were then tested individually over a period of two days. The test set-up consisted of two separate steel frames, both securely bolted to the laboratory strong floor. A 500 kN capacity hydraulic actuator (Instron) was used to apply the load to the tip of the cantilever floor. The Instron was securely fixed to the first steel frame, while the second frame was designed as an A-type frame in order to keep the wall in place during testing. A 152x152x23 H-Section was used as a spreader beam, to spread the point load over the width of the 1m wide specimen. A ball bearing was also introduced in the load train. The bearing ensured that the load was always applied in a vertical direction, while the spreader beam stayed fully connected to floor itself. Figure 3.3, illustrates the full test set-up.

3.2.2 Test Specimens

The four full-scale models presented in this section correspond to the different connection systems, as discussed in section 2. The first specimen was used as the reference model and will hereafter be referred to as Model A. The site-installed pull-out system was used in the second specimen or Model B, while Model C had the prefabricated pull-out system installed. The mechanical couplers with cast-in anchors were used in the last specimen, referred to as Model D hereafter.

The reinforcement used for all four models were standard high yield deformed bars ordered from a local bending yard. The concrete was ordered from a local pre-mix batching plant and was specified as a 40 MPa (CEM II 51.5 A-L) concrete. The concrete was delivered to the laboratory in two separate batches: the first batch was used to cast the walls for all four models and 7 days later the second batch was used for the cantilever floors.

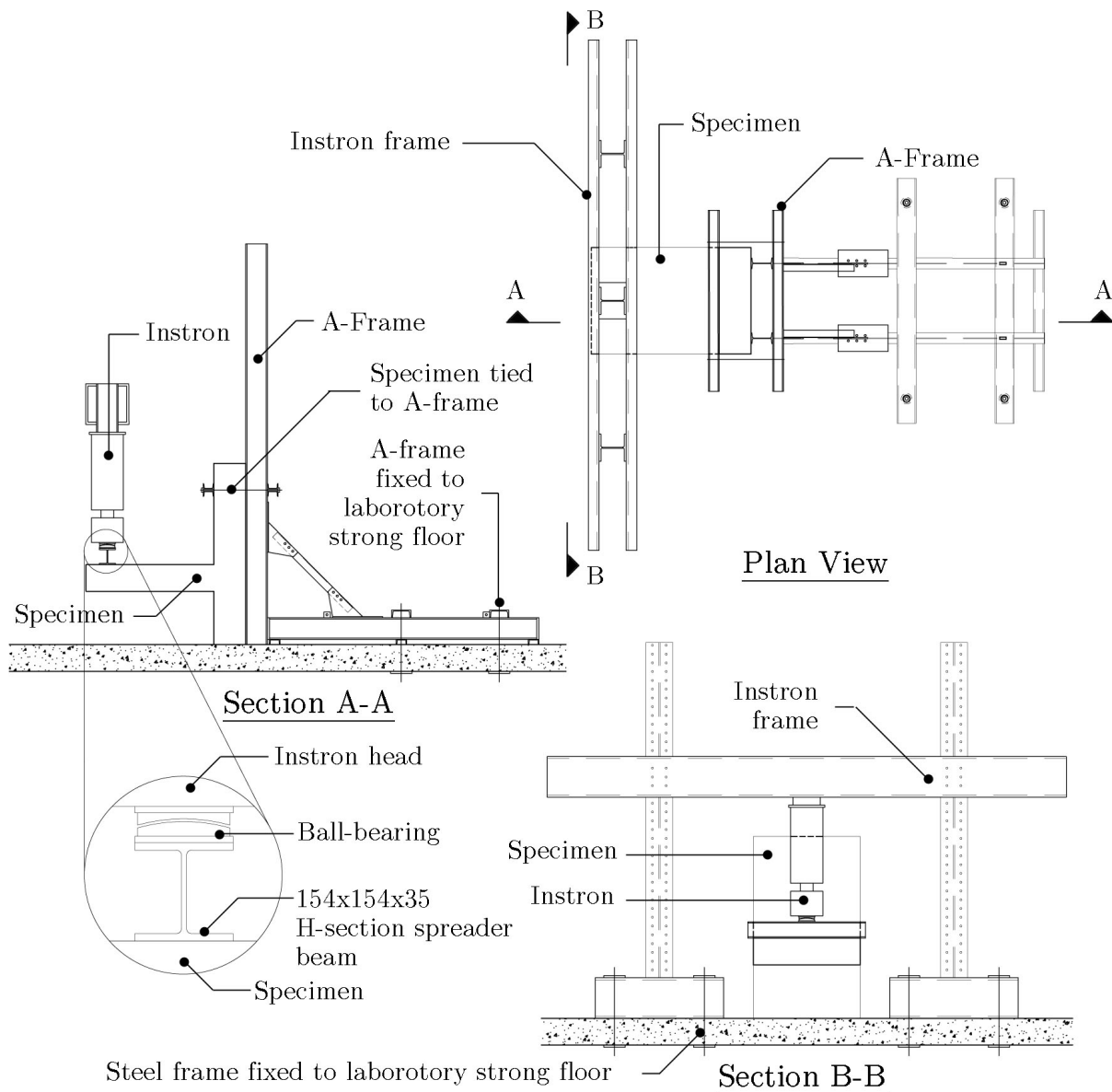


Figure 3.3: Full-scale Test Configuration

This research investigation does not include the design of any vertical elements, such as walls and columns, but in order to simulate practice as closely as possible and to ensure continuity, a typical reinforcement configuration for all the wall sections was used. The vertical reinforcement was Y12 bars, spaced at 150 mm centre-to-centre (c/c) on both sides of the wall, and similarly the horizontal reinforcement was Y12 bars spaced at 200 mm c/c. This configuration complies with the detailing requirements of SANS 10100-1:2000 to minimise cracking in the walls.

3.2.2.1 Design - Model A

The following steps were followed in the design process for the continuous starter-bar system. The format corresponds to the steps defined in section 2.2.2. All the equations as referred to in this section can be found in the detailed design procedure, presented in

Appendix A.

Step 1 - Determine Loads: According to SANS 10160-2:2011 - self-weight and imposed loads, the characteristic value for the variable action associated with general office space is 3 kPa. This was the only variable action applicable to the design and was subsequently also defined as the leading action.

It was further assumed that the permanent actions included the self-weight of the slab, a 50 mm screed and the weight of the ceiling, permanent partitions, lighting and air conditioning equipment below the slab. The density of the reinforced concrete was taken as 24 kN/m³, while the combined weight of the additional permanent actions were considered to be equal to a permanent load of 3.5 kPa.

SANS 10160-1:2011 specifies that two limit state combinations are to be considered when calculating actions for structural resistance. They are defined as the so-called STR and STR-P limit state combination. The partial factors for the actions, to be used in the combinations, are summarized below:

For STR (subscript 1):

- Leading variable action - 1.6
- Permanent actions - 1.2

For STR-P (subscript 2):

- Leading variable action - 1.2
- Permanent actions - 1.3

(SANS, 2011a)

Step 2 - Calculate load combinations: When considering a 4 m wide strip of floor, the total variable action (Q_T) for the two limit state combinations were calculated by Equations A.1 and A.3.

$$\begin{aligned} Q_{T1} &= 1.6 \times 3 \times 4 + 0 \\ &= 19.2 \text{ kN/m} \end{aligned}$$

$$\begin{aligned} Q_{T2} &= 1.0 \times 3 \times 4 \\ &= 12.0 \text{ kN/m} \end{aligned}$$

The total permanent action (G_T) was subsequently calculated by Equations A.2 and A.4.

$$\begin{aligned} G_{T1} &= 1.2 \times (24 \times 0.25 + 3.5) \times 4 \\ &= 45.6 \text{ kN/m} \end{aligned}$$

$$\begin{aligned} G_{T2} &= 1.3 \times (24 \times 0.25 + 3.1) \times 4 \\ &= 47.32 \text{ kN/m} \end{aligned}$$

The combined value for the two limit state combinations were:

$$\begin{aligned} STR &= 19.2 + 45.6 \\ &= 64.8 \text{ kN/m} \end{aligned}$$

$$\begin{aligned} STR - P &= 12.0 + 47.32 \\ &= 59.32 \text{ kN/m} \end{aligned}$$

As the value for the combined STR combination was more than that of the STR-P combination, it was considered as the critical load combination to be used in the ULS design of the structure.

Step 3 - Analyse structure: For the typical office block under consideration, the concrete frame was assumed to be fully braced in both directions. Subsequently, the simplified approach for analysing a structure was adopted, in which only a subframe of the structure is considered. The Continuous Beam module in the Prokon software package was used to analyse the subframe, as illustrated in Figure 3.4 (Prokon, 2015). The subframe was modelled as a 4 m wide strip of floor. In order to convert the results from the analysis to the 1m wide full-scale models, the values are simply divided by four. This simplification is acceptable as the floor is connected to a continuous wall and the analysis was performed to generate the moments and shear forces at the connection only. The walls and columns, above and below the strip, were however included in the subframe, in order to accurately simulate the stiffness of the supporting structure.

The permanent and variable actions were specified in Prokon. The input values were presented in kN/m as un-factored actions. The critical factors were prescribed separately, for both the variable and permanent actions, and Prokon then correctly combined the partial load factors. The density of the reinforced concrete was prescribed and the self-weight of the structure was automatically calculated and factored accordingly. Pattern loading was applied to the different spans, as prescribed in SANS 10100-1:2000, and the results were presented through an envelope of the maximum occurring moments and shear forces along the spans. The diagrams are presented in Figure 3.5. No redistribution of moments was considered.

From the diagrams the maximum moment (M) and shear force (V), at the connection under consideration, were divided by four, as presented below:

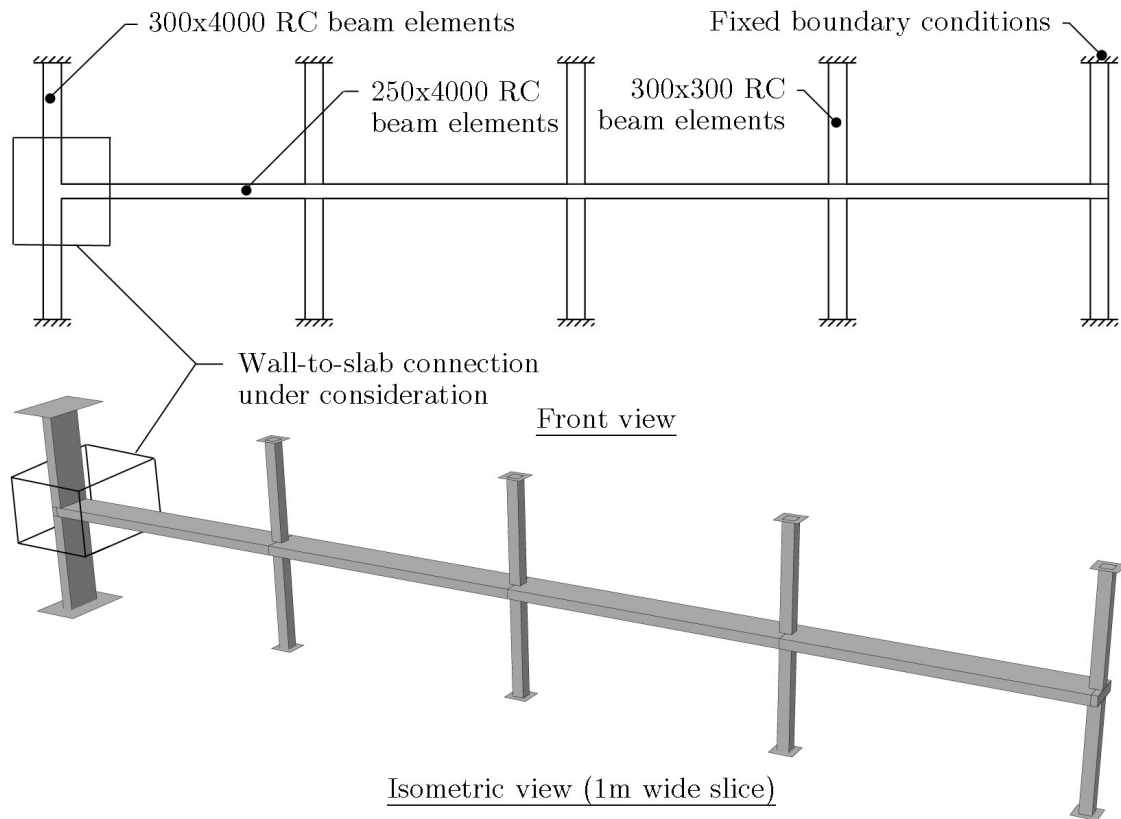


Figure 3.4: Sub Frame Analysis

$$M = 219.9 \times 10^6 / 4 = 54.975 \times 10^6 \text{ N m}$$

$$V = 230.8 \times 10^3 / 4 = 57.700 \times 10^6 \text{ N}$$

These values were used as the ULS load for the design procedure.

Step 4 - Design for Flexure: The area of reinforcement required to resist the ULS design moment was calculated using Equations A.5 to A.9. It was assumed that the reinforcement used in the connection was all Y12 rebar (Φ), with a clear cover of 25 mm. The section width (b) and effective depth (d) was determined as follows:

$$b = 1000 \text{ mm}$$

$$\begin{aligned} d &= 250 - \text{cover} - \Phi/2 \\ &= 250 - 25 - 12/2 \\ &= 219 \text{ mm} \end{aligned}$$

Using the sectional properties and design moment, the value for K was determined:

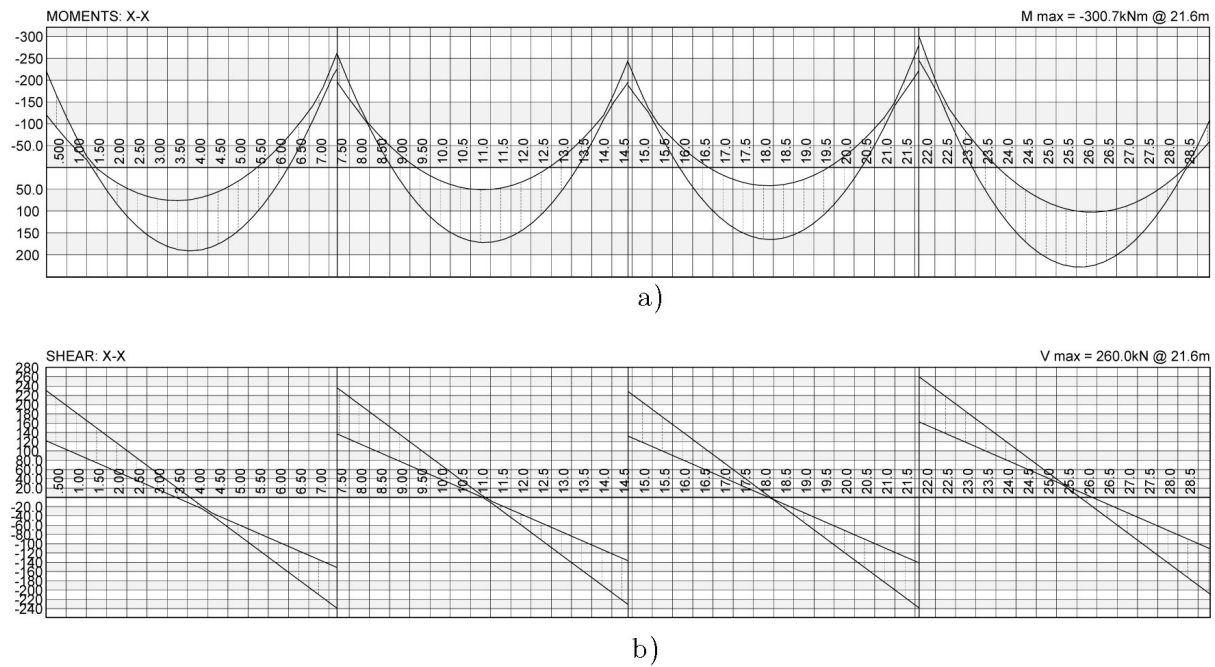


Figure 3.5: a) Moment Diagram Envelope b) Shear Force Diagram Envelope

$$\begin{aligned}
 K &= \frac{M}{bd^2 f_{cu}} \\
 &= \frac{54.975 \times 10^6}{1000 \times 219^2 \times 40} \\
 &= 0.036
 \end{aligned}$$

During the analysis no redistribution of moments was conducted and therefore the value for B_b was equal to 0.9 and K' was determined as follows:

$$\begin{aligned}
 K' &= 0.402(B_b - 0.4) - 0.18(B_b - 0.4)^2 \\
 &= 0.402(0.9 - 0.4) - 0.18(0.9 - 0.4)^2 \\
 &= 0.156
 \end{aligned}$$

Only tension reinforcement was required, as $K \leq K'$. Next, the lever arm (z) and natural axis depth (x) were calculated. The intermediate results were adjusted if the values did not fall within the required limits ($0.755d \leq z \leq 0.95d$), further discussed in section A.4.

$$\begin{aligned}
z &= d \left\{ 0.5 + \sqrt{\left(0.25 - \frac{K}{0.9} \right)} \right\} \\
&= 219 \left\{ 0.5 + \sqrt{\left(0.25 - \frac{0.036}{0.9} \right)} \right\} \\
&= 209.906 \text{ mm} \\
z &> 0.755d = 165.35 \quad OK \\
z &> 0.95d = 208.05 \quad NOT OK \\
\therefore z &= 208.05 \text{ mm}
\end{aligned}$$

$$\begin{aligned}
x &= \frac{d - z}{0.45} \\
&= \frac{219 - 208.05}{0.45} \\
&= 24.33 \text{ mm}
\end{aligned}$$

Finally, the required area of reinforcement was determined:

$$\begin{aligned}
A_{s_{req}} &= \frac{M}{0.87 f_y z} \\
&= \frac{54.975 \times 10^6}{0.87 \times 450 \times 208.05} \\
&= 675 \text{ mm}
\end{aligned}$$

For six Y12 starter-bars, the combined area of reinforcement ($A_{s_{prov}}$) was calculated to be 679 mm. This was more than the required amount and therefore satisfied the design criteria for flexural resistance.

Step 5 - Design for Shear: The design shear stress (v) at the connection was calculated with Equation A.10:

$$\begin{aligned}
v &= \frac{V}{bd} \leq 0.75 \sqrt{f_{cu}} \\
&= \frac{57.7 \times 10^3}{1000 \times 219} \\
&= 0.263 \text{ MPa} < 4.743 \quad OK
\end{aligned}$$

The shear resistance of the section was subsequently determined with Equation A.11, taking the area of reinforcement provided ($A_{s_{prov}}$) and the section properties into account:

$$\begin{aligned}
v_c &= \frac{0.79}{\gamma_m} \left(\frac{f_{cu}}{25} \right)^{\frac{1}{3}} \left(\frac{100A_{sprov}}{bd} \right)^{\frac{1}{3}} \left(\frac{400}{d} \right)^{\frac{1}{4}} \\
&= \frac{0.79}{1.4} \left(\frac{40}{25} \right)^{\frac{1}{3}} \left(\frac{100 \times 678.58}{1000 \times 219} \right)^{\frac{1}{3}} \left(\frac{400}{219} \right)^{\frac{1}{4}} \\
&= 0.52 \text{ MPa}
\end{aligned}$$

The shear resistance for the connection was adequate as $v_c > v$.

Step 6 - Rebar Configuration: From Table 1 in SANS 10100-2:2014, the level of exposure for structural elements inside a typical office block is "moderate". The corresponding minimum cover, defined in Table 3, is 30 mm for a 40 MPa concrete.

The conditions inside the structural laboratory are strictly controlled and the level of exposure could therefore be assumed to be better than only "moderate". The code does not give any recommendations for conditions more favourable than "moderate" and the smallest cover is limited to 25 mm, which corresponds to a concrete strength of 50 MPa exposed to "moderate" conditions. As all the models were constructed, cured and tested in the laboratory under the controlled conditions, the smallest recommended cover of 25 mm was used.

The rebar configuration was based on the rules as set out in section A.6, of Appendix A. The 6 Y12 starter-bars were spaced at 150 mm c/c. In order to simplify the construction process, the secondary steel was also Y12 rebar, but spaced at 200 mm c/c.

Step 7 - Anchorage and lap lengths: Table 24 of SANS 10100-1:2011, gives the ultimate anchorage bond stress (f_{bu}) between a deformed rebar and 40 MPa concrete as 3.4 MPa. Subsequently, the required anchorage length (l) to transfer the load from a fully stressed Y12 bar to the adjacent concrete was calculated by using Equation A.12. The force (F_s) in a fully stressed bar was assumed to be equal to $f_y \times 0.87 \times A_s = 450 \times 0.87 \times 113.097 = 44278$ N.

$$\begin{aligned}
l &= \frac{F_s}{\pi \Phi f_{bu}} \\
&= \frac{44278}{\pi \times 12 \times 3.4} \\
&= 345 \text{ mm}
\end{aligned}$$

The legs of the starter-bars were sized to enable them to project more than 345 mm past the face of the wall. This was translated into a starter-bar configuration, as shown in Figure 3.6.

The cover on the reinforcement in the walls (*cover*) was taken as 30 mm and the diameter of the horizontal wall reinforcement (Φ_{hor}) and vertical wall reinforcement (Φ_{ver}) as 12

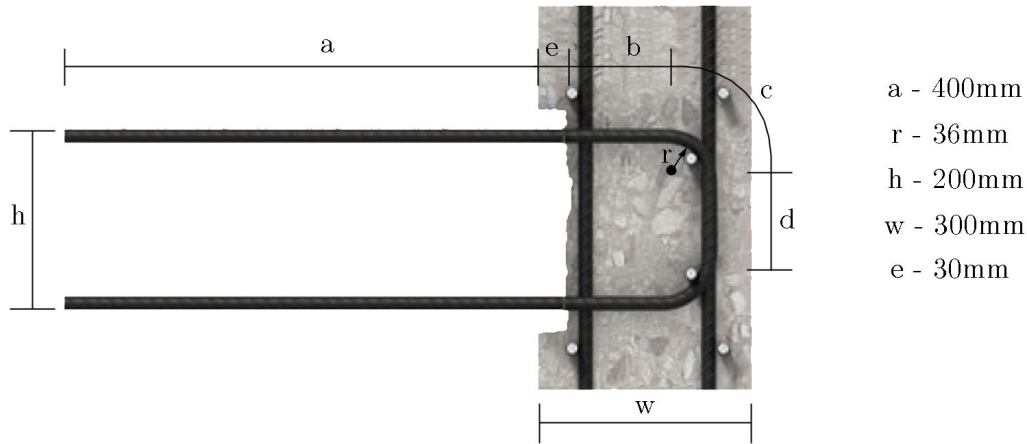


Figure 3.6: Continuous Starter-bar Dimensions

mm. The diameter of the starter-bars (Φ) was also 12 mm. The available anchorage length (l_{ave}) was subsequently determined with Equations A.13 to A.16.

$$\begin{aligned}
 b &= w - cover - \Phi_{hor} - \Phi_{ver} - r - e \\
 &= 300 - 30 - 12 - 12 - 36 - 30 \\
 &= 180 \text{ mm}
 \end{aligned}$$

$$\begin{aligned}
 c &= 8\Phi \\
 &= 8 \times 12 \\
 &= 96 \text{ mm}
 \end{aligned}$$

$$\begin{aligned}
 d &= h - 2\Phi - 2r \\
 &= h - 2 \times 12 - 2 \times 36 \\
 &= 104 \text{ mm}
 \end{aligned}$$

$$\begin{aligned}
 l_{ave} &= b + c + d \\
 &= 180 + 96 + 104 \\
 &= 380 \text{ mm}
 \end{aligned}$$

The available anchorage length (l_{ave}) was more than the minimum value of 345 mm and would prevent any pull-out from occurring.

Step 8 - Detailing Reinforcement: A standard shape code 38 was used to describe the shape of the continuous starter-bar. The minimum dimensions for the shape code, to ensure proper anchorage and lap length, were calculated as follows:

$$\begin{aligned}
 A &= a + e + b + 4\Phi \\
 &= 400 + 30 + 180 + 4 \times 12 \\
 &= 658 \text{ mm}
 \end{aligned}$$

$$\begin{aligned}
 C &= A \\
 &= 658 \text{ mm}
 \end{aligned}$$

$$\begin{aligned}
 B &= h \\
 &= 200 \text{ mm}
 \end{aligned}$$

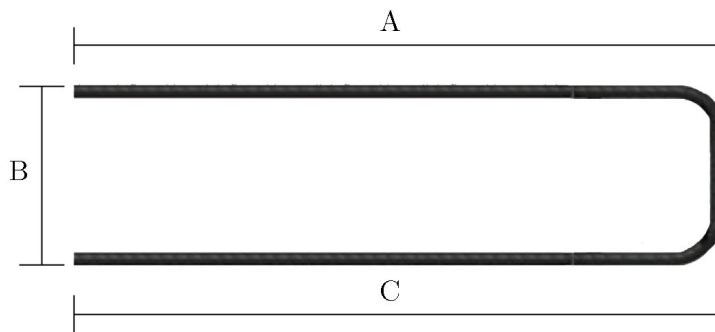


Figure 3.7: Shape Code 38

The length of the starter-bar legs was increased to allow room for error. The minimum values were rounded up to the nearest 100 and an additional 100 mm was added. This brought the final dimension of A and C to 800 mm.

The full set of bending schedules are presented in Appendix E.

3.2.2.2 Design - Model B

The same steps, as described in section 3.2.2.1, were followed for the design of the bend-out system. The only difference was in the detailing of the reinforcement, as discussed below.

Step 8 - Detailing Reinforcement: The shape of the starter-bar for the bend-out system is not a standard shape found in the code. The custom shape, as described in Figure 2.6, was therefore adopted. The values for the specific dimensions were determined as follows:

$$\begin{aligned} A &= h \\ &= 200 \text{ mm} \end{aligned}$$

$$\begin{aligned} C &= a + e \\ &= 400 + 30 \\ &= 430 \text{ mm} \end{aligned}$$

$$\begin{aligned} B &= b + 4\Phi \\ &= 180 + 4 \times 12 \\ &= 228 \text{ mm} \end{aligned}$$

The variables in the equations above are defined in the anchorage configuration presented in Figure 3.6.

3.2.2.3 Design - Model C

The design procedure for the modified bend-out system was similar to the site-installed version. The only difference was that the starter-bars were not scheduled with the reinforcement, but ordered separately. The unit was supplied inside a steel casing and fixed directly to the formwork.

3.2.2.4 Design - Model D

Only step 4 onwards is further presented in this section, as the previous steps are identical to the systems already discussed.

For the connection design, it was assumed that standard Ancon KSN12S Anchors are used. The dimensions of the steel anchors are specified in the product brochure and summarised in Table 3.1.

Table 3.1: Ancon KSN12S Anchor Specifications (mm)

KSN12S Anchor	
Anchor length	115
Anchor head width (d_a)	40
Effective embedment depth (h_{eff})	142

(Ancon Building Products, 2014)

Step 4 - Design for Flexure: The tensile force in the top reinforcement, due to the ULS moment (M) and lever arm (z), was calculated by Equation 2.4:

$$\begin{aligned}
 F_s &= M/z \\
 &= 55.1 \times 10^6 / 208.5 \\
 &= 2.65 \times 10^5 \text{ N}
 \end{aligned}$$

The nominal pull-out strength for a single anchor was determined by Equation 2.1:

$$\begin{aligned}
 N_{Rd}^0 &= k \times f_{ck}^{\frac{1}{2}} \times h_{eff}^{\frac{3}{2}} / \gamma_c \\
 &= 12.5 \times 32^{\frac{1}{2}} \times 142^{\frac{3}{2}} / 1.5 \\
 &= 7.98 \times 10^4 \text{ N}
 \end{aligned}$$

The resistance of a group of anchors is the greater of $N_{Rd,c}$ and $N_{Rd,s}$, but not greater than $N_{Rd,y}$, as discussed in section 2.5.3.1.

The resistance due to the modified cone behaviour ($N_{Rd,s}$) was calculated first. Equations 2.2 and 2.3 were used:

$$\begin{aligned}
 \Psi_{P,N} &= -0.3 + 1.5 \frac{h_{eff}}{d} \leq 1.25 \\
 &= -0.3 + 1.5 \frac{142}{219} \\
 &= 0.673 < 1.25 \quad OK
 \end{aligned}$$

$$\begin{aligned}
 N_{Rd,s} &= n_a \times N_{Rd}^0 \times \Psi_{P,N} \\
 &= 6 \times 7.98 \times 10^4 \times 0.673 \\
 &= 3.22 \times 10^5 \text{ N}
 \end{aligned}$$

Next, the direct pull-out resistance ($N_{Rd,c}$) was calculated using Equations 2.5 to 2.8:

$$\begin{aligned}
\Psi_{A,N,1} &= \frac{S_x}{3 \times h_{eff}} \leq 1.0 \\
&= \frac{150}{3 \times 142} \\
&= 0.352 < 1.0 \quad OK
\end{aligned}$$

$$\begin{aligned}
\Psi_{A,N,2} &= \frac{C_x + S_x/2}{3 \times h_{eff}} \leq 1.0 \\
&= \frac{125 + 150/2}{3 \times 142} \\
&= 0.469 < 1.0 \quad OK
\end{aligned}$$

$$\begin{aligned}
\Psi_{S,N} &= 0.7 + \frac{0.3 \times C_x}{1.5 \times h_{eff}} \leq 1.0 \\
&= 0.7 + \frac{0.3 \times 150}{1.5 \times 142} \\
&= 0.876 < 1.0 \quad OK
\end{aligned}$$

$$\begin{aligned}
N_{Rd,c} &= (n_a - 2) \times N_{Rd}^0 \times \Psi_{A,N,1} + 2 \times N_{Rd}^0 \times \Psi_{A,N,2} \times \Psi_{S,N} \\
&= (6 - 2) \times 7.98 \times 10^4 \times 0.352 + 2 \times 7.98 \times 10^4 \times 0.469 \times 0.876 \\
&= 1.78 \times 10^5 \text{ N}
\end{aligned}$$

The yield strength of the continuation rebar ($N_{Rd,y}$) was determined through Equation 2.9:

$$\begin{aligned}
N_{Rd,y} &= n_a \times f_{yk} \times A_s / \gamma_m \\
&= 6 \times 450 \times 113.09 / 1.15 \\
&= 2.66 \times 10^5 \text{ N}
\end{aligned}$$

The direct pull-out resistance, $N_{Rd,c}$, was less than $N_{Rd,s}$, which indicated an increase in the resistance due to the modified cone behaviour, as discussed in section 2.5.3.1. $N_{Rd,s}$ was, however, more than the yield strength of the bars ($N_{Rd,y}$) and the final capacity of the group was therefore limited to the value of 2.66×10^5 N, which is still more than the applied force, F_s .

Step 5 - Design for Shear: The size and spacing of the continuation rebar used in this model was the same as in the other systems. As the shear resistance in the floor, next to the connection, was adequate in the previous systems, it is assumed to be the same for this case.

The joint shear resistance in the wall ($V_{Rd,s}$), between the top and bottom rebar, was calculated by Equations 2.10 to 2.13. Figure 2.14, defines the variables used in the equations. The dimension a_v , in Figure 2.14, is a function of the width of the cast-in anchor head (d_a), the effective depth of the slab (d) and the height of the natural axis (x), as described in section 3.2.2.1.

$$\begin{aligned} a_v &= d - x - d_a/2 \\ &= 219 - 24.33 - 40/2 \\ &= 175 \text{ mm} \end{aligned}$$

$$\begin{aligned} k_1 &= 1 + \sqrt{\frac{200}{d_w}} \leq 2.0 \\ &= 1 + \sqrt{\frac{200}{142}} \\ &= 2.07 > 2.0 \quad \text{NOT OK} \\ \therefore k_1 &= 2.0 \text{ mm} \end{aligned}$$

$$\begin{aligned} \rho_1 &= \frac{A_{s,w}}{l_v \times d_w} \leq 0.02 \\ &= \frac{791.68}{1000 \times 142} \\ &= 4.52 \times 10^{-3} < 0.02 \quad \text{OK} \end{aligned}$$

$$\begin{aligned} \beta &= \frac{a_v}{2 \times d_w} \\ &= \frac{175}{2 \times 175} \\ &= 0.5 \end{aligned}$$

$$\begin{aligned} V_{Rd,s} &= C_R \times k_1 \times (100\rho_1 f_{ck})^{\frac{1}{3}} \times l_v \times d_w / \beta \\ &= 0.18 \times 2.07 \times (100 \times 4.52 \times 10^{-3} \times 32)^{\frac{1}{3}} \times 1000 \times 175 / 0.5 \\ &= 3.08 \times 10^5 \text{ N} \end{aligned}$$

The limiting minimum value for the resistance ($V_{Rd,s_{min}}$), was further determined by Equation 2.14:

$$\begin{aligned} V_{Rd,s_{min}} &= \left[0.05 \times k_1^{\frac{3}{2}} \times f_{ck}^{\frac{1}{2}} \right] \times l_v \times h_{eff} / \beta \\ &= \left[0.05 \times 2.07^{\frac{3}{2}} \times 32^{\frac{1}{2}} \right] \times 1000 \times 142 / 0.5 \\ &= 2.40 \times 10^5 \text{ N} < 3.08 \quad \text{OK} \end{aligned}$$

and the maximum value ($V_{Rd,smax}$), determined by Equations 2.16 and 2.15:

$$\begin{aligned}\Psi_v &= 0.6 \times \left[1 - \frac{f_{ck}}{250} \right] \\ &= 0.6 \times \left[1 - \frac{32}{250} \right] \\ &= 0.523\end{aligned}$$

$$\begin{aligned}V_{Rd,smax} &= 0.05 \times l_v \times h_{eff} \times \Psi_v \times f_{ck} \\ &= 0.05 \times 1000 \times 142 \times 0.523 \times 32 \\ &= 1.19 \times 10^6 \text{ N} > 3.08 \times 10^5 \text{ OK}\end{aligned}$$

Usually, the design shear force (V) in a joint is calculated by Equation 2.17. V is the difference between the tensile force in the top reinforcement (F_s) and the shear force in the wall, just above the connection. The shear force in the wall is a function of the actual height of the wall and any additional lateral forces acting on it.

As this information was not available, a conservative approach was adopted and the shear force in the wall was ignored, resulting in a larger design shear force equal to $V = 2.66 \times 10^5 \text{ N}$. The resistance was $3.08 \times 10^5 \text{ N}$ and therefore the shear capacity of the connection was sufficient.

Step 6 - Rebar configuration: The rebar configuration for the cast-in anchor system was similar to the other systems. The anchors were spaced at 150 mm c/c and the continuation rebars were also Y12 bars.

With this configuration the edge distance (c_x), as discussed in section 2.5.3.3, is 125 mm. This is less than $1.5 \times h_{eff} = 213 \text{ mm}$ and subsequently no additional edge reinforcement was required.

Step 7 - Anchorage and lap lengths: To simplify the installation process, the continuation bars for the top and bottom anchors were specified to be the same length. The minimum tensile lap length (l), as calculated in section 3.2.2.1 (step 7), was 345 mm. The continuation rebar was therefore specified as 400 mm long Y12 bars.

Step 8 - Detailing Reinforcement: The bending schedules were similar to that of the other systems. With the starter-bars omitted and replaced with details of the pre-ordered anchors and continuation reinforcement. Their position and size were clearly indicated on the bending schedule sketch, with additional information on the installation process. The full set of bending schedules are presented in Appendix E.

3.2.2.5 Construction

The full-scale models were constructed in the Structural Engineering Laboratory at Stellenbosch University. The provisions, as set out in SANS 10100-2:2014, were followed during the construction process. This section describes the processes conducted and is presented in the order of execution.

The formwork for all the models was ordered from a local supplier. The design of the formwork was based on the British Standard - BS 5975. The lateral pressure at the bottom of the formwork was estimated to be about 41 kPa, as the fresh concrete is assumed to adopt hydrostatic behaviour. The formwork was designed by the supplier to resist these pressures.

The material used for the shuttering was 21mm plywood with a filmfaced coating on both sides. The shuttering for the wall was cut to the correct dimensions and delivered to the laboratory. In the vertical direction, the plywood was braced by several timber girders spaced at 200 mm c/c and nailed to the plywood. The entire structure was horizontally braced with steel beams from the one side and square timber blocks from the other, all tied together securely with 15 mm steel rods. The shuttering was pulled together at two points along the height of the structure. Finally, the entire structure was fixed to the laboratory strong floor by diagonal steel props, preventing uplift during the pouring of the concrete and stabilising the formwork laterally. A photo of the formwork is presented in Figure 3.8.

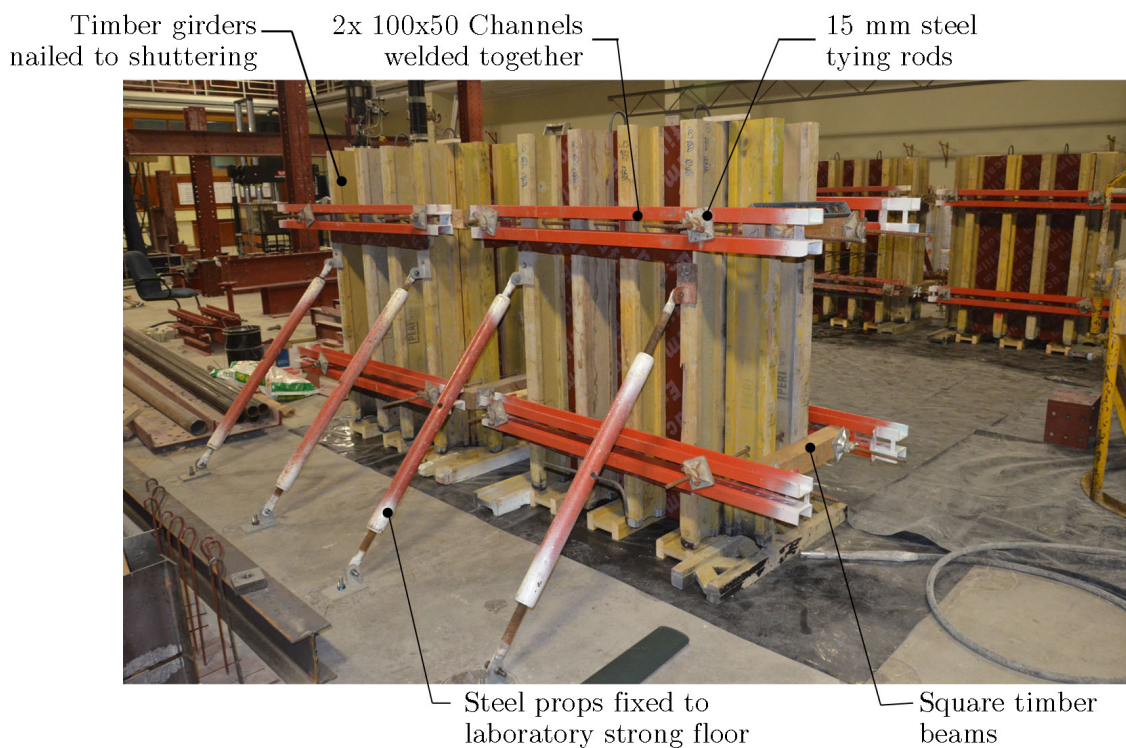


Figure 3.8: Wall Shuttering

The rebar cages for the walls were pre-assembled on the ground. The individual bars were tied together with standard binding wire to create the cages. After completion, universal

cover blocks were attached around the cage to ensure minimum cover was maintained. Two lifting hooks were also bent and tied to the cage. The legs of the hooks were cast into the wall, with the two hoops exposed at the top to create lifting points. The pull-out resistance of the hooks was checked to ensure no pull-out will occur. Standard shutter oil was applied to the inside of the formwork before the rebar cage was put in position.

Only three of the four sides were initially constructed, with the individual connection systems installed to the remaining side. The formwork was only fully closed after the installation was done.

For the continuous system used in Model A, the fourth side was modified by drilling holes into the shuttering in order to line up with the starter-bars for the floor. These starter-bars were pulled through the holes and securely fixed in place. In Model B, the pre-bent starter-bars were fixed to a piece of hardboard at the correct spacing using binding wire. The hard board and starter-bars were then securely screwed to the shuttering at the correct height. The approach adopted for Model C was similar, with the steel casing containing the pre-bent and -assembled starter-bars simply screwed to the shuttering. The timber carriers, containing the steel anchors for Model D, were also screwed directly to the plywood.

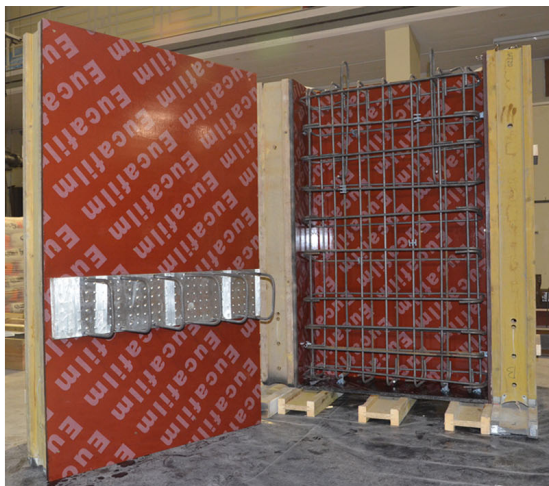
Figure 3.9 shows the four models with their respective systems installed. On the right, the three remaining sides of the shuttering are visible with the steel cage already in place and the lifting hooks projecting past the top of the wall.



Model A
Continuous Starter-bar System



Model B
Site-installed Bend-out Bar System



Model C
Pre-assembled Bend-out Bar System



Model D
Cast-in Anchor System

Figure 3.9: Different Connection Systems

The pre-mix concrete was ordered from a local batching plant. When it arrived, a standard slump test was conducted. The slump was 78 mm and well within the limits to ensure adequate workability. The wet concrete was discharged into a cone bucket and hoisted to the top of the walls. Once on top, the concrete was released in four separate portions, each level being thoroughly vibrated until most air bubbles had dissipated. Refer to Figure 3.10 for a photo of the process. All four walls were cast in less than a hour. 12 test cubes and 12 test cylinders were also cast and properly vibrated.

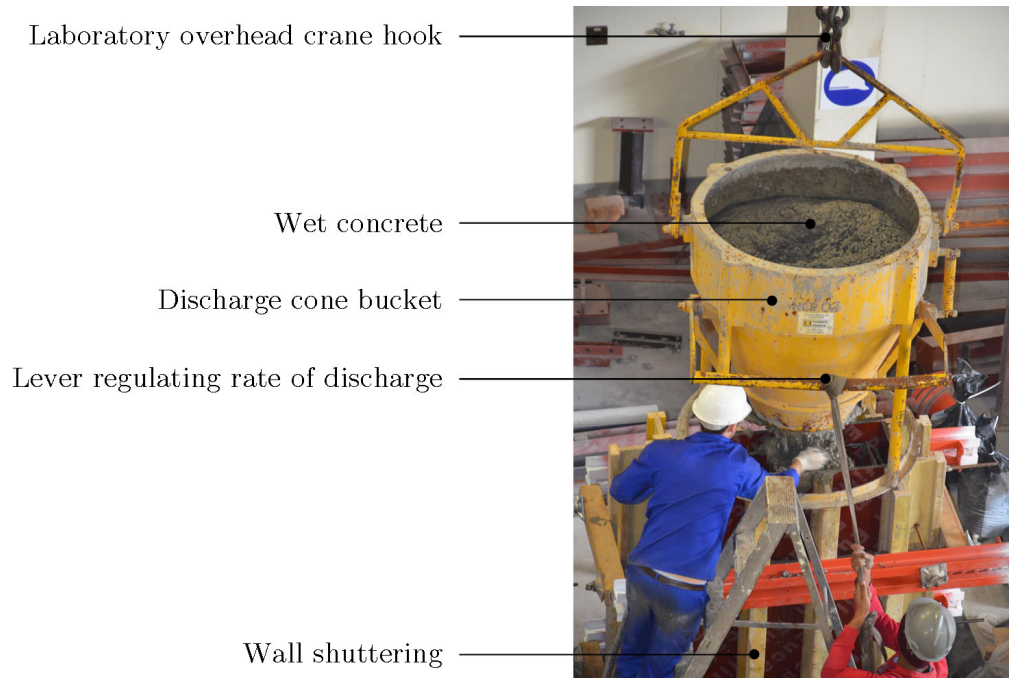


Figure 3.10: Discharging of Concrete

The concrete samples were cured according to the recommendations of SANS 10100-2:2014. A typical strength gain curve was obtained from the concrete supplier, in order to establish the appropriate concrete strength development ratio (r) for the specific concrete mix used. The data for the curve was based on a similar concrete mix, with the samples tested during the first week in May 2015. The ratio, calculated from the values on the graph, was 0.65 and the concrete was therefore classified as a "rapid" strength developing concrete. The corresponding minimum duration of curing, in an environment with a temperature of between 15 °C and 25 °C, is 5 days. The samples were subsequently cured for 7 days, by using moisture retaining blankets wrapped around the walls and slabs. The blankets were kept moist throughout the curing period. The test cubes and cylinders were also wrapped in blankets and left next to the walls.

Further, once the wall shuttering was removed, the individual connection systems were prepared and installed. Figure 3.11 illustrates this process, also described below in more detail.

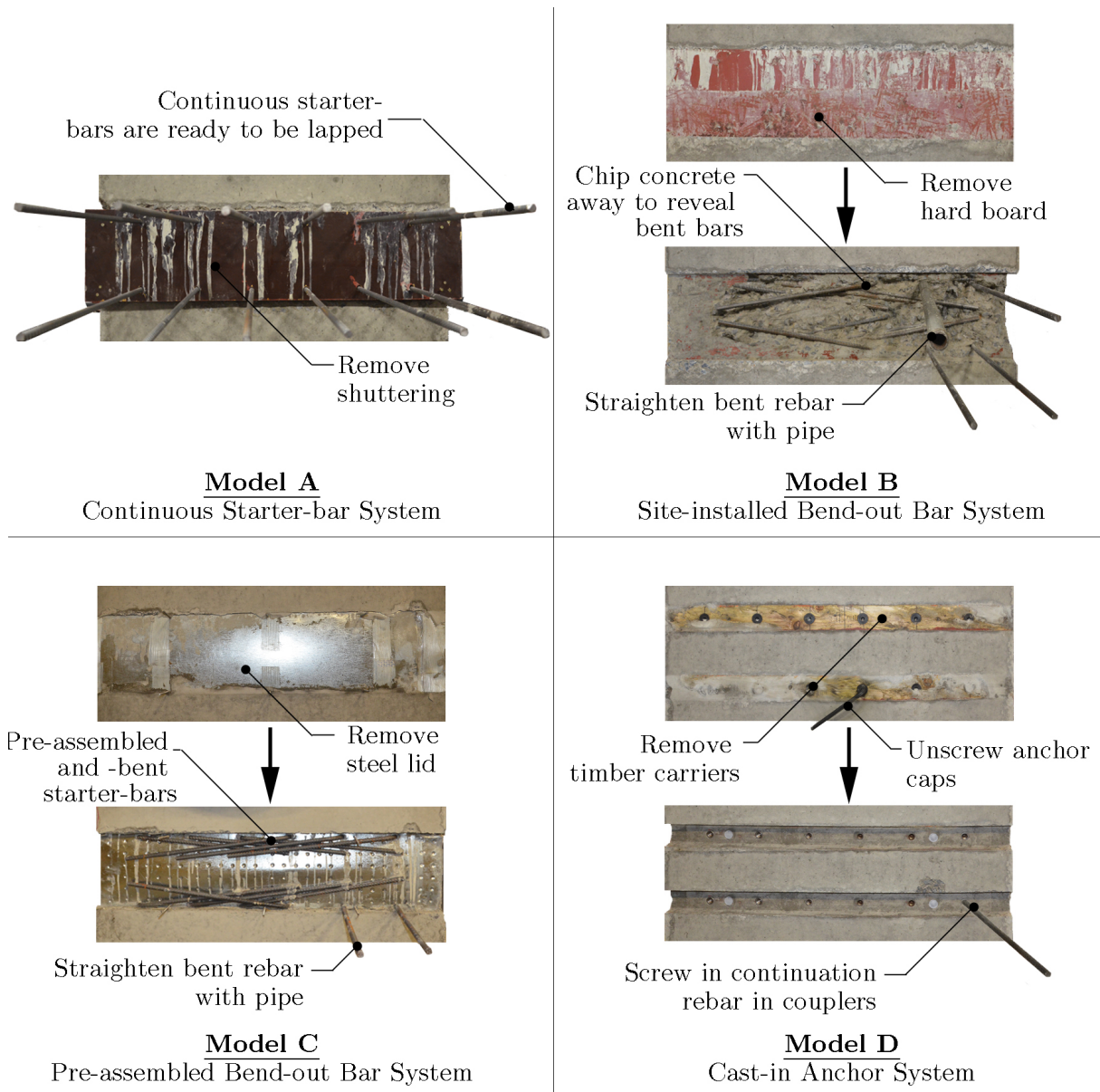


Figure 3.11: Wall-to-slab Joint Preparation

After the shuttering in Model A was removed, a loose piece of the plywood was still kept in place by the legs of the continuous bars, as seen in Figure 3.11. The removal of this piece was a tedious process, as the legs of the deformed rebar were snug inside the pre-drilled holes. However, once the loose piece was removed, the starter-bars were ready to be lapped with the floor rebar.

The pre-bent starter-bars in Model B, also demanded some time and effort. The hard board was relatively easy to remove, but the chipping away of concrete around the bent bars was difficult and time consuming. The jack hammer had to be handled with care in order to avoid any damage to the rebar. Once the bent bars were fully exposed, a pipe was used to straighten them. The bars did not always end up entirely straight after one attempt and additional bending was required.

The process to reveal the bent bars in Model C was much easier and quicker. The steel lid was simply removed and all the bars were exposed. A modified pipe was then used to straighten the starter-bars before lapping them with the rebar intended for the floor.

The preparation time for model D was, however, the quickest. The first step was to unscrew the anchor caps. This released the timber carriers and they were subsequently removed without any hassle. Next, the supplied continuation rebars were screwed into the couplers. Finally the bars were tightened with a hand wrench. All the starter-bars were perfectly straight and aligned at the correct level and this greatly simplified the fixing of the floor rebar.

Three days after stripping the wall, the formwork for the cantilever floor was constructed. A plywood base was supported on timber girders, in order to elevate the structure to the correct height. The sides of the formwork was nailed directly to the base and stabilised by diagonal timber supports. Finally, the entire structure was tied to the already cast wall with 15 mm thick steel rods. Figure 3.12 presents a photo of the shuttering for the cantilever floor.

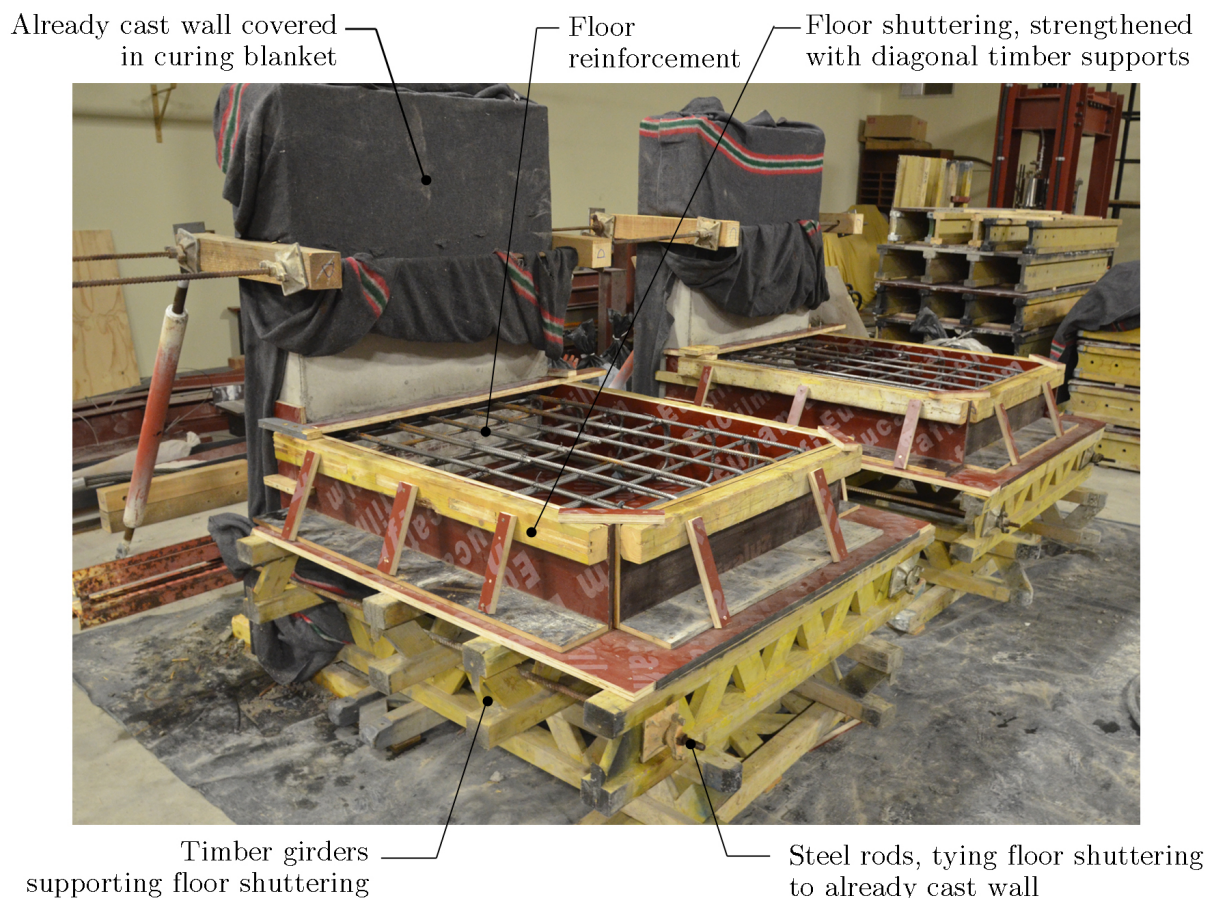


Figure 3.12: Floor Shuttering

The floor rebar was lapped with the starter-bars and placed on cover blocks to ensure the required cover was maintained. The rest of the secondary steel was also fixed and the inside of the plywood was covered with concrete releasing agent, before being closed on both sides.

The same process as described for the walls was used to pour the concrete for the floors. The slump for the pre-mix concrete was measured at 180 mm.

28 days after the cantilever floors were cast, the models were tested one by one. The overhead crane was used to lift the specimens and move them into their testing positions. Once the specimens were lowered, they were tied back to the steel A-frame, which kept them in place for the duration of the test.

3.2.3 Test Frame Design

The steel A-frame had to be designed to withstand an applied load capable of displacing the tip of the cantilever floor up to a point of total failure.

An appropriate failure load was determined with the aid of a spread sheet, containing the design calculations as discussed in Appendix A, and finding the correct values by trial and error. It was found that, for a 100 kN point load, the stress in the bars would amount to 760 MPa, using the standard design calculations found in SANS 10100-1:2000. This was 26 MPa larger than the largest failure stress for a Y12 bar tested during the preliminary tensile testing phase, as presented in section 3.3. It was therefore assumed that the full-scale models would not be able to withstand a load larger than 100 kN. The frame was subsequently designed to resist this load. In order to simplify the analysis, it was further assumed that the material in the specimen would behave in a linear fashion up to the failure load. No crack models or non-linearity in the material was considered. This assumption is conservative as in reality crack formation and reinforcing bar yield will cause disproportionate deflection.

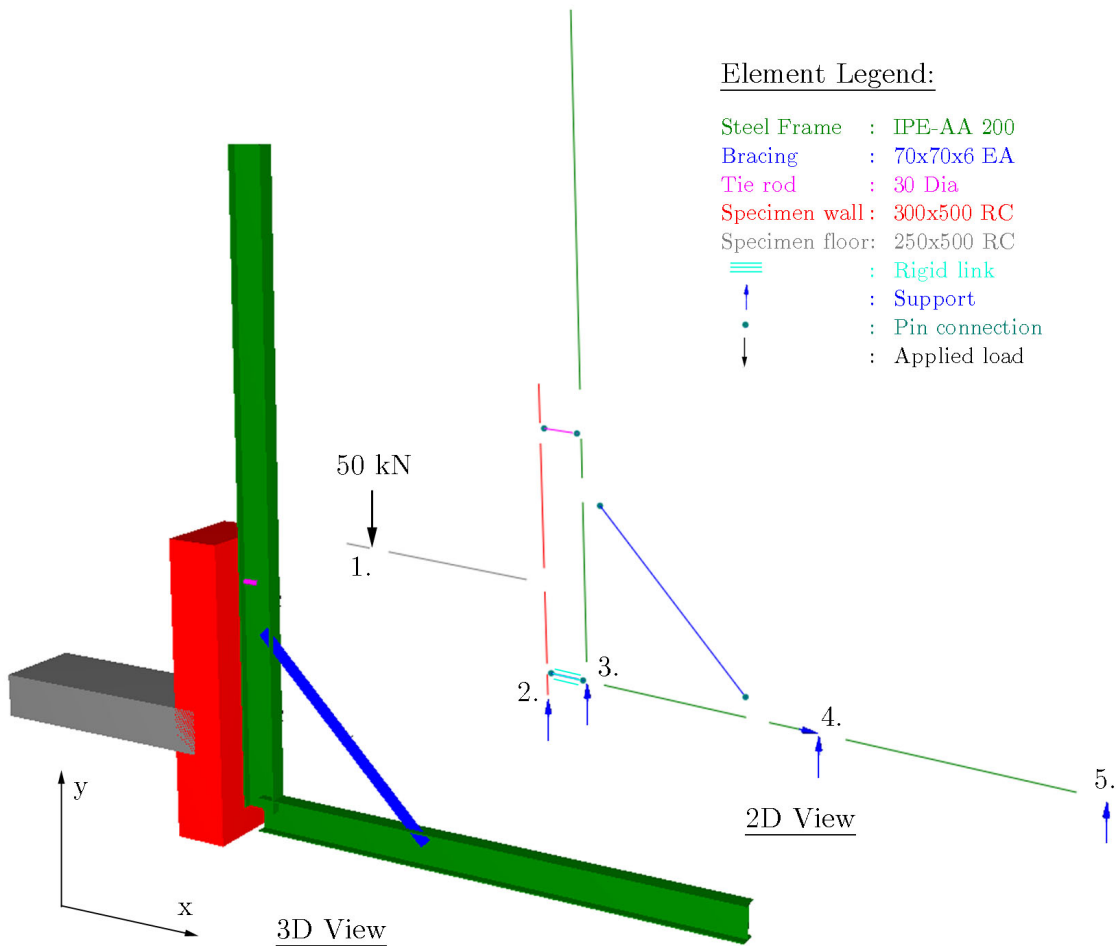


Figure 3.13: Steel A-frame FE Model

The Frame module in the Prokon software package was used for the FEM and analysis. The design of the steel frame included two identical A-frame structures, supporting the specimen at two points 800 mm apart. This symmetry was used to simplify the analysis by only modelling one of the A-frames and assuming that the applied load would be transferred evenly between the two supporting points. Figure 3.13 illustrates the frame model.

Beam elements were used for both the concrete specimen and the steel frame. A rigid link was also defined between the bottom of the wall and the steel frame. This was done to accurately simulate the contact between the specimen and the frame at this point. The load of 50 kN was applied at node 1. While the boundary conditions were defined at node 2, 3, 4 and 5 in the directions as indicated.

A second order analysis was performed and the results are presented in Figure 3.14. Both the deformed shape and axial forces are shown. The moments in the steel elements were insignificantly small and are therefore not included. The elastic displacement at node 1 was 2.37 mm in the x-direction. Although this is a relatively small displacement, a decision was made to put instrumentation in place to measure any movement of the frame and to adjust the measured displacement at the tip of the cantilever floor accordingly.

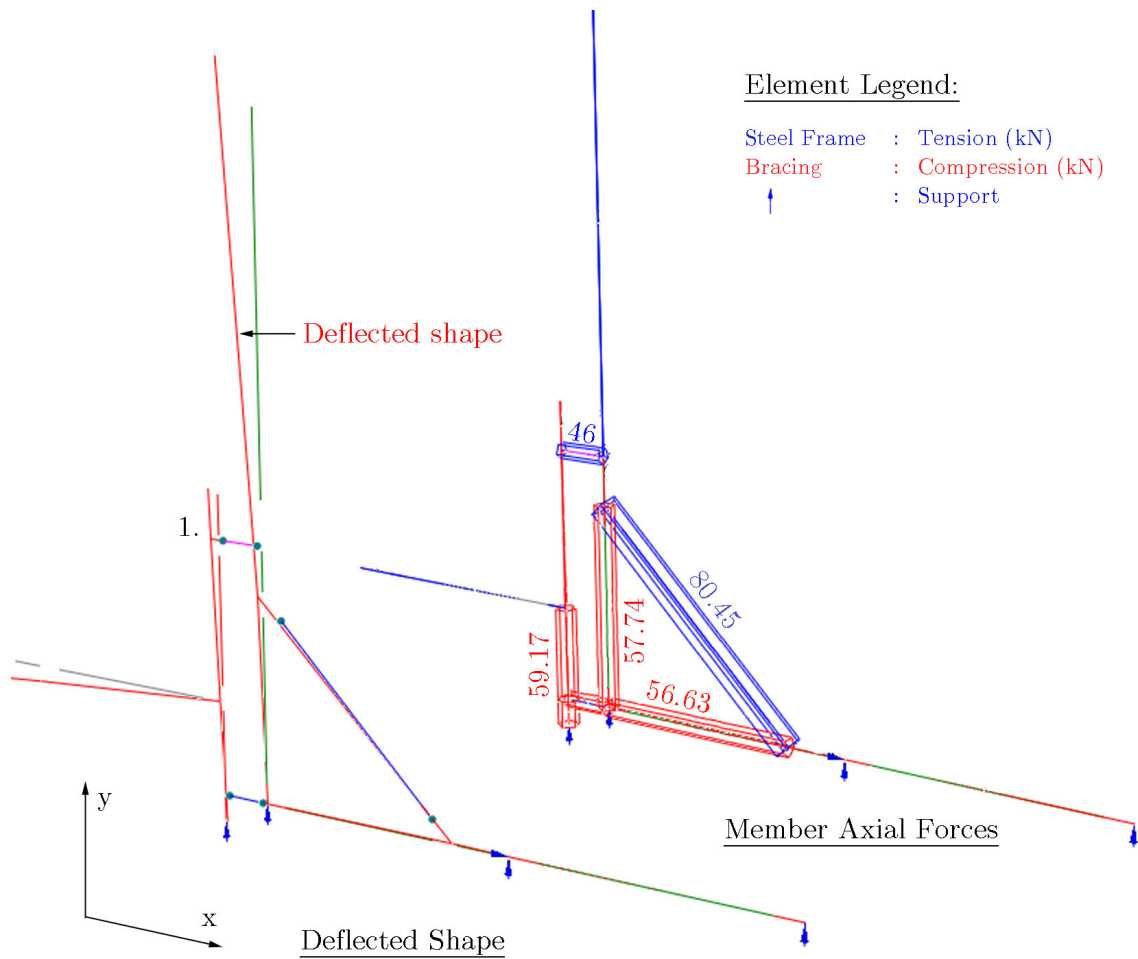


Figure 3.14: Steel A-frame FEA Results

The members and connections for the steel A-frame were designed according to SANS 10162-1:2011. The detailed design calculations are presented in Appendix F. The member sizes were all adequate to transfer the applied load to the wall-to-slab connection. M18 bolts were also found to be sufficient in all the steel connections. A photo of the steel A-frame, with the specimen lowered in position, is presented in Figure 3.15.

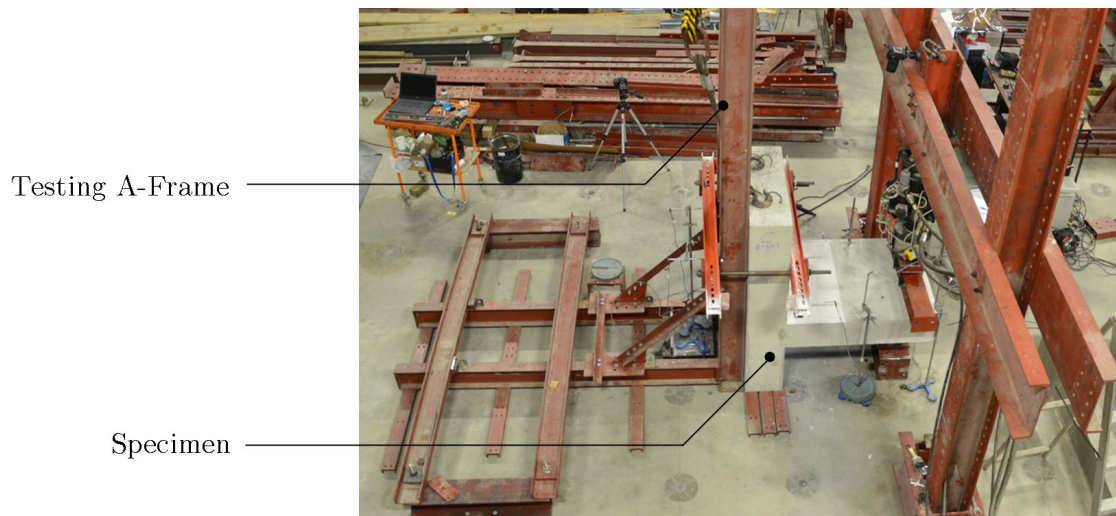
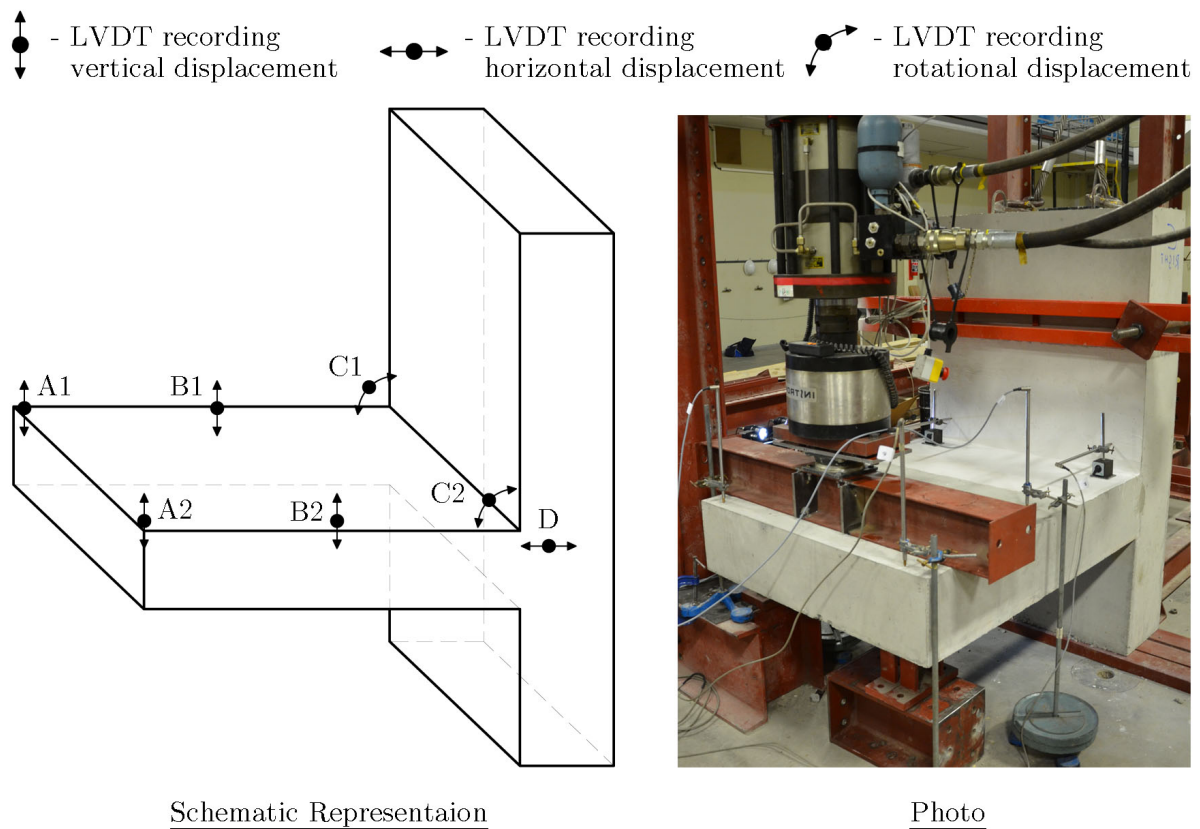


Figure 3.15: Steel A-frame

3.2.4 Measurement Instrumentation

During the experimental testing, the data was captured with the aid of a number of different instruments. A load cell was used to capture the applied load, while seven HBM linear variable differential transformers (LVDT's) were used to measure the structural response of the specimens. The LVDT's were located at specific points along the specimens in order to calculate the relative wall-to-slab displacement. The locations of the LVDT's are presented in Figure 3.16. Any vertical displacement was recorded along the cantilever floor: two LVDT's were located at the tip of the floor, labelled A, and in the middle of the floor, labelled B. At location C, a set-up was installed to record and calculate the joint rotation. The readings on both ends of the floor were recorded to get an average displacement at the centre. An additional LVDT was located at the back of the specimens to record the horizontal movement of the A-frame at a height of 525 mm.



Schematic Representaion

Photo

Figure 3.16: Full-scale Specimen LVDT Set-up

The specimens were covered in a white lime paste, to ensure a smooth and uniform surface and to facilitate location and monitoring of the development of all cracks during the tests. A standard concrete crack width ruler was used to measure the width of all visible cracks at three different stages during the tests. An Aramis camera was also installed to continuously track the crack development in the vicinity of the wall-to-slab joint. The surface of this area was prepared according to the specifications as set out in the Aramis manual. The camera was also calibrated to take the photos at a distance of 900 mm from the specimen. The data was captured on a personal computer and analysed with the Aramis software package (GOM, 2003).

3.2.5 Test Execution Methodology

The overhead crane was used to individually move the specimens, from their original positions, to the testing frame. Great care was taken not to induce excessive handling forces in the specimens. This was accomplished by only lifting the walls by their cast-in lifting hooks thus enabling them to hang freely, during the transport. The only stresses in the connection were thus caused by the self-weight of the cantilever slab.

Once the specimens were in place and tied back to the steel A-frame, the LVDT's were connected at the seven pre-determined positions. The spreader beam was put in place and the Instron was lowered into position, ensuring positive contact between the two sides of the ball-bearing. This was considered the starting position for the tests.

The load was applied at a constant rate, controlled by the displacement of the Instron head. A rate of 1 mm/min was used. The tests were divided into three phases. The first phase continued until the applied load generated a moment and shear force that were equal to the SLS of the connection. This point will hereafter be referred to as stage 1 of the tests and corresponded to an applied load of 40.5 kN. At this point, the tests were paused for 10 minutes, keeping the position of the Instron constant. Visible cracks were measured and photographed.

After the pause, the tests continued into the second phase, with the increased load applied at the same rate. The second phase was terminated when the applied load reached the ULS load, equal to around 49.5 kN. This will be considered as stage 2 of the tests. During the 10 minute pause, the crack widths were once again measured and recorded. Finally, the last phase of the tests continued until the specimens failed. This point was reached, either when the applied load dropped below 50 % of the calculated ULS load, or when the load jack ran out of travel. The maximum travel for the load jack was around 80 mm. This point will hereafter be referred to as stage 3.

3.3 Tensile Tests

In order to understand the effect of cold-bending and straightening on the material properties of reinforcement, a series of tensile tests was also conducted. The specimens included a set of Y10 and Y12 deformed bars. These are typical diameters used in wall-to-slab connections as larger diameters are not suitable for cold bending on site. Half of each set was tested as straight bars, while the remaining bars were cold bent and straightened after two weeks, before being tested.

The reinforcing bars used inside the different full-scale models, as discussed in section 3.2, were also tested to determine their material properties.

3.3.1 Test Configuration

All the tensile tests were performed with a Zwick Universal Testing Machine. The machine has a capacity of 250 kN and is calibrated according to national standards. Two special grips, for clamping the rebar specimens, were installed on the two cross heads of the machine. The grips have triangular grooves, cut in each half, to ensure that the axis of the specimen coincide with the direction of the applied load. The surface of each grip is also sufficiently roughened in order to minimise slippage. Further, the specimens are also clamped in such a way, that the ribs on the deformed bars are placed within the grooves on the grips, to ensure maximum traction. All the tensile tests complied with the specifications of SANS 6892-1:2010 - Metallic materials - Tensile Testing, Part 1: Method of test at room temperature. The test configuration is shown in Figure 3.17.

3.3.2 Test Specimens

Both sets of Y12 and Y10 rebar were ordered from a local bending yard. The reinforcement was locally manufactured at Arcelor Mittal, under the registered trade name NOSTRA[®], and comply with the specifications of SANS 920:2011 for 450 MPa deformed reinforcement bars.

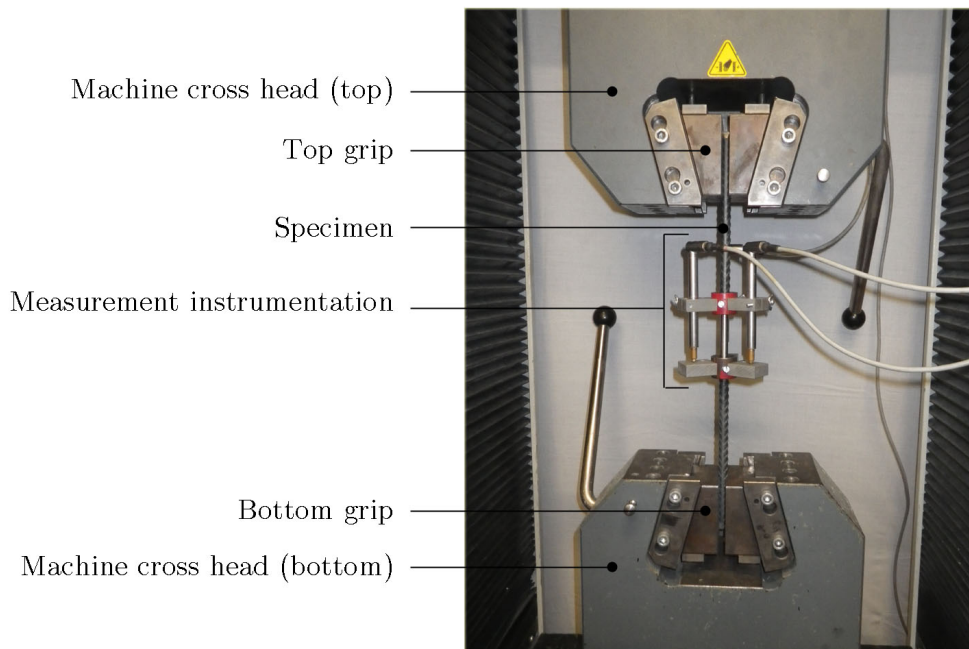


Figure 3.17: Tensile Testing Configuration

In practice, the contractor will order the starter-bars for a bend-out system after receiving the bending schedule from the design engineer. The time between the bending of the rebar at the bending yard and the straightening of the cast-in starter-bars on site will vary between projects. In order to standardise the tensile tests, while trying to simulate practice as closely as possible, the following procedure was adopted:

All the bars in a set were cut from the same batch of steel, into 500 mm lengths. Half of the bars in each set were bent to a 90° angle. The bars were bent using a standard bending table, as shown in Figure 3.18. The diameter of the mandrel used for bending all the rebar was 36 mm, as previous research concluded that the bending radius has little effect on the material properties of the straightened rebar. (Cairns, 2010) The diameter (Φ) does however comply with the minimum bending radius ($3 \times \Phi$) for deformed rebar, as set out in SANS 920:2011 - Steel bars for concrete reinforcement. (SANS, 2011c)

The bent bars were all straightened after 14 days, simulating the usual time lapse between the bending of the rebar and the straightening on site. The bars were placed in a table vice clamp and straightened using a pipe as lever arm, as shown in Figure 3.19. A constant force was applied in a single motion, until the bar was reasonably straight. In some cases the bars were further clamped and straightened, within a tolerance of 3°, to ensure they are straight enough to fit between the cross heads of the testing machine. Refer to Figure 3.19 for an illustration of the straightening process.

It should be noted that, during the straightening process, the bars were not hammered or tampered with in order to apply the principle of best practice. It is acknowledged that, in practice, some hammering may be present on site, which is not simulated in this experimental investigation. The results are therefore a comparison between the material properties after best practice was applied.

The set of Y12 and Y10 straight bars were machined to a constant diameter, according

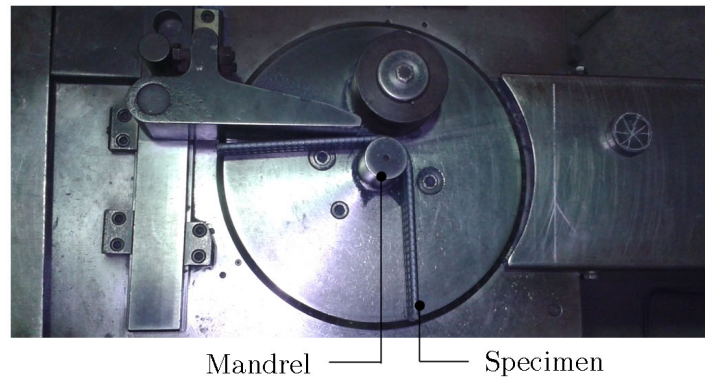


Figure 3.18: Typical Reinforcement Bending Table

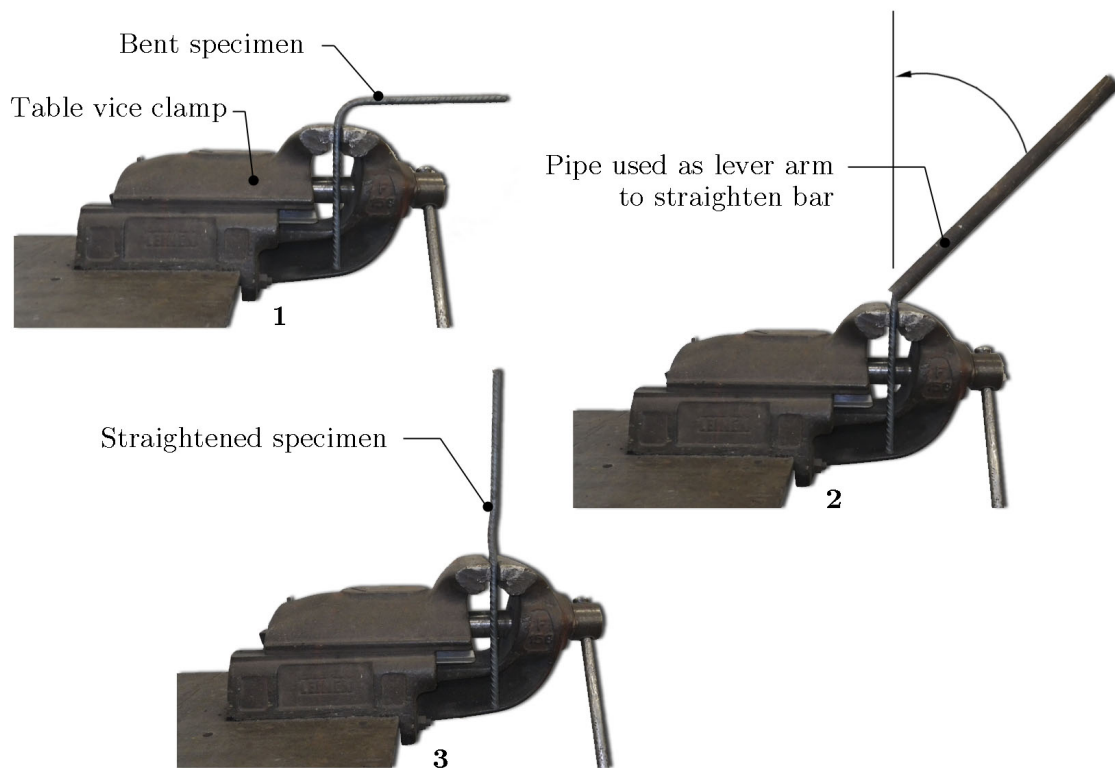
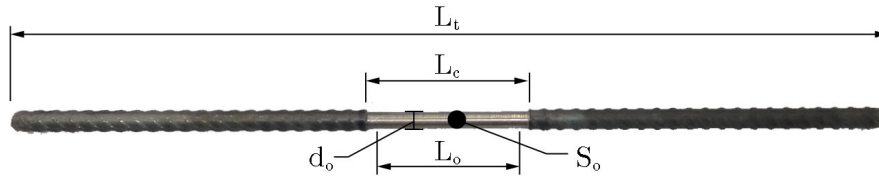


Figure 3.19: Reinforcement Straightening Procedure

to SANS 6982-1:2010. The parameters for the Y10 and Y12 specimens are presented in Table 3.2, while their definitions are illustrated in Figure 3.20.

The reinforcement used in the full-scale models was also tested. Three 500 mm long bars were cut from the same batch of steel and used for the reinforcement in all the walls. Similarly, three additional continuation bars, for the cast-in anchor system, were also cut to 500 mm lengths. Both sets of straight bars were machined to the dimensions as set out in Table 3.2.

The rebar used for the starter-bars, in both the continuous system and the site-installed

**Figure 3.20:** Machined Specimen**Table 3.2:** Parameters for Machined Specimens (mm)

	Y10	Y12
Original diameter (d_o)	8	10
Parallel length (L_c)	100	100
Original gauge length (L_o)	80	80
Total length of test piece (L_t)	500	500
Original cross-sectional area of parallel length (S_o)	50.27	78.54

bend-out system, came from the same batch of steel. Subsequently, six 500 mm bars were cut from this batch. Three were bent at 90° in the same manner as described before. The rebars intended for the modified bend-out system were delivered from the local manufacturer, already assembled inside a steel casing. One additional starter-bar, from the same batch, was requested to be left outside the assembly. The legs of this bar were cut on either side of the 90° turn, in order to be tested once straightened. The bent bars for the tensile testing sets, and the corresponding bars cast inside the full-scale models, were straightened on the same day to ensure consistency.

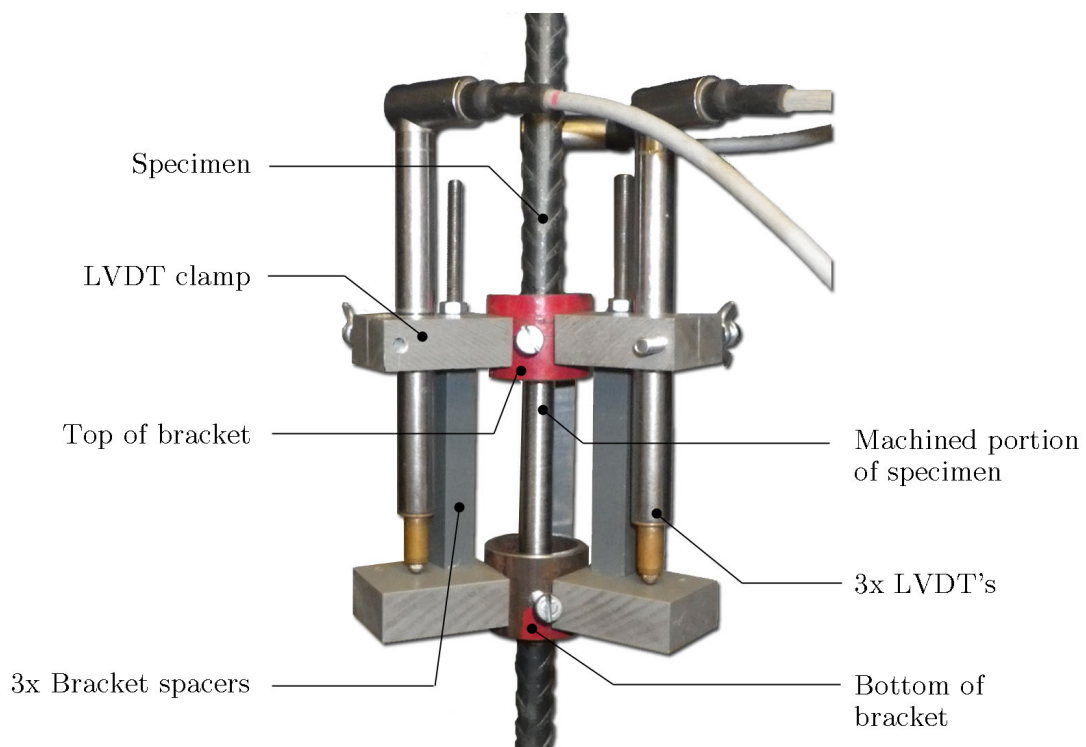
A summary of the specimen sets are presented in Table 3.3, with the abbreviations that will be used hereafter to identify the different sets of rebar.

3.3.3 Measurement Instrumentation

In order to record the relevant information during the tensile testing, three different instruments were used. The applied tensile force was measured with the load cell of the testing machine. The displacement over the total length of the specimen was captured through the cross head separation of the machine, while the extension over the gauge length was recorder by three LVDT's. The three LVDT's were fixed to a custom made bracket manufactured in the structural laboratory workshop. The brackets are designed to fix directly to the specimen, while keeping the three LVDT's at equal spacings around the bar. They are also kept in place at exactly the same distance from the centre, as shown in Figure 3.21. By taking the average reading between the three LVDT's, any eccentricity in the alignment of the specimen did not have an effect on the results. All the data was channelled and recorded with a Spider8 data recorder and stored on a personal computer. The recording frequency was 10 Hz.

Table 3.3: Tensile Testing Specimen Sets

	No. off	Abbreviation
<u>Preliminary Tensile Testing</u>		
Y10 straight bars (Machined)	20	Y10-S
Y10 bent and straightened bars (Not Machined)	20	Y10-B
Y12 straight bars (Machined)	20	Y12-S
Y12 bent and straightened bars (Not Machined)	18	Y12-B
<u>Reinforcement Used in Full-scale Models</u>		
Y12 straight wall bars (Machined)	3	Y12-WR
Y12 straight starter-bars - Model A (Machined)	3	Y12-FRA
Y12 bent and straightened starter-bars - Model B (Not Machined)	3	Y12-FRB
Y12 bent and straightened starter-bars - Model C (Not Machined)	2	Y12-FRC
Y12 straight continuation bars - Model D (Not Machined)	3	Y12-FRD

**Figure 3.21:** Tensile Testing LVDT Set-up

3.3.4 Test Execution Methodology

The tensile testing was conducted according to the specifications of SANS 6892:2010. The gauge length (L_0) for the machined bars was fixed at 80 mm and the LVDT bracket was adjusted accordingly. The gauge length for the straightened specimens had to be adjusted to 100 mm in order to fit over the kink in the bars.

The original diameter for the straight bars was measured with a vernier scale at three different points along the parallel length. The average measurement was used to calculate the original cross-sectional area (S_0). It was not possible to determine an original diameter for the straightened bars, as they were not machined. Equation 3.1 was subsequently used to determine an effective cross sectional area, based on the weight (K) and length (L) of the bar.

$$S_0 = \frac{K}{0.007 \times 85 \times L} \quad (3.1)$$

(SANS, 2010)

The brackets with the three LVDT's were fixed around the specimen and placed inside the testing machine. The gauge spacers were removed and the load cell zeroed before the grips were lowered. Prior to the start of the test, a pre-load of 1000 N was applied to ensure the specimens were securely fixed inside the grips. The pre-load value of a 1000 N falls well within the limit of 5% of the expected yield strength, as proposed by the code, for both the Y12 and Y10 specimens. The speed of the testing was fixed at a constant load rate of 600 N/s. Although this resulted in a range of testing deformation and stress rates due to the difference in original cross sectional areas between the specimens, it always satisfied the minimum requirement of 6 MPa/s without exceeding the upper limit of 60 MPa/s. This requirement can be found in Table 3 of SANS 6892-1:2009, under materials with a modulus of elasticity above 150 MPa. The data was captured at a rate of 10 readings per second to ensure all high and low points were accurately recorded.

It was observed that, once the applied stress passed the yield point and strain hardening started, the LVDT bracket became loose and sometimes shifted, resulting in readings that were not accurate. The test was therefore momentarily paused at this point in order to remove the slipping LVDT bracket and resumed thereafter. It was subsequently impossible to measure the total elongation of the specimens and could therefore not determine the reduced ductility in cold bent reinforcement. The test automatically stopped once the applied load fell below 50% of the ULS load.

The methods as set out in SANS 6892-1:2010 were used to determine the material properties of each specimen.

The average LVDT displacement was determined for each reading and divided by the original gauge length to calculate the strain at each reading. The applied load was similarly divided by the original cross sectional area to determine the corresponding engineering stress. This data was then used to plot a stress-strain curve (SANS, 2010).

The E-modulus (E) was determined by first plotting a trend line for the data in the linear portion of the stress-strain graph and then using the gradient of that line as the value for E (SANS, 2010).

The yield stress (f_y) was determined by one of two possible methods based on the shape of the stress-strain curve. When the curve had a definite linear portion up to a certain

point and then flattened, as seen in Figure 3.22, the yield stress (f_y) was taken as the stress value corresponding to that point on the graph. If, however, the stress-strain curve had no definite point at which it flattened and the gradient for the linear portion just gradually reduced to create a curved graph, then the offset method was used. The South African code does permit the use of this method, but does not provide the necessary details to be followed (SANS, 2010). The ASTM - Standard Test Methods for Tension Testing of Metallic Materials was therefore consulted and the procedure in this code was followed.

A line with a gradient equal to the modulus of elasticity (E) was plotted on the stress-strain graph. The position of the line was chosen so that the x-axis (representing the strain) was intercepted at 0.002 mm/mm or 0.2%. Next, the point of intersection between the offset line and the stress-strain curve was established graphically. The yield stress (f_y) was then assumed to be the stress corresponding to the point of intersection, as illustrated in Figure 3.23 (ASTM Committee on Standards, 2011).

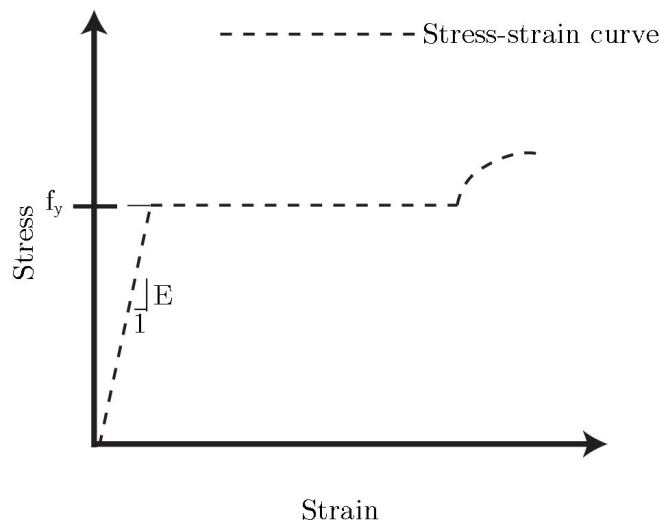


Figure 3.22: Determination of Yield Stress - Direct Method

The ultimate engineering stress (f_u) was recorded as the highest applied load during the test divided by the original cross-sectional area of the rebar.

3.4 Low-cycle Fatigue Tests

Research has shown that, apart from a reduction in the E-modulus and yield strength of steel, cold bending and straightening can also make the steel more brittle due to a reduction in the ductility of the steel. This was especially evident in reinforcing bars due to its high carbon content (Campillo *et al.*, 1996). As cold bending is inevitable when using any of the bend-out systems, brittle failure of the starter-bar legs could occur when they are straightened on site.

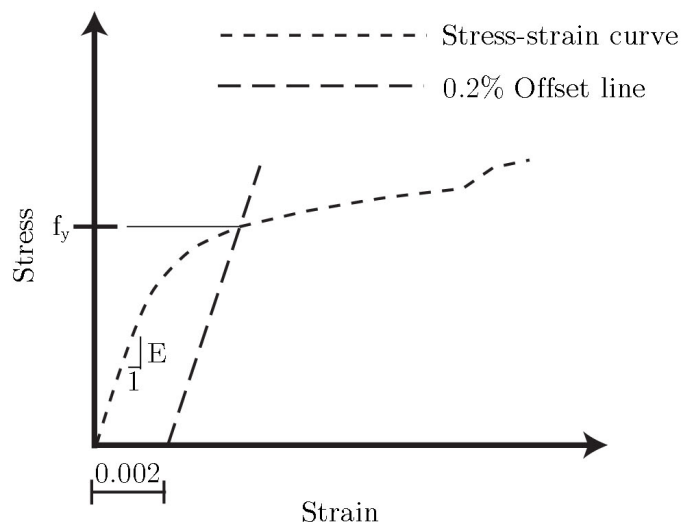


Figure 3.23: Determination of Yield Stress - Offset Method

In order to investigate the effect of this low-cycle bending on the yield strength and ductility of the steel, a series of fatigue tests were conducted by Tino Muzofa at Stellenbosch University.

3.4.1 Test Configuration

The same test configuration, as described in section 3.3 for the tensile testing, was used. The results were also presented through stress-strain curves, from which a yield stress was determined.

3.4.2 Test Specimens

The average results for the Y12-S and Y10-S sets were used as the benchmark yield strength before any cold working has occurred. The results from the Y12-B and Y10-B sets were subsequently used to reflect the corresponding effect of rebar being cold bent and straightened once. Two further sets of Y12 and Y10 bars were taken from the same batch of steel and bent a second and a third time, to simulate two different degrees of cold cycle bending. A summary of the different sets are presented in Table 3.4.

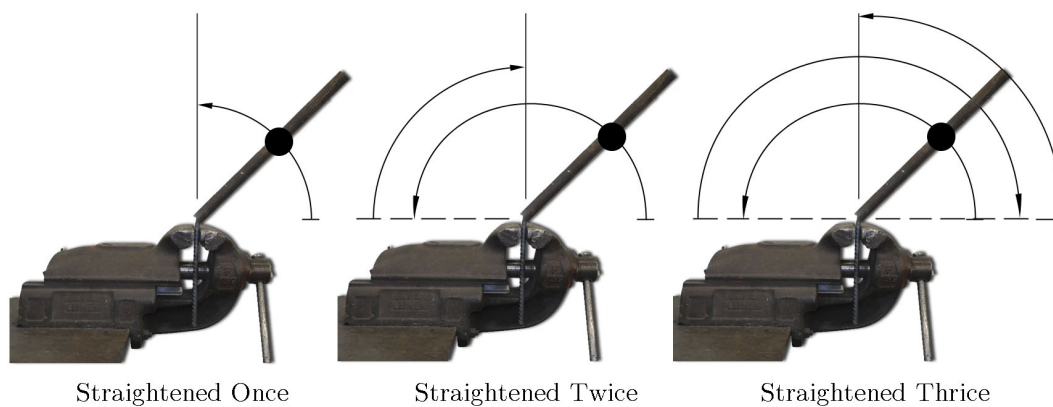
The bending and straightening process was conducted in the same way as described in section 3.3. Figure 3.24 illustrates the three different degrees of cold bending investigated.

3.4.3 Test Execution Methodology

The straight bars, ie. Y10-0 and Y12-0, were tested according to the same procedure as described in section 3.3.4. The sets of straightened bars were subjected to tensile testing according to the specifications as set out in SANS 6892:2010. The gauge length was also set to 100 mm and equation 3.1 was used to determine the original cross sectional area (S_o).

Table 3.4: Low-cycle Fatigue Testing Specimen Sets

	No. off	Abbreviation
Y10 straight bars (Machined)	20	Y10-0
Y12 straight bars (Machined)	20	Y12-0
Y10 bent and straightened once (Not Machined)	20	Y10-1
Y12 bent and straightened once (Not Machined)	18	Y12-1
Y10 bent and straightened twice (Not Machined)	5	Y10-2
Y12 bent and straightened twice (Not Machined)	5	Y12-2
Y10 bent and straightened thrice (Not Machined)	5	Y10-3
Y12 bent and straightened thrice (Not Machined)	5	Y12-3

**Figure 3.24:** Degrees of Low-cycle Bending and Straightening

A stress-strain curve was plotted for each specimen and the yield stress was determined using the offset method, as described in section 3.3.4. The average yield strength was then determined for each set of specimens, in order to determine the effect of multiple low cycle bending on the strength of the bars.

3.5 Supplementary Tests

The E-modulus and compressive strength of the concrete used in the full-scale models had to be determined in order to establish the material properties of the concrete for modelling purposes. The cylindrical and cube specimens, cast on the same day as the full-scale models, were used to determine the material properties of the concrete at the time of the full-scale testing. The specimens were stored and cured in the same manner as the full-scale models in order to simulate the curing and storage conditions as closely as possible. The tests were all conducted by Tino Muzofa, in the Structural Laboratory at Stellenbosch University.

3.5.1 Compressive strength

Concrete cubes were frequently tested to monitor the strength development of the concrete. The first cubes were tested 7 days after they were cast and the remainder of the cubes on the day of the full-scale testing.

An uniaxial compression test was performed to determine the compressive strength. The tests were conducted according to the specifications as set out in SANS 5863. The tests were performed in a Contest Grade A compression test apparatus. A loading rate of 180 N/s was used, as prescribed in the code for a 100 mm x 100 mm cube specimen (SANS, 2006).

The compressive strength (f_{cu}) was calculated using Equation 3.2:

$$f_{cu} = \frac{F_s}{A} \quad (3.2)$$

F_s is the maximum load applied to the specimen, prior to crushing

A is the cross sectional area of the specimen normal to the applied load

(SANS, 2006)

3.5.2 E-modulus

There is no specific South African National Standard that prescribes the procedure to be used when determining the E-modulus of hardened concrete. The British standards were therefore consulted and the procedure, as set out in BS EN 12390-13:2013, was followed.

Cylindrical specimens, 200 mm high and 100 mm in diameter, were used. (BSI, 2013) These E-modulus tests also coincided with the full-scale tests. The floor specimens were tested 42 days after they were cast, while the wall specimens were tested after 48 days.

Cube specimens were crushed on the same day as testing, in order to determine the compressive strength of the concrete. The compressive cube strength (f_{cu}), was multiplied by a factor of 0.8 to convert the strength to a cylindrical compressive strength (f_{ck}). The cylindrical compressive strength was used to calculate the upper and lower limits, σ_a and σ_p , for the loading cycle, using Equations 3.3 to 3.5. Refer to Figure 3.25 for the full loading cycle.

$$\sigma_a = \frac{f_{ck}}{3} \quad (3.3)$$

$$-0.10 \leq \sigma_b \leq 0.15 \times f_{ck} \quad (3.4)$$

$$-0.5 \leq \sigma_p \leq \sigma_b \quad (3.5)$$

The load was applied through a 2000 kN capacity hydraulic actuator (Instron). The strains were measured with three LVDT's. The LVDT's were placed inside custom made

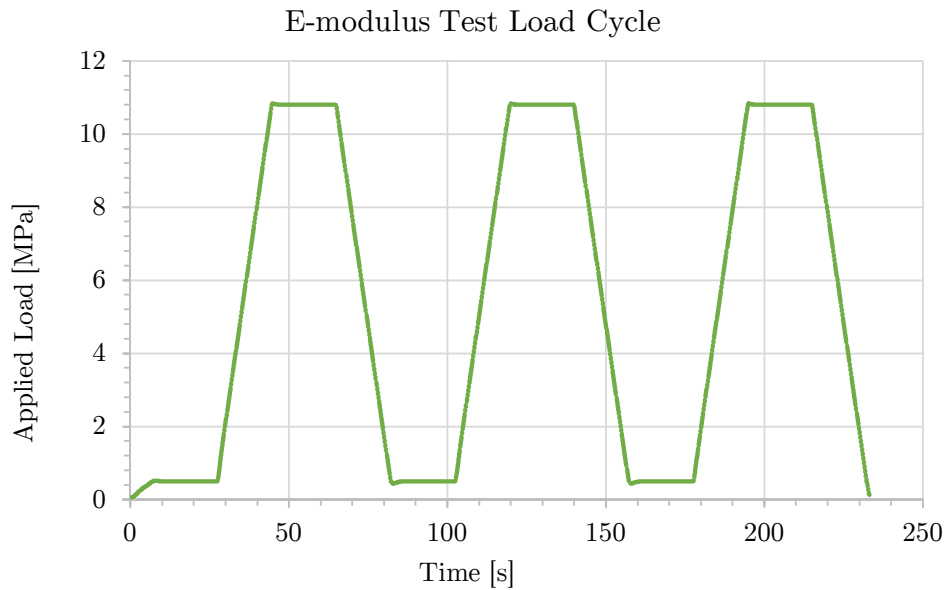


Figure 3.25: E-modulus Test Load Cycle

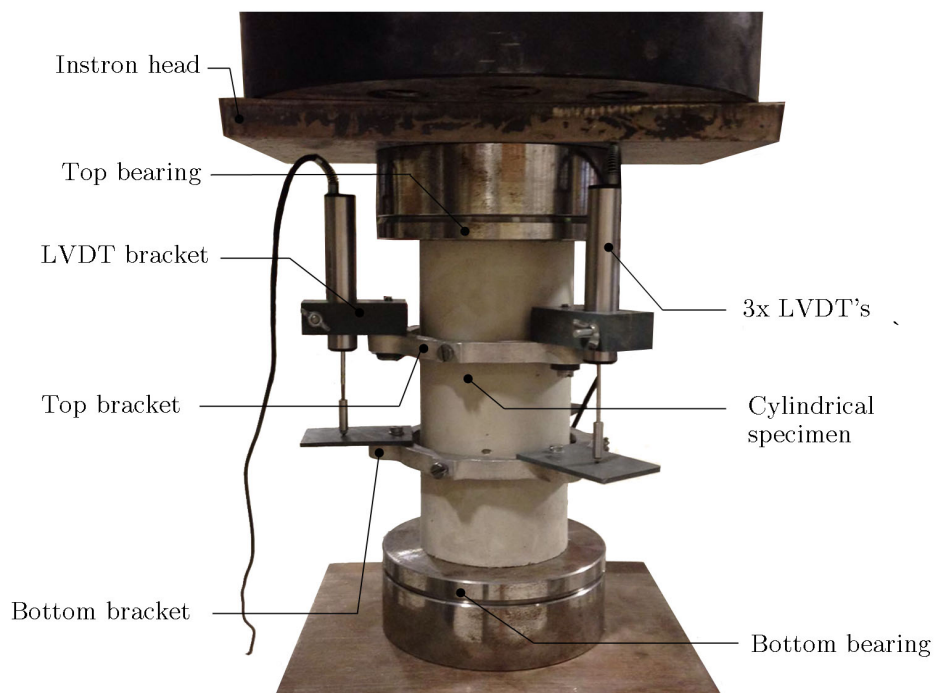


Figure 3.26: E-modulus Test Set-up

brackets, equally spaced around each specimen. The gauge length for the test was 70 mm. Figure 3.26 illustrates the full test set-up.

The data from each test was used to develop a stress-strain curve, from which the E-modulus could be established by using Equation 3.6.

$$E = \frac{\sigma_a^m - \sigma_p^m}{\varepsilon_{a,3} - \varepsilon_{p,2}} \quad (3.6)$$

σ_a^m is the measured stress corresponding to nominal upper stress, σ_a^m

σ_p^m is the measured stress corresponding to nominal preload stress, σ_p^m

$\varepsilon_{a,3}$ is the average strain at upper stress on loading cycle 3

$\varepsilon_{p,2}$ is the average lower stress on loading cycle 2

(BSI, 2013)

Chapter 4

Experimental Results

4.1 Introduction

This chapter presents the results of all the experimental tests conducted in this research investigation. The details surrounding the tests are discussed in section 3.

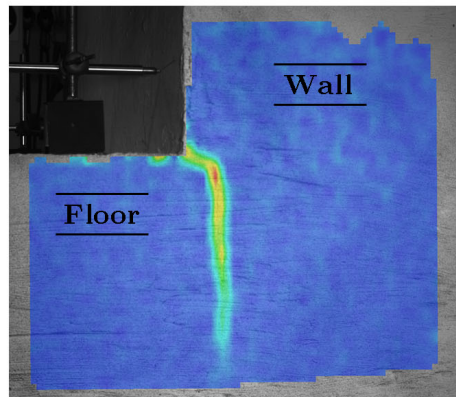
The results and observations for the full-scale tests are presented first in section 4.2, followed by the tensile testing results in section 4.3. The results from the low-cycle fatigue tests and a summary of the supplementary test results are presented in sections 4.4 and 4.5.

4.2 Full-scale Tests

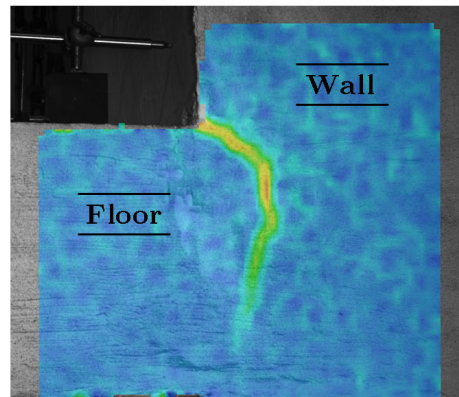
4.2.1 Test Observations

This section provides a summary of the observations made during the full-scale tests with a focus on a comparison between the crack development in the different specimens. The comparisons are drawn at the three different stages during the tests, as described in 3.2.5.

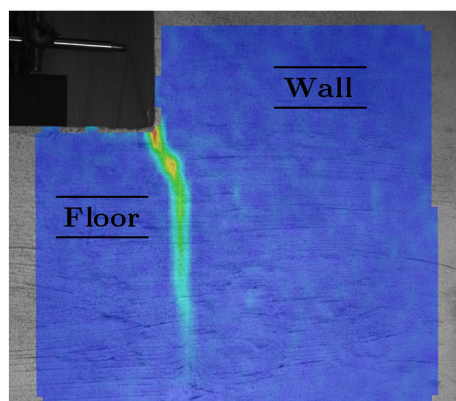
Figure 4.1 presents the crack patterns at stage 1 of the tests. Photos captured by the Aramis camera are superimposed with rendered images indicating the strains measured on the specimens. From these rendered images the crack patterns are clearly visible. The location of the major cracks in all four systems corresponds to the position and shape of the construction joint of the particular system used. All the specimens recorded one major crack of between 0.1 and 0.4 mm, with Model A recording the widest crack of 0.4 mm. This crack was observed on the rear side of the wall and is therefore not visible in Figure 4.1. Apart from this crack, all the other cracks fell within the general limit of 0.3 mm for structures exposed to a serviceability load. (SANS, 2000)



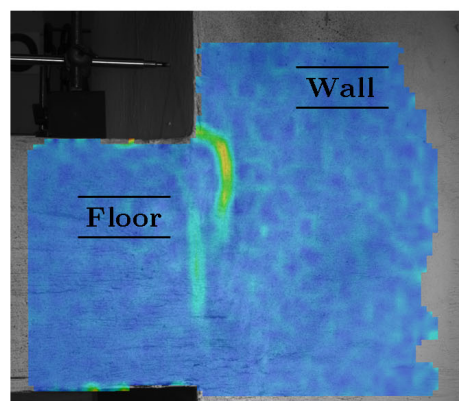
Model A
Continuous Starter-bar System



Model B
Site-installed Bend-out Bar System



Model C
Pre-assembled Bend-out Bar System



Model D
Cast-in Anchor System

Figure 4.1: Cracks at Stage 1 - Wall Joint

Some cracks were also observed on the top of the floor, close to the connecting wall. These cracks were also in the range of 0.1 to 0.4 mm, with the 0.4 mm crack occurring in Model C. Figure 4.2 contains photos of the crack patterns observed in this area.



Figure 4.2: Cracks at Stage 1 - Top of Floor

At stage 2 of the tests, the crack widths increased to a range of between 0.5 and 0.7 mm. The widest crack was observed in Model C. Photos taken at this stage are presented in Figure 4.3, with the largest cracks labelled.

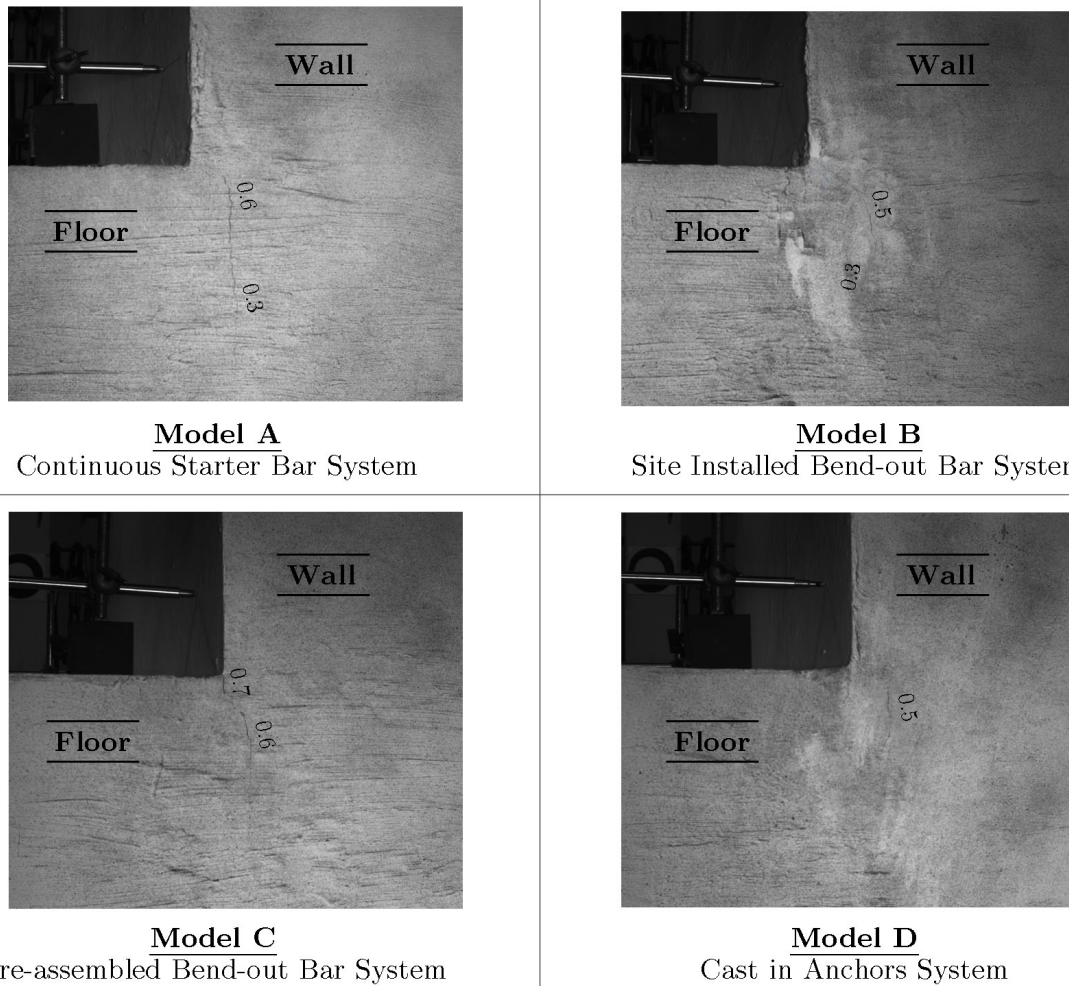


Figure 4.3: Cracks at Stage 2 - Wall Joint

The crack development on top of the floor at stage 2 was similar in size between the different specimens, as seen in Figure 4.4. The structural performance of A and B did however seem slightly better, with Model C and D presenting larger cracks. It was further observed that the number of cracks in all the specimens increased at this stage.

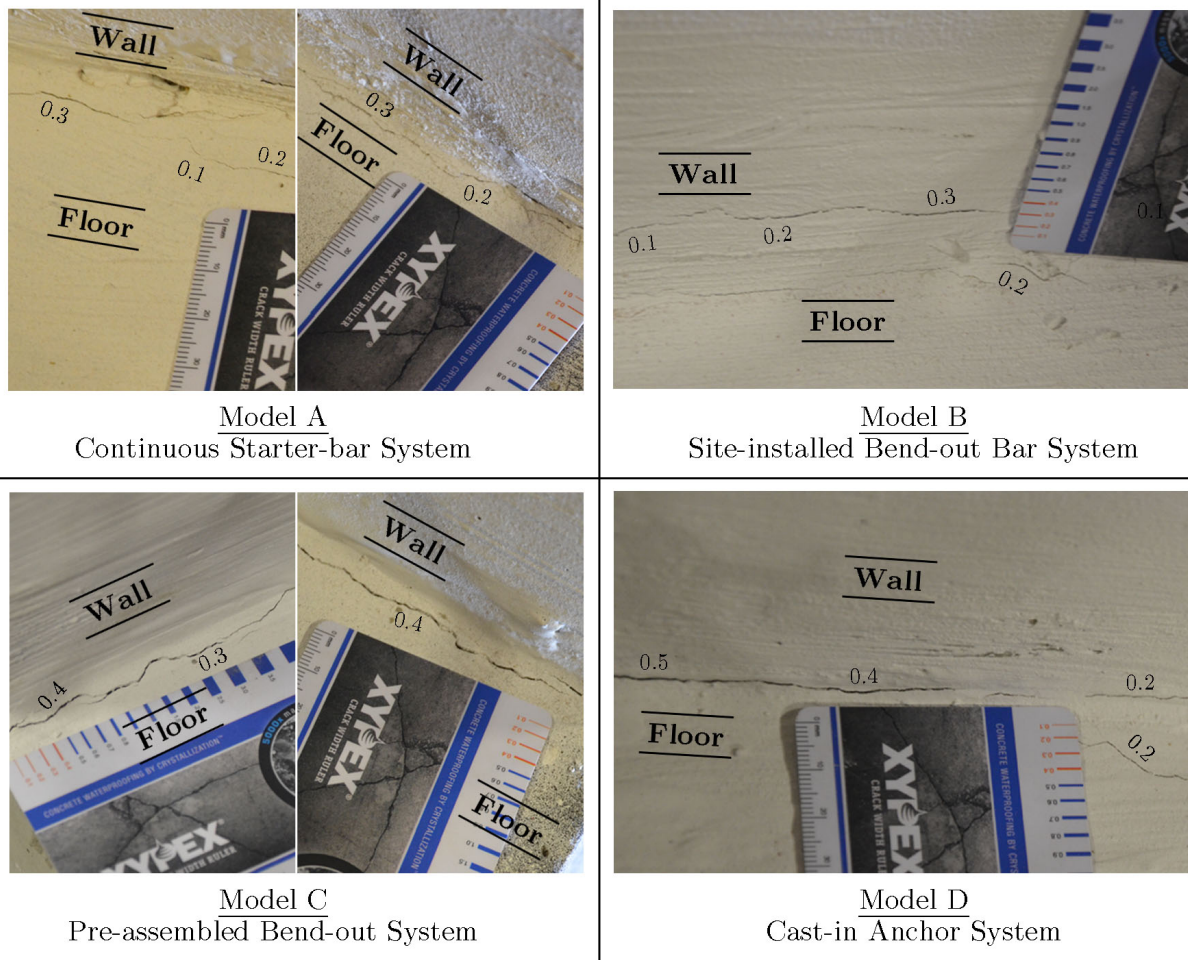


Figure 4.4: Cracks at Stage 2 - Top of Floor

Once the tests went past stage 2, the crack development in the first three systems was similar, both in size and pattern, and was clearly indicative of a connection where the rebar was starting to yield. In contrast to this, the pattern that was observed in Model D strongly suggested a cone pull-out failure.

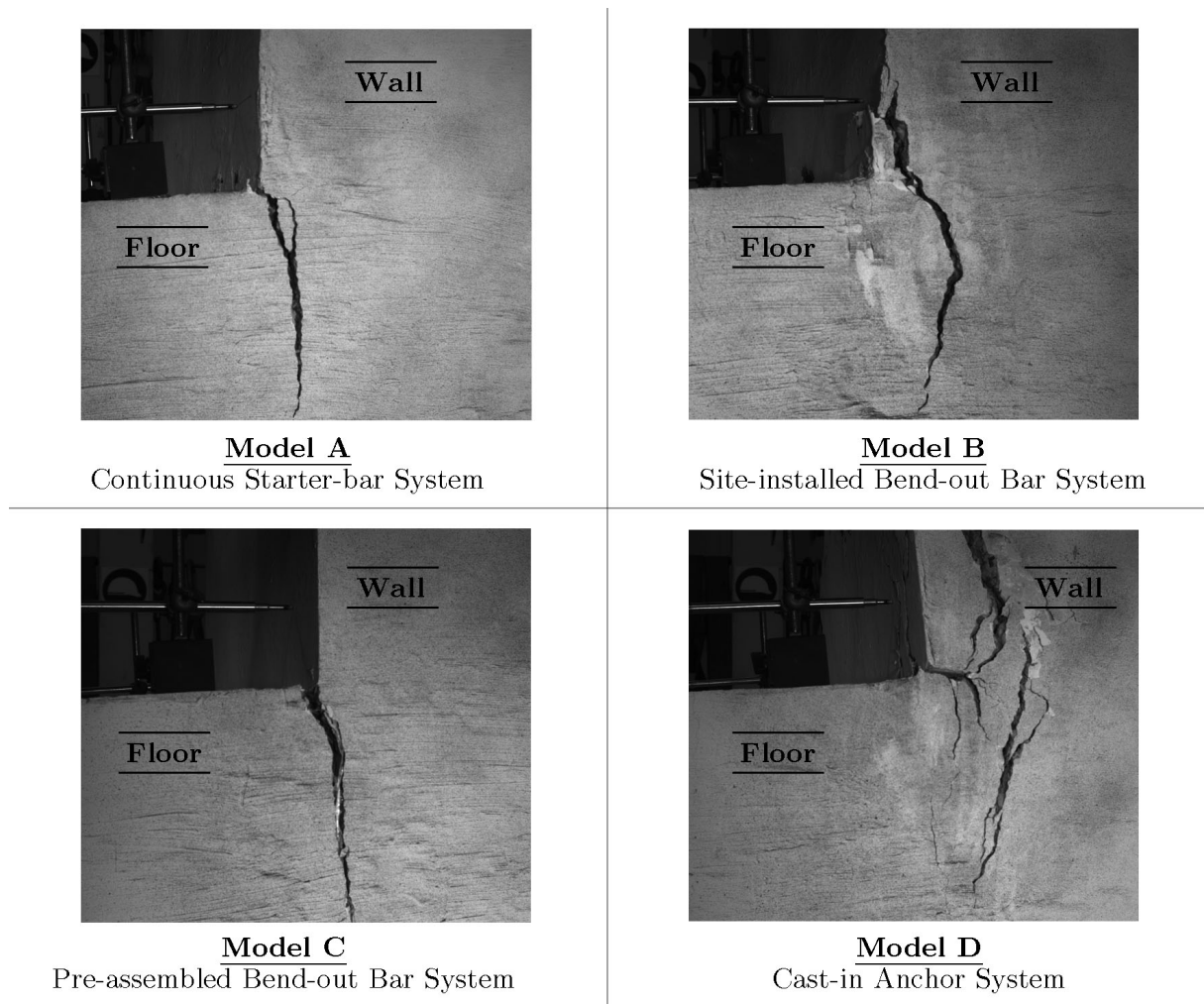


Figure 4.5: Cracks at Stage 3 - Wall Joint

Looking at the photos in Figure 4.5, the cone shaped crack pattern in Model D is clearly visible. Although the initial yielding cracks are also present, the failure mechanism clearly shifted to a cone shaped pull-out failure after stage 2. Looking at Figure 4.6 it is also clear that cone failure was present throughout the width of the specimen.

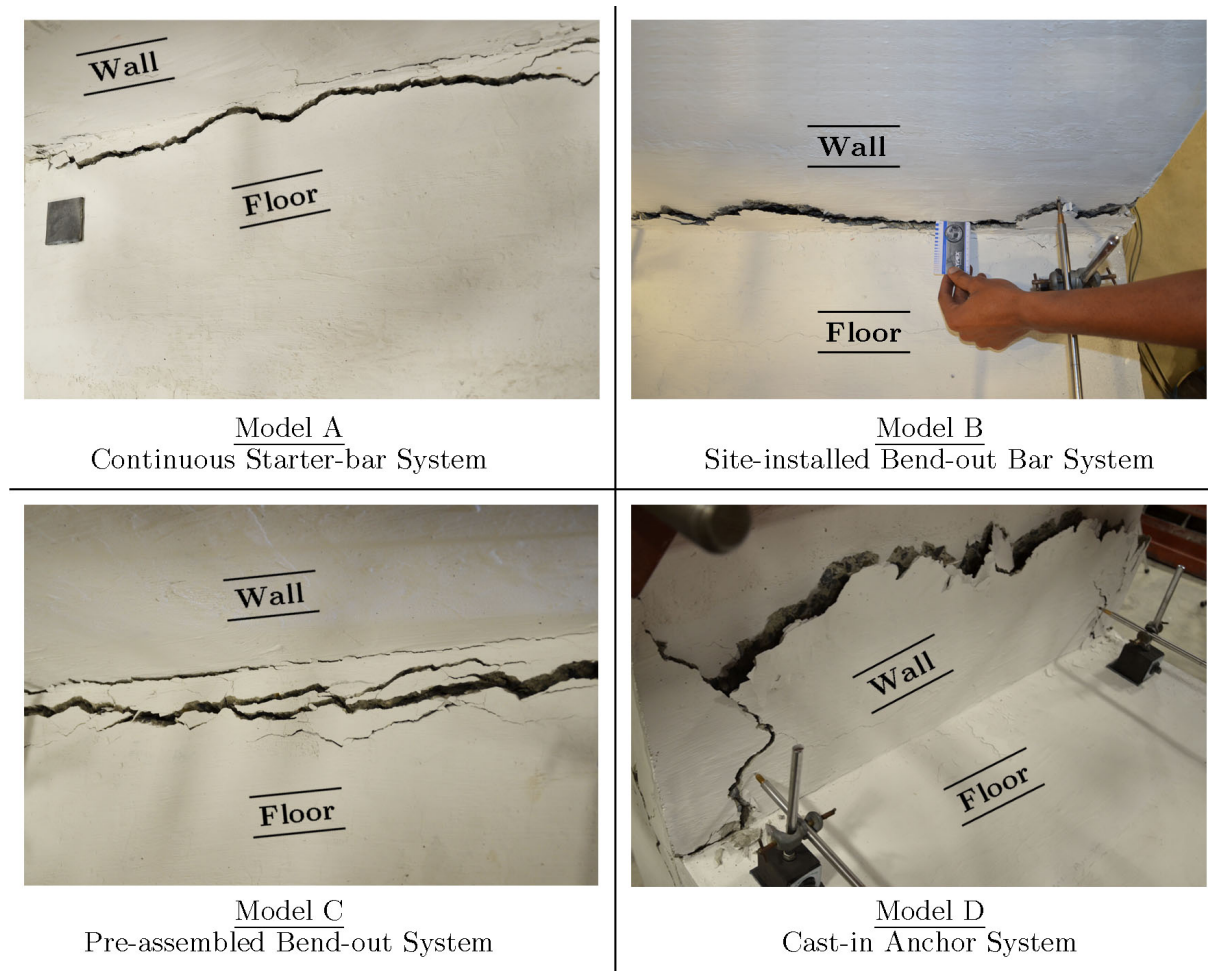


Figure 4.6: Cracks at Stage 3 - Top of floor

4.2.2 Test Results

The data captured during the full-scale tests is presented in this section. The results are presented through several graphs and tables, containing the data for all four models.

The first comparison is between the displacement of the cantilever floor, measured at the tip, for a specific applied load. Figure 4.7 presents this comparison graphically by means of a load displacement curve.

The shapes of all the curves are similar up to a serviceability load of 40.5 kN. However, the graph for Model A does seem to be flatter than the other curves with a perturbation observed just before 40 kN. After this point the graph returns to the general trend observed in the other models. This flatter gradient might have been caused by the bottom portion of the specimen not being fully placed against the supporting frame, resulting in the entire specimen rotating and adding additional displacement at the tip of the cantilever floor. It seems that just before 40 kN this movement suddenly seized, causing the perturbation and bringing the graph back in line with the other models. From this point onwards the curves for Model B and C are flatter compared to that of Model A, indicating a slower tip displacement in Model A for a specific applied load. The shape of the graph for Model A suggests a system that is ductile, ie. can undergo large

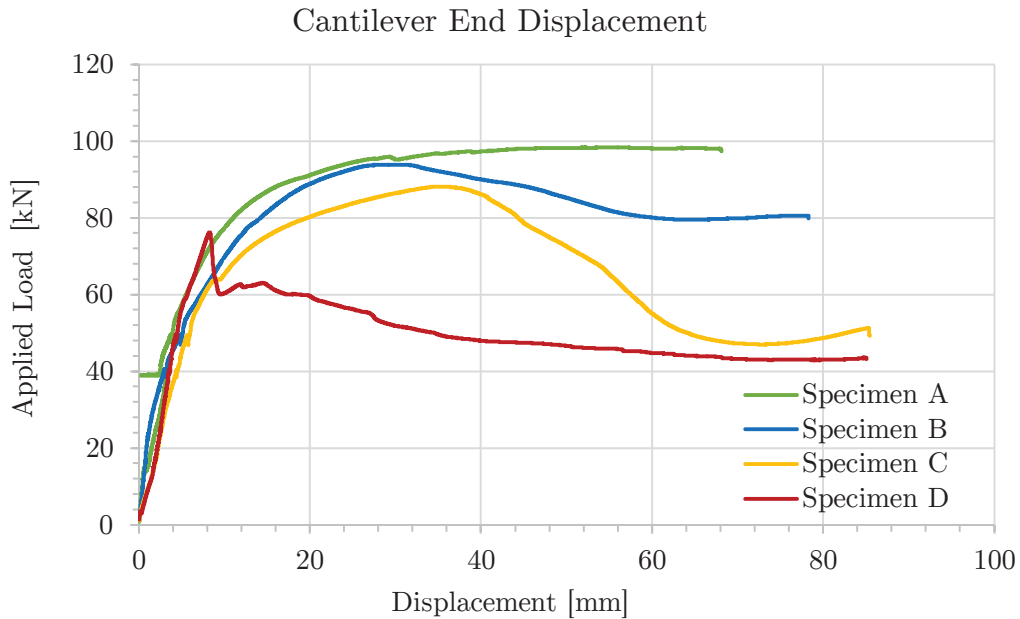


Figure 4.7: Cantilever Tip Displacement vs Applied Load

deformations without total collapse. Ductile failure in connections is preferred over brittle failure, where there is no warning of sudden loss in the resistance (Robberts and Marshall, 2010). Although the behaviour of Model B and C could also be classified as "ductile", the structural performance was not as desirable as in Model A: the point of ultimate resistance was lower with deflection-softening occurring beyond this point. The graph for Model D climbs gradually to the maximum load of 75.86 kN, after which there is a sudden drop in the load. This drop in resistance is followed by a gradual softening response. It has a significantly lower ultimate resistance and the earliest onset of deflection softening of the four models. This behaviour is associated with a pull-out cone failure mechanism, as observed through the crack formation in the previous section.

Figure 4.8 presents a comparison between the displacement, measured at the centre of the cantilever slab, to an applied load at its tip. As expected, the graph produced similar shapes as presented in Figure 4.7. The values are also in the same range relative to one another. Model A once again presented the most ductile behaviour, with the pull-out cone failure mechanism in Model D clearly visible.

The rotation at the connection itself was also recorded and is presented in Figure 4.9. The data for Model D was only reliable up to stage 2 of the test. The cone failure mechanism resulted in a large portion of the wall breaking out just above the connection and rotating with the floor. At this point the readings became inaccurate and the data was therefore not included in the graph. The shape and relative values for the three remaining curves further confirm the observations made in the load-displacement curves already presented.

Table 4.1 presents a summary of the displacements and rotations recorded at the first two stages of the tests.

The tip displacement for Model A, at stage 1, was on average 33 % lower than that of the other Models and 24 % lower at stage 2. Similarly, the displacement of the floor at the middle was 21 % lower at stage 1 and 20 % at stage 2.

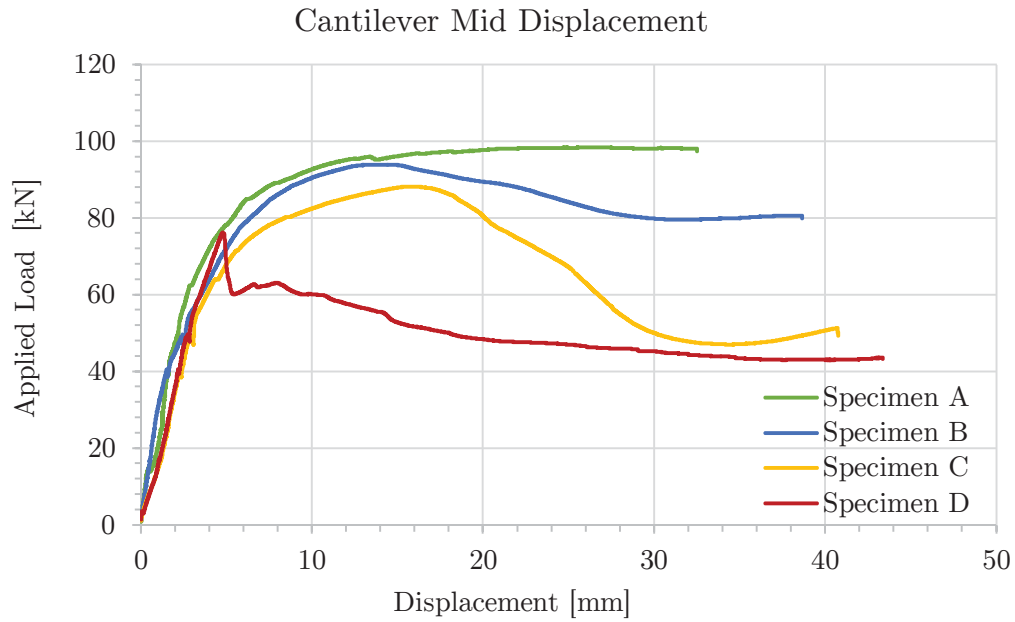


Figure 4.8: Cantilever Centre Displacement vs Applied Load

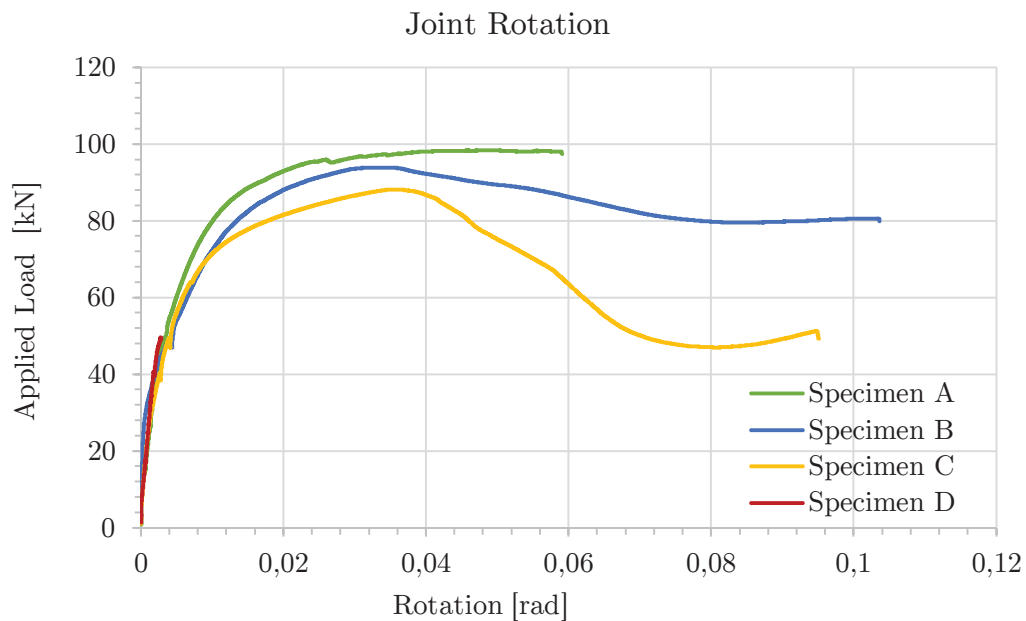


Figure 4.9: Cantilever Rotation vs Applied Load

Table 4.2 presents the ultimate capacities recorded for the models. The ultimate capacity of Model A was 5 % larger than that of Model B, 12 % larger than Model C and 29 % larger than Model D.

Table 4.1: Cantilever Displacement Result Summary

Specimen nr.	Tip Displacement (mm)	Mid Displacement (mm)
Displacement at SLS (Stage 1)		
A	2.5	1.6
B	3.2	1.6
C	4.6	2.4
D	3.6	2.3
Displacement at ULS (Stage 2)		
A	3.8	2.2
B	4.8	2.4
C	6.0	3.1
D	4.5	2.8

Table 4.2: Ultimate Capacity Summary

Specimen nr.	Applied Load kN
A	98.12
B	93.56
C	87.86
D	75.86

4.3 Tensile Tests

The results for the tensile tests are presented and discussed in this section. They are presented through typical stress-strain curves from the different sets of bars, followed by a summary of their calculated yield stresses (f_y), ultimate stresses (f_u) and values for the modulus of elasticity (E). The data from the preliminary tests are presented first, followed by the results for the reinforcement used in the full-scale models.

Any outliers in the experimental results are identified by using the Grubb's test (Grubbs, 1969). The procedure is described in Appendix H.

A full set of all the results can be found in Appendix B. Refer to Table 3.3 for the definitions of the abbreviations used in this chapter.

4.3.1 Preliminary Tests

A stress-strain curve was developed for each specimen tested. The two main sets of bars were the straight bars (S-Series) and bent and straightened bars (B-series). The stress-strain curves of the two sets of specimens were noticeably different. To illustrate this, Figure 4.10 presents a typical stress-strain curve associated with a Y10 bar from the S-series and a Y10 bar from the B-series. Figure 4.11 presents the same comparison, but for a typical Y12-S and Y12-B specimen.

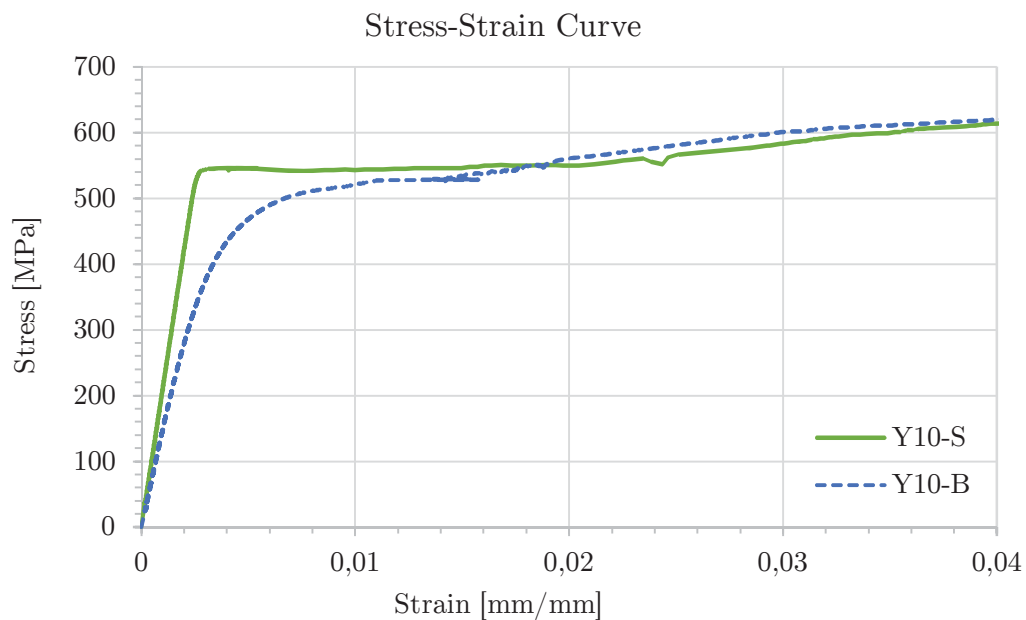


Figure 4.10: Stress-Strain Curve of Y10-S and Y10-B Reinforcement

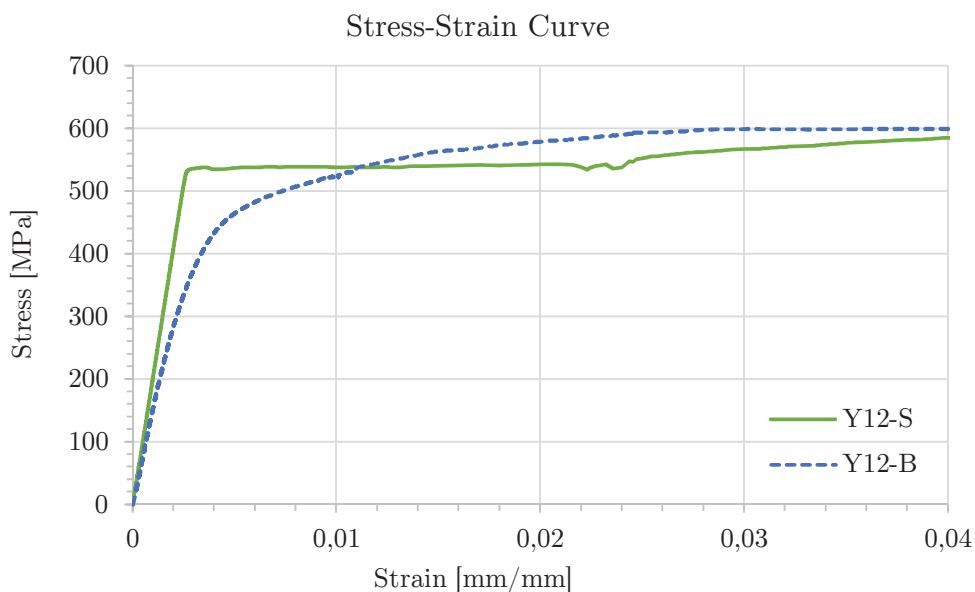


Figure 4.11: Stress-Strain Curve of Y12-S and Y12-B Reinforcement

Both stress-strain curves for the S-series demonstrate a linear-elastic behaviour up to a stress value of about 540 MPa before flattening out. After the yield plateau, the start of strain hardening is observed at around 0.022 mm/mm strain, in both the Y10 and Y12 bars. In contrast to this, the stress-strain curves for the Y10-B and Y12-B specimens present no clear yield plateau and the start of strain hardening is not as clearly defined, especially in the case of the Y12 specimen.

Further, the gradient of the linear portion on the curves for the B-series is notably lower than that of the S-series. This demonstrates a decrease in the modulus of elasticity and is supported by the individual results, presented in Figure 4.12 and 4.13. It is important to note that the value obtained for specimen set number 3 of the Y10-B specimens was identified as an outlier. It is suspected that this specific specimen was locally damaged during the bending or straightening process and this resulted in a disproportionate high reduction in the E-modulus. The data for this specimen is subsequently excluded in the calculation of the average value and standard deviation for the E-modulus. This does, however, prove the importance of ensuring that rebar is not damaged during the straightening process on site, as this can lead to substantially larger negative effects, compared to what is observed in this research investigation.

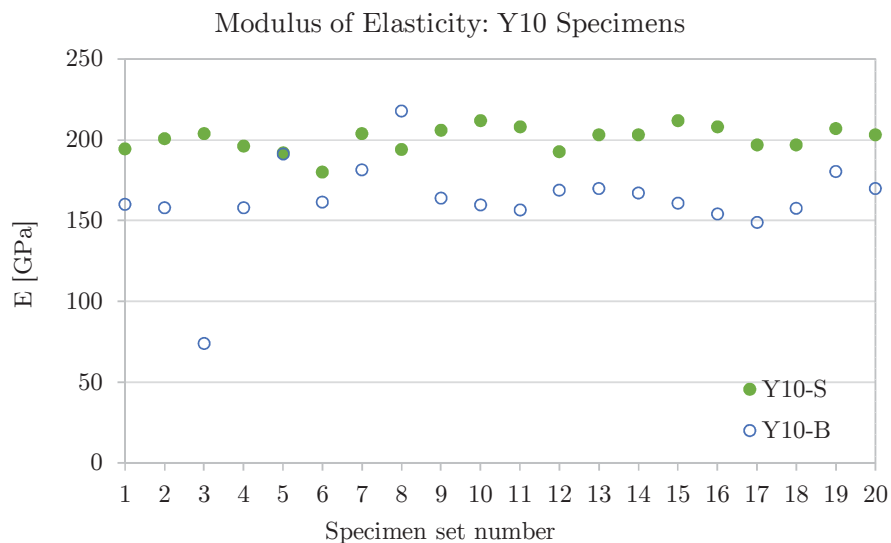


Figure 4.12: E-modulus Results of Y10-S and Y10-B Reinforcement

The average E-modulus for the Y10-B series was 16.5% lower than that of the Y10-S series. For the Y12 equivalent, the reduction was even larger at 23.5%. A summary of the data is contained in Table 4.3.

A reduction in the yield stresses between the S-series and B-series was also observed. This was largely due to the change in shape between the two stress-strain curves. The direct method was used to determine most of the yield stresses in the S-series, while the offset

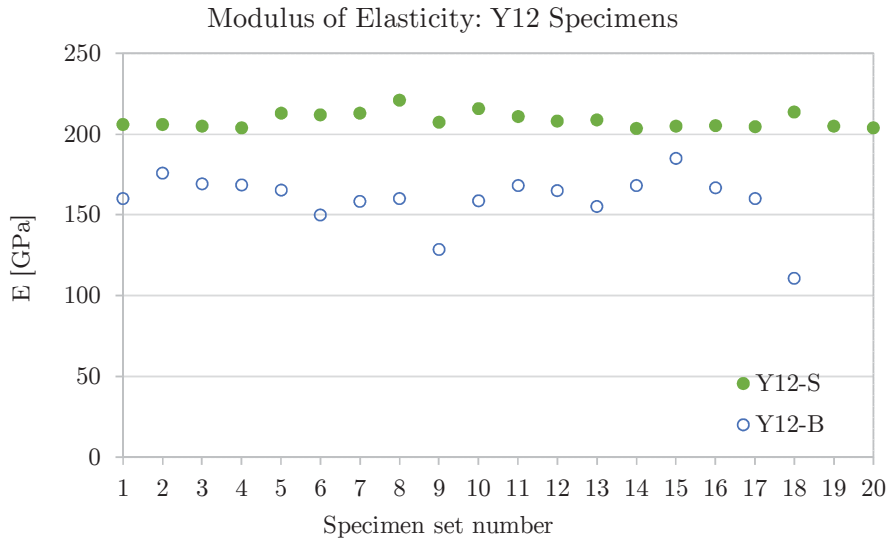


Figure 4.13: E-modulus Results of Y12-S and Y12-B Reinforcement

Table 4.3: Modulus of Elasticity Results Summary (GPa)

	Y10 Rebar		Y12 Rebar	
	S-Series	B-Series	S-Series	B-Series
Average	201	168	209	160
Std deviation	7.9	16.0	4.8	16.8
Coeff of variation	0.039	0.095	0.023	0.105

method had to be used for the bars in the B-series, as they did not present a clear yield plateau.

Figure 4.14 shows a portion of two typical stress-strain curves for a B-series and a S-series specimen respectively. The differences in the stress-strain curves are clearly visible with the corresponding reduction in their yield stresses indicated by the two yield stress lines. In the case of the S-series data, the yield line corresponded to the yield plateau as prescribed in the direct method. On the other hand, the yield line for the B-series specimen was determined through the offset method by plotting the 0.002 offset-line and using the point of intersection with the curve to determine the equivalent yield stress.

The results for the yield stresses of the Y10 and Y12 bars are presented in Figures 4.15 and 4.16.

According to JCSS (2001) the average strength of rebar is expected to be around 2 stan-

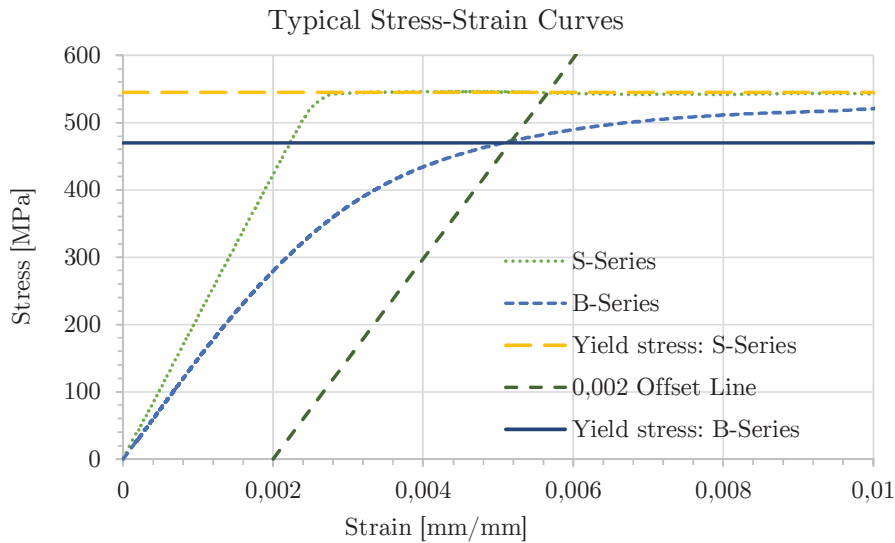


Figure 4.14: Yield Stress Calculation Methods for the Different Reinforcement Sets

standard deviations above the characteristic value, ie. for high strength rebar the average tested strength should be in the range of $450 + 2 \times 30 = 510$ MPa. The Y10-S bars comfortably met this requirement with an average yield strength (f_y) of 550 MPa. However, the average strength for the Y10-B bars dropped by more than 16% to 460 MPa and 5 specimens recorded a value lower than 450 MPa, as seen in Figure 4.15. Further, according to SANS 920:2011, the characteristic yield strength of reinforcement determined through tensile testing is the 5th percentile of the data, ie. the value below which not more than 5% of the results in the series fall. Subsequently, the characteristic yield strength for the Y10-B bars was only 437 MPa. A similar observation for the Y12 set of bars showed a drop in the average yield stress of 19.5%, to 447 MPa and a characteristic value of 422 MPa. A summary of the results is presented in Table 4.4.

Table 4.4: Yield Stress Results Summary (MPa)

	Y10 Rebar		Y12 Rebar	
	S-series	B-series	S-Series	B-Series
Average	550	460	555	447
Characteristic value	502	437	535	422
Std deviation	29.4	14.1	12.2	14.8
Coeff of variation	0.053	0.031	0.022	0.033

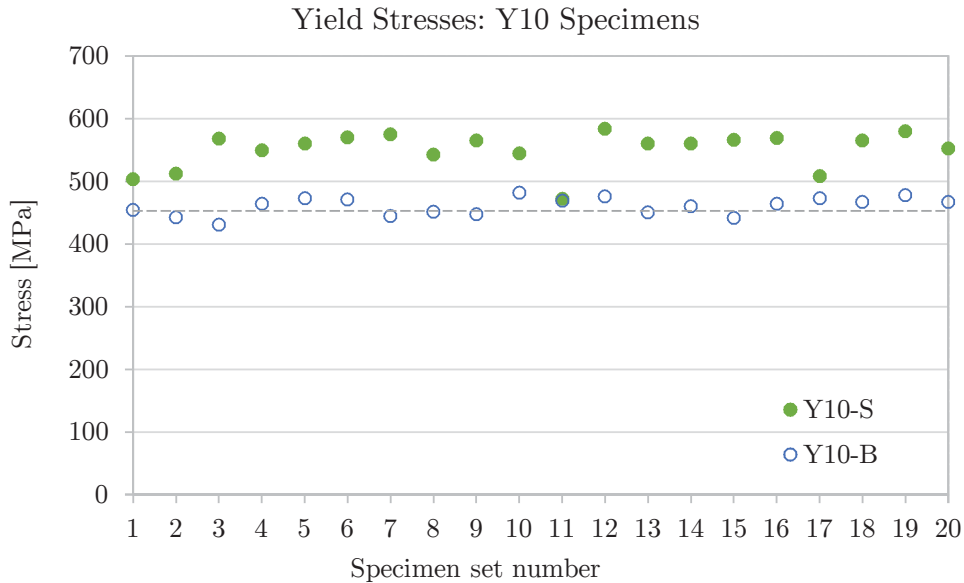


Figure 4.15: Yield Stresses of Y10-S and Y10-B Reinforcement

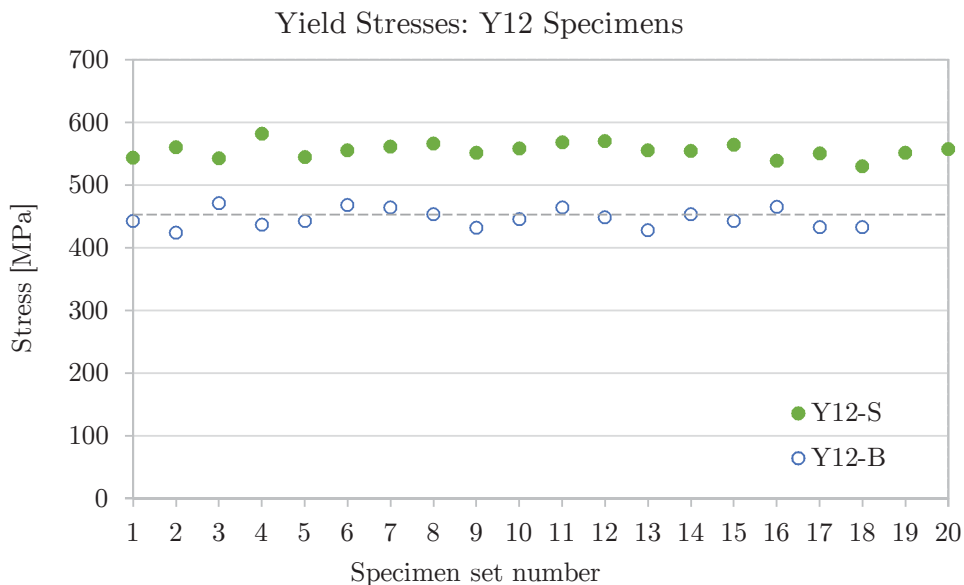


Figure 4.16: Yield Stresses of Y12-S and Y12-B Reinforcement

The average value for the ultimate stress (f_u), determined through the tensile testing, of the S- and B-series, showed only a small reduction of 2% and 4% respectively. Figures 4.17 and 4.18 graphically present the individual results, while Table 4.5 provides a summary of all the data captured.

4.3.2 Reinforcement used in the Full-scale Models

All the rebars used in the full-scale models were high yield deformed bars with a nominal diameter of 12 mm. The wall rebars, used in all the models, were from the same batch and are defined by the abbreviation Y12-WR. The floor starter-bars used in the models

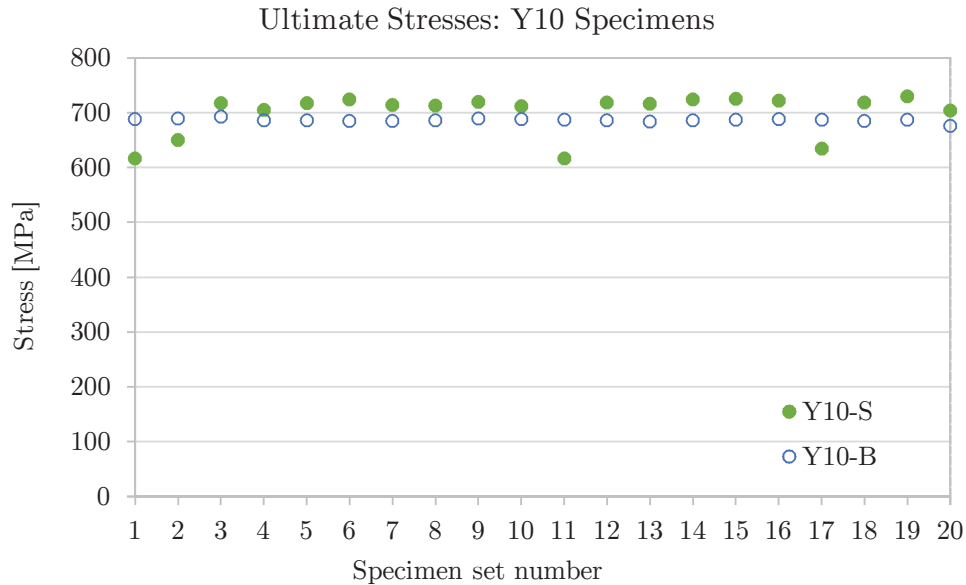


Figure 4.17: Ultimate Stresses of Y10-S and Y10-B Reinforcement

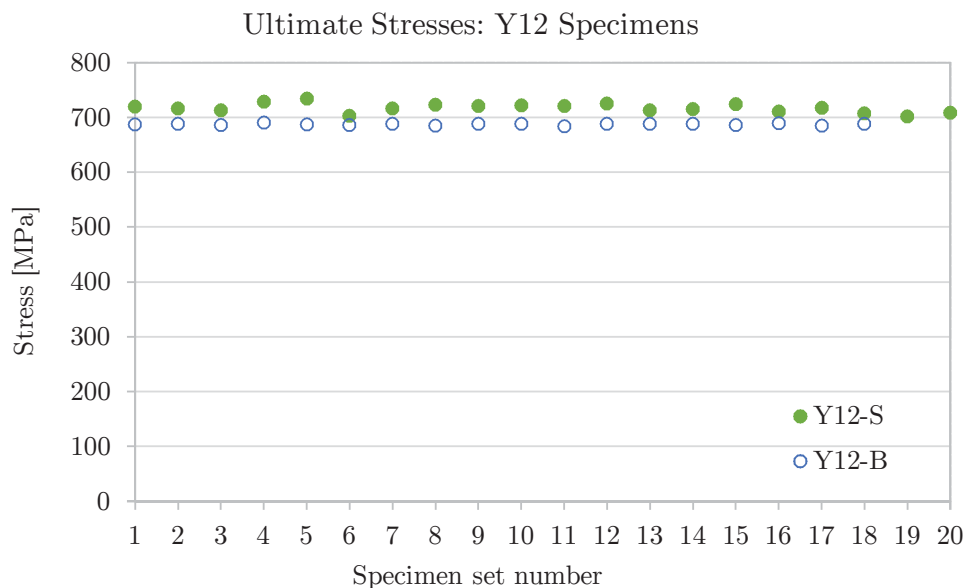


Figure 4.18: Ultimate Stresses of Y12-S and Y12-B Reinforcement

labelled A, B, C and D are defined by Y12-FRA, Y12-FRB, Y12-FRC and Y12-FRD respectively. It is important to note that only the starter-bars in Model A and B were from the same batch of steel and can therefore be directly compared. The starter-bars for Models C and D were ordered directly from the supplier.

Figure 4.19 represents typical stress-strain curves for the five different sets of reinforcement tested. From this graph it is evident that the rebar in the wall (Y12-WR) and, to a lesser degree, the starter-bars in Model D (Y12-FRD) were the only sets that behaved linearly up to a yield stress before turning into a plateau. The yield stress for Y12-FRD was, however, lower than that observed for Y12-WR. Both these sets contained rebar that

Table 4.5: Ultimate Stress Results Summary (MPa)

	Y10 Rebar		Y12 Rebar	
	S-series	B-series	S-series	B-series
Average	700	686	717	687
Characteristic value	639	681	704	684
Std deviation	37.3	3.1	8.2	1.6
Coeff of variation	0.053	0.005	0.011	0.002

was not bent and behaved similarly to the observations made in the preliminary testing. The starter-bars used in Model A (Y12-FRA) were also straight rebar and the shape is therefore expected to be similar. However, the shape is notably different and could be the result of discontinuity in the forging process of reinforcement as the starter-bars in Model A (Y12-FRA) were not cut from the same batch of steel used in the Y12-FRD and Y12-WR sets.

Conversely, the starter-bars in Model B (Y12-FRB) and Model A (Y12-FRA) were from the same batch of steel. Only the bars in the Y12-FRB set were bent and straightened before testing and the effect of this cold bending is clearly evident in Figure 4.19. The linear portion of the stress-strain relationship for Y12-FRB is much smaller and flatter than that of Y12-FRA.

The stress-strain curve for the starter-bars used in Model C (Y12-FRC), which have also undergone cold bending and straightening, is only slightly less linear than that of the Y12-FRA set. The starter-bars are not cut from the same batch of steel and a direct comparison is therefore not possible. The general shapes of the stress-strain curves observed in the preliminary tests do, however, correspond to the behaviour for bars that have been bent and straightened.

Figure 4.20 contains the values for the modulus of elasticity (E-modulus) of the different reinforcement sets used in the full-scale models. The E-moduli for the Y12-WR, -FRA and FRD series were observed to be more or less in the same range of between 210 to 220 GPa. The values recorded for the Y12-FRC bars were on average lower at around 188 GPa, while the Y12-FRB series were the lowest. The average modulus of elasticity for the reinforcement in the Y12-FRB series was 167 GPa, 25% lower than that of the Y12-FRA series. This reduction in the E-modulus between straight and straightened bars, is in line with the phenomena observed in the preliminary tensile testing.

The different values for the modulus of elasticity between the sets are presented in Table 4.6.

A reduction in the the yield stresses between the sets containing straight bars and the sets with straightened bars is also observed and illustrated in Figure 4.21, with the specific values presented in Table 4.7.

The ultimate stresses of the starter-bars were very similar, at around 650 MPa. However, the reinforcement used in the walls presented a higher ultimate stress of about 685 MPa on average. The results are all presented in Figure 4.22 and Table 4.8.

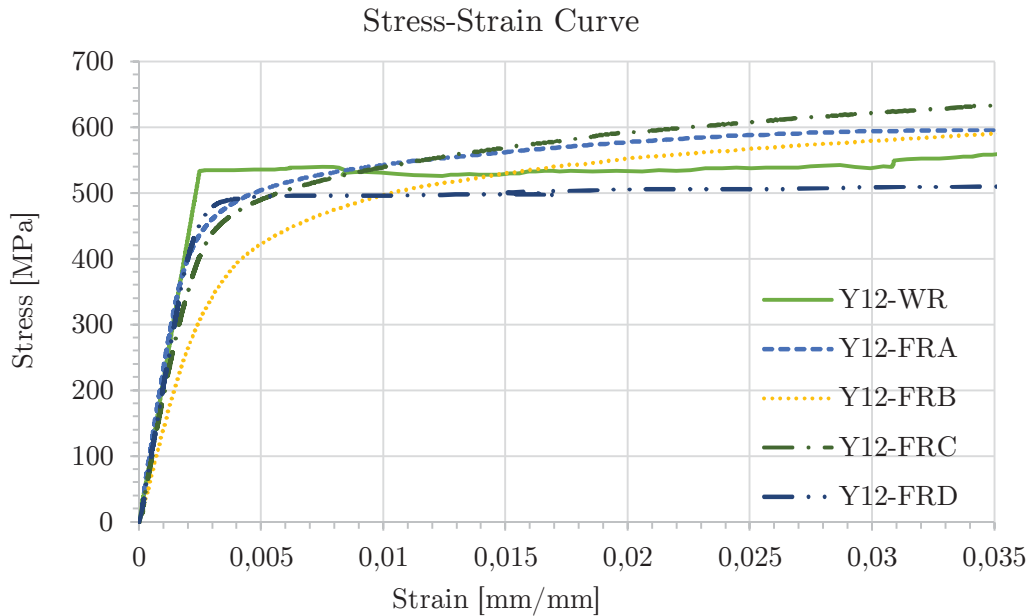


Figure 4.19: Typical Stress-strain Relationships: Full-scale Model Reinforcement

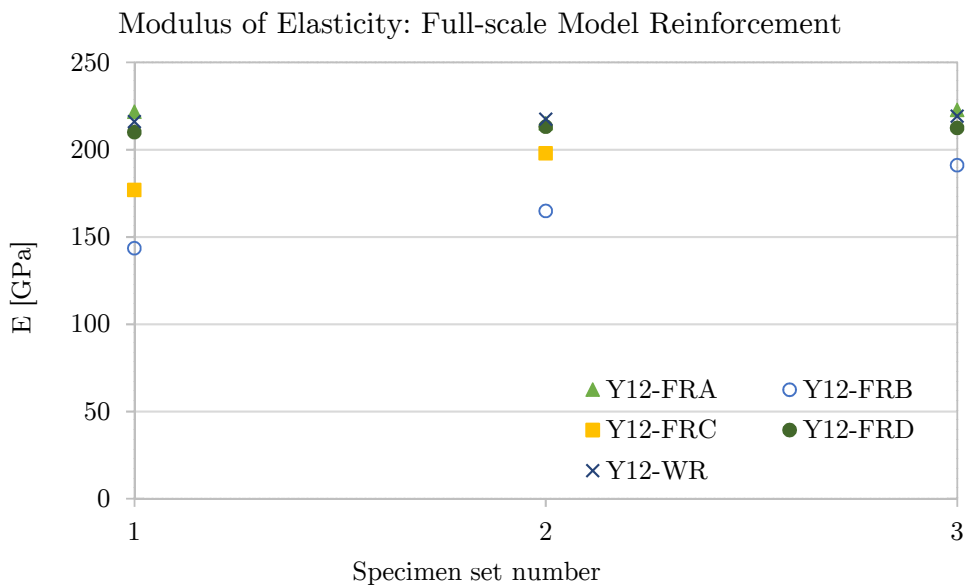


Figure 4.20: E-modulus Results: Full Scale Model Reinforcement

4.4 Low-cycle Fatigue Tests

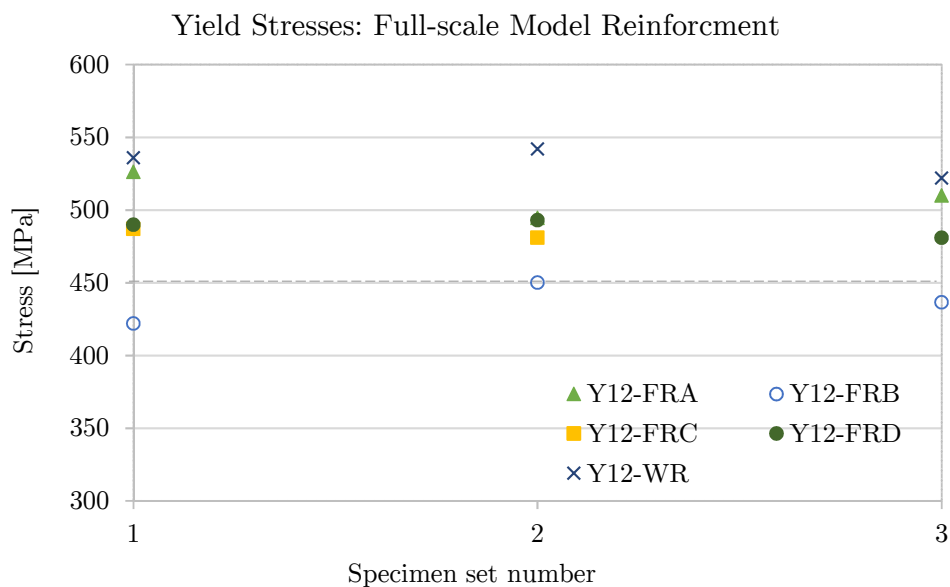
4.4.1 Test Observations

This section presents the observations made during the low-cycle fatigue tests, focussing on the position of failure, crack formation and presence of brittle fracture. The abbreviations used in this section to distinguish between the different sets are explained in section 3.4.

The position of ultimate fracture was different for the various sets. All the specimens in the Y10-0 and Y12-0 sets failed inside the parallel length (machined part of the specimen),

Table 4.6: Rebar used in Full-scale Models - E-modulus Summary (GPa)

	Y12 Rebar				
	WR	FRA	FRB	FRC	FRD
Average	217.6	219.8	166.5	187.4	211.9
Std deviation	1.6	4.2	23.9	14.8	1.6
Coeff of variation	0.0072	0.019	0.1432	0.0795	0.0075

**Figure 4.21:** Yield Stress Results: Full Scale Model Reinforcement**Table 4.7:** Rebar used in Full-scale Models - Yield Stress Summary (MPa)

	Y12 Rebar				
	WR	FRA	FRB	FRC	FRD
Average	533.3	510.3	436.2	484	488
Std deviation	10.3	15.8	14.1	4.2	6.2
Coeff of variation	0.0192	0.0310	0.0322	0.0088	0.0128

but at different locations and with no systematic pattern observed. The bars that were straightened only once (Y10-1 and Y12-1) also fractured at random positions. With the exception of two bars, specimens in the sets that were straightened twice (Y10-2 and Y12-2) failed at the position where the original bend was made. All the bars in the Y10-3 and Y12-3 sets failed at the centre where the bars were bent.

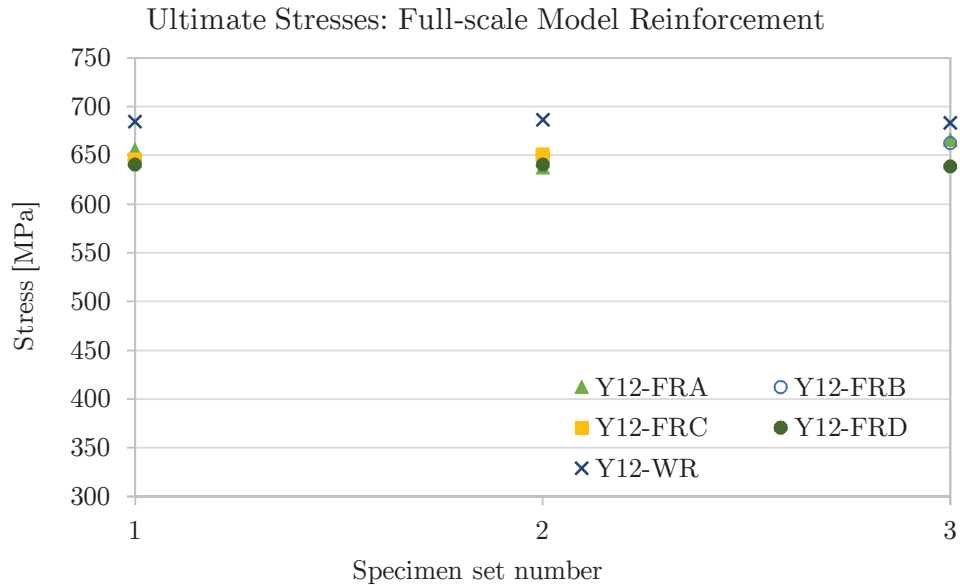


Figure 4.22: Ultimate Stress Results: Full Scale Model Reinforcement

Table 4.8: Rebar used in Full-scale Models - Ultimate Stress Summary (MPa)

	Y12 Rebar				
	WR	FRA	FRB	FRC	FRD
Average	684.8	652.9	653	648.1	639.9
Std deviation	1.5	14.4	8.9	3.7	0.9
Coeff of variation	0.0021	0.0220	0.0136	0.0057	0.0013

It is important to note that two of the specimens in the Y12-3 set experienced brittle fracture during the low-cycle bending and could therefore not be tested as failure had already occurred.

Significant cracks, visible to the naked eye, were observed in the specimens that were bent and straightened three times (Y10-3 and Y12-3) and the cracks were all located near the centre. Figure 4.23 shows the formation of cracks and discolouring at the centre of the bar.

4.4.2 Test Results

Figure 4.24 presents a summary of the yield strengths of the different sets of rebar tested. Refer to Appendix D for the full set of results.

It is clear that after the initial drop in yield strength between the straight bars and the bars that were bent and straightened once, a continuation of the low-cycle bending does not further reduce the yield strength. In contrast, it seems that the work hardening effect of the steel will actually increase the yield strength. Some of the specimens did, however,

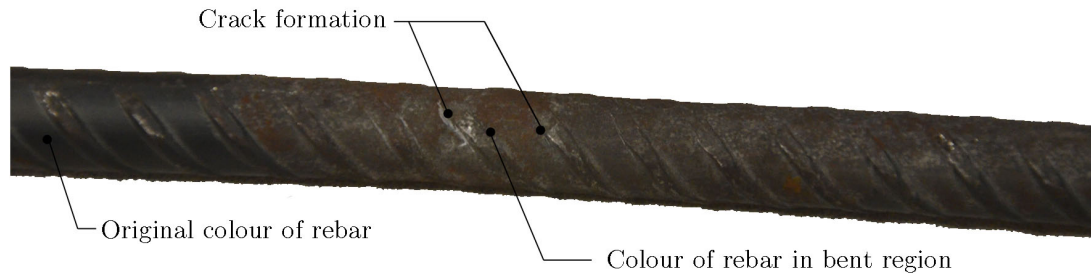


Figure 4.23: Crack Formation and Discolouring of Rebar in Bent Region

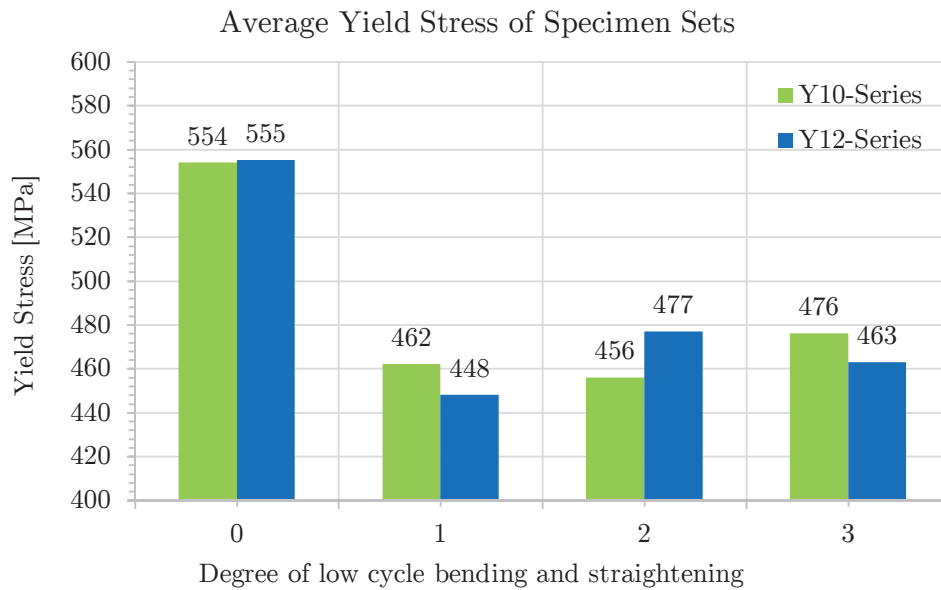


Figure 4.24: Fatigue Test Results Summary

experience brittle fracture during the cold bending and extreme caution should therefore be applied when straightening any rebar on site. These results also prove that there is a reduction in the ductility of steel that has been cold bent and that the possibility remains that these bars will not be able to meet the standardised requirement for ductility as prescribed in SANS 920:2011 (SANS, 2011c).

4.5 Supplementary Tests

4.5.1 Compressive Strength

Figure 4.25 presents a summary of the compressive strengths of the cubes tested. Both the specimens for the wall and the slab are plotted on one graph. The slabs were cast seven days after the walls, but both specimens were tested 7 days after they were cast. The full-scale tests were performed 35 days after the walls were cast and 28 days after the slabs. On the day of the test another batch of cubes were tested in order to establish the material properties of the specimens.

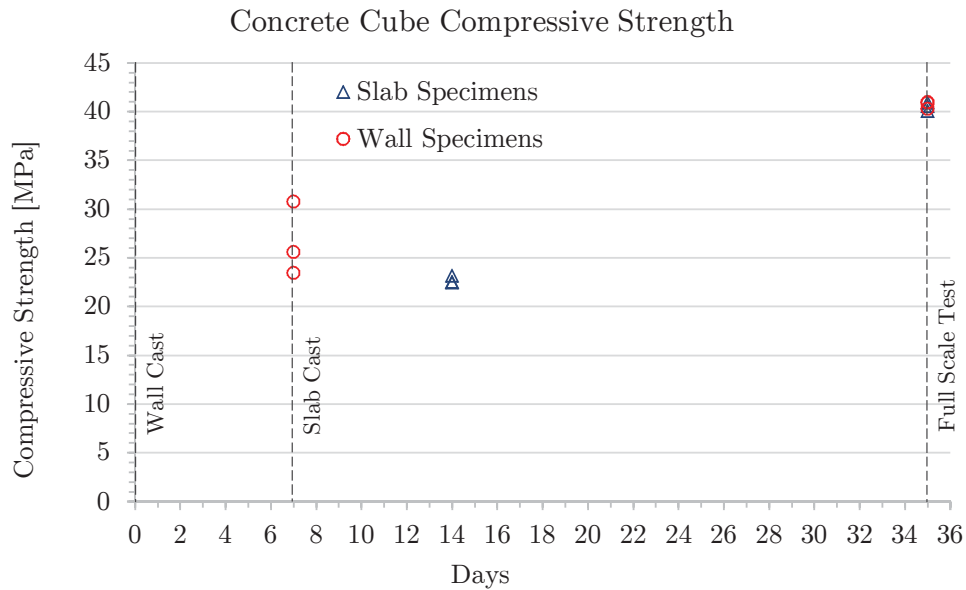


Figure 4.25: Summary of Uniaxial Compression Test Results

Up to seven days the strength development rate in the wall specimens were higher than that of the specimens for the slab. From seven days onwards, the rate slowed and at 35 days the compressive strength of the wall specimens were equal to that of the slab's.

A full set of data is included in Appendix D.

4.5.2 E-Modulus

Table 4.9 includes a summary of the E-modulus results, for both the wall and slab samples.

Table 4.9: Summary of Concrete E-Modulus Results

	Slab Specimens	Wall Specimens
Cube No.	E-Modulus (GPa)	E-Modulus (GPa)
1	33.62	30.69
2	31.09	30.18
3	36.7	
Average	33.8	30.44
Std deviation	2.81	0.36
Coeff of variation	0.083	0.012

Chapter 5

Numerical Analysis

5.1 Introduction

Numerical simulation of experimental results, combined with the correct material models, is a powerful tool to extend the range of variables used in the limited experimental phase. In this research investigation, numerical analysis was used to conduct a sensitivity study on the structural performance of a wall-to-slab connection, by varying the properties of the starter bars and the concrete strength.

The full-scale tests confirmed that there exists a correlation between a reduction in the E-modulus and yield stress of the starter-bars and the overall structural performance of a system. It is, however, difficult to establish the isolated effect of only varying the reinforcement properties, as different connection systems were installed in the various models.

Finite element modelling (FEM) and numerical analysis was therefore conducted, to better understand the isolated effect and sensitivity of the structural performance to a range of reinforcement properties. The different reinforcement material models used in the FEM were all based on actual data captured in the preliminary tensile testing phase. The data used for Finite Element (FE) models, simulating a connection system containing straight bars, was taken from the Y12-S series of specimens, while the data from the Y12-B series was used in the material models for the numerical analysis of the bend-out bar systems. In a separate set of analyses, the effect of using different grades of concrete was also established by keeping the steel properties constant and only varying the characteristic compressive stress of the concrete.

A summary of all the analyses that were performed in this study are presented in Table 5.1, alongside details of the FE model used in each analysis. This includes the type of starter bars simulated, B-series or S-series, the yield strength (f_y) of the modelled reinforcement, the characteristic concrete strength (f_{ck}) and the abbreviations that will be used hereafter.

The development of the various FE models is discussed in section 5.2. A brief overview of previous research is included, while more detail is provided on the actual development of the models, including the type of analysis and elements, mesh configuration, boundary and loading conditions and material models.

All the results are presented in section 5.3, starting with a comparison between the FE model and the experimental results of Model A, followed by the results obtained through

Table 5.1: Summary of FE Analyses

Discription	f_y	f_{ck}	Abbreviation
	(MPa)	(MPa)	
<u>Comparison to Experimental Results</u>			
Y12-S starters, 40 MPa concrete	510	31.83	Y12-A(40)
<u>Sensitivity Study</u>			
Y12-S starters, 30 MPa concrete	570	24	Y12-S(30)
Y12-B starters, 30 MPa concrete	471	24	Y12-B1(30)
Y12-B starters, 30 MPa concrete	431	24	Y12-B2(30)
Y12-S starters, 40 MPa concrete	570	32	Y12-S(40)
Y12-B starters, 40 MPa concrete	471	32	Y12-B1(40)
Y12-B starters, 40 MPa concrete	431	32	Y12-B2(40)
Y12-S starters, 50 MPa concrete	570	40	Y12-S(50)
Y12-B starters, 50 MPa concrete	471	40	Y12-B1(50)
Y12-B starters, 50 MPa concrete	431	40	Y12-B2(50)

the sensitivity study.

5.2 Model Development

Research done by Deaton (2013), on non-linear finite element analysis (FEA), provided essential information in the development of the FE models used in this investigation. The focus of his study was specifically on RC beam-to-column joints. Key issues and best-practice principles were extensively researched in the study by Deaton (2013). The literature study incorporates 60 research papers, all published over the past 30 years and mostly focusses on the analysis of RC building joints. A short summary of the information used in this study, is listed below:

- Non-linearity in the analyses was introduced by specifying non-linear material models for both the concrete and the reinforcement.
- The expression proposed by Thorenfeldt was established as the preferred non-linear uniaxial compression response and was validated against experiments conducted by Karsan and Jirsa (1969) and Sinha *et al.* (1964).
- An elasto-plastic behaviour for the reinforcement was adopted in most cases, often with the von Mises failure criterion. The introduction of strain hardening made

the material models more accurate, but has also shown to increase the numerical instability.

- Modelling the concrete as three-dimensional (3D) solid elements was recommended over the use of two dimensional (2D) plane stress elements. A 3D model allows for the spatial placement of reinforcement at the joint and the confinement provided by the transverse reinforcement is more accurately accounted for.
- One study successfully simulated the construction joint, adjacent to the connection, by introducing a weak plane in the finite element mesh.
- The *total strain rotating smeared crack model*, implemented in the Diana software package, was established as the most suitable in the analysis of RC joints.

(Deaton, 2013)

Crack models can be categorised in two groups: a discrete crack concept and a smeared crack concept. The former approach deals with cracks as a separation between element edges, while the smeared approach imagines a cracked solid to be a continuum. The discrete crack approach more closely represents the actual behaviour of concrete, but has two major shortcomings. This approach implies a discontinuity in the connectivity of the element nodes, which does not fit the nature of the finite element displacement method. The second problem is that the cracks develop along a pre-determined path, coinciding with the edges of elements. Conversely, the smeared crack approach starts from the notion of stress strain relations within a continuum. The smeared crack model switches from an initial isotropic stress-strain law to an orthotropic law as soon as a crack is formed, with the axes of orthotropy being a function of the condition of crack initiation. The model further preserves the configuration of the finite element mesh and does not impose restrictions on the orientation of the crack planes. For this reason it makes computational sense to rather use the smeared crack approach, which has been proven to produce accurate simulations. (Rots and Blaauwendraad, 1989)

Further research conducted by Gregory Maybery, at Stellenbosch University, on the structural performance of a RC corbel, showed good correlation between experimental results and numerical analysis done with the Diana software package. The research formed part of his final year project. The FE model was developed using both 2D and 3D elements with embedded reinforcement. The results from the 3D model produced a better fit to the experimental data than the 2D equivalent (Maybery, 2014). This is in agreement with the recommendations made in Deaton (2013).

Research conducted by Monnier (1987) also showed that a perfect-bond model or *embedded reinforcement model*, as implemented in Diana, gives satisfactory results in the prediction of the structural performance of RC structures.

The research and recommendations were subsequently used to develop the FE models in this research investigation. A summary containing the general details, applicable to all the models, are presented in Table 5.2, with a more in-depth discussion provided in sections 5.2.1 to 5.2.5:

Table 5.2: Finite Element Model Summary

Element Types
Concrete: CHX60, 20 node, Solid Brick Element
Reinforcement: Embedded Reinforcement
Mesh Configuration
Concrete: 50x50x50 mm Elements
Reinforcement: Automated post processing of reinforcement locations
Material Models
Concrete: Total strain rotating crack model [TOTCRK ROTATE]
Tensile Behaviour - Hordijk [TENCRV HORDYK]
Compressive Behaviour - Thorenfeldt [COMCRV THOREN]
Reinforcement: Von Mises plasticity model [YIELD VMISES]
Tensile Behaviour - User defined [EPSSIG]
Hardening hypothesis - Work Hardening [WORK]
Boundary Conditions
Wall toe: Fixed against translation horizontally and vertically
Floor support: Fixed against translation horizontally
Steel tie-back: Fixed against translation horizontally
Load Conditions
Applied load: Line load over floor width
Control: Displacement controlled
Increments: 0.01 mm x 20 steps; 0.1mm onwards
Analysis Method
Method: Non-Linear Analysis [NONLIN]
Iteration process: Newton-Raphson Regular [METHOD NEWTON]
Convergence criteria: Energy - 0.001 Tolerance [ENERGY TOLCON 0.001]

5.2.1 Elements

The FE model, as shown in Figure 5.1, consists of three main parts: the concrete representing the cantilever slab and wall, the weaker concrete simulating the position of the construction joint and the reinforcement bars embedded in the concrete structure. The reinforcement is further divided into two sets: the general reinforcement, used inside the wall and floor and the starter bars, running through the construction joint.

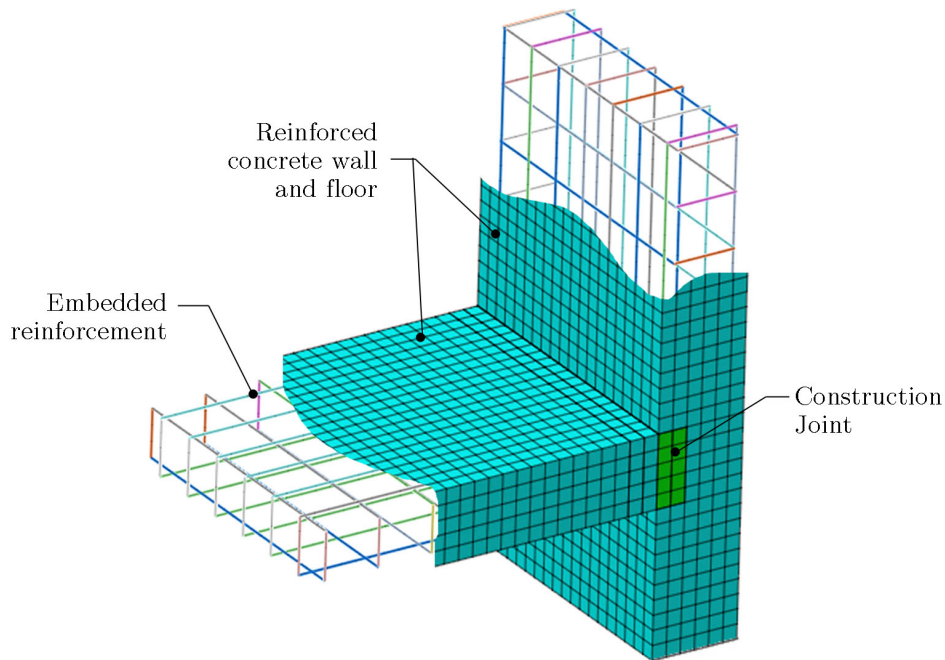


Figure 5.1: Finite Elements

The concrete was modelled using twenty node, isoparametric solid brick elements (CHX60), with three degrees of freedom at each node, as shown in Figure 5.2. Gauss integration was applied on the element, with a 3x3x3 integration scheme, as per the default setting in Diana. (Diana, 2014)

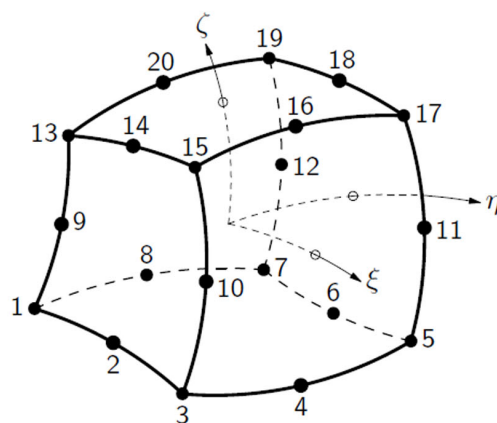


Figure 5.2: CHX60, 20-node Solid Brick Element (Diana, 2014)

The reinforcement was modelled as *embedded reinforcement* positioned in the concrete or *mother element*.

Embedded reinforcement does not have any degrees of freedom of its own, but the sectional and material properties add stiffness to the elements that it intersects. The stress and strain in the rebar are computed from the displacement field of the mother elements and therefore implies that there is a perfect bond between the rebar and the embedding material. The location of the *embedded reinforcement* can be random and does not have to follow the mesh lines of the *mother element*. (Diana, 2014)

The *embedded reinforcement* is divided into segments that correspond to the position of intersection with the brick elements, as shown in Figure 5.3. The location points are automatically established relative to the element nodes. Diana performs numerical integration of each reinforcement segment separately. (Diana, 2014)

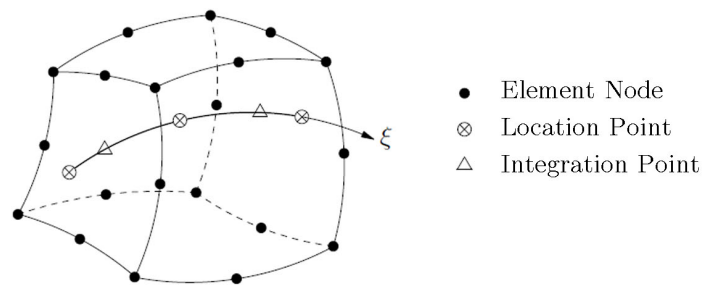


Figure 5.3: Embedded Reinforcement Element in Solid (Diana, 2014)

Figure 5.4 presents the isoparametric axis and the two integration points in two consecutive segments of reinforcement. At each integration point, Diana establishes a \hat{x} -axis, which is tangential to the axis of the rebar. The strains (ε_{xx}) and stresses (σ_{xx}), oriented in the \hat{x} -axis, are the two variables calculated for a reinforcement bar element. The strains and stresses are finally coupled to the degrees of freedom of the embedding element to simulate the composite action of the reinforcement in the concrete. (Diana, 2014)

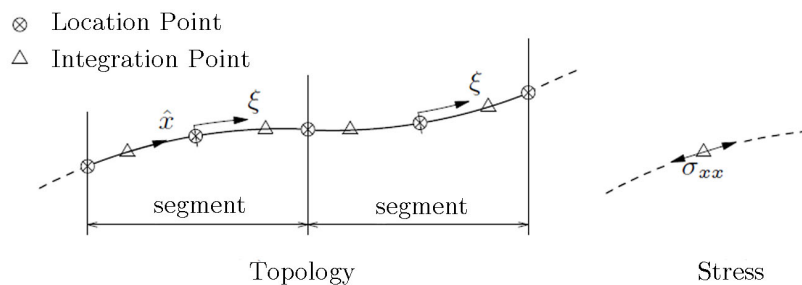


Figure 5.4: Reinforcement Segment Integration Points (Diana, 2014)

5.2.2 Mesh Configuration

The concrete was initially meshed by 80 x 80 x 80 mm elements. The analysis did, however, struggle to converge and a finer mesh of 50 x 50 x 50 mm was considered. The smaller mesh did not experience any convergence issues and produced results that were closer to the experimental data, as shown in Figure 5.5.

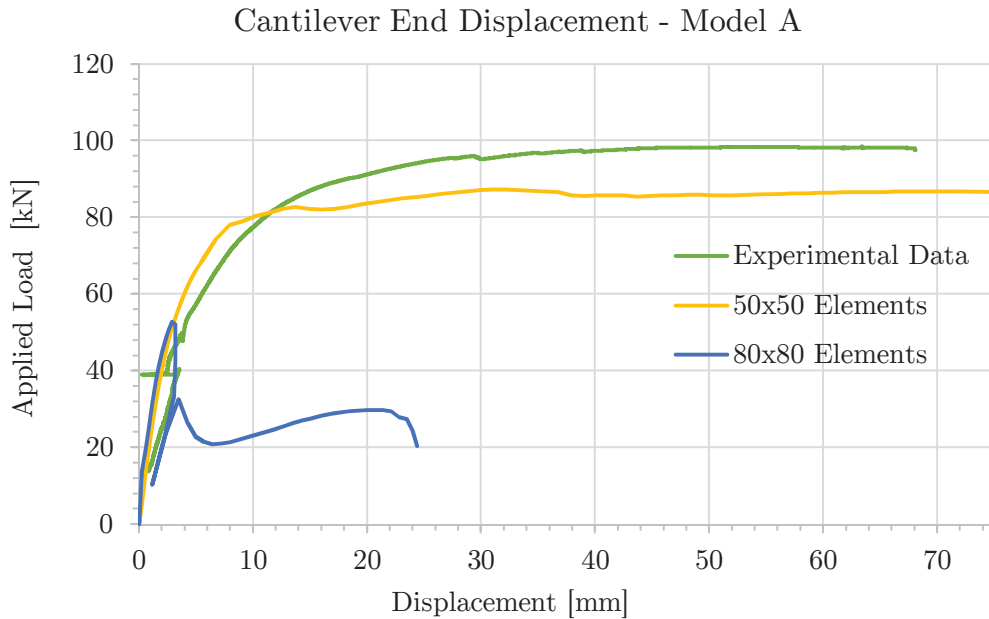


Figure 5.5: Effect of Mesh Size on FEM Results

The 50x50x50 mesh configuration was subsequently incorporated in all the FE models. The construction joint was located at the wall-to-slab intersection and two rows of elements were used to simulate the joint. All the reinforcing bars were modelled at the same location as in the physical specimen and are shown in Figure 5.6(a). The concrete elements, Figure 5.6(b), were specified as the *mother elements* for the *embedded reinforcement*. No specific mesh configuration was applied to the reinforcement as the Diana package automatically runs the *preprocessing* of reinforcement locations in order to divide the reinforcement into their respective segments, as discussed in section 5.2.1. (Diana, 2014)

5.2.3 Material Models

5.2.3.1 Concrete Models

The smeared cracking approach was adopted as it is the only model that can accurately simulate the non-linearities present in RC structures and include the effect of crack formation on the internal stresses and strains. Diana further distinguishes between a fixed smeared crack model and a rotating smeared crack model. Unlike the fixed approach, the rotating smeared crack approach assumes that the crack direction (axis of orthotropy) co-rotates with the axes of principle strain. This results in the element shear vanishing with the continually updated principle planes, thus circumventing the requirement to provide a shear retention factor. This approach was subsequently adopted for all the models. (Diana, 2014)

Model Y12-A(40) was developed to simulate the experimental testing conducted on Model A. The basic properties of the concrete model were based on the supplementary tests conducted on actual concrete specimens, while the fib Model Code was consulted to provide additional properties that could not be derived from the experimental data (fib, 2010).

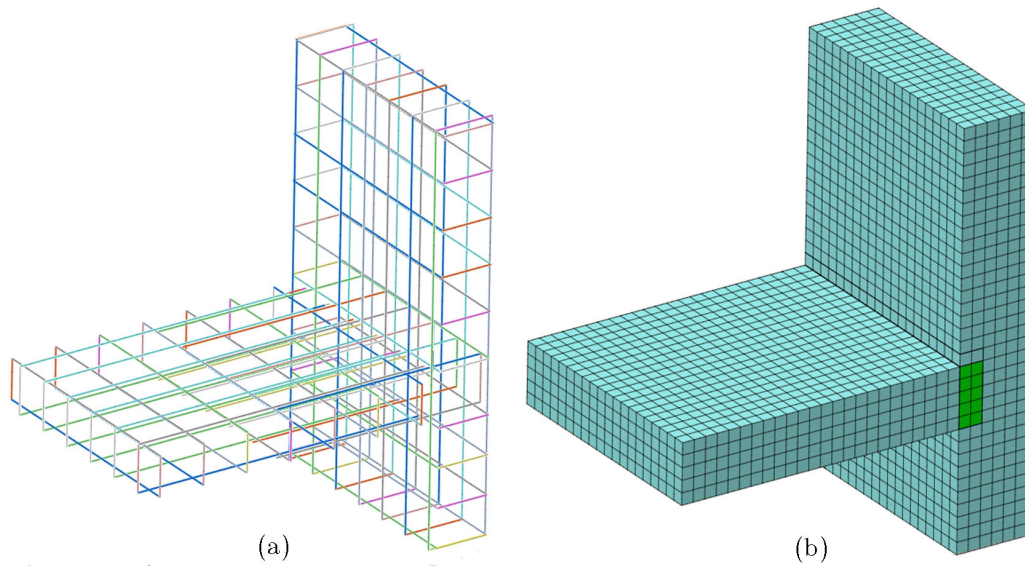


Figure 5.6: a) Reinforcement Elements b) Concrete Mesh

The E-modulus was taken as the average value of the specimens tested, while the fib Model Code was used to determine the density and the poisson's ratio of the concrete. The density was based on the assumption that the models have a reinforcement ratio of 1 %, while the general acceptable value of 0.15 was used for the Poisson's ratio. (fib, 2010)

The characteristic cylindrical compressive strength of the concrete (f_{ck}) was calculated from the experimental data. Although the experiments were conducted on cube specimens, the values were converted to a cylindrical equivalent by multiplying the data with a factor of 0.8, based on BS EN 12504-1:2000 (BSI, 2000). The characteristic strength was taken as the 5th percentile value of the results and determined with Equation 5.1:

$$f_{ck} = f_{cm} - z_{0.05} * std(f_c) \quad (5.1)$$

$std(f_c)$ Standard deviation of concrete compressive strength results

f_{cm} Average of compressive strength results

$z_{0.05}$ 5 Percentage Point of the random variable = 1.64

(Montgomery and Runger, 2007)

For the models used in the sensitivity study, the modulus of elasticity was fixed at 30 GPa. Three different grades of concrete was modelled: 30 MPa, 40 MPa and 50 MPa. The respective characteristic cylindrical compressive strength was subsequently calculated to be 24 MPa, 32 MPa and 40 MPa. The same values used in Model Y12-A(40) for the density and the Poisson's ratio were assumed for these models.

The Tensile behaviour for the concrete models was based on the curve by Hordijk. The general shape of the curve is presented in Figure 5.7(a).

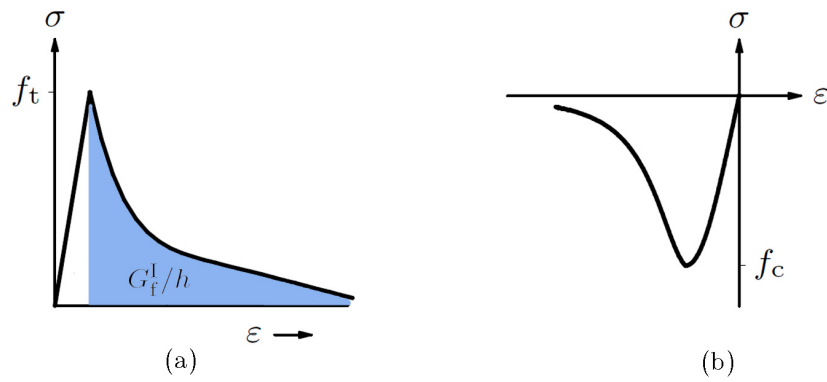


Figure 5.7: a) Tensile Behaviour by Hordijk b) Compressive Behaviour by Thorenfeldt (Diana, 2014)

The tension softening curve requires three input values. The first is the tensile strength (f_t) of the concrete. This characteristic value is determined by Equation 5.2. As no experimental data was available for Model Y12-A(40), the value for the tensile strength was varied within the lower and upper bound limits, as allowed for in the fib Model Code, to establish the best fit between the numerical and experimental data. The basic value, as calculated from Equation 5.2, was however assumed for all the models used in the sensitivity study.

$$f_t = 0.3 \times f_{ck}^{2/3} \quad (5.2)$$

(fib, 2010)

The second variable is the Mode-I fracture energy (G_f^I), which relates to the energy that is required to create a square unit of fracture surface or crack. The fib Model Code defines the G_f^I as a function of the mean cylindrical compressive strength, as presented in Equation 5.3.

$$G_f^I = 73 \times f_{cm}^{0.18} \quad (5.3)$$

(fib, 2010)

The last variable is the crack bandwidth (h). The default value, as assumed by Diana, was used in all the models. This value is determined through Equation 5.4.

$$h = \sqrt[3]{V_e} \quad (5.4)$$

(Diana, 2014)

V_e Volume of the element

The compressive behaviour of the concrete was based on the function by Thorenfeldt, presented in Figure 5.7(b). The only input value required to establish this basic function is the compressive strength (f_{ck}) of the concrete. This value was subsequently supplied for all the models, while the Diana default values were assumed for any additional parameters required.

The material models for the concrete interface simulating the construction joint were defined in a similar manner as the rest of the concrete, with the only adjustment in the tensile strength. This value was reduced significantly to 1.00×10^{-5} MPa in all the models. This configuration enabled the concrete elements to still retain their full compressive strength without any significant contribution to the tensile resistance of the elements in the interface zone.

A list of all the specific values used in the models is presented in Appendix G.

5.2.3.2 Reinforcing Steel Models

For the *embedded reinforcement* a Von Mises plasticity model available in Diana (2014) was used.

The data from the preliminary tensile tests was used to create user defined Von Mises plasticity Models. The hardening curve was specified by providing a series of yield stresses (σ_y) and the corresponding total strain values (ε) that best fit the actual stress-strain curves recorded in the rebar tensile testing phase.

Diana further requires two additional input values. The first value relates to the maximum stress at the end of the linear portion (σ_y) and the modulus of elasticity (E_s) that correspond to the strain at that point.

The steel models for all the reinforcement in model Y12-A(40) were based on the experimental results of specimen F3 tested in the preliminary tensile testing phase. This specimen came from the same batch of steel that was used in the physical model. The stress-strain curve from the experimental results is presented in Figure 5.8. The numerical equivalent, used in defining the material model, is also presented on the graph. As the experimental data was only reliable up to a certain point, the numerical equivalent was extended with an assumed gradient up to the ultimate stress recorded for the specific specimen. Further, due to a lack of accurate experimental data, no softening in the stress-strain curves was modelled.

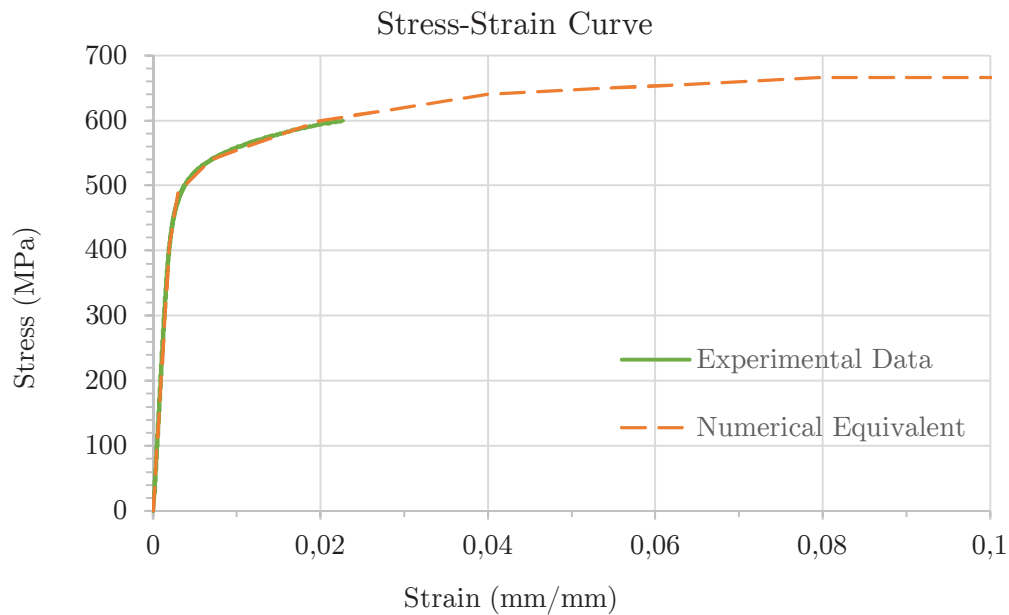


Figure 5.8: Equivalent Stress-strain Curve for the Reinforcement Material Model in Y12-A(40)

For the sensitivity study, three different stress-strain curves were selected. The first set of data was taken from a straight specimen (Y12-S) and presents a close to perfect elastic response up to the yield stress after which a plastic yield plateau is clearly visible. The two other sets of data, came from specimens that were bent and straightened before they were tested. The first B-series specimen, Y12-B1, recorded a reduction of 17 % in the yield stress and 19 % in the E-modulus. The second specimen, Y12-B2, produced an even larger reduction of 24 % for the yield stress and 38 % for the E-modulus. Both specimens recorded a 5 % reduction in their ultimate stresses. The reductions are all calculated as a percentage of the values obtained for the Y12-S specimen. The general reinforcement in the wall and slab was based on the Y12-S data, while the properties for the starter-bars were varied between the data obtained in the Y12-S, Y12-B1 and Y12-B2 specimens. Figure 5.9 presents the three different stress-strain relationships.

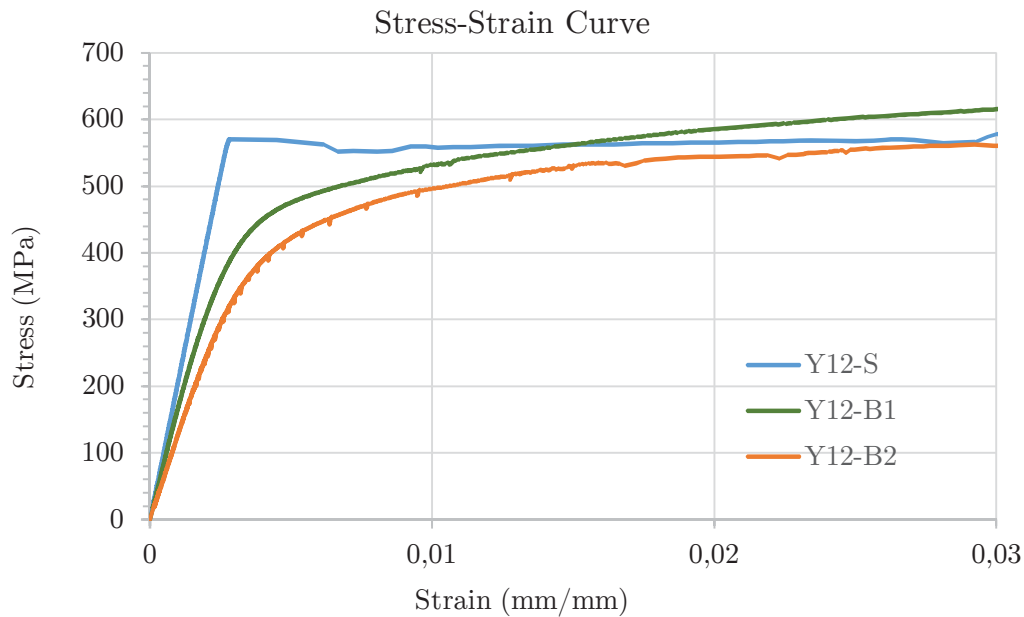


Figure 5.9: Rebar Stress-Strain Relationships used in Sensitivity Study

The full set of data and graphs used to create all the steel material models, are presented in Appendix G.

5.2.4 Boundary Conditions

The boundary conditions for all the models were the same and a visual representation is presented in Figure 5.10. The red arrows indicate the direction of constraint. The entire base of the wall was fixed in the x-direction, with the toe of the wall fixed in both the x- and y-direction. This configuration allows for some degree of rotation around the toe without any translation horizontally or vertically. This corresponds to the physical set-up where the models were placed against the A-frame, preventing horizontal movement, without being tied directly to the strong floor, i.e not preventing uplift or rotation. The tie-back beam was simulated by the horizontal restraints at the top of the wall above the floor connection.

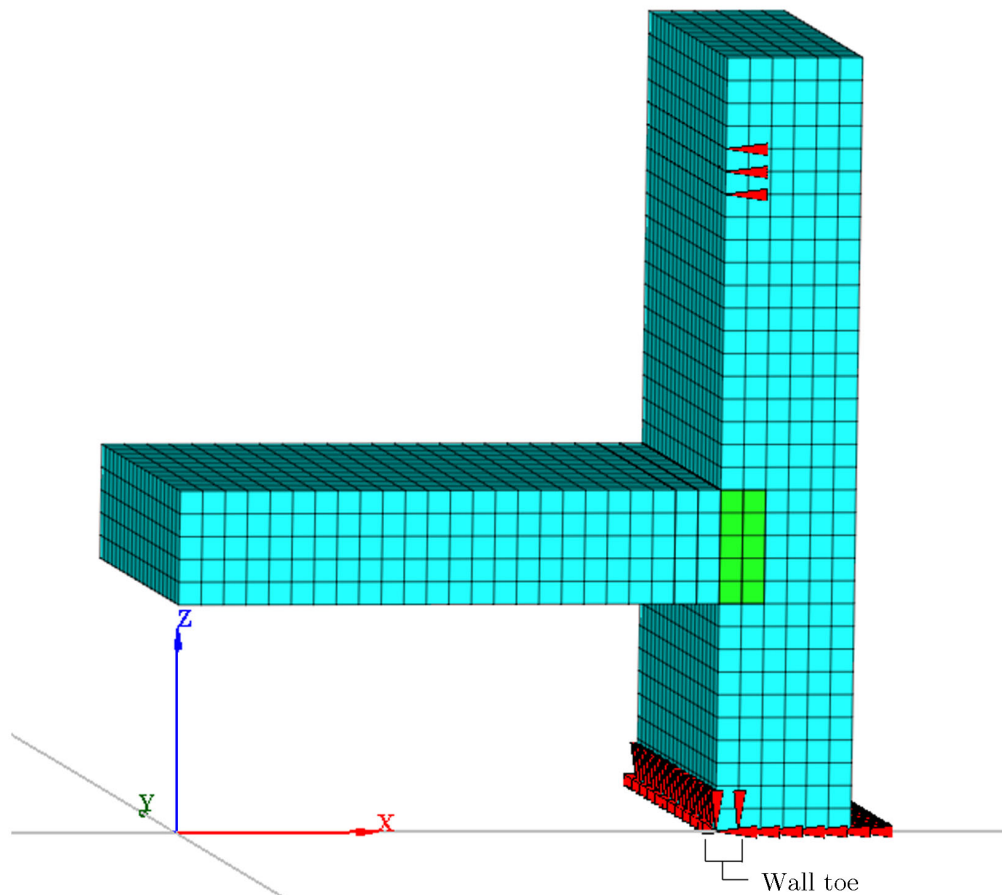


Figure 5.10: FE Model Boundary Conditions

5.2.5 Load Conditions

The applied load at the tip of the cantilever floor was modelled by specifying a predetermined displacement of the nodes at the point of contact with the spreader beam. This configuration resulted in a displacement controlled environment which is preferred when dealing with non-linear material models. It also reduces the computational effort of the analysis while the iterative process is more stable and converges faster. (Diana, 2014)

The load was applied in increments that represented a fraction of the specified displacement. The applied load or displacement was simplified into a single line of nodes coinciding with the centre of the spreader beam, as shown in Figure 5.11.

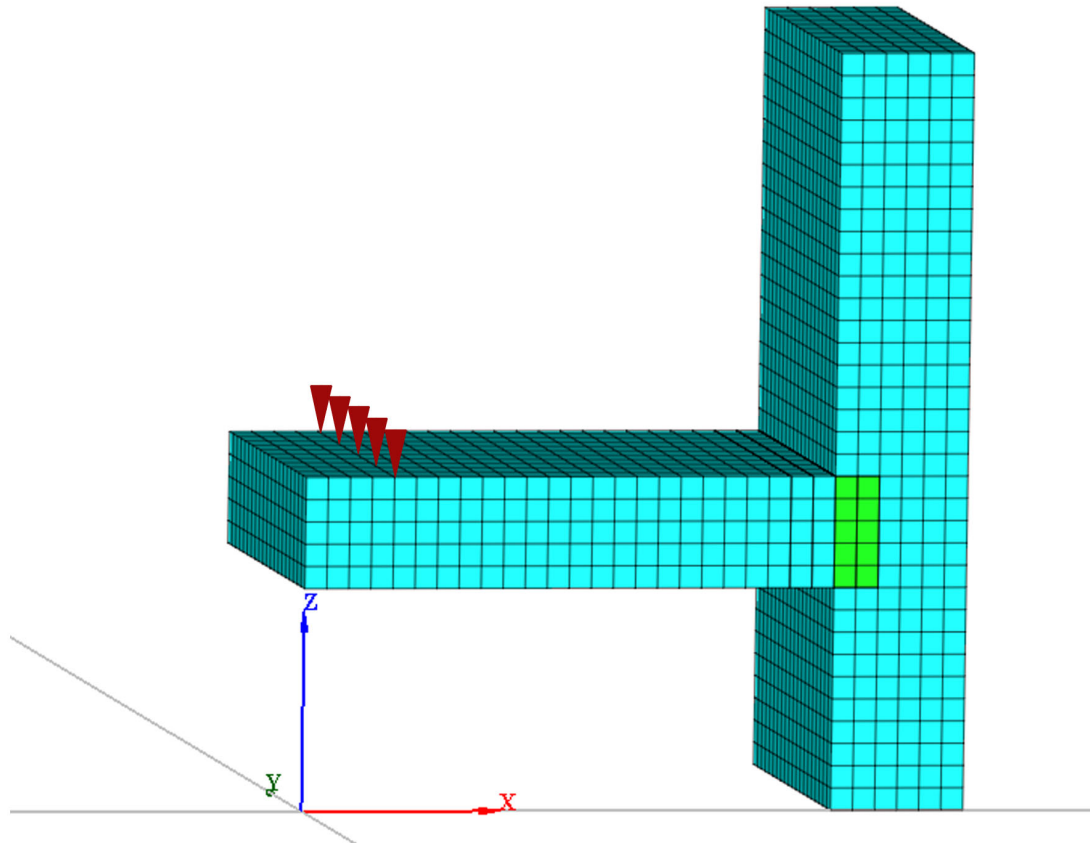


Figure 5.11: FE Model Applied Displacement/Load

The displacement was added in 0.025 mm increments for the first 20 steps and was increased to 0.1 mm increments for the remainder of the analysis.

The self weight was not added as a volume force, but was compensated for by its contribution to internal forces and bending moments at the wall-to-slab connection, i.e. the moments and shear forces due to the self-weight of the cantilever floor was calculated and added to the results obtained through the FEA.

5.3 Results

This section includes the results for the FEA.

The experimental results for Model A are compared to the FEA by means of a load displacement curve and the formation of cracks at SLS and ULS. The measured cracks in the physical model is compared to the principal crack widths (ω_{cr}), determined through the FEA and calculated by multiplying the principle crack strain (ε_{cr}) with the crack bandwidth (h), as shown in Equations 5.5.

$$\omega_{cr} = h \times \varepsilon_{cr} \quad (5.5)$$

(Schreppers and Frissen, 2011)

$$\varepsilon_{cr} = \varepsilon_1 - \frac{\sigma_1}{E} = \varepsilon_1 - \varepsilon_{1,e} \quad (5.6)$$

(Schreppers and Frissen, 2011)

ε_1 Total Principle Strain

$\varepsilon_{1,e}$ Elastic Principle Strain

σ_1 Principle Stress

E Young's Modulus

Finally, the results from the sensitivity study focus on the structural behaviour of a typical wall-to-slab connection, under varying steel and concrete properties. The structural performances are compared through a series of load-displacement curves.

5.3.1 Comparison to Experimental Results

It is important to ensure that any FE model is correctly calibrated to produce similar results expected in a physical equivalent. The data capture in Model A was therefore used to calibrate and confirm the accuracy of the FE model before the sensitivity study was conducted.

Figure 5.12 presents a comparison of the data captured during the experimental phase and the data from the numerical analysis.

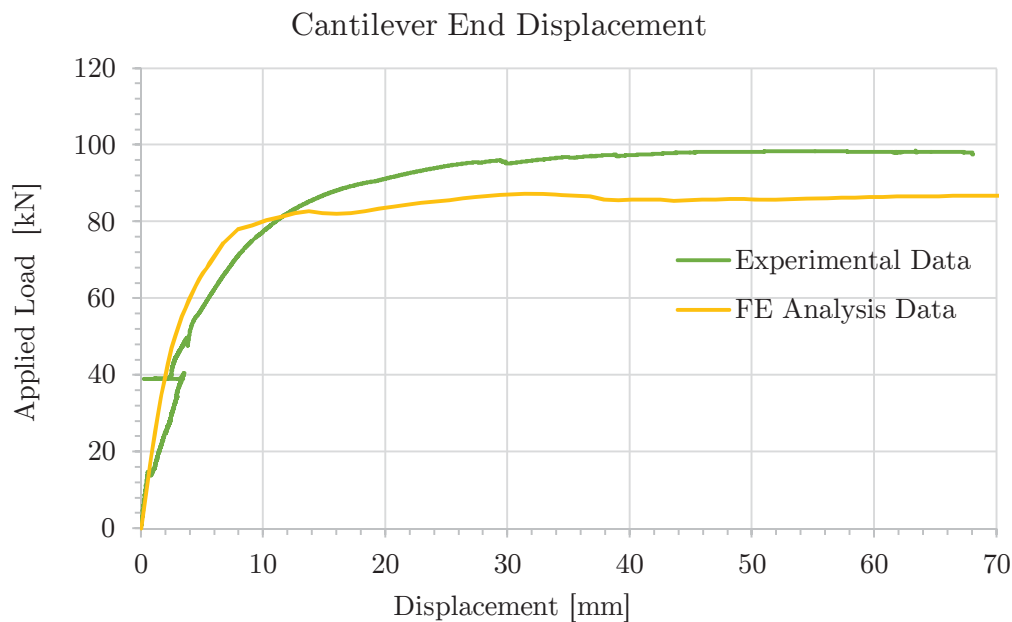
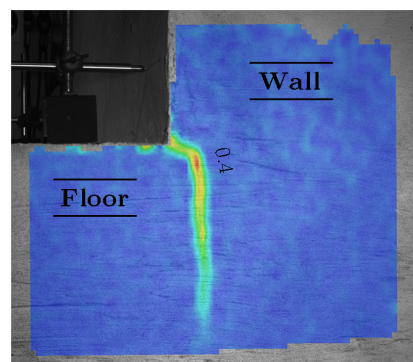


Figure 5.12: Comparison of Experimental data with FEA data of Model A

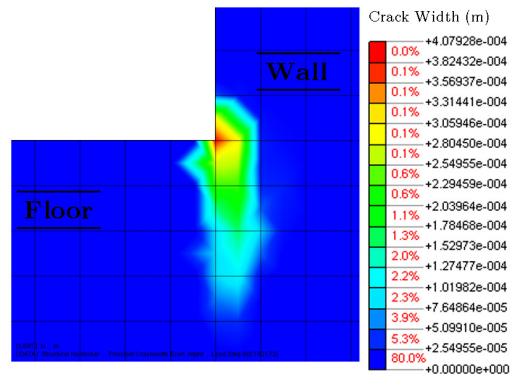
The data from the FEA shows reasonable agreement with the experimental load-displacement response. Both graphs start in a linear fashion and then gradually lose stiffness until the respective yield plateaus are reached. The physical model was able to withstand a maximum applied load of 98.12 kN, while the numerical equivalent came within 11 % of this

value with an ultimate load of 87.24 kN. The displacement of the physical model at stage 1 of the test (SLS) was 2.5 mm, while the FEA recorded a tip displacement of 2.02 mm. At stage 2 (ULS) of the tests, the displacements were 3.8 mm and 2.72 mm respectively.

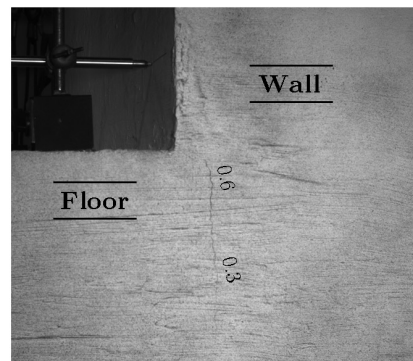
Figure 5.13 contains images comparing the crack development at the two stages of testing. The images on the right show the crack patterns and associated crack widths in the FE model, while the images on the left are the photos taken during the experimental test. A rendered image is superimposed on top of the first photo, as the cracks were not visible with the naked eye. This rendered image was captured with the Aramis camera and processed to show the associated strains at stage one of the physical test.



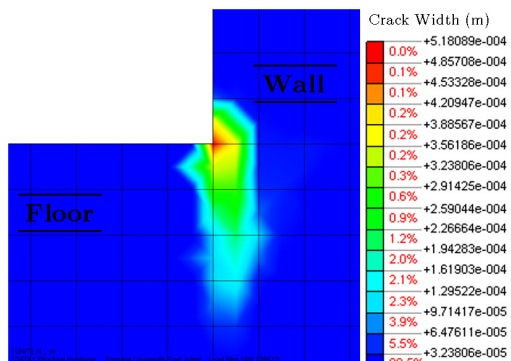
Physical experiment
Crack pattern and width at SLS



Numerical Analysis
Crack Pattern and width at SLS



Physical experiment
Crack pattern and width at ULS



Numerical Analysis
Crack Pattern and width at ULS

Figure 5.13: Comparison Of Experimental and Numerical Analysis of Model A

The general pattern of the experimental photos and the numerically rendered images are similar, both in appearance and in crack widths. At stage one the largest crack measured on Model A was 0.4 mm, while the maximum crack width in the numerical equivalent was also 0.4 mm. At the second stage of the tests, the cracks on the physical model were 0.6 mm in width compared to the 0.52 mm in the FE model.

This overall good correlation between the numerical and physical responses, serves as a validation of the FE model and shows that the structural response of a wall-to-slab connection can be simulated with the Diana package with reasonable accuracy.

5.3.2 Sensitivity Study

Table 5.3 presents the summary of the main variables that were measured in the FE analyses. The responses were compared in three categories: the tip displacement of the cantilever floor, the crack widths at SLS and ULS and the ultimate resistance of the connection.

Table 5.3: Summary of Sensitivity Study Results

Analyses	Tip Displacement		Crack Width		Ultimate Resistance (kN)
	(mm)		(mm)		
	SLS	ULS	SLS	ULS	
Y12-S(50)	1.87	2.44	0.3	0.41	90.92
Y12-S(40)	1.92	2.53	0.31	0.43	89.24
Y12-S(30)	2.01	2.72	0.33	0.47	89.5
Y12-B1(50)	2.07	2.73	0.35	0.48	88.82
Y12-B1(40)	2.14	2.84	0.36	0.5	87.31
Y12-B1(30)	2.24	3.08	0.39	0.55	88.02
Y12-B2(50)	2.37	3.21	0.42	0.6	83.5
Y12-B2(40)	2.45	3.4	0.44	0.64	81.66
Y12-B2(30)	2.6	3.82	0.47	0.72	82.06

The sensitivity study was conducted for two parameters. The first is the sensitivity of the structural response to variation in the starter bar steel properties, while keeping the concrete properties constant. The three different steel properties were based on the stress-strain curves as presented in Figure 5.9.

Figure 5.14 includes the responses of the first three models. In this set, the concrete grade was kept at 30 MPa while the material properties for the starter-bars were changed. Similarly, Figure 5.15 presents the structural responses of another set of FE models, this time with a characteristic compressive stress of 40 MPa. Finally, Figure 5.16 presents the results for the models with a concrete grade of 50 MPa.

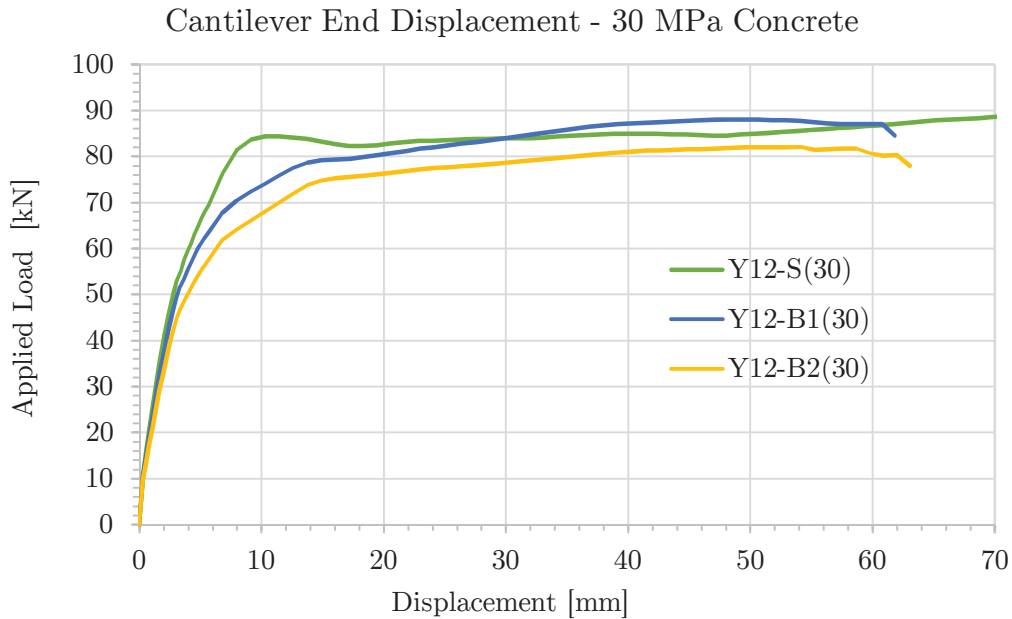


Figure 5.14: Results for Finite Element Analyses - 30 MPa Models

All three graphs show a similar trend: the structural performance is greatly dependant on the tensile properties of the starter-bars. The effect of cold bending is clearly visible as the B-series models all produced less desirable structural responses. The shapes of the stress-strain curves for the starter-bars, presented in Figure 5.9, are closely mirrored here in the load displacement curves of their corresponding models. The E-modulus of the Y12-S bar is noticeably higher than the other bars and this resulted in a connection that performed better at the SLS and ULS. The Y12-B2(30) model produced the weakest structural response spectrum with a maximum resistance equal to 82.06 kN, 8 % lower than the Y12-S(30) model. The tip displacement for the Y12-S(30) model was 2.01 mm at SLS and 2.72 mm at ULS. At the same applied load, model Y12-B1(30) recorded an 11 % increase in the displacement at SLS and 14 % at ULS. The reduction in the yield stress of the starter-bars had the biggest effect on the stiffness of Model Y12-B2(30) and resulted in a tip displacement of 2.6 mm at SLS and 3.82 mm at ULS, a 29 % and 41 % increase respectively. The onset of deflection softening was also much earlier for the Y12-B models and this corresponded to the observations made in Figure 5.9: the stress-strain curve for the bent and straightened bars (B-series) did not have a definite point at which it flattened and the gradient for the linear portion just gradually reduced to create a curved graph. Similar observations were made in the models with a concrete grade of 40 MPa, as shown in Figures 5.15.

The structural response of the models with a concrete grade of 50 MPa showed a significant increase in the ultimate resistance of the connection before experiencing a sudden loss in stiffness. This drop could be the result of the concrete reaching its maximum compressive resistance just before it starts to fail in the compression zone of the section. This can be seen in Figure 5.16.

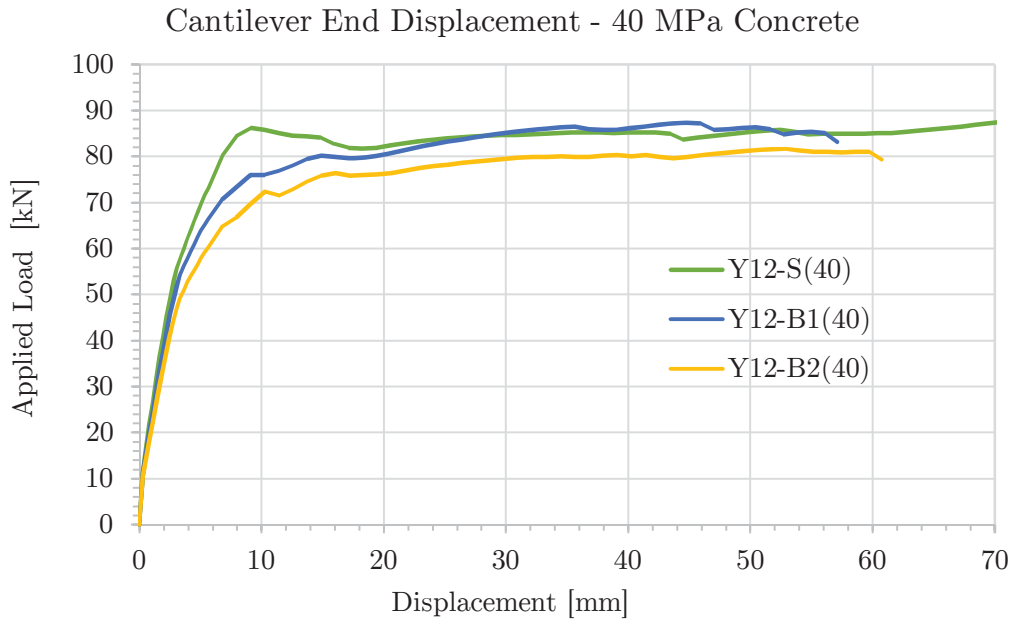


Figure 5.15: Results for Finite Element Analyses - 40 MPa Models

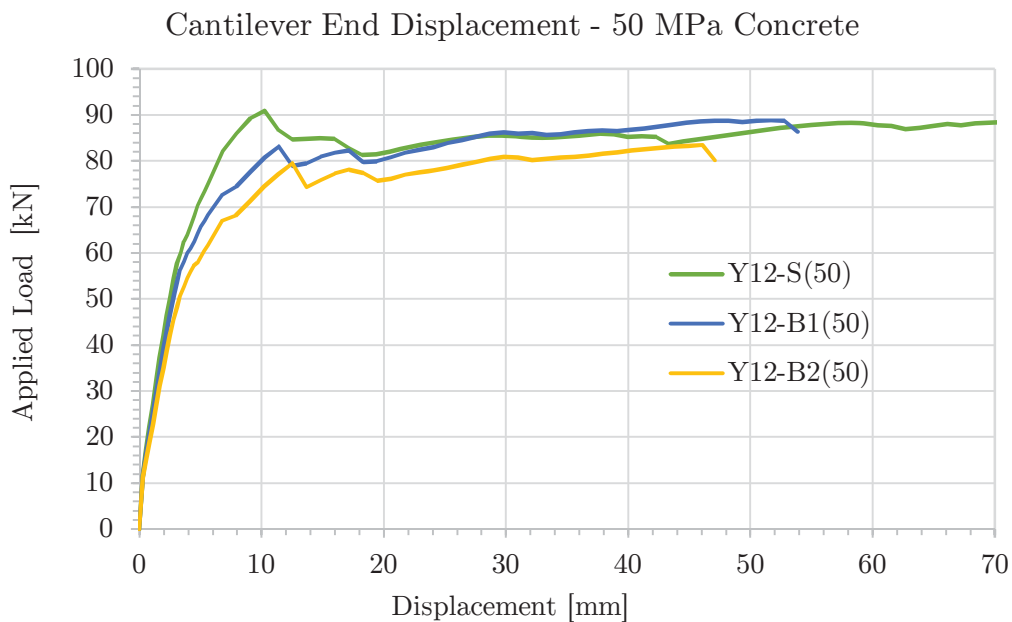


Figure 5.16: Results for Finite Element Analyses - 50 MPa Models

The second parameter study is the concrete class. In this case the sensitivity of the structural response to the use of different concrete classes is studied, while the steel properties are kept constant. The results are presented through Figures 5.17 to 5.19. Each figure displays the structural response of three models, all with the same steel properties, but with different grades of concrete.

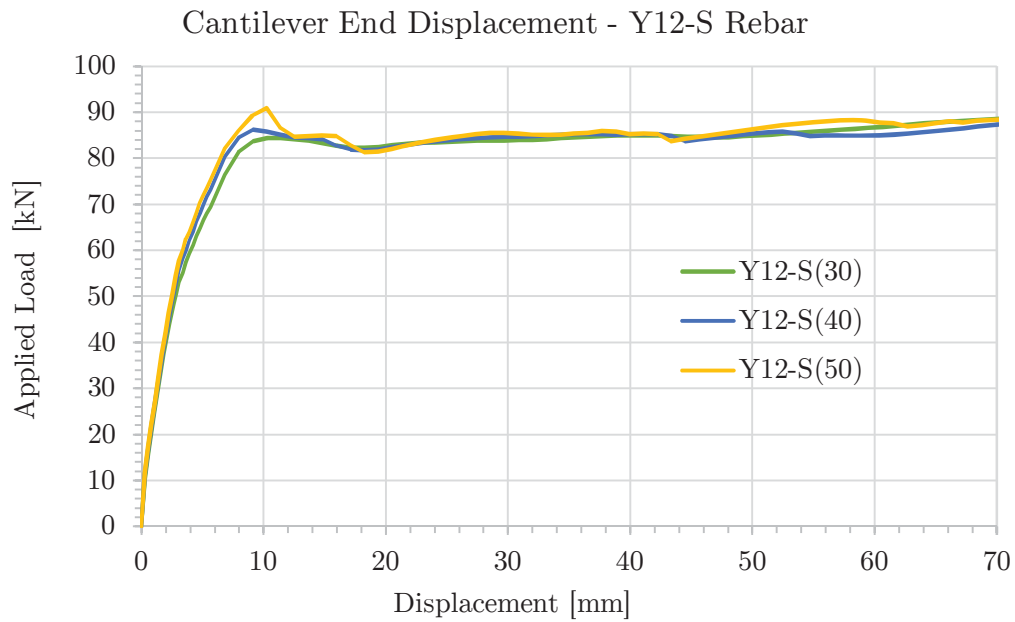


Figure 5.17: Results for Finite Element Analyses - S-Series Models

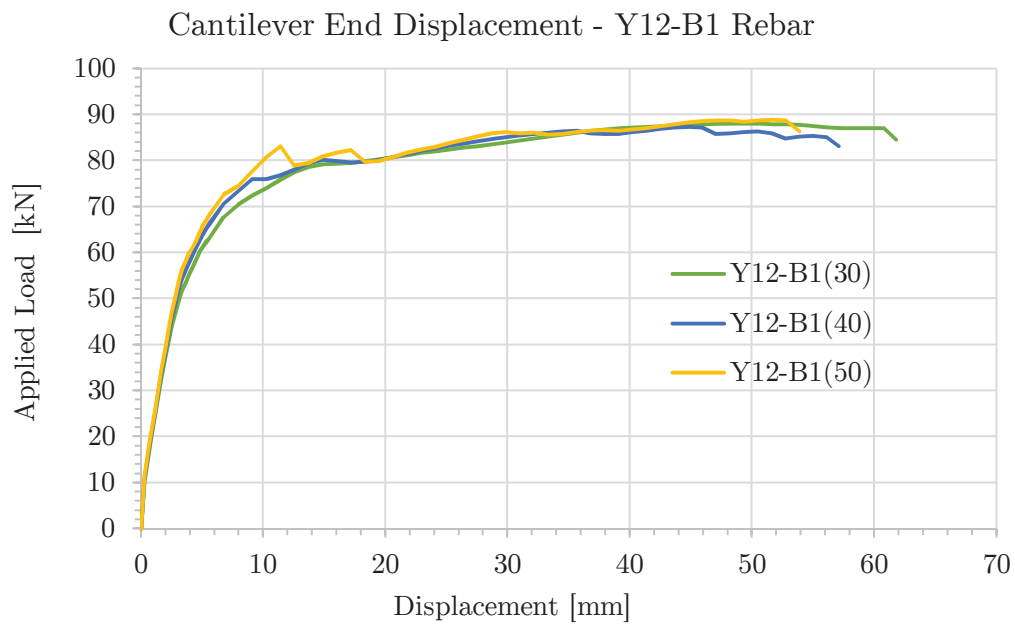


Figure 5.18: Results for Finite Element Analyses - B1-series Models

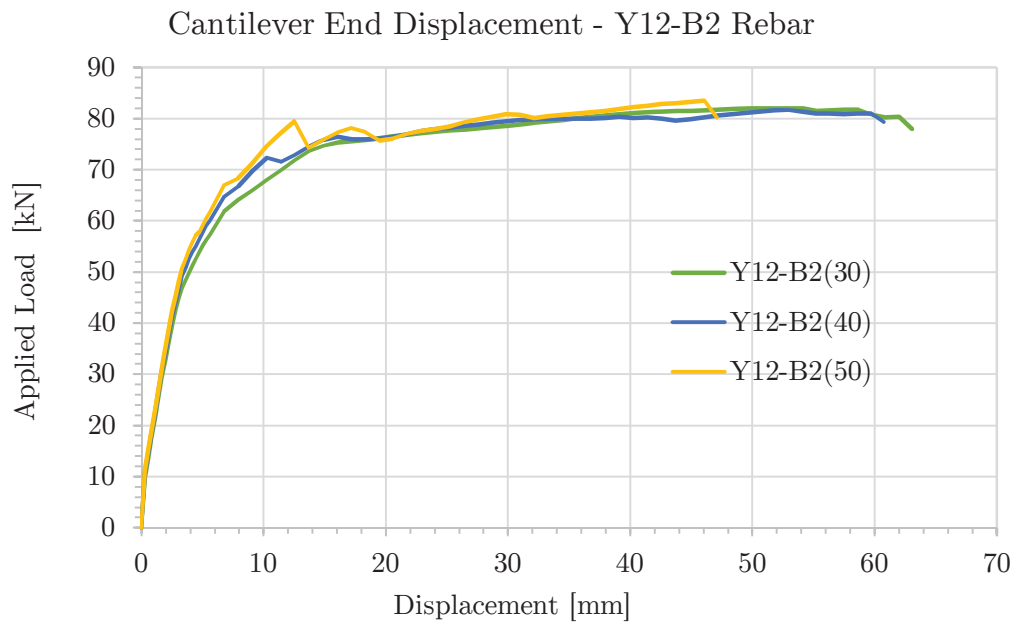


Figure 5.19: Results for Finite Element Analyses - B2-series Models

Although the stiffness increased slightly with an increase in the concrete strength, it is clear that the structural performance is significantly more sensitive to a change in the properties of the starter bars than to a change in the concrete grade. There is, however, a noticeable increase in the ultimate resistance of the models using a 50 MPa concrete. It is important to note that only the properties of the starter-bars were varied and not the rest of the general reinforcement in the wall or the slab. This mimics the situation in practice where only the starter-bars are subjected to cold working.

The final section of the sensitivity study presents a sensitivity graph. The percentage reduction in the yield stress, or concrete compressive stress, is located on the y-axis and the resulting percentage increase in the tip displacement on the x-axis, as shown in Figure 5.20. The data is captured only for the SLS. The crack widths were also measured and a similar graph is presented in Figure 5.21.

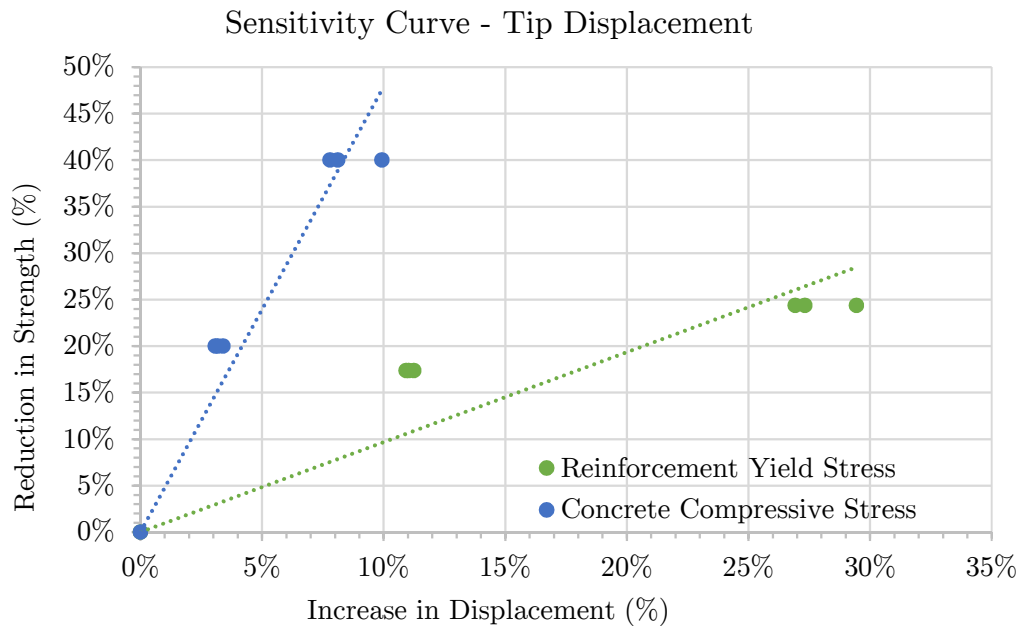


Figure 5.20: Tip Displacement Sensitivity to Change in Steel and Concrete Properties

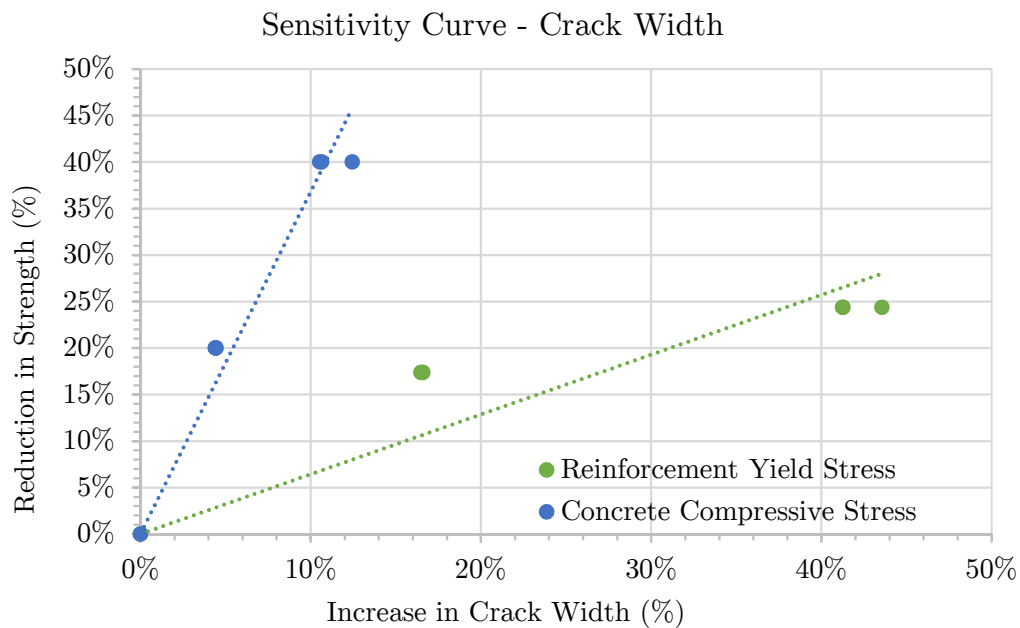


Figure 5.21: Crack Width Sensitivity to Change in Steel and Concrete Properties

The dotted lines in both Figures 5.20 and 5.21 resemble a best-fit linear function to the data points on the graph. This shows that the structural performance of RC slab-to-wall connections is more sensitive to a change in the starter-bar properties than to a change in concrete grade. For a wall-to-slab connection with the same configuration as described in Chapter 3, a 20% decrease in the yield stress of the reinforcement could result

in an 24% larger displacement of the slab at its tip, with the largest crack being 34 % wider. Once again, the percentages are relative to the values obtained for a connection system with continuous starter-bars that have not been subjected to any cold bending and straightening.

Chapter 6

Conclusions and Recommendations

6.1 Introduction

The main aim of this research investigation was to provide recommendations on how to design and construct the most effective wall-to-slab moment-fixed connection. The focus was on high rise construction, but similar applications where floors are connected to already cast walls are also applicable.

Four different connection systems were studied, focussing on the aspects in each system that might improve or impair the structural performance of the wall-to-slab joint. Full-scale testing was performed on the four systems in order to compare their performances and constructibility. The results from the full scale tests indicated that the structural performance in some of the connection systems might be compromised by the cold working of the starter bars. This observation was confirmed with a series of tensile tests conducted on individual reinforcing bars.

Finally, numerical analyses verified the results obtained in the full scale tests, while further development of a series of FE models studied the sensitivity of the structural performance to a range of different concrete strengths and reinforcing bar stress-strain behaviours.

6.2 Conclusions

6.2.1 Constructibility of Systems

The installation procedure for the continuous starter-bar system is a tedious and time consuming process. The starter-bars have to be fixed one-by-one while ensuring the correct level is always maintained. It is also challenging to cut the holes in the shuttering for the starter-bar legs at the correct position and to make them big enough to fit comfortably around the bars, without making them so big that the wet concrete spills from the gaps around the bars. This system is not compatible with jump or slip formwork, as the protruding bars will hinder the sliding nature of the systems. Further, the exposed bars are impractical on site and they are a safety hazard for workers moving in the vicinity.

The constructibility of the site-installed bend-out system is also far from ideal: the pre-bent bars need to be fixed individually and great care should be taken to ensure that they are properly tied to prevent any shifting during concreting. A downward shift will compromise the effective depth of the flexural reinforcement and in turn decrease the

moment capacity of the connection. If the bars are cast too high, the cover on the reinforcement is reduced and this could lead to the connection not meeting the required level of serviceability.

The use of power tools to chip the concrete away and reveal the bent bars is not only labour intensive, but there is a great risk of damaging the reinforcement during the process. One of the specimens in section 4.3.1 recorded a significant lower E-modulus of 74 GPa that could be explained by damage caused to the specimen prior to it being tested. It is therefore very important to ensure that no bars are damaged when removing the concrete surrounding them. Once the bars are revealed, a standard pipe can be used to straighten them. During the construction of the models it became clear that the modified pipe does not make the process any easier or produce significantly straighter bars. It is more important to properly expose the bent rebar before attempting to straighten them. The straightening process should also be done in one smooth motion without over working the steel to reduce the risk of brittle fracture. Although the site-installed bend-out system has many drawbacks it can produce a proper floor-to-wall joint under the correct supervision without the hassle of drilling holes in the formwork or exposing anyone to the hazards of protruding rebar on site. The bend-out bars can also be ordered from any bending yard, bringing the material cost of the system in line with the continuous starter-bar alternative, as seen in Table 6.1.

The pre-assembled bend-out system addresses two of the major shortcomings of the site-installed version: the pre-assembled starter-bars speed up the fixing process and once the wall is cast the steel lid is simply removed to reveal the bent reinforcement. Due to the speed with which the system can be installed, it is the preferred system to use with any form of jump or slip formwork. The only drawback is the price, as the material cost is nearly double that of the first two systems. However, in large projects where the cost of the connection systems are insignificantly small compared to the overall building cost, their use can easily be justified. It is also important to ensure that the reinforcement supplied in the boxes conform to the minimum requirements of SANS 920:2011 - the company should be able to produce the relevant certification when supplying the product.

Another, even more elegant solution is the use of cast-in anchors with couplers. This is particularly useful in walls where the concentration of reinforcement is already high as the anchors take up little space. The installation process is simple, fast and effective. Once the wall is cast, the timber carriers are removed and the continuation rebars are screwed in and tightened with a hand wrench. Good quality-control is essential to ensure that all the bars are fully screwed in. In terms of material cost this system is the most expensive. This product is not currently available in South Africa and a realistic cost comparison is therefore not possible. However, in a market where all the systems are locally manufactured the material cost for this system is 3 times that of the pre-assembled bend-out system, as presented in Table 6.1.

Table 6.1 presents a summary of the material costs for the respective systems. Both the local rates and the rates in the United Kingdom are included. The rates are all based on a connection between a 300 mm wall and a 250 mm floor, with Y12 rebar spaced at 150 mm c/c and 25 mm cover.

It is important to note that, depending on the size of the project and the specific application, the material cost of all the slab-to-wall connections might be insignificantly small compared to the overall cost of the project or building. Although it is important to design

Table 6.1: Combined Material Cost Comparison

System.	Rate (UK) (£/m)	Rate (RSA) (R/m)
Continuous Starter-bar	11	130
Site-installed Bend-out Bar	11	130
Pre-assembled Bend-out Bar	27	245
Cast-in Anchor	83	*

* system not locally available

as economically as possible, this material cost comparison should not be used in isolation, but rather as a guide to consider all possible options.

6.2.2 Effect of Cold Bending and Straightening

Through this research investigation it has become clear that the cold bending and straightening of reinforcement have a significant effect on the properties of the steel. The stress-strain relationship is affected and the result is a reduction in the E-modulus, maximum elongation and yield stress of the steel.

A significant drop in the E-modulus can be expected, with an average reduction of 16.5% for the Y10 specimens and 23.5% for the Y12 bars. These reductions relate to an average E-modulus of 168 GPa and 160 GPa respectively, with only 3 specimens recording a value below 150 GPa. A modified value for the E-modulus of 150 GPa should therefore be used when conducting the design for connections that contain bars that have been cold bent.

Although this study was unable to quantify the amount of reduction in the ductility of cold bent bars, the phenomena was observed during the low cycle fatigue tests where some bars fractured after being cold bent and straightened more than twice. Previous research showed that a reduction of up to 50% can be expected (Chun and Ha, 2014). This could lead to bars failing the ductility requirements as set out in SANS 920:2011. The full scale specimens did, however, behave in a ductile manner and no fracture of any reinforcement was observed. It is subsequently concluded that further research is required to better understand and quantify the reduction in ductility of cold bent rebar and the effect it has on the structural performance of slab-to-wall connection systems.

On average, a 16% reduction in the yield stress can be expected for Y10 reinforcement and a 19.5% reduction for Y12 bars. Although the reduction in the ultimate stress is not as significant, a small reduction of between 2% and 4% should be accounted for in the design. It should be noted that despite the number of tests (20 or more), the pool of data is limited and only represents one manufacturer's steel. It is concluded that the characteristic yield stress for cold bent rebar should be reduced by 20% in any design calculations.

The phenomena of Age-Hardening can reverse the negative effect of cold working, but should not be relied upon during the design process as the time, for this re-strengthening

mechanism to realise between bending and straightening of reinforcement, is rarely available in practice. It should be noted that the time between bending and straightening for all the specimens in this research investigation was two weeks.

The reduction in the yield stress, observed by bending and straightening reinforcement once, will not necessarily continue if the process is to be repeated. The risk of brittle fracture does, however, increase with each cycle and a further reduction in the ductility of the steel can be expected. Repeated cold working of reinforcement on site should therefore be avoided as far as possible.

6.2.3 Structural Performance of Systems

The structural response of all the systems can be categorised as ductile, although the performance of the continuous starter-bar system was the most desirable. This is expected, as the starter-bars in this system are not subjected to cold bending and straightening.

Between the two bend-out bar systems, the site-installed version (Model B) performs slightly better in both displacement and crack widths at SLS and ULS. This enhancement could be the result of better aggregate interlock, as the concrete surface is roughened with the jack hammer when exposing the rebar. This is compared to the pre-assembled alternative (Model C) where the steel box is cast into the wall and prevents any concrete contact across the joint. The point of ultimate resistance for Model C was also 6 % lower and the deflection softening after this point more significant when compared to Model B. The structural performance of both systems is, however, inferior to that of the continuous starter-bar system (Model A) and larger displacements and crack widths can be expected when using a bend-out system.

The performance of the cast-in anchor system (Model D) is very similar to the site-installed bend-out system at SLS and ULS, but not equal to that of the continuous starter-bar system. A difference in behaviour was observed beyond the ULS with a sudden drop in the stiffness, followed by the earliest onset of deflection softening of the four models. Although the system did perform satisfactory at the SLS and ULS, larger displacements and cracks should also be expected when using this system.

6.2.4 FEM and Sensitivity Study

The structural performance of a moment fixed slab-to-wall connection joint can be successfully simulated using finite element analysis. Using the Diana software package, results in reasonable agreement with experimental data were obtained with the combination of the *total strain rotating smeared crack model* for RC elements and modelling the reinforcement as *embedded reinforcing bars*.

The sensitivity study clearly highlighted that a change in the properties of the reinforcement has a much greater effect on the structural performance of a connection, than the use of a different grade of concrete. A 25% increase in the tip displacement of a cantilever floor can be expected when reducing the starter-bar yield stress by 20%, compared to only a 5% increase in the displacement when lowering the concrete strength by the same amount. Similarly, a reduction of 20% in the yield stress could result in 35% wider cracks at SLS.

6.3 Recommendations

- If the use of jump or slip formwork is not a requirement, any of the alternative systems can be used. Although the structural performance of the site-installed system is slightly superior and the material costs 47% less, practical considerations and project specific aspects might be of greater influence when choosing the most desirable system. It is therefore recommended that the suitability of a specific alternative system should be evaluated against all the aspects for any given project.
- If one of the bend-out systems are chosen, the design should be conducted with a modified yield stress and E-modulus for the flexural reinforcement in the joint. The recommended value for the yield stress is $0.8 \cdot f_y$ and 150 GPa for the E-modulus. The design engineer should also strive to keep the elongation of the reinforcement in the connection to a minimum as a reduction in the ductility of the bars can be expected.
- The size of the reinforcement to be used in any bend-out system should be limited to a diameter of 12 mm. Larger bars are not recommended for cold-bending on site and the effect on the steel properties are not covered in this research investigation. This study has found that the negative effects on the steel were worse for the Y12 bars than for the Y10 bars. A further reduction is, therefore, believed to occur in larger diameter bars.
- When using the site-installed bend-out systems, good site supervision and quality control is necessary to ensure that the starter-bars are fixed securely and at the correct level. It is recommended that the future floor level is clearly indicated on the horizontal wall reinforcement to help identify starter-bars that are fixed out of place.
- Care should be taken when chipping away the concrete surrounding the pre-bent rebar in the site installed bend-out system. It is recommended that a small jack hammer is used that will fit easily between the bars. The pre-bent rebar should first be fully exposed, with at least 30 mm clear spacing behind the bend, before any form of straightening is considered. A steel pipe should be used to straighten the bars. The pipe should be placed over the reinforcement and continuously pushed inwards as far as possible, while straightening the rebar in one smooth motion. If the bar is not entirely straight after the first attempt, not more than one further adjustment should be considered.
- Once the starter-bars are straightened, the concrete at the joint should be properly scabbled to ensure aggregate interlock. All starter-bars should be checked to verify that they have not been damaged in any way during the straightening process. All damaged bars should be considered unusable and the design will have to be re-checked ignoring these bars.
- Any reinforcement that has been cold bent past 45° should be considered to have a reduced capacity and ductility and the design of the specific element should be checked, using the modified yield stress and E-modulus as recommended above. If possible, conduct tensile tests on reinforcement cut from the same batch of steel and the reduction in the properties may be determined. Tables 5.20 and 5.21 can then be used as a guideline to predict the performance of the structure at SLS.

- If a slip or jump formwork method necessitates the use of pre-assembled starter-bars, it is recommended that the design is conducted with the modified steel parameters and that the possibility of larger deflections and cracks, in the order of 5%, are accounted for.
- The use of cast-in anchors could be a feasible option in highly congested walls or when larger moment capacities are required. The enhancing effect of the modified cone behaviour can be adopted to produce more economical designs, but once again larger deflections and cracks should be expected and accounted for.
- The manufacturer's specifications and installation procedures should also be strictly followed when using the cast-in anchor system. A proper tightness check of all the continuation rebar should be conducted before the fixing of the reinforcement for the floor commences. The tightness can be checked by using a standard hand wrench.
- The thread at the end of the continuation reinforcement, supplied by the manufacturer, should be a size larger than the nominal diameter of the bar. Couplers with tapered threads should be avoided as they only obtain their tensile capacity when they are fully screwed in. The constant diameter couplers, as used in this study, gradually build up their capacity with each turn of the continuation bar.
- When creating a non-linear finite element model of RC structures, the Diana software package is recommended. A non-linear analysis should be performed with the *total strain rotating smeared crack model*. The reinforcement can be successfully modelled as *embedded reinforcing bars*, but should be placed in a full 3D structure.
- In order to incorporate the effect of a construction joint, it is recommended that a plane of elements is modelled with modified properties at the location of the joint. The compressive properties should be kept unchanged, while the characteristic tensile stress can be significantly reduced to simulate the loss in tensile transfer across the construction joint.

6.4 Future Work

The following recommendations are made for further research:

- The reduction in the ductility of cold bent reinforcement should be studied and quantified in order to ensure that the standardised ductility requirements of SANS 920:2011 are met when using bend-out bar systems. It could be beneficial to perform further research using reinforcement from a variety of South African suppliers to determine if there is any variation in the steel properties.
- In-depth research is needed on all the practical aspects of the alternative slab-to-wall connection systems. These results can be used to determine the actual costs of the systems for various project sizes, configurations and applications. This will greatly assist the engineer when choosing the most suitable connection system for the project at hand.
- Further sensitivity studies should be performed on the various slab-to-wall systems, in order to determine the effect of different variables that might be encountered on

a construction site or in a specific application. These include different wall and slab configurations, the misplacement or damaging of starter-bars, concrete not being properly vibrated when being poured or placed in extreme weather conditions and starter-bars that have been cold bent more than once.

Appendices

Appendix A

Detailed Design Procedure - Continuous Starter-bar System

This Appendix includes a detailed description of the design procedure for a wall-to-slab connection, making use of continuous starter-bars for continuity.

A.1 Step 1 - Determine loads

SANS 10160:2011 forms the basis for structural design in South Africa. It provides information on typical forces or actions that can be expected to act on a structure and also provides the necessary principles to apply when conducting a structural design or analysis. This code is subsequently consulted to determine the characteristic values of actions for a specific project. The code defines all actions as being one of the following:(SANS, 2011a)

Permanent Action (G) - action that is likely to act throughout a given reference period and for which the variation is always in the same direction (monotonic), until the action attains a certain limit value. (SANS, 2011a)

Variable Action (Q) - action for which the variation in magnitude with time is neither in relation to the mean value, nor monotonic. (SANS, 2011a)

Seismic Action (A_E) - action that arises due to earthquake ground motion. (SANS, 2011a)

Accidental Action (A_A) - action, usually of short duration but of significant magnitude, that is unlikely to occur on a given structure during the design working life. (SANS, 2011a)

The code is further divided into eight parts:

Part 1: Basis of structural design – This part serves as a general standard in order to provide a procedure to determine the actions on structures and to calculate their resistance in accordance with the partial limit state design approach.

Part 2: Self-weight and imposed loads – In this part methods are discussed in which self-weight and non-structural materials are applied as permanent loads. The code also specifies minimum values to be used for imposed loads on floors and how to apply them as variable actions divided as a function of occupancy. It further

includes an extended range of imposed loads associated with industrial buildings, horizontal loads on parapets, railings or other balustrades, typical loads on roofs and also light weight partitions.

Part 3: Wind actions – Actions caused by natural wind on land-based structures are dealt with in this part.

Part 4: Seismic actions and general requirements for buildings – This part deals with the actions on buildings induced by earthquakes. It provides strategies and rules for the design of buildings required to resist these loads.

Part 5: Basis for geotechnical design and actions – This part forms the basis for geotechnical design and provides guidelines to deal with vertical earth loading, pressures arising from ground water and actions caused by ground movement.

Part 6: Actions induced by cranes and machinery – Imposed loads induced by overhead travelling bridge cranes are discussed in this part. It also includes a limited amount of information on harmonic loading caused by machinery and how to incorporate this into a design.

Part 7: Thermal actions – This part introduces new procedures to calculate thermal actions on buildings.

Part 8: Actions during execution – Introduces new procedures and general rules to determine the actions that need to be considered in the construction phase of a building or structure.

(SANS, 2011a)

The location, occupancy, use and size of a structure is subsequently used to determine all the relevant actions required for the design process.

A.2 Step 2 - Calculate load combinations

This study only considers ultimate limit state design and subsequent discussions will therefore focus on the conditions at ultimate limit state.

SANS 10160-1:2011 specifies that two limit state combinations are to be considered when calculating actions for structural resistance. They are defined as the so called STR and STR-P limit state combination. The STR combination scheme is for structures with significant imposed loads, while the STR-P scheme is for self-weight dominated structures. The suffix P indicates the dominant effect of permanent actions. These two combinations were found to produce a more uniform level of reliability than the use of a single load combination (Retief and Dunaiski, 2009).

The design load is determined by considering the worst combination that will result in the largest load being applied to the structure. The combinations are determined by multiplying specific factors to the corresponding characteristic value, as determined in section A.1, before adding them together. The partial factors (γ) are set out in Table 3 of SANS 10160-1:2011. (SANS, 2011a)

Further to these partial factors, the code also specifies combination factors (ψ) for variable actions. These factors are applicable when two independent variable actions are to be considered. They account for the probability of simultaneous occurrence of these variable actions - one being the leading action with the rest as accompanying actions. The factors are also found in Table 2 of SANS 10160-1:2011. (SANS, 2011a)

The total variable action (Q_T) and total permanent action (G_T) are calculated by these equations:

For STR (subscript 1):

$$Q_{T1} = \gamma_{Q,1} \times Q_{k,1} + \sum_{i>1} \gamma_{Q,i} \times \psi_i \times Q_{k,i} \quad (\text{A.1})$$

$\gamma_{Q,1}$ is the partial factor for the leading variable action

$Q_{k,1}$ is the characteristic value of the leading variable action

$\gamma_{Q,i}$ is the partial factor for the accompanying variable action

ψ_i is the action combination factor for the accompanying variable action, i

$Q_{k,i}$ is the characteristic value of the accompanying variable action

$$G_{T1} = \sum_{j>1} \gamma_{G,j} \times G_{k,j} \quad (\text{A.2})$$

$\gamma_{G,j}$ is the partial factor for the permanent action, j

$G_{k,j}$ is the characteristic value of the permanent action, j

For STR-P (subscript 2)

$$Q_{T2} = \gamma_{Q,1} \times Q_{k,1} \quad (\text{A.3})$$

$$G_{T2} = \sum_{j>1} \gamma_{G,j} \times G_{k,j} \quad (\text{A.4})$$

All possible load combinations are considered and the combination that is most detrimental to the specific structure is used as the ultimate design load in the next step.

A.3 Step 3 - Analyse structure

The primary objective of a structural analysis is to obtain the internal design forces and moments, so that they are in equilibrium with the applied actions from a specific limit state. SANS 10100-1:2000 provides a simplified approach of analysing a structure, given that it only has to resist vertical loads i.e. the frame is fully braced in both directions. (SANS, 2000)

Design moments, loads and shear forces are determined by elastic analysis of a series of subframes as opposed to running a full 3D analysis. These subframes represent only the beams or slabs in one direction and on one specific floor of the structure. The columns or walls above and below the floor are also modelled to simulate the stiffness of the supporting structure. An example of a subframe is presented in Figure A.1. (SANS, 2000)

In order to simulate the worst case scenario, SANS 10100-1:2000 recommends that at least three loading arrangements are considered when analysing a subframe. It further comments that the STR limit state is in most reinforced concrete structures, the critical state and subsequently there is no need to include both limit states when applying pattern loading. (SANS, 2000) The three loading arrangements (or pattern loading) are applied as presented in Figure A.1.

The maximum design moments and shear forces are extracted from the analysis and used in the following steps.

A.4 Step 4 - Design for Flexure

In this step, the cross sectional properties of the floor is used to calculate the amount of reinforcement needed to resist the design moment at the connection. The design methodology as described in SANS 10100:2000-1 is used and it is based on the follow fundamental principles: (SANS, 2000)

- Simplified stress-strain relationships for both the steel and concrete are adopted. Refer to Figures 1 and 2 in the code for these stress-strain curves
- Plane cross-sections remain plane during bending
- Flexural stresses must be in equilibrium at every section along the element
- The material factor (γ_m) for reinforcement is taken as 1.15
- The material factor (γ_c) for concrete is taken as 1.5
- The tensile strength of the concrete is ignored

(SANS, 2000)

The design process starts by calculating the value for the constant (K) using the design moment (M), concrete compressive cube stress (f_{cu}) and the equivalent section depth (d) and width (b), in Equation A.5:

$$K = \frac{M}{bd^2 f_{cu}} \quad (\text{A.5})$$

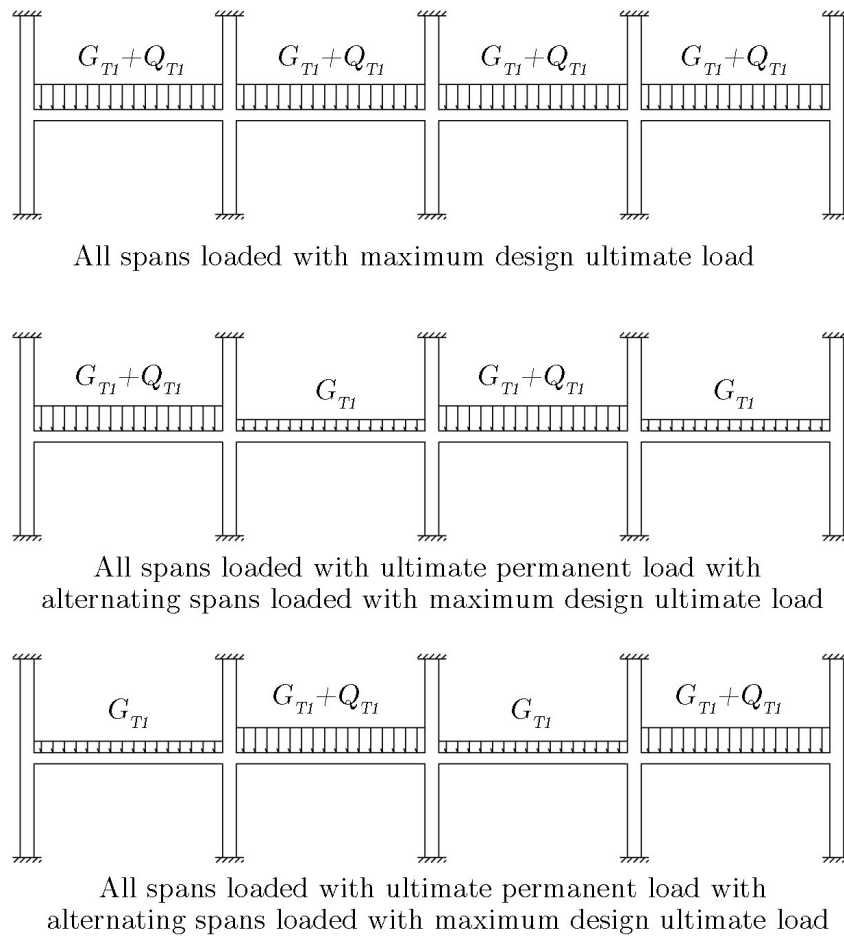


Figure A.1: Pattern Loading on a Typical Subframe

K' is equal to 0.156 when the redistribution of moments does not exceed 10%, otherwise it is calculated with Equation A.6. If this is not the case, K' is calculated using the percentage of redistribution (B_b) used.

$$K' = 0.402(B_b - 0.4) - 0.18(B_b - 0.4)^2 \quad (\text{A.6})$$

If $K \leq K'$ (which is the only case that will be considered here) only tension reinforcement is required. The lever arm (z) and natural axis depth (x) are determined using Equations A.7 and A.8 respectively. The length of the lever arm (z) is limited to the following two values:

- $0.775d \leq z$: This lower limit is to account for a reduction in the effective stress block due to weaker concrete found at the surface of the concrete
- $z \leq 0.95d$: This upper limit is to ensure that the connection is of ductile behaviour and that a brittle failure will not occur

$$z = d \left\{ 0.5 + \sqrt{\left(0.25 - \frac{K}{0.9}\right)} \right\} \quad (\text{A.7})$$

$$x = \frac{d - z}{0.45} \quad (\text{A.8})$$

The amount of reinforcement required (A_{sreq}) is calculated by considering the equilibrium of forces and moments over the section. The characteristic yield stress of the steel (f_y) is multiplied by a material factor of 0.87 to account for any inaccuracies in the assessment of the resistance of the section. Finally, when the equation of equilibrium is re-arranged, the amount of reinforcement is determined with Equation A.9.

$$A_{sreq} = \frac{M}{0.87f_y z} \quad (\text{A.9})$$

The rebar configuration (size and spacing) is chosen in such a way that the actual area of reinforcement (A_{sprov}) is more than the required area (A_{sreq}). More information on the detailing and configuration of the rebar is provided in section A.6.

(SANS, 2000)

A.5 Step 5 - Design for Shear

In contrast to flexural design, where there is a close agreement between experimental results and the numerical predictions, the methods available for shear design is not yet fully understood. Consequently there is a big difference between what is numerically predicted and what experimental data reveals. For this reason beams and slabs are designed in such a way that they will fail in flexure before failing in shear. (Robberts and Marshall, 2010)

The method, as described in SANS 10100:2000, starts with determining the design shear stress (v) by dividing the design shear force (V) by the effective area of the section ($b \times d$):

$$v = \frac{V}{bd} \quad (\text{A.10})$$

The design stress value (v) is limited to the lesser of $0.75\sqrt{f_{cu}}$ or 4.75 MPa.

The shear resistance of a section (v_c) is determined by Equation A.11. The resistance is a function of the characteristic concrete cube stress (f_{cu}) (which is limited to 40 MPa), the effective depth (d) and the effectively anchored tension reinforcement ratio $\left(\frac{100A_{sprov}}{bd}\right)$:

$$v_c = \frac{0.79}{\gamma_m} \left(\frac{f_{cu}}{25}\right)^{\frac{1}{3}} \left(\frac{100A_{sprov}}{bd}\right)^{\frac{1}{3}} \left(\frac{400}{d}\right)^{\frac{1}{4}} \quad (\text{A.11})$$

γ_m is the partial safety factor for materials = 1.4

If the resistance (v_c) is more than the design stress (v) the criteria is met.

(SANS, 2000)

A.6 Step 6 - Rebar configuration

Although the SLS design procedures are not explicitly covered in this paper, certain rules to minimise cracking are considered in this step when deciding on a specific rebar configuration.

SANS 10100-1:2000 is consulted to determine the maximum spacing for the longitudinal reinforcement. Table 25 provides a simplified approach by limiting the maximum clear spacing for high yield bars in slabs to 170 mm. This approach is effective to limit crack widths to 0.3 mm. (SANS, 2000)

In order to ensure the required level of durability is maintained the specific condition of exposure is selected from Table 1 in SANS 10100-2:2014. The cover for the reinforcement is subsequently determined as a function of the exposure. (SANS, 2014)

Further detailing requirements are found in SANS 10144:2012 - Detailing of steel reinforcement for concrete. Some important considerations are listed below:

- The minimum clear spacing for bottom rebars, is the sum of the aggregate size plus 5 mm
- The minimum clear spacing for top rebars is a 100 mm. This ensures that a vibrator can fit through the rebar
- The minimum area of main reinforcement is equal to 0.13% of the effective cross-sectional area of the slab
- The minimum area of secondary steel is the greater of 0.06% of the cross-sectional area of the slab, or one-quarter of the area of main reinforcement

Once the reinforcement configuration is established, the anchorage and lap lengths are determined.

A.7 Step 7 - Anchorage and lap lengths

In order for the connection to transfer the design moment in the floor to the connecting wall, the tension rebar has to be properly anchored in the wall and lapped with the floor reinforcement. The reasoning behind the methodology for the design of anchorage, as set out in SANS10100-1:2011, is that if a rebar is properly anchored it will yield before pull-out occurs. (Robberts and Marshall, 2010)

The ultimate anchorage bond stress (f_{bu}) is given in Table 24 of SANS10100-1:2011. It is a function of the type of rebar and the characteristic cube stress of the concrete (f_{cu}). The bond stress is assumed to be constant over the effective anchorage length of the bar. The required anchorage length (l) to transfer a force (F_s) in a bar to the surrounding concrete is calculated by:

$$l = \frac{F_s}{\pi\Phi f_{bu}} \quad (\text{A.12})$$

Φ is the effective bar diameter

The legs of the continuous starter-bars should project at least a lap length from the face of the wall when it is installed i.e. it should project at least a distance equal to the length as calculated in Equation A.12. F_s is taken as the ultimate yield force for reinforcement ($f_y \times 0.87 \times A_s$). This will ensure that the bars yield before any slippage occurs. Refer to Figure 2.1 where the lap length is indicated.

The anchorage of the tensile (top) reinforcement in the connection is determined by considering the anchorage length available in the connecting wall as shown in Figure A.2.

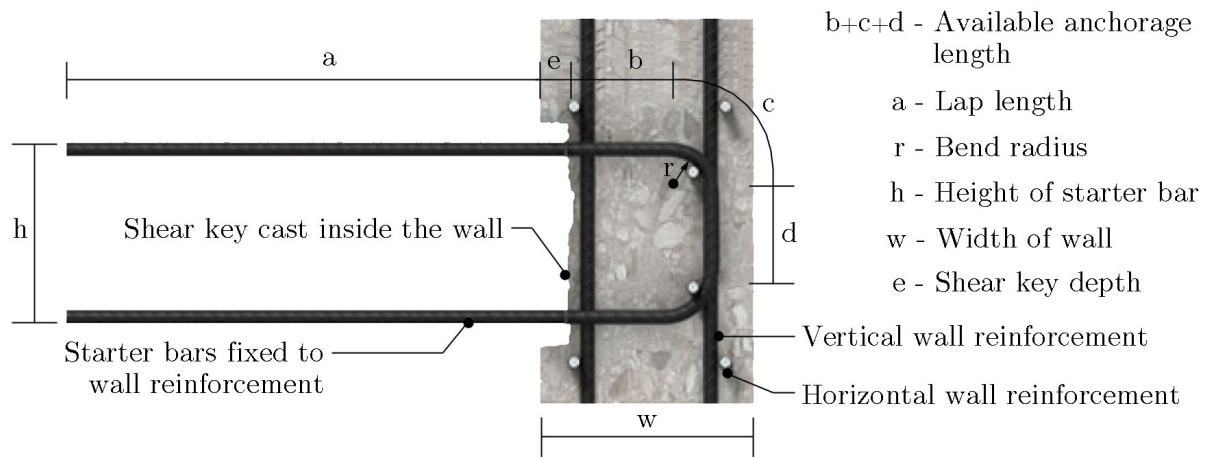


Figure A.2: Cast-in Starter-bar Anchorage Detail (reworked from Ancon Building Products (2014))

The equation to determine the available anchorage length (l_{ave}) is given in Robberts and Marshall (2010) as:

$$l_{ave} = b + c + d \quad (\text{A.13})$$

with

$$b = w - cover - \Phi_{hor} - \Phi_{ver} - r - e \quad (\text{A.14})$$

$$c = 8\Phi \quad (\text{A.15})$$

$$d = h - 2\Phi - 2r \quad (\text{A.16})$$

Φ is the starter-bar diameter

Φ_{hor} is the horizontal wall reinforcement bar diameter

Φ_{ver} is the vertical wall reinforcement bar diameter

The available anchorage is further used to determine the maximum stress that can be transferred through the top rebar to the wall in a specific connection. The available anchorage length is substituted into Equation A.12 and re-arranged so that F_s can be determined. F_s is then divided by the starter-bar area (A_s) to determine the engineering stress (f_s) that can be transferred to the wall. If $f_s \geq 0.87f_y$ then it can be assumed that the rebar will yield before pull-out will occur. If, however, $f_s \leq 0.87f_y$ then the bars will start to pull-out before their yield stresses are reached and in such a case the available anchorage length will have to be increased i.e changing the wall or floor thickness. Alternatively, f_y will have to be decreased in all the design calculations. If the latter is opted for, f_y will become a value equal to $f_s/0.87$. (SANS, 2000)

Recent experimental data, however, suggests that the values for the ultimate bond stress in Table 24 of SANS10100-1:2011 are conservative and therefore pull-out failure in this type of connection is highly unlikely. (De Villiers, 2015)

A.8 Step 8 - Detailing Reinforcement

The final step in the design process is to create a bending schedule with the correct dimensions and shape codes according to the guidelines set out in SANS10144:2012. The starter-bars are usually a shape code 38.

A shape code 38 is defined by three dimensions A, B and C as illustrated in Figure A.3. A and C are the same length and will be equal to $a + e + b + 4\Phi$ as defined in Figure A.2. While B will be equal to the starter-bar height (h).

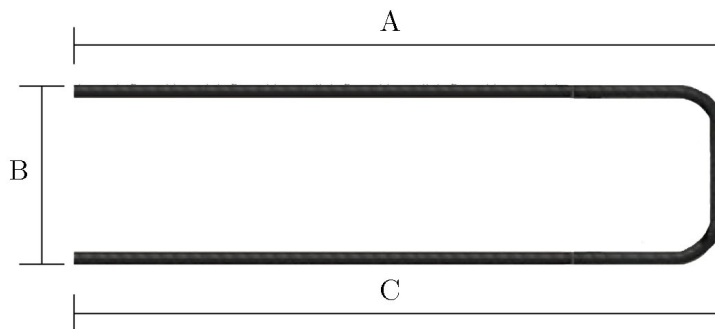


Figure A.3: Shape Code 38

Appendix B

Tensile Test Results

The full set of data recorded in the tensile tests conducted in this research investigation is presented in this Appendix. The first four tables contain the data from the preliminary tests. Table B.1 contains the data for the tensile tests on the machined Y10 straight bars, while Table B.2 contains the data for the straightened Y10 bars. Similarly does Table B.3 and Table B.4 contains the data for the Y12 machined and straightened bars.

The last five tables contain the data for the tensile tests done on the reinforcement used in the full scale models. Table B.5 contains the data of the reinforcement used for starter bars in Model A. Similarly, Table B.6 contains the data for Model B and Table B.7 for Model C. The data for the tensile tests conducted on the continuation rebar of the cast in anchor system of model D, is presented in Table B.8. Finally the test results for the reinforcement used in the walls, for all the full scale models, are presented in Table B.9.

The tables contain the following information captured during each test.

Set nr. - the set number that correlates to the numbers used in the graphs in section 4.3

Specimen nr. - the individual number marked on each specimen

$S_0(mm^2)$ - the average original cross sectional area over the parallel length

$L_0(mm)$ - the gauge length

$E(GPa)$ - the modulus of elasticity rounded off to the nearest whole number

$f_y(MPa)$ - the yield stress rounded off to the nearest whole number

$f_u(MPa)$ - the ultimate stress rounded off to the nearest whole number

Average - the average value rounded off to the nearest whole number

Std deviation - the standard deviation

Coeff of variation - the coefficient of variation

The average values, standard deviation and coefficient of variation is determined using the precise values of the data, before they were rounded off as presented in the tables.

Table B.1: Preliminary Tensile Testing Results - Y10 Straight Rebar

Y10 Straight bars						
Set nr.	Specimen nr.	$S_o(mm^2)$	$L_o(mm)$	$E(GPa)$	$f_y(MPa)$	$f_u(MPa)$
1	40	52	80	194	503	616
2	41	52	80	201	512	650
3	42	50	80	204	568	718
4	43	52	80	196	549	705
5	44	51	80	192	560	717
6	45	50	80	180	570	724
7	46	51	80	204	575	714
8	47	50	80	194	542	713
9	48	50	80	206	565	719
10	49	50	80	212	544	712
11	50	50	80	208	472	617
12	51	50	80	193	584	718
13	52	52	80	203	560	716
14	53	51	80	203	560	724
15	54	50	80	212	566	726
16	55	51	80	208	569	721
17	56	50	80	197	508	634
18	57	50	80	197	565	718
19	58	50	80	207	580	730
20	59	50	80	203	552	704
Average				201	550	700
Std deviation				7.9	29.4	37.3
Coeff of variation				0.039	0.053	0.053

Table B.2: Preliminary Tensile Testing Results - Y10 Straightened Rebar

Y10 Straightened bars						
Set nr.	Specimen nr.	$S_o(mm^2)$	$L_o(mm)$	$E(GPa)$	$f_y(MPa)$	$f_u(MPa)$
1	18	78	100	160	454	689
2	19	78	100	158	443	689
3	20	78	100	74*	431	692
4	21	78	100	158	464	686
5	22	78	100	191	472	686
6	23	78	100	161	470	685
7	24	78	100	182	445	685
8	25	78	100	218	451	686
9	26	78	100	164	447	689
10	27	78	100	160	482	689
11	28	78	100	157	469	687
12	29	78	100	169	476	686
13	30	78	100	170	451	684
14	31	78	100	167	460	686
15	32	78	100	161	441	687
16	33	78	100	154	464	688
17	34	78	100	149	473	687
18	35	78	100	158	467	685
19	36	78	100	181	478	687
20	37	78	100	170	467	676
Average				168	460	686
Std deviation				16	14.1	3.1
Coeff of variation				0.095	0.031	0.005

*outlier, excluded in the calculation of the average and standard deviation

Table B.3: Preliminary Tensile Testing Results - Y12 Straight Rebar

Y12 Straight bars						
Set nr.	Specimen nr.	$S_o(mm^2)$	$L_o(mm)$	$E(GPa)$	$f_y(MPa)$	$f_u(MPa)$
1	60	79	80	206	543	719
2	61	80	80	206	560	716
3	62	80	80	205	542	713
4	63	80	80	204	582	728
5	64	80	80	213	544	735
6	65	80	80	212	555	703
7	66	80	80	213	561	716
8	67	80	80	221	566	723
9	68	80	80	208	551	720
10	69	80	80	216	558	722
11	70	80	80	211	568	721
12	71	80	80	208	570	726
13	72	80	80	209	555	713
14	73	80	80	203	554	716
15	74	80	80	205	564	724
16	75	80	80	205	538	711
17	76	80	80	205	550	717
18	77	80	80	214	530	707
19	78	80	80	205	551	702
20	79	80	80	204	557	709
Average				209	555	717
Std deviation				4.8	12.2	8.2
Coeff of variation				0.023	0.022	0.011

Table B.4: Preliminary Tensile Testing Results - Y12 Straightened Rebar

Y12 Straightened bars						
Set nr.	Specimen nr.	$S_o(mm^2)$	$L_o(mm)$	$E(GPa)$	$f_y(MPa)$	$f_u(MPa)$
1	1	79	100	160	442	687
2	2	80	100	176	424	688
3	3	82	100	169	471	686
4	4	78	100	168	437	690
5	5	82	100	165	442	687
6	6	80	100	150	468	686
7	7	78	100	158	464	688
8	8	79	100	160	453	685
9	9	79	100	129	431	688
10	10	79	100	159	446	688
11	11	79	100	168	464	684
12	12	80	100	165	449	688
13	13	80	100	155	428	688
14	14	80	100	168	453	688
15	15	80	100	185	442	686
16	16	80	100	167	465	689
17	17	80	100	160	433	685
18	38	80	100	111	432	688
Average				160	447	687
Std deviation				16.8	14.8	1.6
Coeff of variation				0.105	0.033	0.002

Table B.5: Full Scale Model A Floor Reinforcement - Y12 Straight Rebar

Y12 Straight bars						
Set nr.	Specimen nr.	$S_o(mm^2)$	$L_o(mm)$	$E(GPa)$	$f_y(MPa)$	$f_u(MPa)$
1	F1	80	80	222	526	656
2	F2	80	80	215	495	637
3	F3	78	80	223	510	666
Average				220	510	653
Std deviation				4.2	15.8	14.4
Coeff of variation				0.019	0.031	0.022

Table B.6: Full Scale Model B Floor Reinforcement - Y12 Straightened Rebar

Y12 Straightened bars						
Set nr.	Specimen nr.	$S_o(mm^2)$	$L_o(mm)$	$E(GPa)$	$f_y(MPa)$	$f_u(MPa)$
1	FLS1	112	100	144	422	645
2	FLS2	115	100	165	450	651
3	FLS3	113	100	191	437	663
Average				167	436	653
Std deviation				23.9	14.1	8.9
Coeff of variation				0.143	0.032	0.014

Table B.7: Full Scale Model C Floor Reinforcement - Y12 Straightened Rebar

Y12 Straightened bars						
Set nr.	Specimen nr.	$S_o(mm^2)$	$L_o(mm)$	$E(GPa)$	$f_y(MPa)$	$f_u(MPa)$
1	FSC1	112	100	177	487	645
2	FSC2	111	100	198	481	651
Average				187	484	648
Std deviation				14.9	4.2	3.7
Coeff of variation				0.079	0.009	0.006

Table B.8: Full Scale Model D Floor Reinforcement - Y12 Straight Continuation Rebar

Y12 Straight bars						
Set nr.	Specimen nr.	$S_o(mm^2)$	$L_o(mm)$	$E(GPa)$	$f_y(MPa)$	$f_u(MPa)$
1	A1	79	80	210	490	640
2	A2	79	80	213	493	640
3	A3	77	80	212	481	639
Average				212	488	640
Std deviation				1.6	6.2	0.9
Coeff of variation				0.007	0.013	0.001

Table B.9: Full Scale Models Wall Reinforcement - Y12 Straight Rebar

Y12 Straight bars						
Set nr.	Specimen nr.	$S_o(mm^2)$	$L_o(mm)$	$E(GPa)$	$f_y(MPa)$	$f_u(MPa)$
1	W1	79	80	216	536	685
2	W2	79	80	218	542	686
3	W3	79	80	219	522	683
Average				218	533	685
Std deviation				1.6	10.3	1.5
Coeff of variation				0.007	0.019	0.002

Appendix C

Low Cycle Fatigue Test Results

All the results for the low cycle fatigue tests, for the bars that were bent and straightened more than once, are presented in this Appendix ie. -2 and -3 series. The results for the straight bars are included in Appendix B. Table B.1 and Table B.3 contains the results for the Y10-0 and Y12-0 sets. While the results captured for the bars that were bent and straightened once (Y10-1 and Y12-1), are presented in Table B.2 and Table B.4.

The tables in this Appendix contain the following information captured during each test.

Specimen nr. - the individual number marked on each specimen

$f_y(MPa)$ - the yield stress rounded off to the nearest whole number

Average - the average value rounded off to the nearest whole number

Std deviation - the standard deviation

Coeff of variation - the coefficient of variation

The average values, standard deviation and coefficient of variation are determined using the precise values of the data, before they were rounded off as presented in the tables.

Table C.1: Fatigue Test results - Y10-2 Set (straightened twice)

Specimen nr.	$f_y(MPa)$
T1	433
T2	420
T3	512
T4	460
Average	456
Std deviation	40.6
Coeff of variation	0.089

Table C.2: Fatigue Test results - Y10-3 Set (straightened thrice)

Specimen nr.	$f_y(MPa)$
T5	525
T6	456
T7	446
T8	*
Average	476
Std deviation	43.3
Coeff of variation	0.091

* one LVDT failed to record any data

Table C.3: Fatigue Test results - Y12-2 Set (straightened twice)

Specimen nr.	$f_y(MPa)$
T8	483
T9	485
T10	454
T11	487
Average	477
Std deviation	15.4
Coeff of variation	0.032

Table C.4: Fatigue Test results - Y12-3 Set (straightened thrice)

Specimen nr.	$f_y(MPa)$
T12	441
T13	485
T14	**
T15	**
Average	463
Std deviation	30.9
Coeff of variation	0.067

** bar fractured while being straightened

Appendix D

Supplementary Test Results

The full set of data recorded for the uniaxial compression tests, are presented in this Appendix. The results for the slab specimens are presented in Table D.1 and the results for the wall specimens in Table D.2.

Table D.1: Uniaxial Compression Test Results - Slab Specimens

Cube No.	Mass (kg)	Axial Force (kN)	Crushing Strength (MPa)
At 7 days			
1	2.434	231.5	23.15
2	2.445	224.5	22.45
3	2.436	224.9	22.49
Average	2.44	226.97	22.7
Std deviation	0.01	3.93	0.39
Coeff of variation	0.004	0.017	0.017
At 28 days			
1	2.431	409.1	40.91
2	2.445	400.5	40.05
3	2.4	405.2	40.52
Average	2.43	404.93	40.49
Std deviation	0.02	4.31	0.43
Coeff of variation	0.008	0.011	0.011

Table D.2: Uniaxial Compression Test Results - Wall Specimens

Cube No.	Mass (kg)	Axial Force (kN)	Crushing Strength (MPa)
At 7 days			
1	2.421	307.79	30.779
2	2.475	234.5	23.45
3	2.4	256.2	25.62
Average	2.43	266.16	26.62
Std deviation	0.04	37.65	3.76
Coeff of variation	0.016	0.141	0.141
At 35 days			
1	2.4	410.1	41.01
2	2.379	409.2	40.92
3	2.399	403.2	40.32
Average	2.39	407.5	40.75
Std deviation	0.01	3.75	0.38
Coeff of variation	0.004	0.009	0.009

Appendix E

Bending Schedules for Full Scale Models

The bending schedules for the four full scale models are presented in this Appendix.

E.1 Continuous Starter-bar System

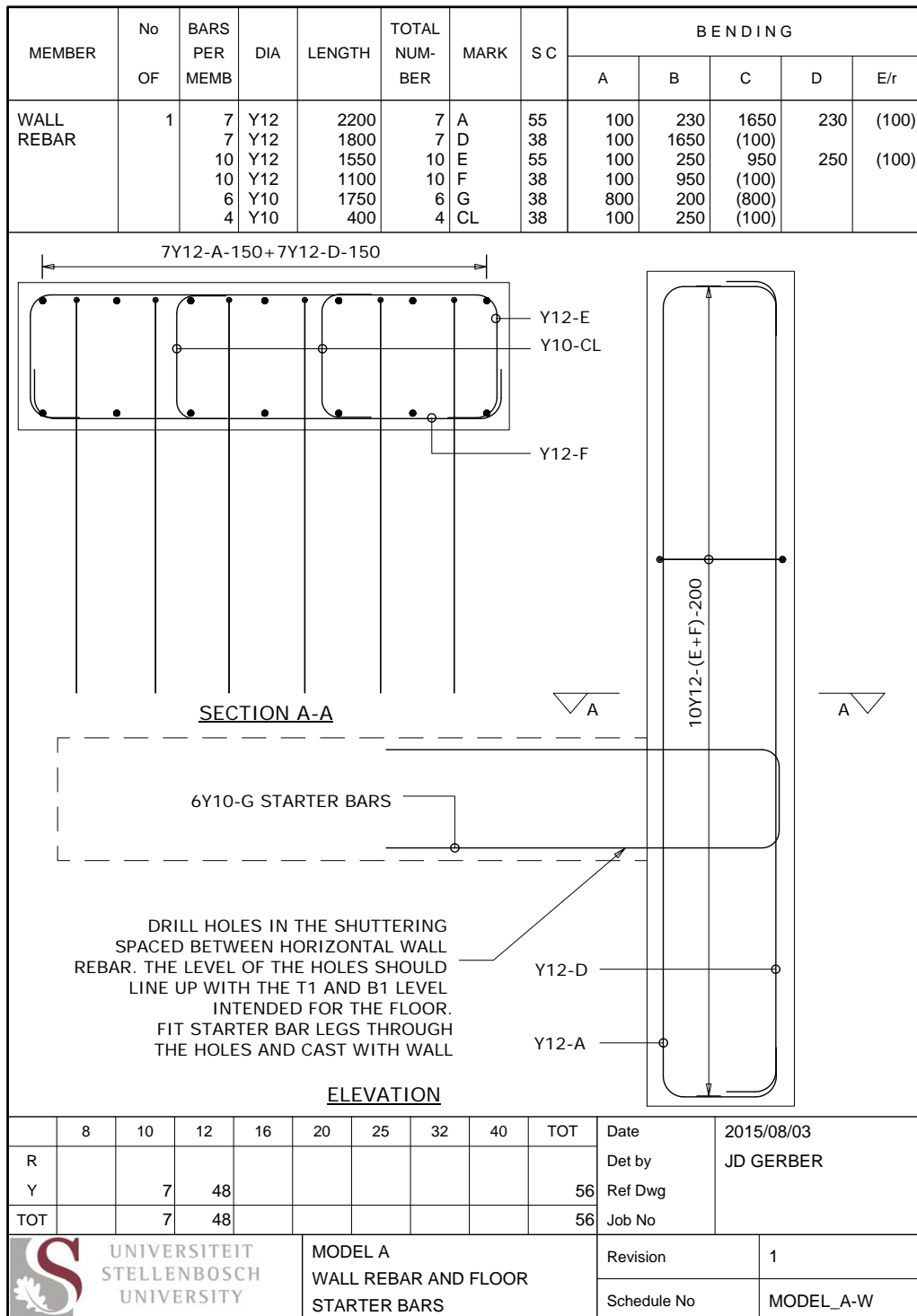


Figure E.1: Model A Wall Reinforcing Bending Schedule

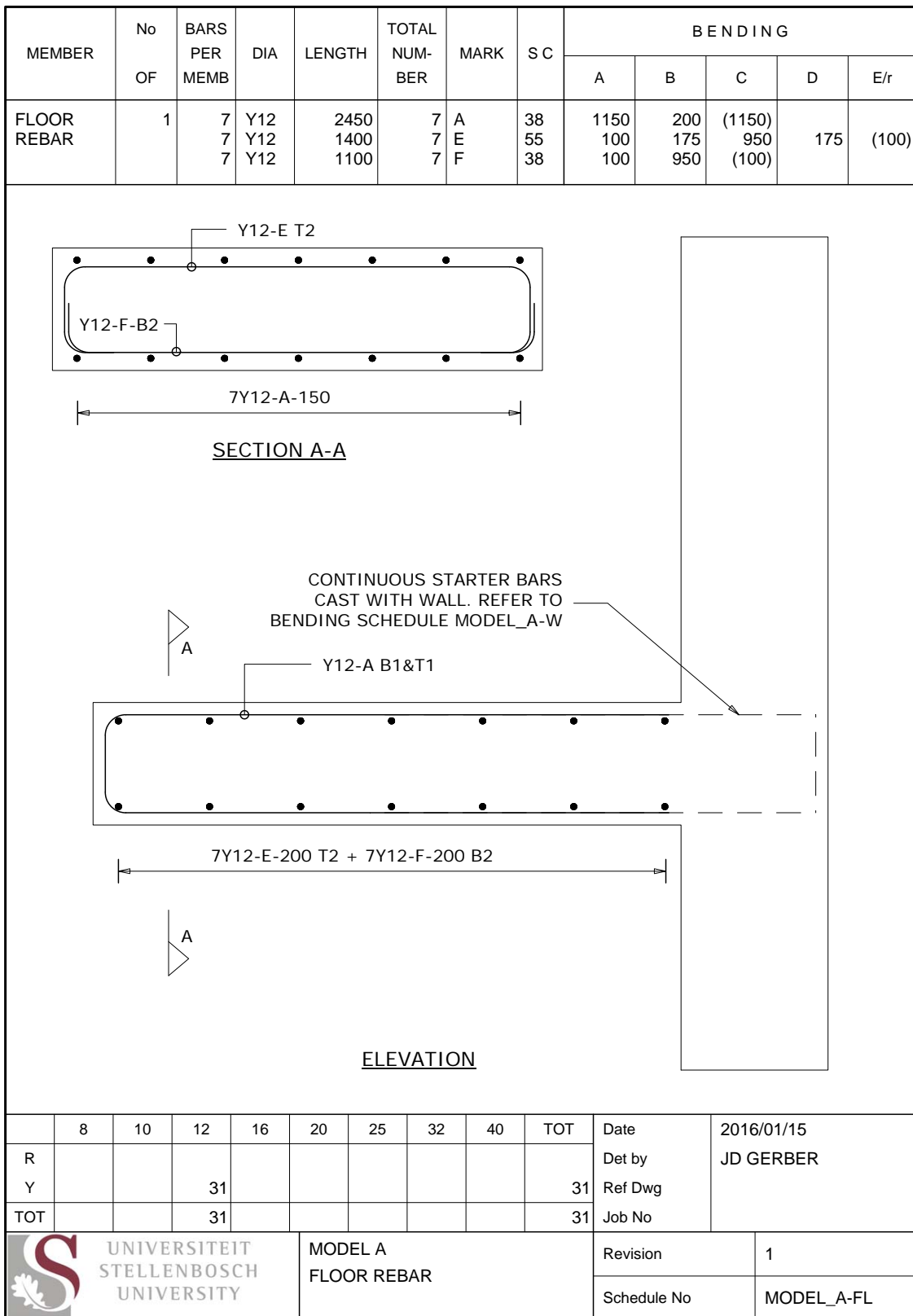


Figure E.2: Model A Floor Reinforcing Bending Schedule

E.2 Site-installed Bend-out Bar System

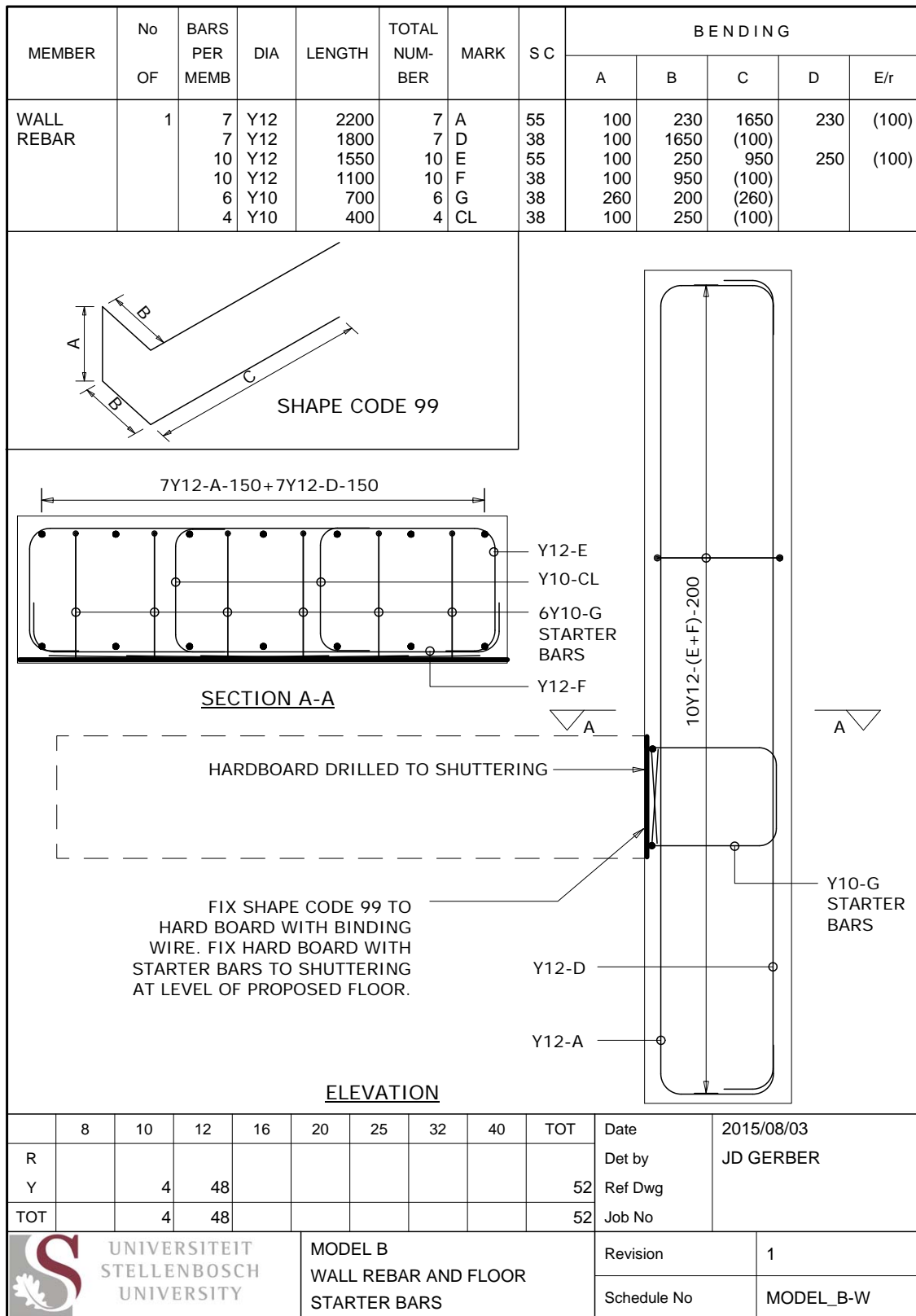


Figure E.3: Model B Wall Reinforcing Bending Schedule

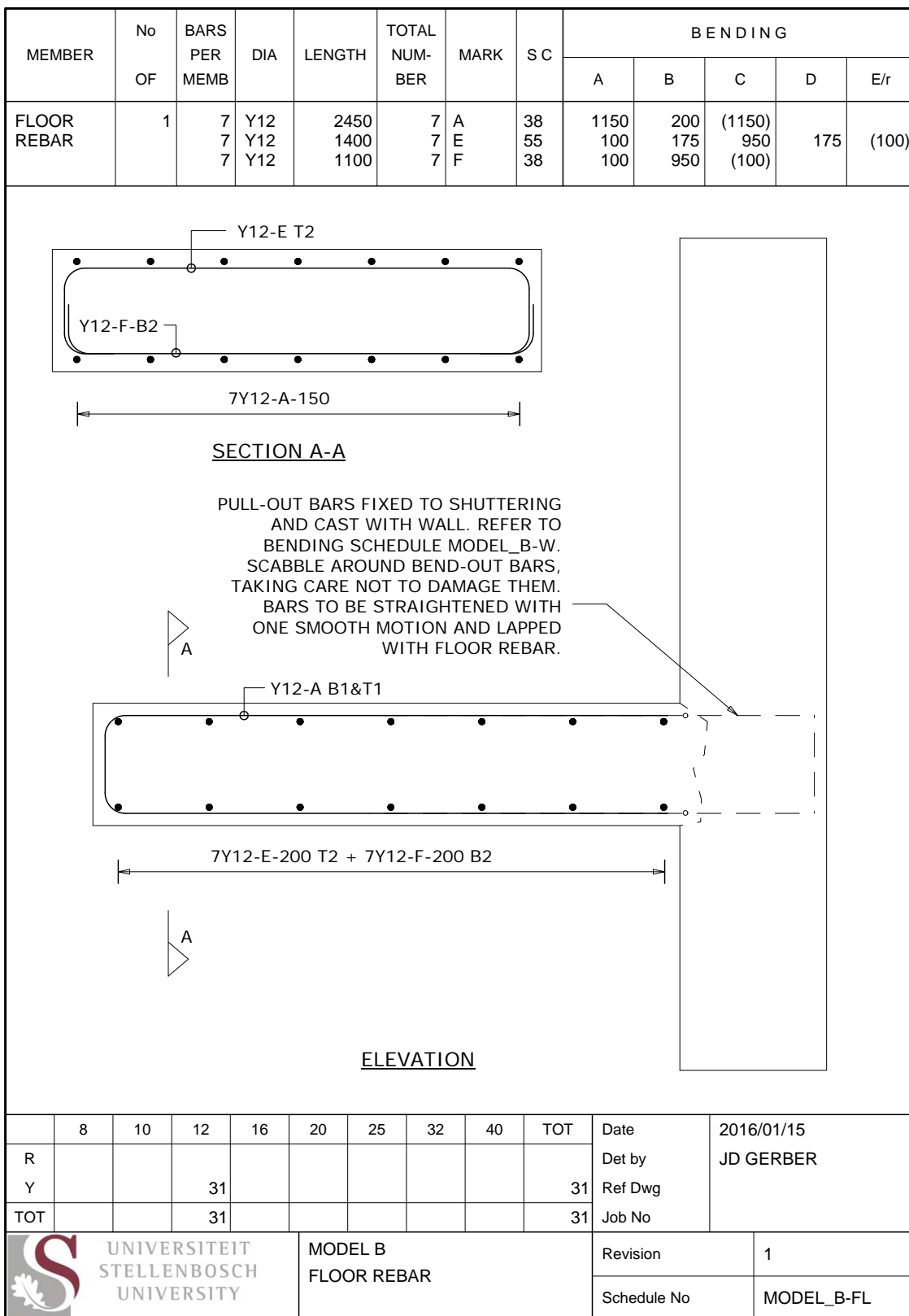


Figure E.4: Model B Floor Reinforcing Bending Schedule

E.3 Pre-assembled Bend-out Bar System

The bending schedule for the wall rebar in Model C, was identical to the schedule for Model A, presented in Figure E.1.

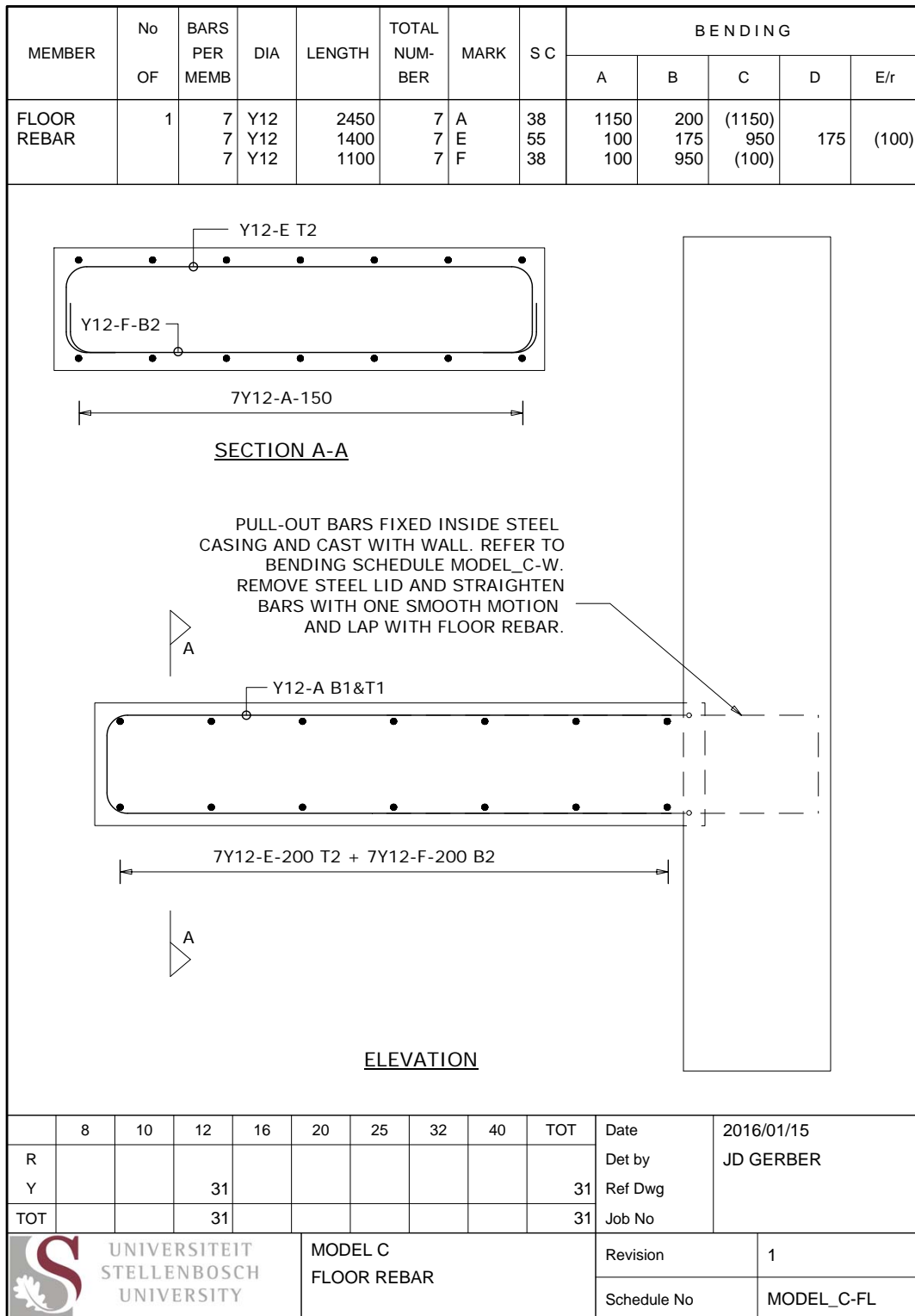


Figure E.5: Model C Floor Reinforcing Bending Schedule

E.4 Cast-in Anchors System

The bending schedule for the wall rebar in Model D, was identical to the schedule for Model A, presented in Figure E.1.

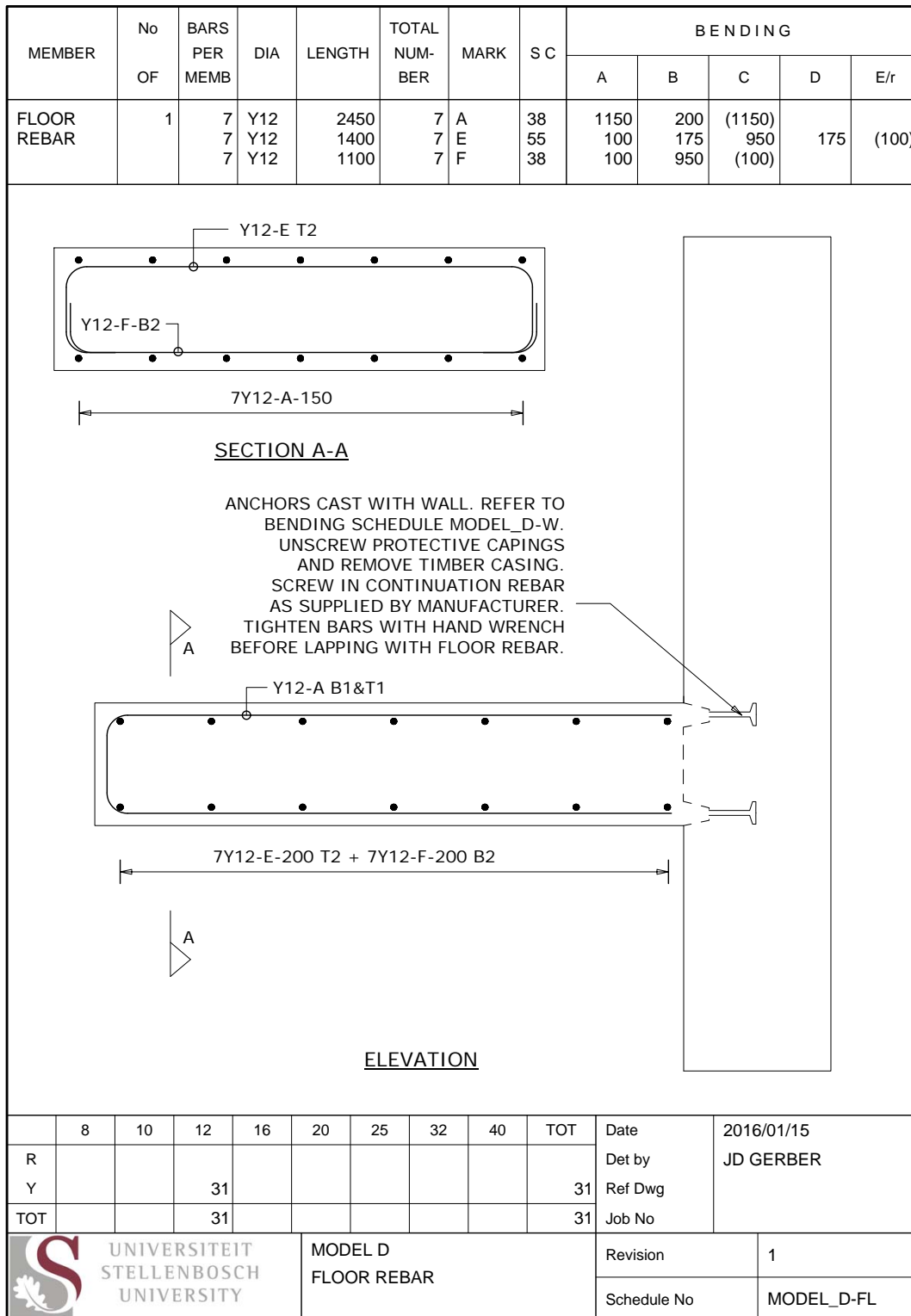


Figure E.6: Model D Floor Reinforcing Bending Schedule

Appendix F

Steel A-Frame Design Calculations

This Appendix includes the design calculations for the A-frame. Figure F.1 presents the node numbers for the respective steel members. The calculations that follow, include the design checks for each member corresponding to the relevant node numbers. The construction drawings of the full A-frame set-up is also included at the end of the Appendix.

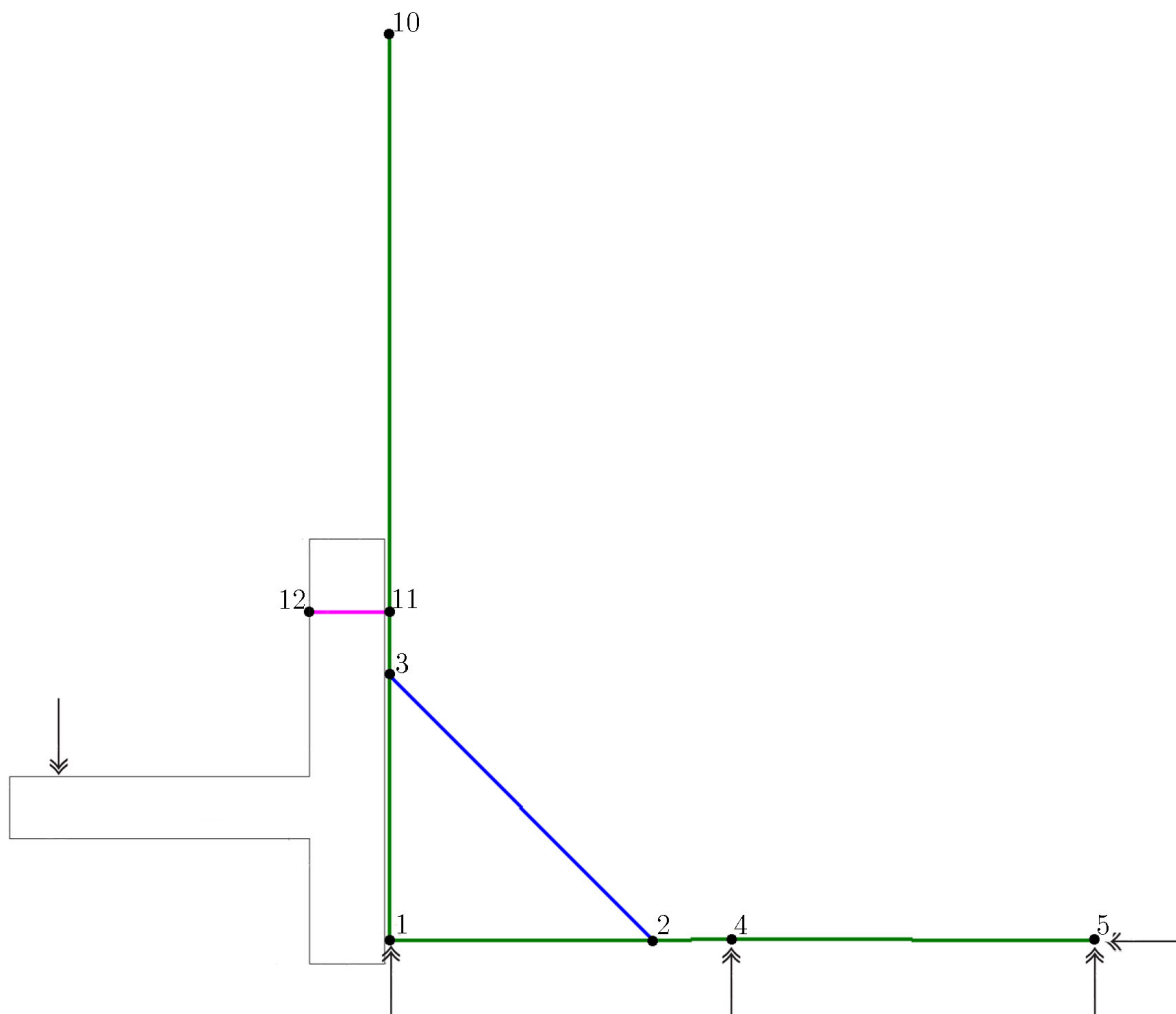


Figure F.1: Steel A-frame Nodes

<p>Software Consultants (Pty) Ltd Internet: http://www.prokon.com E-Mail: mail@prokon.com</p>	Job Number 15422828	Sheet
	Job Title Steel A-Frame	
	Client	
	Calcs by JD Gerber	Checked by

Member Design for Combined Stresses

MOMENTS: X-X M max = 11.49kNm @ 1.06m

MOMENTS: Y-Y M max = 0.000kNm @ 0.00m

AXIAL FORCE P max = 57.83kN @ 0.00m

Ver W2.6.25 - 18 Nov 2015
 Combine Ver W2.6.25
 Element 1-3 Evaluate current section
 Section name FR

Lx Eff = 0.903 m Wlx = 0.61
 Ly Eff = 0.903 m Wly = 1.00
 Le Eff = 1.062 m W2 = 1.73
 Fy = 350 MPa Fu = 480 MPa
 Tension area factor (Ane/Ag) = 1.00
 Flange class: 1 Web class : 1

Critical Load Case : C1

Section IPE-AA 200 I-sections (Web vert)

SANS 10162 - 2005 13.8.2 :

a) Cross-sectional strength (Crit. pos.= 1.062 m)
 Cu 0.85Mux 0.60Muy 57.7 9.77 0.00
 --- + --- + --- = --- + --- + --- = 0.26 OK
 Cr Mrx Mry 721 55.4 11.0

b) Overall member strength
 Cu 0.85U1xMux U1yMuy 57.8 5.94 0.00
 --- + --- + --- = --- + --- + --- = 0.21 OK
 Cr Mrx Mry 589 55.4 11.0

c) Lateral torsional buckling strength
 Cu 0.85U1xMux U1yMuy 57.8 9.77 0.00
 --- + --- + --- = --- + --- + --- = 0.27 OK
 Cr Mrx Mry 624 55.4 11.0

d) Additional check for class 1 I sections
 Mux Muy 11.5 0.00
 --- + --- = --- + --- = 0.21 OK
 Mrx Mry 55.4 11.0

13.4:Shear

Vux < Vrx 10.6 < 183.7 OK
 Vuy < Vry 0.0 < 116.1 OK

Slenderness Ratio: L/r = 41 OK

<p>Software Consultants (Pty) Ltd Internet: http://www.prokon.com E-Mail: mail@prokon.com</p>	Job Number 15422828	Sheet
	Job Title Steel A-Frame	
	Client	
	Calcs by JD Gerber	Checked by

MOMENTS: X-X M max = -9.070kNm @ 1.05m

Combine Ver W2.6.25
Element 1-2
Section name FR

Evaluate current section

Lx Eff = 0.894 m Wlx = 0.61
Ly Eff = 0.894 m Wly = 1.00
Le Eff = 1.052 m W2 = 1.72
Fy = 350 MPa Fu = 480 MPa
Tension area factor (Ane/Ag) = 1.00
Flange class: 1 Web class : 1

Critical Load Case : C1

MOMENTS: Y-Y M max = 0.000kNm @ 0.00m

Section IPE-AA 200 I-sections (Web vert)

SANS 10162 - 2005 13.8.2 :

a) Cross-sectional strength (Crit. pos. = 1.052 m)

Cu	0.85Mux	0.60Muy	56.6	7.71	0.00	
-- +	----- +	----- =	----- +	----- +	----- =	0.22
Cr	Mrx	Mry	721	55.4	11.0	OK

b) Overall member strength

Cu	0.85U1xMux	ISUlyMuy	56.6	4.71	0.00	
-- +	----- +	----- =	----- +	----- +	----- =	0.18
Cr	Mrx	Mry	591	55.4	11.0	OK

c) Lateral torsional buckling strength

Cu	0.85U1xMux	ISUlyMuy	56.6	7.71	0.00	
-- +	----- +	----- =	----- +	----- +	----- =	0.23
Cr	Mrx	Mry	626	55.4	11.0	OK


d) Additional check for class 1 I sections

Mux	Muy	9.07	0.00	
---	---	----- +	----- =	0.16
Mrx	Mry	55.4	11.0	OK

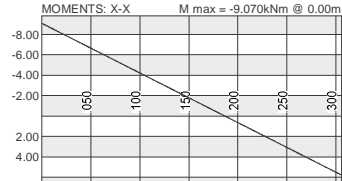
13.4: Shear

Vux < Vrx	8.5 < 183.7	OK
Vuy < Vry	0.0 < 116.1	OK

Slenderness Ratio: L/r = 40

 <p>Software Consultants (Pty) Ltd Internet: http://www.prokon.com E-Mail: mail@prokon.com</p>	Job Number 15422828	Sheet
	Job Title Steel A-Frame	
	Client	
	Calcs by JD Gerber	Checked by

MOMENTS: X-X M max = -9.070kNm @ 0.00m

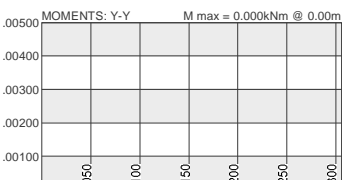


Combine Ver W2.6.25
Element 2-4 Evaluate current section
Section name FR

Lx Eff = 0.260 m Wlx = 0.40
Ly Eff = 0.260 m Wly = 1.00
Le Eff = 0.306 m W2 = 2.50
Fy = 350 MPa Fu = 480 MPa
Tension area factor (Ane/Ag) = 1.00
Flange class: 1 Web class : 1

Critical Load Case : C1

MOMENTS: Y-Y M max = 0.000kNm @ 0.00m



Section IPE-AA 200 I-sections (Web vert)

SANS 10162 - 2005 13.8.2 :

a) Cross-sectional strength (Crit. pos.= 0.000 m)

Cu	0.85Mux	0.60Muy	.320	7.71	0.00	
--- + ----- + ----- = ----- + ----- + ----- = 0.14						OK
Cr	Mrx	Mry	721	55.4	11.0	

b) Overall member strength

Cu	0.85U1xMux	ISUlyMuy	.320	3.08	0.00	
--- + ----- + ----- = ----- + ----- + ----- = 0.06						OK
Cr	Mrx	Mry	700	55.4	11.0	

c) Lateral torsional buckling strength

Cu	0.85U1xMux	ISUlyMuy	.320	7.71	0.00	
--- + ----- + ----- = ----- + ----- + ----- = 0.14						OK
Cr	Mrx	Mry	702	55.4	11.0	


d) Additional check for class 1 I sections

Mux	Muy	9.07	0.00			
--- + --- = ----- + ----- = 0.16						OK
Mrx	Mry	55.4	11.0			

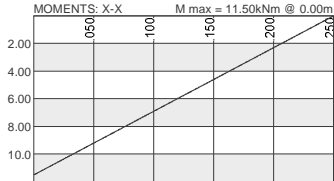
13.4: Shear

Vux < Vrx	48.6 < 183.7	OK
Vuy < Vry	0.0 < 116.1	OK

Slenderness Ratio: L/r = 12 OK

 <p>Software Consultants (Pty) Ltd Internet: http://www.prokon.com E-Mail: mail@prokon.com</p>	Job Number 15422828	Sheet
	Job Title Steel A-Frame	
	Client	
	Calcs by JD Gerber	Checked by

MOMENTS: X-X M max = 11.50kNm @ 0.00m



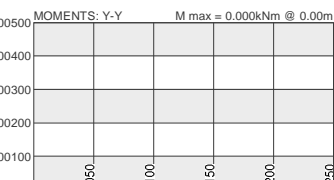
Combine Ver W2.6.25
Element 3-11
Section name FR

Evaluate current section

Lx Eff = 0.212 m Wlx = 0.60
Ly Eff = 0.212 m Wly = 1.00
Le Eff = 0.250 m W2 = 1.75
Fy = 350 MPa Fu = 480 MPa
Tension area factor (Ane/Ag) = 1.00
Flange class: 1 Web class : 1

Critical Load Case : C1

MOMENTS: Y-Y M max = 0.000kNm @ 0.00m



Section IPE-AA 200 I-sections (Web vert)

SANS 10162 - 2005 13.8.2 :

a) Cross-sectional strength (Crit. pos.= 0.000 m)

Cu	0.85Mux	0.60Muy	.450	9.78	0.00	
--- + ----- + ----- = ----- + ----- + ----- = 0.18						OK
Cr	Mrx	Mry	721	55.4	11.0	

b) Overall member strength

Cu	0.85U1xMux	U1yMuy	.450	5.87	0.00	
--- + ----- + ----- = ----- + ----- + ----- = 0.11						OK
Cr	Mrx	Mry	703	55.4	11.0	

c) Lateral torsional buckling strength

Cu	0.85U1xMux	U1yMuy	.450	9.78	0.00	
--- + ----- + ----- = ----- + ----- + ----- = 0.18						OK
Cr	Mrx	Mry	703	55.4	11.0	

d) Additional check for class 1 I sections

Mux	Muy	11.5	0.00			
--- + --- = ----- + ----- = 0.21						OK
Mrx	Mry	55.4	11.0			

13.4: Shear

Vux < Vrx	46.0 < 183.7	OK
Vuy < Vry	0.0 < 116.1	OK

Slenderness Ratio: L/r = 10 OK

<p>Software Consultants (Pty) Ltd Internet: http://www.prokon.com E-Mail: mail@prokon.com</p>	Job Number 15422828	Sheet
	Job Title Steel A-Frame	
	Client	
	Calcs by JD Gerber	Checked by

MOMENTS: X-X M max = 5,800kNm @ 0.00m

Combine Ver W2.6.25
Element 4-5 Evaluate current section
Section name FR

Lx Eff = 1.244 m Wlx = 0.60
Ly Eff = 1.244 m Wly = 1.00
Le Eff = 1.464 m W2 = 1.75
Fy = 350 MPa Fu = 480 MPa
Tension area factor (Ane/Ag) = 1.00
Flange class: 1 Web class : 1

Critical Load Case : C1

MOMENTS: Y-Y M max = 0.000kNm @ 0.00m

Section IPE-AA 200 I-sections (Web vert)

SANS 10162 - 2005 13.8.2 :

a) Cross-sectional strength (Crit. pos.= 0.000 m)

Cu	0.85Mux	0.60Muy	.010	4.93	0.00	
--- + ----- + ----- = ----- + ----- + ----- = 0.09						OK
Cr	Mrx	Mry	721	55.4	11.0	

b) Overall member strength

Cu	0.85U1xMux	ISU1yMuy	.010	2.96	0.00	
--- + ----- + ----- = ----- + ----- + ----- = 0.05						OK
Cr	Mrx	Mry	482	55.4	11.0	

c) Lateral torsional buckling strength

Cu	0.85U1xMux	ISU1yMuy	.010	4.93	0.00	
--- + ----- + ----- = ----- + ----- + ----- = 0.09						OK
Cr	Mrx	Mry	543	55.4	11.0	


d) Additional check for class 1 I sections

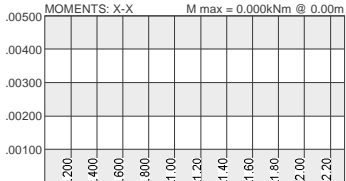
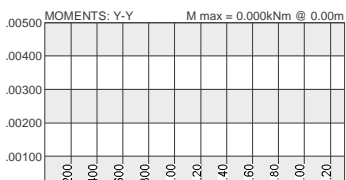
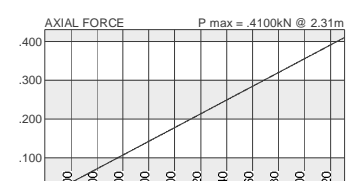
Mux	Muy	5.80	0.00			
--- + ----- = ----- + ----- = 0.10						OK
Mrx	Mry	55.4	11.0			

13.4: Shear

Vux < Vrx	4.1 < 183.7	OK
Vuy < Vry	0.0 < 116.1	OK

Slenderness Ratio: L/r = 56 OK

 <p>Software Consultants (Pty) Ltd Internet: http://www.prokon.com E-Mail: mail@prokon.com</p>	Job Number 15422828	Sheet
	Job Title Steel A-Frame	
	Client	
	Calcs by JD Gerber	Checked by

Combine Ver W2.6.25
Element 10-11 Evaluate current section
Section name FR

Lx Eff = 1.963 m Wlx = 1.00
Ly Eff = 1.963 m Wly = 1.00
Le Eff = 2.310 m W2 = 1.00
Fy = 350 MPa Fu = 480 MPa
Tension area factor (Ane/Ag) = 1.00
Flange class: 1 Web class : 1

Critical Load Case : C1

Section IPE-AA 200 I-sections (Web vert)

SANS 10162 - 2005 13.8.2 :

a) Cross-sectional strength (Crit. pos. = 2.310 m)

Cu	0.85Mux	0.60Muy	.410	0.00	0.00	
--- + ----- + ----- = ----- + ----- + ----- = 0.00						
Cr	Mrx	Mry	721	55.4	11.0	OK

b) Overall member strength

Cu	0.85U1xMux	U1yMuy	.410	0.00	0.00	
--- + ----- + ----- = ----- + ----- + ----- = 0.00						
Cr	Mrx	Mry	288	55.4	11.0	OK

c) Lateral torsional buckling strength

Cu	0.85U1xMux	U1yMuy	.410	0.00	0.00	
--- + ----- + ----- = ----- + ----- + ----- = 0.00						
Cr	Mrx	Mry	357	42.9	11.0	OK


d) Additional check for class 1 I sections

Mux	Muy	0.00	0.00			
--- + --- = ----- + ----- = 0.00						
Mrx	Mry	42.9	11.0			OK

13.4: Shear

Vux < Vrx	0.0 < 183.7	OK
Vuy < Vry	0.0 < 116.1	OK

Slenderness Ratio: L/r = 89

 <p>Software Consultants (Pty) Ltd Internet: http://www.prokon.com E-Mail: mail@prokon.com</p>	Job Number 15422828		Sheet	
	Job Title Steel A-Frame			
	Client			
	Calcs by JD Gerber		Checked by	Date 05.05.2015

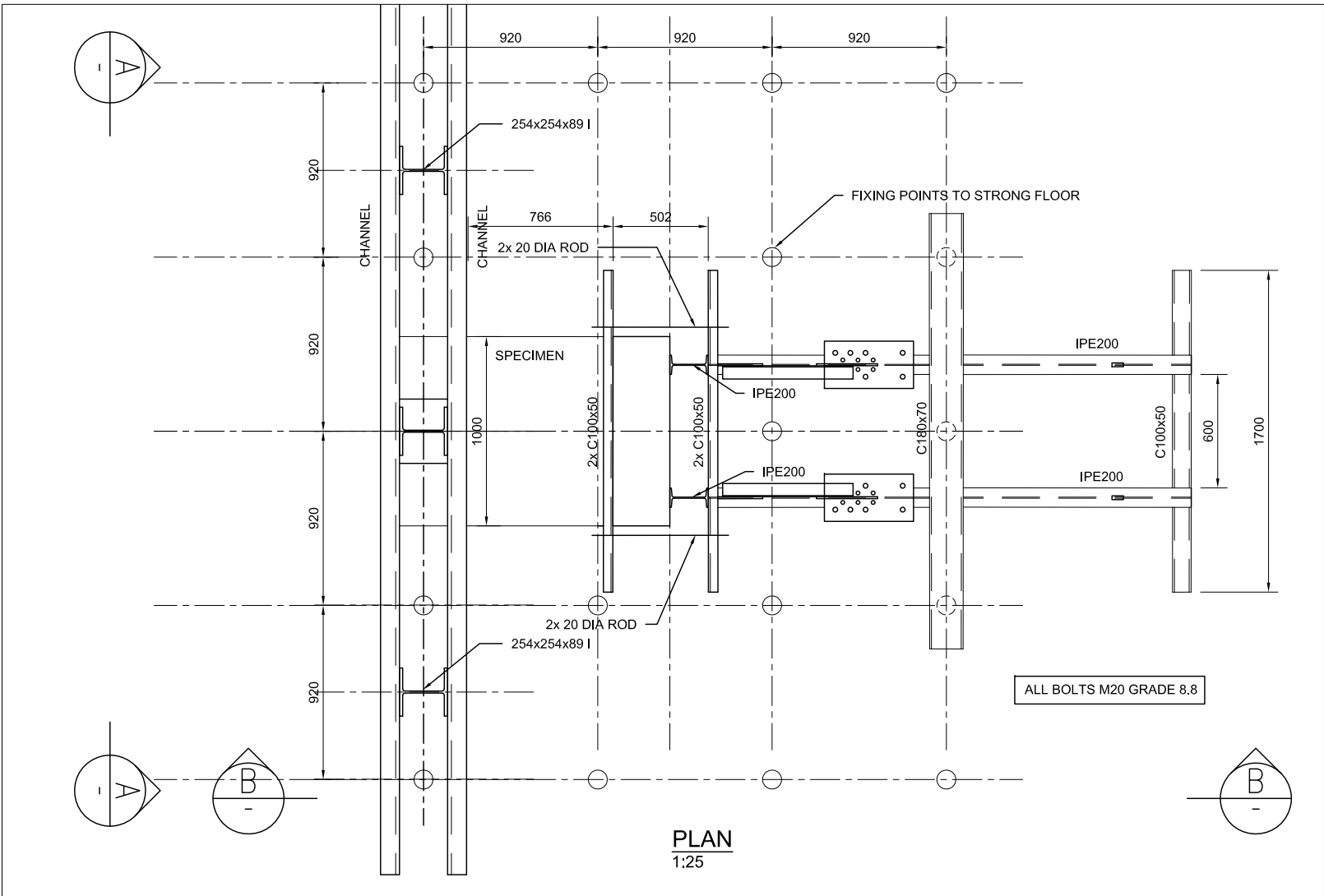
Member Design for Axial Force - Strut Ver W2.6.05

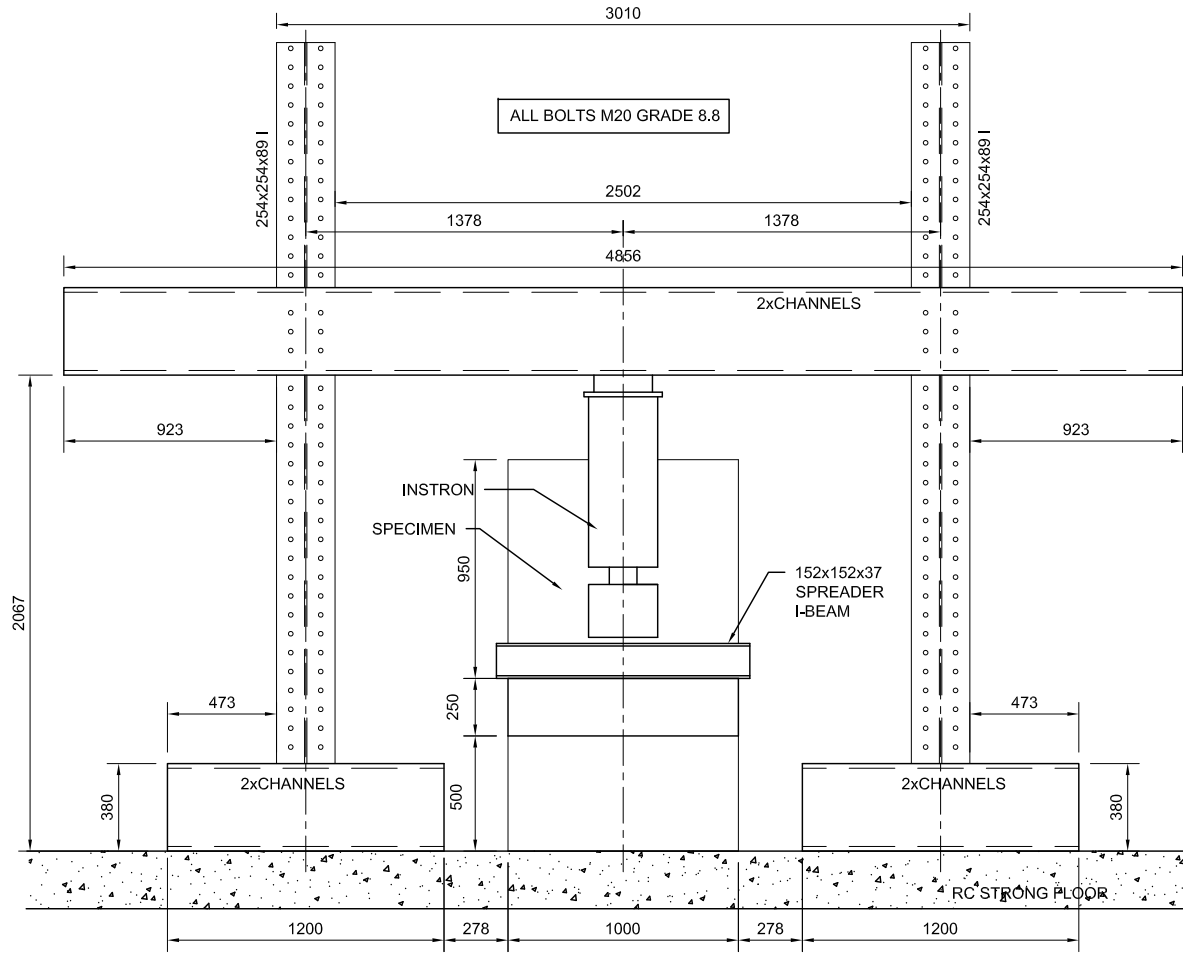
Code of practice: SANS 10162 - 2005
Design approach: Evaluate current sections

Design parameters		Maximum L/r ratios		
Kv factor	0.85	L Case	Compr.	Tension
Kx factor	0.85	C1	200	300
Ky factor	1.00			
Kz factor	1.00			
Ane/Ag	1.00			
Fy	MPa 350.00			
Fu	MPa 480.00			

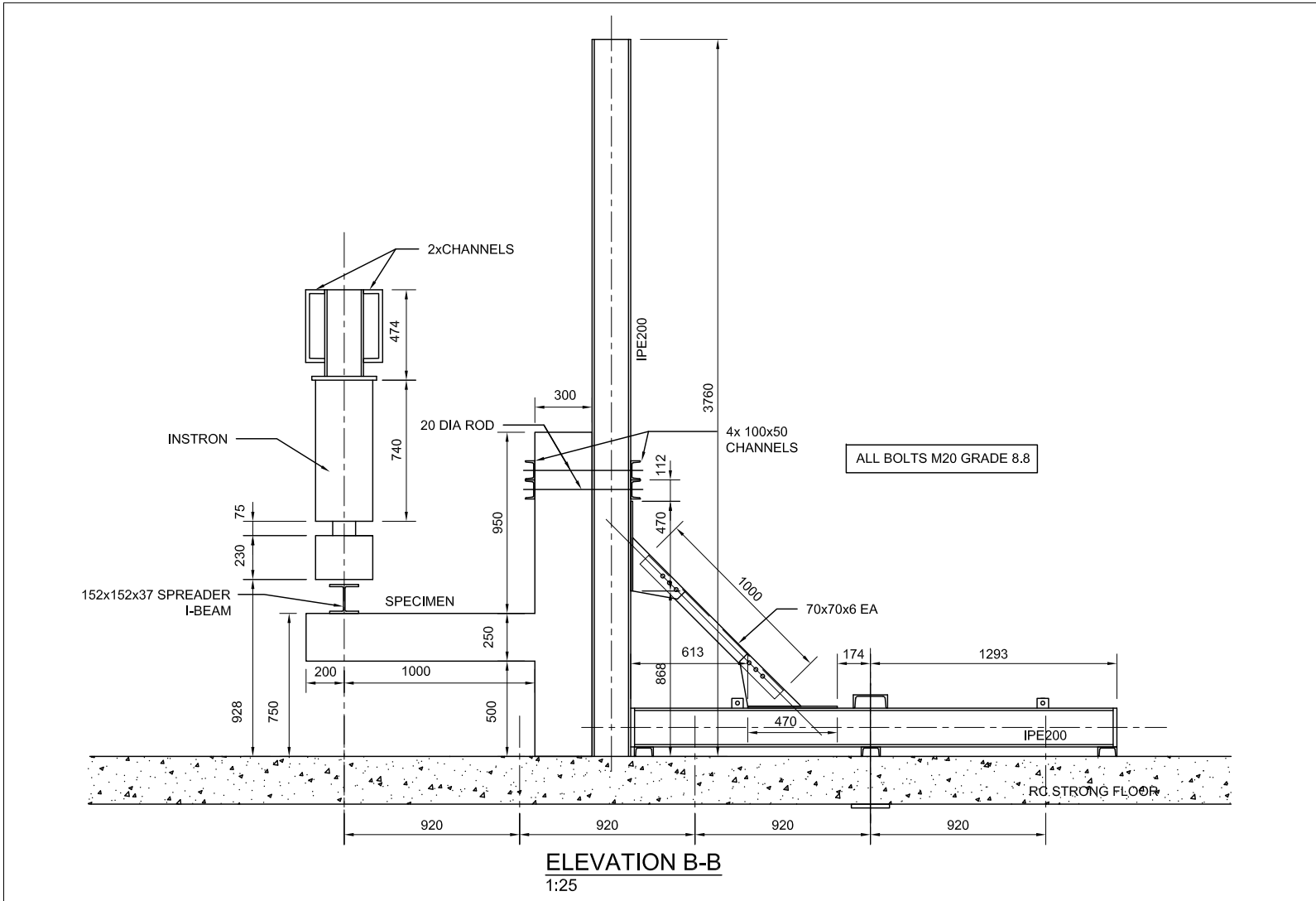
Element	Length (m)	L.C. Force (kN)	L/R	Crit Axis	Section	Pc (MPa)	σc (MPa)	Result

GROUP BR	Angles (Equal leg)							
2-3	1.495	C1 -80.48	93	V	70x70x6	315.0	99.0	OK
Group mass = 9.5 kg								
GROUP TIE	Circular solid sections							
11-12	0.252	C1 -46.01	34	Y	Dia 30	315.0	65.1	OK
Group mass = 1.4 kg								
Total mass for task = 10.9 kg								





ELEVATION A-A
1:25



Appendix G

Finite Element Material Models

This Appendix includes all the input values used to create the material models used in the numerical analyses. The values for both the concrete and steel models are summarised in Table G.1.

For the analysis of Model Y12-A(40), the steel material model for the wall, slab and starter-bar reinforcement were all based on specimen F3, taken from the same batch of steel as the floor reinforcement used in the full-scale Model A. The stress-strain curve, with the numerical equivalent is presented in Figure 5.8.

For the Y12-S analyses, the steel material model for the wall, slab and starter-bar reinforcement were all based on specimen 71, taken from the S-series of specimens in the preliminary tensile testing phase. The stress-strain curve is presented in Figure G.1.

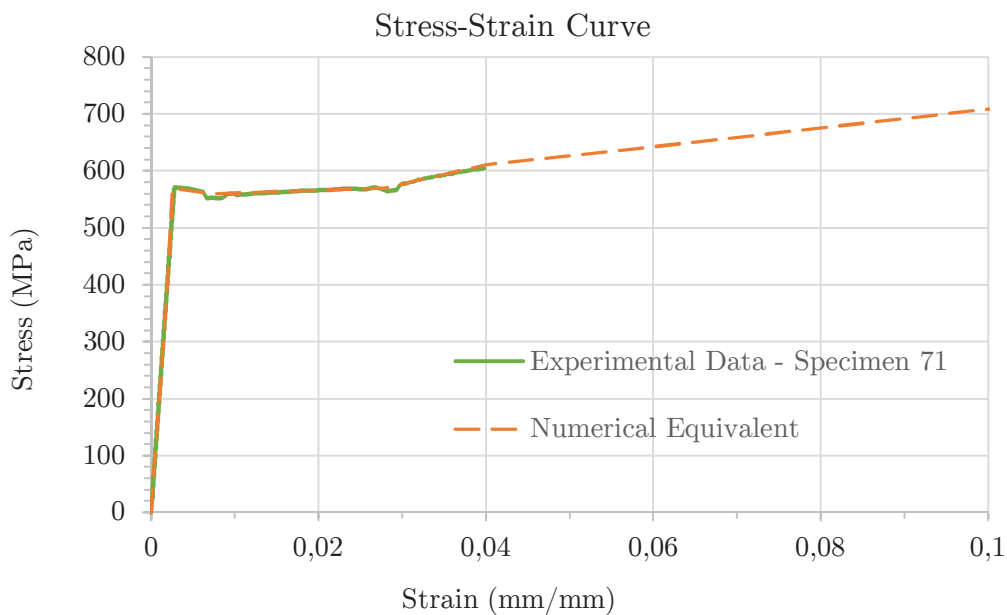


Figure G.1: Equivalent Stress-strain Curve for the Reinforcement Material Model in Y12-S(30-50)

For the Y12-B1 analyses, the steel material model for the wall and the slab reinforcement were based on the data as presented in Figure G.1. The starter-bars were however based

on the results from specimen 3, taken from the B-series of specimens in the preliminary tensile testing phase. The stress-strain curve is presented in Figure G.2.

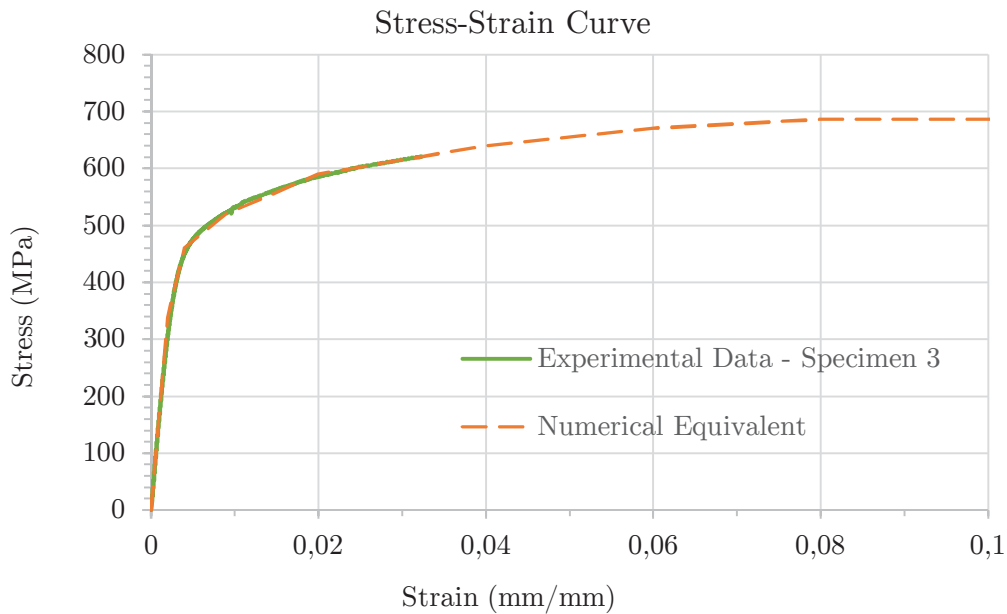


Figure G.2: Equivalent Stress-strain Curve for the Reinforcement Material Model in Y12-B1(30-50)

Similarly are the starter-bars in the Y12-B2 analyses, based on the data gathered from specimen 9 and the stress-strain curve is presented in Figure G.3.

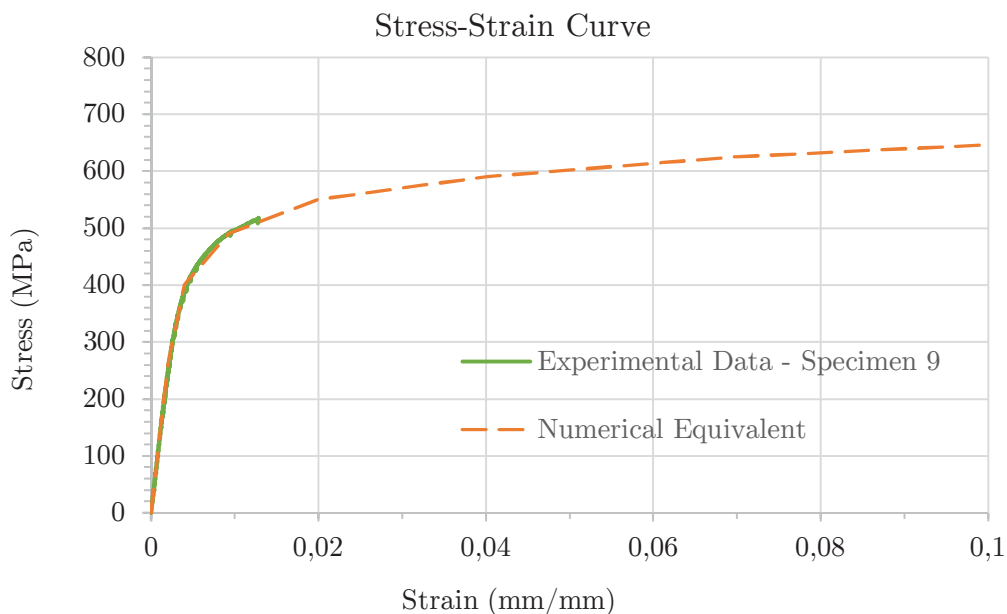


Figure G.3: Equivalent Stress-strain Curve for the Reinforcement Material Model in Y12-B2(30-50)

Table G.1: FE Analysis - Material Model Inputs

FE Model	Wall and Slab Concrete					Interface Concrete					Wall and Slab Rebars			Starter-bars		
	f_{ck}	f_t	G_f^I	ν	E_c	f_{ck}	f_t	G_f^I	ν	E_c	f_y	f_u	E_s	f_y	f_u	E_s
	MPa	MPa	N/m		GPa	MPa	MPa	N/m		GPa	MPa	MPa	GPa	MPa	MPa	GPa
Y12-A(30)	40.49	2.11	136.52	0.15	33.8	40.49	1×10^{-5}	136.52	0.15	33.8	510	666	223	510	666	223
Y12-S(30)	24	2.5	129.35	0.15	30	24	1×10^{-5}	129.35	0.15	30	570	725	208	570	725	208
Y12-S(40)	32	3.02	136.22	0.15	30	32	1×10^{-5}	136.22	0.15	30	570	725	208	570	725	208
Y12-S(50)	40	3.51	141.81	0.15	30	40	1×10^{-5}	141.81	0.15	30	570	725	208	570	725	208
Y12-B1(30)	24	2.5	129.35	0.15	30	24	1×10^{-5}	129.35	0.15	30	570	725	208	471	686	169
Y12-B1(40)	32	3.02	136.22	0.15	30	32	1×10^{-5}	136.22	0.15	30	570	725	208	471	686	169
Y12-B1(50)	40	3.51	141.81	0.15	30	40	1×10^{-5}	141.81	0.15	30	570	725	208	471	686	169
Y12-B2(30)	24	2.5	129.35	0.15	30	24	1×10^{-5}	129.35	0.15	30	570	725	208	431	688	129
Y12-B2(40)	32	3.02	136.22	0.15	30	32	1×10^{-5}	136.22	0.15	30	570	725	208	431	688	129
Y12-B2(50)	40	3.51	141.81	0.15	30	40	1×10^{-5}	141.81	0.15	30	570	725	208	431	688	129

 f_{ck} Concrete Compressive Cylinder Stress G_f^I Mode-I Fracture Energy E_c Modulus of Elasticity for the Concrete f_u Ultimate Stress of Reinforcement Bar f_t Concrete Tensile Stress ν Poisson's Ratio f_y Yield Stress of Reinforcement Bar E_s Modulus of Elasticity for the Steel

Appendix H

The Grubb's Test

This Appendix includes the procedure to detect a single outlier in a data set of N -values that are nearly normally distributed. The first step in the procedure is to calculate the Grubbs G -value (G_{exp}) as defined with Equation H.1:

$$G_{exp} = |x_{out} - \bar{x}|/s \quad (\text{H.1})$$

x_{out} is the suspected outlier

\bar{x} is the mean of the N values

s is the standard deviation of the N values

This value is subsequently compared to the constant G_{crit} , obtained from Table H.1, for data with different confidence levels and number of values N in a set. If the calculated G_{exp} is found to be:

- $G_{exp} < G_{crit}$ then the point in question is not an outlier
- $G_{exp} > G_{crit}$ then the point in question is indeed an outlier

Table H.1: Critical values of Grubbs Test

Percentage Confidence Level				Percentage Confidence Level			
N	95%	97.5%	99%	N	95%	97.5%	99%
3	1.15	1.15	1.15	19	2.53	2.68	2.85
4	1.46	1.48	1.49	20	2.56	2.71	2.88
5	1.67	1.71	1.75	21	2.58	2.73	2.91
6	1.82	1.89	1.94	22	2.6	2.76	2.94
7	1.94	2.02	2.1	23	2.62	2.78	2.96
8	2.03	2.13	2.22	24	2.64	2.8	2.99
9	2.11	2.21	2.32	25	2.66	2.82	3.01
10	2.18	2.29	2.41	30	2.75	2.91	
11	2.23	2.36	2.48	35	2.82	2.98	
12	2.29	2.41	2.55	40	2.87	3.04	
13	2.33	2.46	2.61	45	2.92	3.09	
14	2.37	2.51	2.66	50	2.96	3.13	
15	2.41	2.55	2.71	60	3.03	3.2	
16	2.44	2.59	2.75	70	3.09	3.26	
17	2.47	2.62	2.79	80	3.14	3.31	
18	2.5	2.65	2.82	90	3.18	3.35	
				100	3.21	3.38	

(Grubbs, 1969)

List of References

- ACI (2008). *ACI 318-08: Building Code Requirements for Structural Concrete and Commentary, Appendix D*. Michigan.
- Ancon Building Products (2011). Reinforcement Continuity Systems for the Construction Industry - Eazistrip. Available at: <http://www.ancon.co.uk>, accessed June 2016.
- Ancon Building Products (2014). Reinforcement Continuity Systems for the Construction Industry - KSN Anchors. Available at: <http://www.ancon.co.uk>, accessed June 2016.
- ASTM Committee on Standards (2011). *E8/E8M-11: Standard Test Method for Tension Testing of Metallic Materials*.
- BSI (1992). *BS EN 1992-1-1:2004 Eurocode 2 - Design of Concrete structures, Part 1-1: General Rules and rules for Buildings*. London.
- BSI (2000). *BS EN 12504-1:2000 - Testing concrete in structures. Cored specimens. Taking, examining and testing in compression*.
- BSI (2013). *BS EN 12390-13:2013 - Testing hardened concrete, Determination of secant modulus of elasticity in compression*.
- Cairns, J. (2010). Design Analysis for moment connections with KS Threaded Anchors (unpublished report). Tech. Rep., Heriot Watt University, Edinburgh.
- Campillo, B., Perez, R. and Martinetz, L. (1996). Study of Aging and Embrittlement of Microalloyed Steel Bars. *Jmeppeg*, vol. 5, pp. 615–620.
- Chun, S. and Ha, T. (2014). Cyclic Behavior of Wall-Slab Joints with Lap Splices of Cold-Straightened Rebars and Mechanical Splices. *Journal of Structural Engineering*, vol. 141, no. 2. ISSN 0733-9445.
- Chun, S.-C., Kim, S.-K. and Oh, B. (2003). Re-bar Joints between RC Core-wall and Slab in High-rise Buildings - Using Steel Plates with Mechanical Splice and Anchorage. *Architectural Institute of Structural Engineering*, vol. 19, no. 9, pp. 181–189.
- De Villiers, J. (2015). *Bond behaviour of deformed steel in lightweight foamed concrete*. Master's thesis, Stellenbosch University.
- Deaton, J.B. (2013). *Nonlinear Finite Element Analysis of Reinforced Concrete Exterior Beam-Column Joints With Nonseismic Detailing Nonlinear Finite Element Analysis of Reinforced Concrete Exterior Beam-Column Joints With Nonseismic Detailing*. Ph.D. thesis, Georgia Institute of Technology.
- Diana, T. (2014). *Diana User's Manual*. TNO Diana, Delft.
- fib (2010). *fib Model Code for Concrete Structures*.

- GOM (2003). *GOM Aramis User Manual - 3.11 Software*, vol. 49.
- Grubbs, F. (1969). Procedure for detecting outlying observations in samples. *Technometrics*, vol. 11, no. 1, pp. 1–21.
- JCSS (2001). *Probabilistic Model Code, Part III*.
- Karsan, I. and Jirsa, J. (1969). Behavior of concrete under compressive loadings. *ASCE Journal of the Structural Division*, vol. 95, pp. 2543–2563.
- Maybery, G. (2014). *Setting up testing and modelling of a typical reinforced concrete beam to column structural connection, BEng (Civil) final year Project Report number 14-2-100*. Department of Civil Engineering, Stellenbosch University.
- Monnier, T. (1987). Examples of non-linear numerical analysis with DIANA. *IABSE*, vol. 54, no. 1, pp. 405–415.
- Montgomery, D. and Runger, G. (2007). *Applied Statistics and Probability for Engineers*. 4th edn. John Wiley & Sons, Inc.
- NZS (2006). *Concrete Structures Standard NZS 3101-Part 1:2006*. Wellington.
- Prokon (2015). Help for PROKON Structural Analysis and Design version 3.0. Available at: <http://www.prokon.com>, accessed June 2016.
- Retief, J. and Dunaiski, P. (2009). *Background to SANS 10160*. SUN Press, Stellenbosch.
- Robberts, J.M. and Marshall, V. (2010). *Analysis and Design of Concrete Structures*. Nuclear Structural Engineering, Johannesburg.
- Rots, J. and Blaauwendraad, J. (1989). CRACK MODELS FOR CONCRETE: DISCRETE OR SMEARED?, FIXED, MULTI-DIRECTIONAL OR ROTATING? *Heron*, vol. 34, no. 1.
- Rupasinghe, R. and Nolan, É. (2007). *FORMWORK FOR MODERN, EFFICIENT CONCRETE CONSTRUCTION*. IHS BRE Press, Garston, Watford.
- SANS (2000). *SANS 10100-1:2000 - The structural use of concrete, Part 1: Design*.
- SANS (2006). *SANS 5863:2006 - Concrete testing - Compressive strength of hardened concrete*.
- SANS (2010). *SANS 68921-1:2010 - Metallic materials - Tensile Testing, Part 1: Method of test at room temperature*.
- SANS (2011a). *SANS 10160-1:2011 - Basis of structural design and actions for buildings and industrial structures, Part 01: Basis of structural design*.
- SANS (2011b). *SANS 10160-4:2011 - Basis of structural design and actions for buildings and industrial structures, Part 4: Seismic actions and general requirements for buildings*.
- SANS (2011c). *SANS 920:2011 - Steel bars for concrete reinforcement*.
- SANS (2012). *SABS 0144:1995 - Detailing of Steel Reinforcement For Concrete*. 2nd edn. The South African Bureau Of Standards, Pretoria.
- SANS (2014). *SANS 10100-2:2014 - The structural use of concrete, Part 2: Materials and execution of work*.
- Schreppers, G. and Frissen, Cand Kang, H. (2011). Prediction of Crack-width and Crack-pattern.

- Sinha, B., Gerstle, K. and Tulin, L. (1964). Stress-strain relations for concrete under cyclic loading. *ACI Journal Proceedings*, vol. 61, no. 2, pp. 195–212.
- Telford, T. (1997). *Design of fastenings in concrete*. CEB, London.
- Totten, G.E. and Howes, M.A.H. (1997). *Steel Heat Treatment Handbook*. Marcel Dekker, New York.